



UNIVERSITÀ DEGLI STUDI DI TRENTO
FACOLTÀ DI SCIENZE MATEMATICHE, FISICHE E NATURALI
DIPARTIMENTO DI FISICA

**Impurities in a Bose-Einstein condensate
using quantum Monte-Carlo methods:
ground-state properties**

Thesis submitted for the degree of
Doctor in Physics

Supervisor:
Prof. Stefano Giorgini

Candidate:
Luis A. Peña Ardila

Trento, Italy. April 27 2015

Acknowledgements

ENGLISH VERSION (To the BEC crew)

It has been a long road until arrive here, sometimes a snaky road. But out of doubt getting this point it wouldn't have been possible without many people who push me forwards in the moments of frustration and dismay.

From the bottom of my heart I am tremendously grateful with Stefano Giorgini, no only because his role as advisor, but for his invaluable guidance, patience and love for physics. I learnt from him an invaluable lesson that quality work always comes in a price: time, patience and discipline. Along the PhD many question popping into my mind and he was there to show me a light. I always will thanks Stefano, not only for his encourage but also for pointing out my weakness as well as to highlight in every meeting we had "...you must learn..."

I want to extend my thanks to Professor Sandro Stringari who allowed me to be part of this family and permit me to learn from outstanding people when I participated in conferences and workshops. Every single conference was an opportunity to inspire myself to continue in this beautiful path of research. Also being inspired every single day by the brilliant team at Trento Lev Pitaevskii, Franco Dalfovo, Iacopo Carusotto, Chiara Menotti, Alessio Recati, Gabriele Ferrari and Giacomo Lamporesi.

Heartfelt thanks to all the crew of the BEC group. In particular to David Papoular and Marta Abad for their help in many concerns and to my friends Grazia Salerno, Giovanni Martone and Yan-Hua Hou. As well as Giulia De Rosi, José Lebreuilly Nicola Bartolo, Simone Donadello, Stefano Finazzi, Marco Larcher, Pierre-Elie Larre, Natalia Matveeva, Tomoki Ozawa, Hannah Price, Riccardo Rota, Alberto Sartori, Robin Scott, Simone Serafini, Marek Tylutki, Zeng-Qiang Yu, Peng Zou, Li yun, and Onur Umucalilar.

My thanks are extended to the wonderful secretaries, Flavia Zanon, Micaela Paoli, Rachele Zanchetta and the technician Giuseppe Fronter whom provided the elements to be my stay more pleasant.

To Professor Jacques Tempere at the University of Antwerp for invite me to give a seminar in Belgium, where interesting and fruitful discussion arose concerning the theoretical aspects of

this thesis. On the other hand, I would like to thank to Professor Rudolf Grimm and Marko Cetina who gave me the opportunity for discussing about the experimental issues of the polaron problem. It was really tough but amazing, to learn and get involved in the discussions.

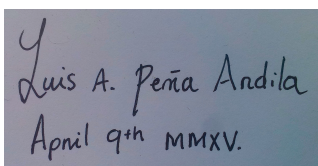
ITALIAN VERSION (To my girlfriend and the open space people)

Vorrei ringraziare la mia ragazza roberta, é stata al mio fianco anche nei momenti di sgomento e tristezza (...) Ha sempre trovato il modo di incoraggiarmi. Senza dubbio ho trovato un tesoro prezioso sulla mia strada del dottorato. Questa tesi é dedicata alla mia famiglia e alla mia Roby.

Grazie a Giovanna e Mary perché hanno fatto dell' open space un posto più piacevole. Ringrazio la sua amicizia

SPANISH VERSION (To my family and my friends) Las más grandes gracias a mis padres, que a pesar de la distancia han estado siempre conmigo en este proceso desde que era un niño. Ellos son los únicos que han estado al tanto de mis pasos desde mi primera vez, cuando hice mi primaria en escuela muy vieja donde nos sentabamos en el suelo debido a la precaria situación económica hasta el punto el que he sido muy el privilegio y he aprendido un montón de cosas. Esta thesis es dedicada a ellos y mi adorada novia.

La sinfonia no hubiera concluido sin ustedes chicos. Gracias por haber estado conmigo durante este tiempo y sacarme un poco de tantos números y ecuaciones. Realmente he encontrado una gran familia en ustedes. Estoy muy agradecido por el apoyo, amabilidad y cariño por parte de Luz, Jackie, Jhonfa, Manu, Juan y el querido maestro Julian Lombana quienes me recibieron y me acogieron en su familia. No me senti solo aqui en italia desde ese momento. Luego la familia se extendio y llegaron los demas muchachos con quienes he aprendido y disfrutado muchas cosas y que hicieron cada segundo inmemorables, a todos y cada uno muchas gracias. Espero llevarme de Trento esos bonitos recuerdos y una gran amistad.



Luis A. Peña Andila
April 9th MMXV.

Contents

Acknowledgements	3
Abstract	1
1 Introduction	11
1.1 Fröhlich solid-state polaron	14
1.1.1 Perturbative treatment	17
1.2 Ultracold gases and Bose Einstein condensates	21
1.2.1 Interatomic interactions and Feshbach resonances	26
2 Impurities and ultracold gases	31
2.1 Fermi Polarons	31
2.2 Bosonic polaron	36
3 Quantum Monte-Carlo Methods	43
3.1 Introduction	43
3.2 Analytical vs numerical tools. Why Monte-Carlo methods?	44
3.3 Preliminary Concepts	45
3.3.1 Importance Sampling	49
3.3.2 Stochastic Process and Metropolis Algorithm $\mathbf{M(RT)^2}$	50
3.4 Variational Monte-Carlo (VMC)	53
3.4.1 Time-dependent algorithm in VMC	56
3.5 Smart Variational Monte-Carlo (SVMC)	57
3.6 Trial wave functions	59

3.6.1	Potential 1: Hard sphere (HS)	61
3.6.2	Potential 2: Attractive square-well (ASW) potential	61
3.7	Diffusion Monte-Carlo (DMC)	63
3.7.1	How does DMC work?	65
3.7.2	Importance Sampling	66
3.7.3	DMC with importance sampling	67
3.8	Observables	69
3.8.1	Energy	69
3.8.2	Pair correlation function	72
3.8.3	Effective mass	74
3.9	Test case: Bose gas	75
3.9.1	Time step	76
3.9.2	Number of Walkers	76
3.9.3	Finite-size Effects	77
3.9.4	Equation of state. Gas parameter $n_B a^3$	78
3.9.5	Pair correlation function	78
4	Single impurity problem	81
4.1	Statement of the problem	81
4.2	Perturbation Theory	84
4.2.1	Ground-state energy and effective mass	84
4.2.2	Effective mass	88
4.3	Variational principle: the Jensen-Feynman formalism	90
4.4	Strongly interacting regime: mean-field techniques and QMC calculation	93
4.4.1	Local energy for the impurity problem	93
4.4.2	Binding energy of the polaron	95
4.5	Effective mass	98
4.6	Pair correlation functions	99

5	Impurity interacting resonantly with the bosonic bath	103
5.1	Binding energy of the impurity	103
5.2	Effective mass	106
5.3	Pair correlation functions	108
5.4	Efimov physics	109
5.5	Discussion	110
6	Many impurities in a Bose-Einstein condensate	113
6.1	Theoretical model	114
6.2	Perturbation theory	117
6.3	Collective variables method	120
6.3.1	Low concentration limit $x = M/N \ll 1$	121
6.4	Monte-Carlo calculation	123
6.5	Energy dependence on the concentration of impurities	127
6.6	Interaction between polarons	127
6.7	Stability conditions and phase diagram	129
6.7.1	Phase I: homogeneous mixture	129
6.7.2	Phase II: phase separated state	132
7	Conclusions and Perspectives	137
7.1	Conclusions	137
7.2	Perspectives	138
	Appendix A: Error estimates for Markov chains	139
	Appendix B: The two-body problem.	143
	Bibliography	145

Abstract

In this thesis we investigate the properties of impurities immersed in a dilute Bose gas at zero temperature using quantum Monte-Carlo methods. The interactions between bosons are modeled by a hard sphere potential with scattering length a , whereas the interactions between the impurity and the bosons are modeled by a short-range, square-well potential where both the sign and the strength of the scattering length b can be varied by adjusting the well depth. We calculate the binding energy, the effective mass and the pair correlation functions of a impurity along the attractive and the repulsive polaron branch. In particular, at the unitary limit of the impurity-bosons interaction, we find that the binding energy is much larger than the chemical potential of the bath signaling that many bosons dress the impurity thereby lowering its energy and increasing its effective mass. We characterize this state by calculating the bosons-boson pair correlation function and by investigating the dependence of the binding energy on the gas parameter of the bosonic bath. We also investigate the ground-state properties of M impurities in a Bose gas at $T=0$. In particular, the energy and the phase diagram by using both quantum Monte-Carlo and mean field methods.

List of Figures

1.1	The ions placed on the lattice feel the attraction by the electron, therefore there is a distortion of the lattice. This electron and this distortion can be described by a quasiparticle with different mass and energy respect the naked electron and this quasiparticle is called polaron.	14
1.2	A) The ground state energy (in units of $\hbar\omega_0$) for the Fröhlich polaron as a function of the electron-phonon coupling, calculated with the weak coupling, strong coupling and Feynman variational formalism. B) Diagramatic Monte-Carlo (Dashed line) and Feynman variational formalism (Solid line).	16
1.3	Representation of the process of an electron with momentum ($\mathbf{P} - \mathbf{k}$) and a phonon of momentum \mathbf{k}	19
1.4	Velocity distribution of Rb atoms at different temperatures [1]. The atoms exhibit a Maxwell distribution at 400 nK (left), but at 200 nK a macroscopic fraction of the atoms occupies the state corresponding to velocity zero (center) and for $T = 50\text{ nK}$ almost all the atoms are in this fraction (right).	22
1.5	Representation of the interatomic potential V and the effective potential V_{eff}. The details of the potential for short distances are irrelevant. For large distance both yields the same s -wave scattering length.	24
1.6	Basic two-channel model for a Feshbach resonance: two atoms colliding with energy E (dashed green line) in the open channel (red line) corresponding to the interaction potential is resonantly coupled to a closed channel (purple line). Then a bound state appears on the closed channel with an energy close to zero. The position of the closed channel can be changed with respect to the open channel by varying the magnetic field.	28

1.7	Observation of a magnetically tuned Feshbach resonance in an optically trapped BEC of Na atoms. Scattering length normalized to the a_{bg} as a function of the external magnetic field B . The resonant point is placed at $B_0 = 907\text{G}$. Dots represents the experimental data, whereas the solid line is the theoretical formula [2].	29
2.1	Fermi Polarons: from polarons to molecules. (a) For weak attraction, an impurity (blue) experiences the mean field of the medium (red). (b) For stronger attraction, the impurity surrounds itself with a localized cloud of environment atoms, forming a polaron. (c) For very strong attraction, molecules of size a are formed despite Pauli blocking of momenta $k < k_F \leq a^{-1}$ by the environment. . .	32
2.2	Attractive and repulsive Fermi polarons in 2D: (a) Energy spectrum displaying the many-body ground state of the system, characterized by both the attractive polaron, the molecular state and the repulsive polaron lying in a metastable branch as a function of the interaction strength written in typical experimental units $\ln(k_F a)$. The single particle spectral function (b) displays a well-defined pick for weak attractive interactions, thus characterizing the attractive polaron. When the interaction strength is driven near to the resonance the pick is not well-defined (c) and the single particle spectral function will display an incoherent feature as soon as the resonance is crossed and enters into the molecular branch (d)	33
2.3	Mean results from the Köhl team about 2D fermionic polarons [2.2]: (a) Energy normalized as a function of the strength parameter defined as $\ln(k_F a)$. Theory [3] and experiments are plotted. (b) The effective mass was investigated for both the attractive (red squares) and the repulsive polaron (blue circles) as a function of the strength parameter as well as a (c) function of the temperature and (d) the impurity concentration. All previous results for the effective mass displays non-self trapping for the impurity. The life-time (e) of the repulsive polaron is plotted as a function of the coupling strength.	35
2.4	Results from the Grimm team concerning 3D fermionic polarons [2.4]: similar to the case in two dimensions the energy spectrum displays two polaronic branches as a function of the strength parameter defined here as $1/(k_F a_{k-Li})$: the attractive (green line) and the repulsive polaron (red line). The gray region between E_m and $E_m - \epsilon_F$ is the molecular continuum. The inset illustrates the radio-frequency spectroscopy scheme used in experiments in which the impurity is transferred from a non-interacting state $ 0\rangle$ to an interacting state $ 1\rangle$	36

2.5	Radio Frequency spectroscopy (rf) for investigating the spectral properties of a BEC: The mean idea of RF spectroscopy is drive a non-interacting system to a interacting system form two internal states of the impurity (a) a small concentration of impurities with two internal levels $ \downarrow\rangle$ and $ \uparrow\rangle$ (red spheres) is immersed into a BEC (blue spheres), in which the interaction between the impurity-boson is featured by the s -wave scattering length a_{IB} . A radio frequency pulse transfers impurities from a non-interacting state $ \downarrow\rangle$ to a interacting state $ \uparrow\rangle$. (b) The transition from $ \downarrow\rangle$ to $ \uparrow\rangle$ is made by a coherent well-defined peak centered at a frequency correspondig to the energy polaron. The picks show up for both attractive ($a_{IB\uparrow} < 0$) and repulsive interactions ($a_{IB\uparrow} > 0$) . Moreover the high-frequency power-law tail is associated to the low energy excitations in the BEC.	37
2.6	(A) single spin impurity is flipped at the center site of a 1D spin chain. Each spin is coherently coupled to its neighbors through the superexchange coupling. (B) Quantum evolution of the spins as a function of the time.	39
2.7	Experimental array for impurities in a one dimensional gas: (A) species-selective dipolar potential localizes the impurities into the center of a one dimensional Rb atoms. (B) The ultracold Rb atoms with K impurities are loaded into a one dimensional array. (C) The axial width $\sigma = \sqrt{\langle x^2 \rangle}$ is plotted as a function of the time for different ratios $\eta = g_{K,Rb}/g_{Rb}$ displaying the effects of the K impurities on the Rb atoms.	39
2.8	^{133}Cs atoms are immersed in a ultracold gas of ^{87}Rb	40
3.1	Representation of the matrix [3.27]: each column of the matrix is a state where the system lies. In our example we have $N = 4$ particles distributed on W walkers.	52
3.2	The ground-state energy per particle is calculated with the SVMC. Green points represent the SVMC data and orange line represents the linear fitting. The time dependent VMC algorithms [3.4.1] are affected by a time-step bias. By using the SVMC that relies on a transition probability defined by Eq. [3.53] and an acceptance probability given by Eq. [3.54] the time-step dependence is eliminated.	59
3.3	Periodic boundary conditions (p.b.c): when a particle (green) leaves the box on the left side, a virtual particle (gray) enters the box on the right side.	59
3.4	Cut off radius $r < L/2$ for inter-particle correlations. Particle B lies inside the radius and images of particle B lies outside.	60
3.5	DMC moves	69

3.6	Ground state energy per particle as a function of the iteration number in VMC for a weakly interacting Bose gas with gas parameter $(n_B a^3) = 10^{-5}$. Green line direct estimator E_D given by Eq. [3.107] and red line, force estimator E_F given by Eq. [3.112].	72
3.7	Example of the boson-boson pair correlation function $g_{BB}(r)$: (A) For short distances, this is related to how the particles are distributed in the simulation box. For example, consider hard spheres (bosons). The spheres can't overlap (HS potential), so the closest distance between two centers is equal to the diameter of the spheres. Further away, the bosons get more diffuse, and so for large distances, the probability of finding two bosons with a given separation is essentially constant. This is represented by the boson-boson correlation function. (B) histogram representing the statistics.	74
3.8	SDMC ground-state energy per particle as a function of the time-step: For $\delta\tau \rightarrow 0$ we obtain $E_D^0(N_B)/N_B = (1.2617 \pm 0.0020) \times 10^{-4}$	76
3.9	Number of walkers dependence: ground-state energy per particle of a Bose gas with $n_B a^3 = 10^{-5}$ as a function the inverse on the number walkers. For $1/N^W \rightarrow 0$ we obtain a value $E_D^0(N_B)/N_B = (1.2625 \pm 0.0010) \times 10^{-4}$	77
3.10	Finite-size effects: ground-state energy per particle as a function $1/N_B$ of a weakly interacting Bose gas with $n_B a^3 = 10^{-5}$. For $n_B = \frac{N_B \rightarrow \infty}{V \rightarrow \infty} = \text{constant}$, one gets $E_D^0(N_B)/N_B = (1.266 \pm 0.010) \times 10^{-4}$	77
3.11	Ground-state energy per particle of a Bose gas as a function of parameter $(n_B a^3)^{1/3}$. Red line from the Bogoliubov theory Eq. [1.34] and green points are the DMC simulations.	78
3.12	boson-boson correlation pair function as a function of the inter-boson distance. For a Bose gas with $n_B a^3 = 10^{-5}$	79
4.1	Perturbation of the impurity in the bosonic bath: A) The initial state has an impurity of momentum p and no phonons B) an excited state is represented by the impurity with momentum $\mathbf{p} + \hbar\mathbf{k}$ and a phonon with momentum $-\hbar\mathbf{k}$	85
4.2	Variational model for an impurity interacting with a BEC: the impurity with mass m_I harmonically coupled to the bosonic bath with total mass M with spring constant MW^2	91

4.3	Reduced binding energy ($F = \mu - \mu_{MF}$) in units of $\frac{4\pi\hbar^2 n_B a}{m}$ as a function of the coupling strength a/b computed with perturbation theory (dashed black line), using the Jensen-Feynman variational formalism (solid orange line) and the DMC method for two different ASW potential ranges $a/R_0 = 5$ (filled green circles) and $a/R_0 = 20$ (filled red diamonds) and the HS potential (blue square).	95
4.4	(A) Binding energy as a function of the strength interaction, for both the attractive and repulsive branch. In the inset we show the binding energy for $a/b > 0$ along the attractive branch. The red line shows the two-body binding energy (B) Reduced binding energy as a function of the coupling strength a/b for both the attractive and the repulsive branch.	97
4.5	Mean square displacement of the impurity as a function of the imaginary time for the case where the impurity and the bosons do not interact (purple), $a/b = -1$ (yellow); $a/b = -0.2$ (blue), $a/b = -0.1$ (red) and $a/b = 0$ (green).	98
4.6	Effective mass as a function of a/b: perturbation theory (red dashed line), Jensen-Feynman (solid blue line), DMC simulations with ASW potential (green points). The range of the potential in the DMC simulations is $R_0 = 0.2a$	99
4.7	Boson-boson pair correlation function $g_{BB}(\mathbf{r})$ on the repulsive branch ($\frac{b}{a} = +30$) (green solid line), at the unitary limit (red solid line) on the attractive branch and for the case where the impurity is absent (blue solid line).	100
4.8	Density profiles $n(r)$ (in logarithmic scale) as a function of the distance in units of the healing length ξ . The profiles are computed for both the attractive (solid blue line) and the repulsive (green solid line) branches for coupling strengths: $b/a = \pm 10, \pm 20$ and $b/a = \pm 30$. The dashed line represents the equilibrium density n_B . In the insets the number of bosons as a function of the distance in units of the healing length for the attractive and repulsive branch.	101
4.9	Enhancement for the attractive branch (right) and depletion for the repulsive branch (left) of the density profile. The dashed line represents the equilibrium density n_B	102
5.1	Binding energy at the unitary limit as a function of the inverse number of the walker (time-step fixed $\delta\tau = 0.05$) (A) $n_B a^3 = 3.375 \times 10^{-6}$ and (B) $n_B a^3 = 10^{-6}$ and as a function of the time step $\delta\tau$ (number of walkers $N_W = 400$) (C) $n_B a^3 = 3.0 \times 10^{-7}$ and (D) $n_B = 10^{-6}$	104

5.2	Binding energy as a function of the gas parameter $(n_B a^3)^{1/3}$ at the unitary. Green points represent DMC simulations.	105
5.3	Dependence on the binding energy with $(n_B a^3)^{1/3}$ at the unitary limit: Green points stand for DMC, whereas the red line is a power law fitting.	106
5.4	Effective mass of the polaron at the unitary limit as a function of the gas parameter $n_B a^3$ of the bosonic bath.	107
5.5	Boson-boson pair correlation function at the $a/b = 0$ for different values of the gas parameter $n_B a^3$.	108
5.6	Density profile (in logarithmic scale) at the unitary limit as a function of the inter particle distance for different values of $n_B a^3$: green ($n_B a^3 = 3 \times 10^{-6}$), red ($n_B a^3 = 1 \times 10^{-5}$), blue ($n_B a^3 = 1 \times 10^{-4}$). Inset: parameter C contact as a function of $(n_B a^3)^{2/3}$. The dashed line represents the equilibrium density n_B	109
5.7	Total energy in units of \hbar^2/ma^2 for a system consisting of two bosons and one impurity with resonant interspecies interaction as a function of the inverse of the size of the simulation box a/L.	110
6.1	Generalized binding energy in units of $gn_B x$ as a function of b/a along the repulsive branch for different concentrations $x = 3/64, 5/64, 7/64$ and $x = 9/64$. Both perturbation theory (blue dashed line) and DMC results (filled green circles).	126
6.2	Generalized binding energy (in units of $gn_B x$) as a function of b/a for different concentrations $x = 3/64, 5/64, 7/64$ and $x = 9/64$.	126
6.3	Generalized binding energy (in units of $gn_B x$) once the mean-field term (μ_{MF}) is subtracted as a function of b/a for different concentrations $x = 3/64, 5/64, 7/64$ and $x = 9/64$. Perturbation theory (blue dashed line) and DMC results (filled green circles).	127
6.4	Generalized binding energy in units of $gn_B N$ as a function of the concentration x. For $b/a = -5$ (lower branch) and $b/a = +5$ (upper branch) computed with perturbation theory (blue dashed line), collective variables method (solid red line) and DMC results (filled green circles).	128
6.5	Residual function $F(x)$ as a function of the concentration x for both (left) attractive interactions $b/a = -5$ and (right) repulsive interactions $b/a = +5$. Perturbation theory (blue dashed line), collective variables method (solid red line) and DMC results (filled green circles).	129

6.6	Homogeneous phase: M bosons of type A (green balls) and N bosons of type B (blue balls) immersed in a cubic box of size L	130
6.7	Representation of $h_1(n_B a^3, \frac{b}{a})$ for different values of $\frac{b}{a}$ and $n_B a^3$. For values of $h_1 > 0$, the homogeneous phase is stable.	132
6.8	Phase II: (left) M bosons in the region A and N bosons in the region B distributed in different volumes $V_A \neq V_B$. (right) stability of the phase separated state,	132
6.9	Plot of $h_2(n_B a^3, \frac{b}{a})$ as a function of $\frac{b}{a}$ for different values of $n_B a^3$. For values of $h_2 < 0$, the phase separated state is unstable.	134
6.10	Phase diagram for different values of $n_B a^3$ as a function of the coupling strength b/a . The stable homogeneous phase is represented by the green region, whereas the stable phase separated state is represented by the blue region. The horizontal dashed lines represent the interval where perturbation theory works.	135
7.1	Bunching data algorithm for a sample of correlated data. Taking from Ref. [4]. .	140
7.2	Bunching data algorithm taking from Ref. [4].	140
7.3	Estimation of the true error in a DMC simulation for 10000 iterations of the total energy for a system of bosons in a cubic box.	140
7.4	Plotting of Eq. [3.63]. For $R_0/a = 0.2$. By tuning the depth and range of the ASWP , one can access either to attractive interactions when $K_0 R_0 < \pi/2$ ($a < 0$) and or repulsive when, $K_0 R_0 > \pi/2$ ($a > 0$) and there is one bound state.	144

Chapter 1

Introduction

In this thesis we investigate the properties of an impurity immersed in a dilute Bose gas at zero temperature using quantum Monte-Carlo methods. The interactions between bosons are modeled by a hard sphere potential with scattering length a , whereas the interactions between the impurity and the bosons are modeled by a short-range, square-well potential where both the sign and the strength of the scattering length b can be varied by adjusting the well depth. We calculate the binding energy and the effective mass of the impurity along the attractive and the repulsive polaron branch. In particular, at the unitary limit of the impurity-bosons interaction, we find that the binding energy is much larger than the chemical potential of the bath while the effective mass remains on the order of the bare mass. We characterize the ground state of the impurity by calculating the bosons-boson pair correlation function and by investigating the dependence of the binding energy on the gas parameter of the bosonic bath. Additionally, we present some results concerning the problem of many impurities immersed in a Bose quantum gas by using both perturbative and Monte-Carlo methods.

In the first chapter, we review two important topics that are involved in this study: ultracold gases and polarons in solid-state systems. The latter is a standard problem in many-body physics, where an impurity interacts with the quantum fluctuations of its environment. The Fröhlich solid-state polaron problem is briefly reviewed, which consists in investigating the properties of a charged particle interacting with the lattice vibrations in a polar crystal. The electron and the distortion of the lattice can be described by a quasiparticle with different mass and energy with respect to the bare electron. The Hamiltonian for this problem is described and a second-order perturbation theory is used to calculate both the ground-state energy and the effective mass. In the second part of the chapter we briefly review the physics of ultracold, dilute gases. In particular, we discuss the regimes where these gases exist (density and temperature conditions) and how interactions in the gas can be controlled. The Hamiltonian for a weakly interacting Bose gas is considered and Bogoliubov transformations are used to calculate the

ground-state energy.

In the second chapter we provide a review of experiments concerning impurities immersed in quantum gases. We briefly discuss the Fermi polaron, which consists in a dressed spin-down impurity in a Fermi sea of spin-up particles. The Fermi polaron displays an energy spectrum formed by two branches: a metastable repulsive and the ground-state attractive branch. The metastable polaron may decay eventually into the attractive branch consisting of a molecular state formed by the impurity and a particle from the Fermi sea. Various properties, such as the polaron effective mass and lifetime, are investigated experimentally. The Fermi polaron are observed both in two and three dimensions. In the second part of the chapter we summarize some experiments concerning impurities immersed in a Bose gas. We start with experiments in one dimensional systems where the dynamics of a single impurity is studied. Properties such as the energy and the effective mass are investigated as a function of the coupling strength between the impurity and the bosonic bath. At the end of the chapter we mention an important experiment that could be linked to our project: the dynamics of neutral impurities immersed in an ultracold Bose gas in three dimensions.

The third chapter is devoted to develop the concepts of the Quantum Monte-Carlo (QMC) methods. These are techniques I used to study the problem of the polaron immersed in a degenerate Bose gas at zero temperature. We start by mentioning the importance of the computational methods compared to more analytical tools in the regime of strong correlations and we explain some preliminary concepts such as: random variables and stochastic processes and how observables are calculated in QMC techniques, in particular energy, correlation functions and effective mass of an impurity. The specific techniques that I used are them introduced: the Variational Monte-Carlo (VMC) and the Diffusion Monte-Carlo methods (DMC). The technical details are explained for both methods and the chapter closes with a case study: the calculation of the ground-state energy for a Bose gas as a function of the gas parameter.

The fourth chapter addresses specifically the problem of investigating the ground-state properties of an impurity immersed in a Bose gas at zero temperature. We start by writing down the Hamiltonian for a system consisting of one single impurity immersed in a dilute degenerate gas of bosons by using the Bogoliubov approximation introduced in the first chapter. This system is cast in the form of the Fröhlich's Hamiltonian, similar to the solid-state problem discussed in the first chapter. Here, the low-energy (Bogoliubov) excitations play the role of phonons. From this Hamiltonian and following a similar procedure to the one introduced in the first chapter, where the coupling between the electron and the lattice vibrations is weak we tackle the problem with perturbation theory. The relevant coupling strength is the interaction between the impurity and the Bogoliubov excitations and it is defined by the ratio b/a of the two scattering length. The ground-state energy and the effective mass are obtained within the perturbation theory. Another theoretical tool that can address this problem was

devised using a variational principle. The Jensen-Feynman free energy approach allows one to calculate the ground-state energy for the impurity problem immersed in a Bose gas for all the values of the coupling strength. A functional action can be written using the Fröhlich's Hamiltonian; then this action is introduced into the Jensen-Feynman inequality and the free energy of the system is obtained by a minimization procedure. Furthermore, the effective mass of the impurity is calculated using this technique. We then address the problem using QMC methods. In particular, the Diffusion Monte-Carlo technique is used to study the ground-state properties of the bath-impurity system. This system is characterized by N bosons plus one impurity in a cubic box with periodic boundary conditions. We calculate the binding energy of the impurity defined as the difference of the ground-state energy $E(N + 1)$ of the system plus the impurity and the ground-state energy $E_0(N)$ of the system without impurity. Similarly to the Fermi polaron problem, we find two branches: a repulsive and an attractive branch corresponding to effective repulsive and attractive interactions between the impurity and the bath. We compared the polaron binding energy with the mean-field results obtained at the beginning of the chapter. In the weak-coupling regime the polaron binding energy is obtained with both perturbative and variational methods are in good agreement with the QMC results, however significant differences appear at strong coupling. In addition, both the boson-boson and the impurity-bosons correlation functions are calculated for all values of the coupling strength, in order to understand the effects of the impurity on the bosonic bath when the interaction is either attractive or repulsive. The effective mass has been computed by using QMC techniques and agreement is found with mean-field results in the weak-coupling regime. In the strongly interacting limit we find a finite value of the effective mass. This is in contrast with the results of the mean-field methods where the effective mass is predicted to diverge and self-localization of the impurity is claimed.

The fifth chapter treat separately the regime of strongest coupling between the impurity and the Bose gas known as the unitary limit. We investigate the dependence of the binding energy with the gas parameter. At low densities the binding energy is much larger than the chemical potential of the bath. On the other hand, the effective mass is found to reach a value around twice the bare mass of the impurity. The chapter closes by investigating the possible existence of a three-body bound state in our model.

The sixth chapter treats the problem of many bosonic impurities immersed in a degenerate Bose gas. We study the ground-state energy as a function of the coupling strength and the concentration (number of impurities/number of bosons). For weak coupling and low concentrations, the QMC results agree with the predictions of mean-field methods. Interaction effects between polarons are observed. The stability of the system is studied from the equation of state obtained from the QMC calculations. The pair correlation functions are also computed and instability of the system is displayed above a critical concentration x and value of the coupling

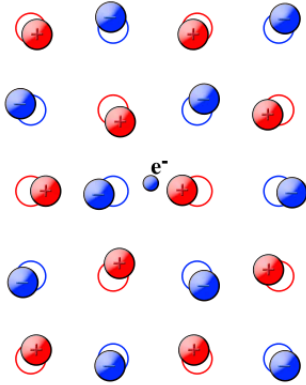


Figure 1.1: The ions placed on the lattice feel the attraction by the electron, therefore there is a distortion of the lattice. This electron and this distortion can be described by a quasiparticle with different mass and energy respect the naked electron and this quasiparticle is called polaron.

strength b/a .

At the end of the thesis some conclusions and remarks are drawn from the theoretical point of view. In addition we will discuss some interesting features about possible experimental realizations of impurities immersed in a bosonic bath.

1.1 Fröhlich solid-state polaron

In this section, we turn our attention to the polaron problem in solid-state physics. In this context, a central problem is the study of electrons and phonons and their interactions. When an electron at rest or in movement interacts with the ions placed in the lattice, then the negative charge of the electron will attract the positively charged ions and repel the negatively charged ones Fig [1.1]. The electron together with its self-polarisation cloud will form a new quasiparticle called polaron. The energy and the mass of this quasiparticle are different from the bare electron.

The concept of polaron was introduced by Landau and Pekar [5] in 1933. The distortion of the lattice can be described in terms of phonons. The Fröhlich Hamiltonian derived by Fröhlich [6] in 1954 describes the interaction between electrons and the longitudinal optical phonons (LO) due to the lattice distortion. The Hamiltonian can be written as:

$$\mathcal{H} = \sum_{\mathbf{p}} \frac{P^2}{2M} \hat{c}_{\mathbf{p}}^{\dagger} \hat{c}_{\mathbf{p}} + \sum_{\mathbf{q}} \hbar\omega_{\mathbf{q}} \hat{a}_{\mathbf{q}}^{\dagger} \hat{a}_{\mathbf{q}} + \sum_{\mathbf{q}, \mathbf{p}} V_{\mathbf{q}} \hat{c}_{\mathbf{p}+\mathbf{q}}^{\dagger} \hat{c}_{\mathbf{p}} (\hat{a}_{\mathbf{q}}^{\dagger} + \hat{a}_{\mathbf{q}}). \quad (1.1)$$

Here $\hat{c}_{\mathbf{p}}^{\dagger}$ ($\hat{c}_{\mathbf{p}}$) is the creation (annihilation) operator of electrons and $\hat{a}_{\mathbf{q}}^{\dagger}$ ($\hat{a}_{\mathbf{q}}$) is the creation (annihilation) operator of optical phonons with energy $\hbar\omega_{\mathbf{q}}$. This Hamiltonian is derived and

deeply discussed in Reference [7]. The first term in Eq. [1.1] represents the kinetic energy of the unperturbed electrons with momentum P and mass M . The second term is the energy of the phonon bath. The last term describes the interaction between optical phonons and electrons in terms of a k -dependent $V_{\mathbf{k}}$. The particular case of just one single electron reduces the Hamiltonian Eq. [1.1] to:

$$\mathcal{H} = \frac{P^2}{2M} + \hbar\omega_0 \sum_{\mathbf{q}} \hat{a}_{\mathbf{q}}^\dagger \hat{a}_{\mathbf{q}} + \sum_{\mathbf{q}} V_{\mathbf{q}} \exp(i\mathbf{q} \cdot \mathbf{r}) (\hat{a}_{\mathbf{q}}^\dagger + \hat{a}_{\mathbf{q}}). \quad (1.2)$$

where the longitudinal phonons are described by the Einstein model with frequency ω_0 and the interaction amplitude between electrons and phonons is given by $V_{\mathbf{q}} = \frac{M_0}{\nu^{1/2}} \frac{1}{|q|}$, ν being the volume, $M_0^2 = \frac{4\pi\alpha\hbar(\hbar\omega_0)^{3/2}}{(2M)^{1/2}}$ and $\alpha = \frac{e^2}{\hbar} \left(\frac{M}{2\hbar\omega_0}\right)^{1/2} \left(\frac{1}{\epsilon_\infty} - \frac{1}{\epsilon_0}\right)$ where ϵ_∞ and ϵ_0 are the static and high-frequency dielectric constant respectively and depend on the specific material. Then the Hamiltonian Eq. [1.1] is reduced to:

$$\mathcal{H} = \frac{P^2}{2M} + \omega_0 \sum_q a_q^\dagger a_q + \sum_q \frac{M_0}{\nu^{1/2}} \frac{\exp(iq \cdot r)}{|q|} (a_q^\dagger + a_q). \quad (1.3)$$

A couple of features must be pointed out: the result above is obtained independently of the statistics of the particle and the model assumes that the motion is isotropic in space and the energy bands are nondegenerate.

However if $\omega_{\mathbf{q}}$ is kept general in Eq. [1.1], this Hamiltonian describes in general the problem of a particle with mass M coupled to a bath of bosons with dispersion relation $\omega_{\mathbf{q}}$, mediated through an interaction amplitude $V_{\mathbf{q}}$. Aside from the optical phonons studied in solid-state physics and described by the Hamiltonian Eq. [1.3]; the electron-phonon interaction can be mediated by acoustical phonons as well, which are known as acousto-polarons or piezo-polarons [8, 9]. Other examples are the ripplon-polarons which consist of one electron on a Helium film and the excitations of the system are described by surface waves called ripplons [10, 11, 12, 13]; the plasmaron is a quasiparticle arising from the strong interaction between plasmon and electron, the plasmaron is a quasiparticle formed by quasiparticle-quasiparticle interactions [14, 15, 16]. When a photon is absorbed by a semiconductor an exciton is formed. This quasiparticle is represented as an excitation of an electron from the valence band into the conduction band. [17, 18, 19]. A more general case are the polaritons. These are quasiparticles resulting from strong coupling of electromagnetic waves with an electric dipole-carrying excitation.

The Fröhlich Hamiltonian has been a relevant problem in mathematical physics. Quite a few mathematical techniques have been employed in solving this problem because this Hamiltonian resists exact diagonalization. In the literature there are many methods attempting to tackle this problem. One of the standard techniques is perturbation theory, which calculates

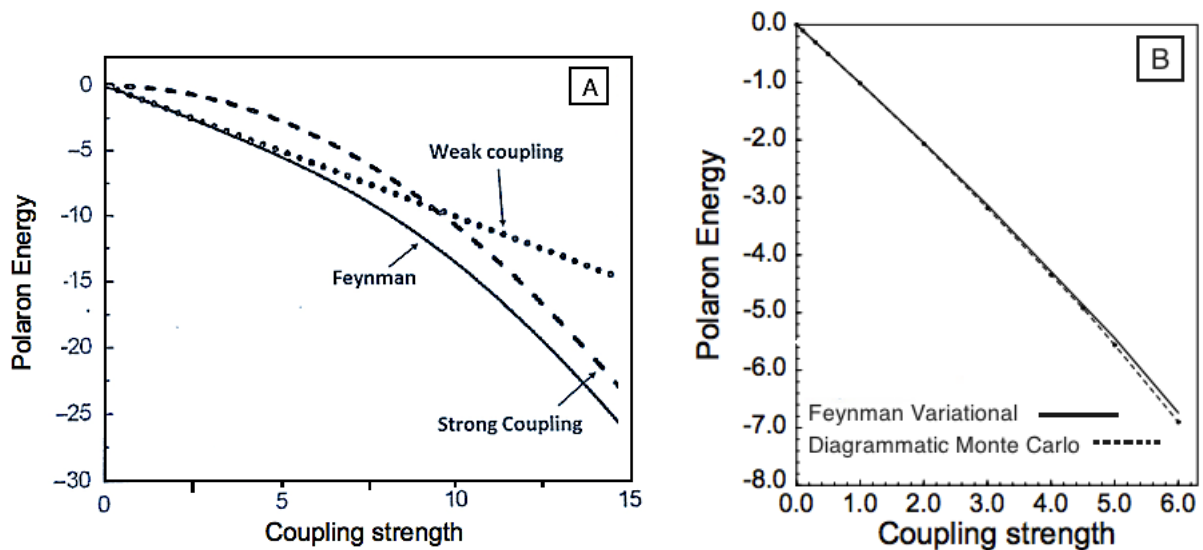


Figure 1.2: A) The ground state energy (in units of $\hbar\omega_0$) for the Fröhlich polaron as a function of the electron-phonon coupling, calculated with the weak coupling, strong coupling and Feynman variational formalism. B) Diagrammatic Monte-Carlo (Dashed line) and Feynman variational formalism (Solid line).

the ground-state energy and the effective mass of the polaron as a function of the coupling parameter between the electron (impurity) and the lattice vibrations (bosons); this method was applied for the first time by Fröhlich [6]. The Brillouin-Wigner and Rayleigh-Schrödinger perturbation theory are introduced as predecessors of the modern formulation of the Green's function formalism and the properties of the electron are described in terms of the spectral function. The latter is obtained from the self-energy contained in the phonon-electron Green's function. Both theories are linked directly with the T -matrix theory and the reaction matrix theory. Both the ground-state energy of the electron and its effective mass are calculated. These methods are described in large detail in Ref. [7].

The methods listed above work quite well for weak coupling, it means, small values of the interaction strength between the electron and the bosons. On the other hand, the strong-coupling regime was investigated by Bogoliubov, Tyablikov [20] and by Landau and Pekar [5] using canonical transformations. This strong coupling limit is based on a strong assumption: the localization of the electron with a Gaussian wave function resulting in a bound state of the electron in the self-induced potential. Later on, the problem was most accurately treated by Feynman. He developed a theory valid for all the coupling strengths introducing a variational method based on the path-integral formalism [21, 22]. The ground-state energy and effective mass was calculated for all the coupling strengths [23]. In chapter 4 we will describe this method for investigating the ground-state properties of the impurity interacting with the bosonic bath. The polaron energy and the effective mass are calculated.

In Fig. [1.2] the ground-state energy of the electron (impurity) is calculated for different coupling strengths. In Fig. [1.2, A] the ground-state energy is plotted for the weak-coupling formalism (e.g perturbative methods), the strong-coupling regime (e.g Landau-Pekar strong coupling theory) and the Feynman variational formalism which reproduces very well the weak-coupling limit and provides an upper bound in the strong-coupling limit. Furthermore it interpolates between the two regimes. The strong-coupling regime has been widely investigated with diagrammatic expansions, where Feynman diagrams are drawn and sampled using Monte-Carlo methods. This method is known as Diagrammatic Monte-Carlo (DiagMC). In Fig. [1.2, B] both results of Feynman variational formalism and Diagrammatic Monte-Carlo methods [24, 25, 26] are shown for all values of the coupling strength and they are in good agreement. The DiagMC method is the most powerful technique describing the strong-coupling regime.

The problem of two and more impurities has been widely investigated as well. In particular, an extension of the Feynman variational formalism was developed for two electrons [27]. This study shows that if the polaronic coupling strength is large enough the impurities will form a bound state of two electrons with weak effective Coulomb interaction (the bipolaron). [28]. Under certain circumstances the formation of multipolaron are linked with clusters of polarons [29].

In the subsequent section, we will derive the Fröhlich Hamiltonian describing the phonon-electron interaction and a perturbative calculation will be presented in order to estimate both the energy and the effective mass.

1.1.1 Perturbative treatment

In this section we will treat the problem of one electron interacting with the lattice vibrations by means of perturbative methods. One assumes that the electron interacts with the lattice and therefore there is a periodic potential acting on the electron. The lattice is displaced from its equilibrium position and there is a potential $\Delta V_1(x)$ “felt” by the electron due to the change of the charge density $\rho(x)$. This statement is contained in the Poisson equation:

$$\nabla^2 \Delta V_1(\mathbf{x}) = e\rho(\mathbf{x}) = -\nabla \cdot \mathbf{P}(\mathbf{x}). \quad (1.4)$$

Let us suppose that the lattice is formed by a positive and a negative ion placed in each unit cell. Then, there are six total modes for each k number. Three of the modes are characterized by the ions moving in the same direction; as $k \rightarrow 0$ such modes do not provide important contributions to the polarization $\mathbf{P}(\mathbf{x})$, because there is not a net relative displacement (acoustic branch). On the contrary, the other three modes associated with the opposite motion of the positive and

negative ions produce a polarization that is proportional to the amplitude of the mode (optical branch). For these modes, a gap is present in the excitation frequency $\omega_0 \neq 0$ for $k \rightarrow 0$.

Let us consider $\hat{a}^\dagger(\mathbf{k})$ and $\hat{a}(\mathbf{k})$ the creation and annihilation operators of phonons respectively. The polarization can be written as:

$$\mathbf{P}(\mathbf{x}) = \alpha' \int \frac{d^3\mathbf{k}}{(2\pi)^3} \sum_{i=1}^3 \left[\hat{a}_i(\mathbf{k}) \exp(i\mathbf{k} \cdot \mathbf{x}) \hat{e}_{\mathbf{k},i} + \hat{a}_i^\dagger(\mathbf{k}) \exp(-i\mathbf{k} \cdot \mathbf{x}) \hat{e}_{\mathbf{k},i}^* \right] \quad (1.5)$$

Where $\hat{e}_{\mathbf{k},i}$ ($\hat{e}_{\mathbf{k},i}^*$) is the unitary polarization vector (and its complex conjugate) in the direction \mathbf{k} . The polarization $\mathbf{P}(\mathbf{x})$ is proportional to the net displacement of the ions. In fact the previous equation is obtained by the quantization of the harmonic oscillations of the crystal (see for instance [21]). The proportionality constant is α' and it depends on the material. From Eq. [1.4] and Eq. [1.5] the charge density is then given by:

$$e\rho(\mathbf{x}) = -\nabla \cdot \mathbf{P}(\mathbf{x}) = i\alpha' \int \frac{d^3\mathbf{k}}{(2\pi)^3} \sum_{i=1}^3 \left[\hat{a}_i(\mathbf{k}) \exp(i\mathbf{k} \cdot \mathbf{x}) \mathbf{k} \cdot \hat{e}_{\mathbf{k},i} - \hat{a}_i^\dagger(\mathbf{k}) \exp(-i\mathbf{k} \cdot \mathbf{x}) \mathbf{k} \cdot \hat{e}_{\mathbf{k},i}^* \right]. \quad (1.6)$$

Evidently the longitudinal mode parallel to $\hat{e}_{\mathbf{k},i}$ has a non-zero contribution ($\hat{e}_{\mathbf{k},i} \parallel \mathbf{k}$). It turns out that

$$\rho(\mathbf{x}) = i\alpha' \int \frac{d^3\mathbf{k}}{(2\pi)^3} \mathbf{k} \left[\hat{a}_{\mathbf{k}} \exp(i\mathbf{k} \cdot \mathbf{x}) - \hat{a}_{\mathbf{k}}^\dagger \exp(-i\mathbf{k} \cdot \mathbf{x}) \right]. \quad (1.7)$$

The potential energy of the electron due to the lattice vibration can be obtained as

$$\begin{aligned} \Delta V_1(\mathbf{x}) &= -ie\alpha' \int \frac{d^3\mathbf{k}}{(2\pi)^3} \frac{1}{\mathbf{k}} \left[\hat{a}_{\mathbf{k}} \exp(i\mathbf{k} \cdot \mathbf{x}) - \hat{a}_{\mathbf{k}}^\dagger \exp(-i\mathbf{k} \cdot \mathbf{x}) \right] \\ &= i \left(\sqrt{2\pi}\alpha \right)^{1/2} \frac{\hbar^5 \omega^3}{M} \int \frac{d^3\mathbf{k}}{(2\pi)^3} \frac{1}{\mathbf{k}} \left[\hat{a}_{\mathbf{k}} \exp(i\mathbf{k} \cdot \mathbf{x}) - \hat{a}_{\mathbf{k}}^\dagger \exp(-i\mathbf{k} \cdot \mathbf{x}) \right], \end{aligned} \quad (1.8)$$

where $\alpha' = \left(\sqrt{2\pi}\alpha \right)^{1/2} \left(\hbar^5 \omega^3 / M \right)^{1/4}$, $\alpha = \frac{1}{2} \left(\frac{1}{\varepsilon_\infty} - \frac{1}{\varepsilon_0} \right) \frac{e^2}{\hbar\omega} \left(\frac{2M\omega}{\hbar} \right)^{1/2}$ and ε_∞ , ε_0 are the static and high-frequency dielectric constants of the crystal respectively. The total Hamiltonian reads as

$$\mathcal{H} = \frac{P^2}{2} + \sum_{\mathbf{k}} \hat{a}_{\mathbf{k}}^\dagger \hat{a}_{\mathbf{k}} + i \left(\sqrt{2\pi}\alpha \right)^{1/2} \sum_{\mathbf{k}} \frac{1}{|\mathbf{k}|} \left(\hat{a}_{\mathbf{k}}^\dagger \exp(-i\mathbf{k} \cdot \mathbf{r}) - \hat{a}_{\mathbf{k}} \exp(i\mathbf{k} \cdot \mathbf{r}) \right), \quad (1.9)$$

where $\hbar = M = \omega_0 = 1$. On the Hamiltonian [1.9] one uses perturbation theory in order to

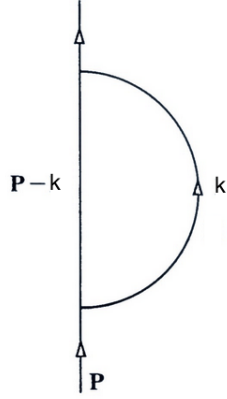


Figure 1.3: Representation of the process of an electron with momentum $(\mathbf{P} - \mathbf{k})$ and a phonon of momentum \mathbf{k} .

estimate the energy of the polaron. Therefore, one assumes a perturbative parameter, in this case the coupling constant $\alpha \ll 1$.

In perturbation theory one splits the Hamiltonian Eq. [1.9] as $\mathcal{H} = \mathcal{H}_0 + \mathcal{H}_{pert}$, where

$$\mathcal{H}_0 = \frac{P^2}{2} + \sum_k \hat{a}_k^\dagger \hat{a}_k \text{ and} \quad (1.10)$$

$$\mathcal{H}_{pert} = i (\sqrt{2\pi\alpha})^{1/2} \sum \frac{1}{|\mathbf{k}|} \left(\hat{a}_k^\dagger \exp(-i\mathbf{k} \cdot \mathbf{r}) - \hat{a}_k \exp(i\mathbf{k} \cdot \mathbf{r}) \right),$$

and the energy is written as a perturbative expansion, namely:

$$\Delta E_0 = \langle 0 | \mathcal{H}_{pert} | 0 \rangle + \sum_n \frac{\langle 0 | H_{pert} | n \rangle \langle n | H_{pert} | 0 \rangle}{E_0^0 - E_n^0} + \dots$$

As it is standard in perturbation theory, $|n\rangle$ and E_n are the eigenvectors and eigenvalues of \mathcal{H}_0 respectively. Since \mathcal{H}_{pert} acting on a state changes the number of phonons, the first term of the perturbative series vanishes.

In the Fig. [1.3] the *initial state* is represented by an electron with momentum \mathbf{P} and no phonons. In an *intermediate state* the electron has a momentum $(\mathbf{P} - \mathbf{k})$ and there is one phonon emitted. Therefore the energies of these states are:

$$\text{Initial state : } E_0^0 = \frac{P^2}{2}. \quad (1.11)$$

$$\text{Intermediate state : } E_n^0 = \frac{(\mathbf{P} - \mathbf{k})^2}{2} + 1. \quad (1.12)$$

Notice that in the units used the energy of the phonon is $\hbar\omega_0 = 1$ therefore, the matrix element

is given by:

$$\langle n | \mathcal{H}_{pert} | 0 \rangle = i (\sqrt{2\pi\alpha})^{1/2} \left\langle n \left| \sum_{\mathbf{k}} \frac{1}{|\mathbf{k}|} \left(\hat{a}_{\mathbf{k}}^\dagger \exp(-i\mathbf{k} \cdot \mathbf{r}) - \hat{a}_{\mathbf{k}} \exp(i\mathbf{k} \cdot \mathbf{r}) \right) \right| \mathbf{P}, no\ phonons \right\rangle. \quad (1.13)$$

It vanishes unless $|n\rangle$ is a state with one phonon and one electron with momentum \mathbf{P}' , namely $|n\rangle = |\mathbf{P}', 1\ phonon\rangle$. If the phonon has momentum k , it turns out that,

$$\langle n | \mathcal{H}_{pert} | 0 \rangle = i (\sqrt{2\pi\alpha})^{1/2} \left\langle \mathbf{P}', no\ phonons \left| \frac{1}{|\mathbf{k}|} \exp(-i\mathbf{k} \cdot \mathbf{r}) \right| \mathbf{P}, no\ phonons \right\rangle. \quad (1.14)$$

Since $\exp(-i\mathbf{k} \cdot \mathbf{r}) |\mathbf{P}\rangle = |\mathbf{P} - \mathbf{k}\rangle$, $\mathbf{P}' = \mathbf{P} - \mathbf{k}$ is expected by the momentum conservation. Then

$$\langle n | \mathcal{H}_{pert} | 0 \rangle = i (\sqrt{2\pi\alpha})^{1/2} \frac{1}{|\mathbf{k}|} \delta_{\mathbf{P}', \mathbf{P} - \mathbf{k}}, \quad (1.15)$$

$$\Delta E_0 = -\sqrt{2\pi\alpha} \sum_{\mathbf{k}} \frac{1}{|\mathbf{k}|^2} \left(\frac{1}{(\mathbf{P} - \mathbf{k})^2/2 + 1 - \mathbf{P}^2/2} \times 2 \right). \quad (1.16)$$

The factor 2 in the previous expression is due to the spin of the electron. By writing the sum as an integral using $\sum_{\mathbf{k}} = V \int \frac{d^3\mathbf{k}}{(2\pi)^3}$ it turns out

$$\Delta E_0 = -2\sqrt{2\pi\alpha} \int \frac{d^3\mathbf{k}}{(2\pi)^3} \frac{1}{|\mathbf{k}|^2} \left(\frac{2}{\mathbf{k}^2 - 2\mathbf{P} \cdot \mathbf{k} + 2} \right). \quad (1.17)$$

The integral is computed using the fact that $\int \frac{d^3\mathbf{k}/(2\pi)^3}{|\mathbf{k}^2 + a|^2} = \frac{1}{8\pi\sqrt{a}}$. Adding both the kinetic energy and the second order correction of the energy, one obtains

$$E = \frac{P^2}{2} - \alpha - \frac{p^2}{12}\alpha + \dots = \frac{P^2}{2(1 + \alpha/6)} - \alpha + \dots \quad (1.18)$$

As it can be inferred from the previous equation the electron mass is increased due to the polarisation of the media. The polaron is described as a free particle with $m^*/m = 1 + \alpha/6$.

Experimentally in the solid state context, both weak and intermediate coupling regimes have been tested and they are in good agreement with the theoretical approaches mentioned in this chapter [30, 31]. Nevertheless, there are materials with large values of the coupling parameter where perturbative theories are not longer adequate.

Until now, the interaction between bosonic excitations and the impurity was considered in the context of solid-state physics. However as it will be seen soon, one neutral impurity immersed in a homogeneous degenerate Bose gas can also display a polaron behaviour.

1.2 Ultracold gases and Bose Einstein condensates

The first ideas of Bose Einstein condensation (BEC) appeared in 1925 when A. Einstein expanded the ideas of S.N Bose about the quantum statistics of light quanta (now called photons) [32]. Einstein considered a non-interacting system of massive bosons and he established that below a certain critical temperature, a large finite fraction of bosons would occupy the lowest-energy single-particle state [33]. In 1938, after the discovery of the superfluidity in liquid ^4He [34], F. London suggested that there was a connection between superfluidity and Bose Einstein condensation [35]. The first theoretical explanation of superfluidity was provided by Landau in 1941 [36] in terms of the elementary excitations of the fluid. Later on, Bogoliubov developed the first microscopic approach in order to describe an interacting Bose gas [37]. In 1951 simultaneously Landau and Lifshitz [38] and Penrose [39] realized that there was an intrinsic relation between the one-body density matrix and the macroscopic occupation of the single particle state where bosons are condensed. The concept of non-diagonal long-range order came out as a key point in order to understand BEC. This concept was also helpful in order to make the link between superfluidity and BEC clearer [40]. On the other hand, Landau's predictions concerning the excitation spectrum in superfluid ^4He were verified experimentally. Furthermore the momentum distribution was measured for the superfluid ^4He yielding information about the condensed fraction. Starting, from the experimental observations about the specific heat in superfluid ^4He [41] Landau proposed the existence of a quasiparticle named roton, that is an elementary excitation in the fluid, responsible of the behaviour of the specific heat. After, the theoretical prediction of quantized vortices by Onsager [42] and Feynman [43] were experimentally confirmed by Hall and Vinen [44].

In 1970, many experimental techniques aiming at the study of atomic physics appeared; such techniques are based on magnetic and optical trapping. In the 1980's laser-based techniques, such as laser cooling and magneto-optical trapping were developed for cooling and trapping neutral atoms [45, 46, 47]. Furthermore, alkali atoms were found as very suitable candidates in the laser-based methods, since their optical transitions can be excited by a laser and their internal energetic structure allows one to cool them to low temperatures (a theoretical description of trapping and cooling of atoms can be found in chapter 4 of Ref. [48]). Once atoms are trapped their temperature can be lowered further by using evaporative cooling. Finally, in 1995, by using the evaporative cooling techniques, Bose Einstein condensation was achieved for dilute atomic gases of ^{87}Rb atoms by Cornell and Wieman at Boulder [1] and simultaneously by Ketterle at MIT using ^{23}Na atoms [49]. The different species were cooled down to very low temperatures on the order of fractions of μK . In the same year Bradley and colleagues achieved BEC of ^7Li [50, 51]. Since then, BEC was achieved in many other atomic species such as spin polarized H [52], metastable ^4He [53], ^{41}K [54], and ^{133}Cs [55]. Moreover alkali atoms

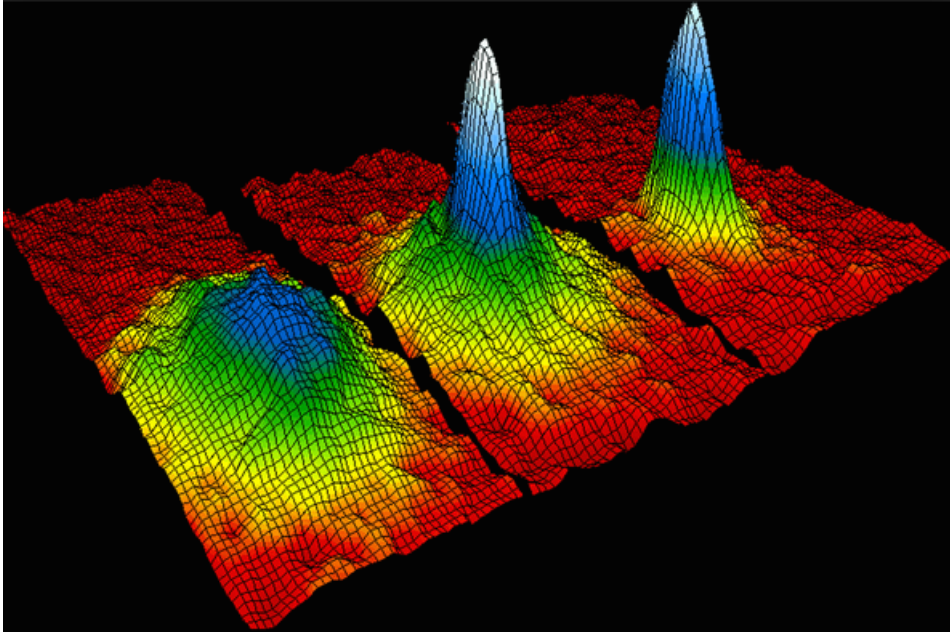


Figure 1.4: **Velocity distribution of Rb atoms** at different temperatures [1]. The atoms exhibit a Maxwell distribution at 400 nK (**left**), but at 200 nK a macroscopic fraction of the atoms occupies the state corresponding to velocity zero (**center**) and for $T = 50nK$ almost all the atoms are in this fraction (**right**).

are not the unique species displaying BEC: it has been achieved with ytterbium isotopes [56], strontium [57], and erbium atoms [58] as well as with molecules [59, 60].

It is very convenient to observe and analyze BEC's in dilute cold gases. The experiments are very clean and the basic theoretical description is much less involved than in traditional condensed-matter systems such as superfluid ^4He . Diluteness and low temperatures are the main features of these cold gases.

Diluteness: Let us consider a gas of bosons of mass m and density $n_B = N_B/V$. Where N_B is the number of bosons and V the volume. In a dilute homogeneous gas the range R_0 of the interatomic forces is much smaller than the average distance between particles; namely $d = n_B^{-1/3}$. In other words,

$$n_B R_0^3 \ll 1. \quad (1.19)$$

In fact, in alkali atoms interacting via a van der Waals potential, the typical range of the interactions is around two orders of magnitude greater than the size of the atom a_0 (the Bohr radius) and is much smaller than the typical interparticle separation $\sim 10^3 a_0$ [48]. Corresponding to typical densities ranging from $10^{13}/\text{cm}^3$ to $10^{15}/\text{cm}^3$.

The condition [1.19] makes the simple “mean field” description valid. Three-body collisions rarely happen and can be neglected, however, they do occur and cause losses. A consequence

derived from the diluteness condition establishes that pair collisions are well described by a single parameter, the s -wave scattering length [48]. All the properties of the system are described in terms of this parameter and do not depend on the specific details of the two-body potential (see. Section 1.2.1).

Low temperatures: BEC is achieved for temperatures lower than a critical temperature $K_B T_c = \frac{2\pi\hbar^2}{m} \left(\frac{n_B}{2.612}\right)^{2/3}$, with m the mass of the bosons [61]. In fact, the thermal de Broglie wavelength $\Lambda = h/\sqrt{2\pi m K_B T}$ for massive particles must be on the order of the interparticle distance $n_B \Lambda^3 \sim 1$. In addition if

$$\Lambda \gg R_0, \quad (1.20)$$

the scattering amplitude becomes independent of the collisional energy as well as of the scattering angle and a low-energy approximation can be used. According to the scattering theory at low energy, this scattering amplitude is determined by the s -wave scattering length which characterizes the effects of the interaction without specific knowledge of the potential details. The condition of diluteness Eq. [1.19] can be re-written in terms of the s -wave scattering length as:

$$n_B |a_{BB}|^3 \ll 1. \quad (1.21)$$

If a quantum gas satisfies the condition [1.21], mean-field theories are suitable for its theoretical description. On the contrary, if the gas parameter is not small enough the system is no longer weakly interacting and other tools must be used, e.g beyond mean-field techniques or quantum Monte-Carlo methods.

In section [1.2.1] we will discuss the scattering length and how it can be tuned in order to change the interaction between atoms. Before let us calculate the ground-state energy of a dilute Bose gas at low temperatures using the Bogoliubov mean-field approach.

The Hamiltonian for a uniform dilute gas of bosons is written in the form:

$$\mathcal{H} = \sum_{\mathbf{p}} \frac{p^2}{2m} \hat{a}_{\mathbf{p}}^\dagger \hat{a}_{\mathbf{p}} + \frac{1}{2V} \sum_{\mathbf{p}_1, \mathbf{p}_2, \mathbf{q}} V_{\mathbf{q}} \hat{a}_{\mathbf{p}_1+\mathbf{q}}^\dagger \hat{a}_{\mathbf{p}_2-\mathbf{q}}^\dagger \hat{a}_{\mathbf{p}_1} \hat{a}_{\mathbf{p}_2}, \quad (1.22)$$

with $V_{\mathbf{q}} = \int V(r) \exp[-i\mathbf{q} \cdot \mathbf{r}/\hbar] d\mathbf{r}$, the Fourier transform of the interatomic potential. In real systems, for instance ^4He , interaction can be modelled by a two-body potential. However, in general details of the potential are important and the solution of the many-body Schrödinger equation is a difficult task. In virtue of the diluteness condition, the actual form of the two-body potential is not important for describing the properties of the gas. Therefore, it is convenient to replace the microscopic potential $V(r)$ by an effective one, namely $V_{eff}(r)$, in such a way that the provided potential gives the proper value of the scattering length (see Fig. [1.5]).

Since only small momenta are relevant in the solution of the many-body problem, one considers

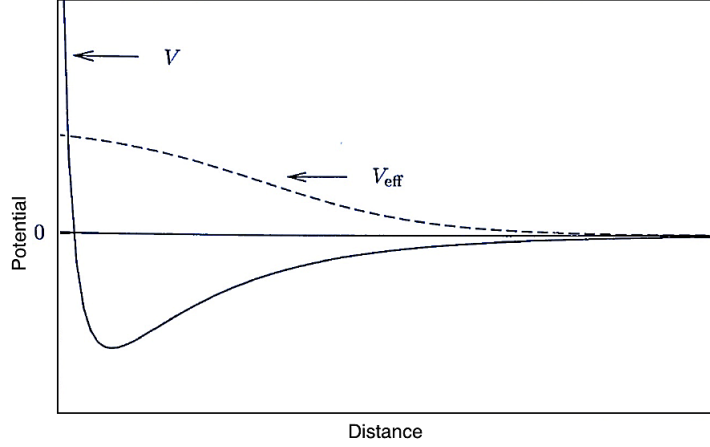


Figure 1.5: **Representation of the interatomic potential V and the effective potential V_{eff} .** The details of the potential for short distances are irrelevant. For large distance both yields the same s -wave scattering length.

the $q = 0$ component of the Fourier transform of the effective potential :

$$V_0 = \int V_{eff}(\mathbf{r}) d\mathbf{r} \quad (1.23)$$

Then the Hamiltonian Eq. [1.22] is written as:

$$\mathcal{H} = \sum_{\mathbf{p}} \frac{p^2}{2m} \hat{a}_{\mathbf{p}}^\dagger \hat{a}_{\mathbf{p}} + \frac{1}{2V} V_0 \sum_{\mathbf{p}_1, \mathbf{p}_2, \mathbf{q}} \hat{a}_{\mathbf{p}_1+\mathbf{q}}^\dagger \hat{a}_{\mathbf{p}_2-\mathbf{q}}^\dagger \hat{a}_{\mathbf{p}_1} \hat{a}_{\mathbf{p}_2}. \quad (1.24)$$

In the Bogoliubov approximation one makes the crucial substitution $\hat{a}_0 \rightarrow \sqrt{N_0}$. For an ideal Bose gas at zero temperature the occupation number for $p \neq 0$ vanishes because all the atoms are in the condensed state $N_0 = N$. In a dilute gas the occupation number for states with $p \neq 0$ is finite but small. To lowest order, it is plausible to neglect all the terms in the Hamiltonian containing terms with $p \neq 0$ and therefore $\hat{a}_0 \equiv \sqrt{N_0} = \sqrt{N}$. Within these approximations the ground-state energy is given by

$$E_0 = \frac{N_B^2}{2V} V_0. \quad (1.25)$$

As it was mentioned before, the two-body potential merely depends on the scattering length a_{BB} . In fact, $V_0 = (4\pi\hbar^2/m) a_{BB}$ is obtained by using the Born approximation (See Sec [1.2.1]). The ground-state energy can be written in terms of the coupling strength $g_{BB} = (4\pi\hbar^2/m) a_{BB}$:

$$E_0 = \frac{1}{2} g_{BB} n_B N_B. \quad (1.26)$$

By computing the total pressure for the interacting gas one obtains $P = -\frac{\partial E_0}{\partial V} = \frac{g_{BB} n_B^2}{2}$, which does not vanish at zero temperature in contrast with the non-interacting Bose gas. By

computing the compressibility of the gas one obtains $\kappa = \frac{\partial n_{BB}}{\partial P} = \frac{1}{g_{BB}n_{BB}}$. Thermodynamic stability requires that $\kappa > 0$ and therefore a weakly interacting Bose gas is stable if $a_{BB} > 0$ (repulsive interactions).

The ground-state energy in Eq. [1.26] has been derived within the lowest-order mean-field approach. Higher-order approximation scheme can be used where quantum fluctuations are included.

In order to go beyond the lowest-order mean-field approximation, one must consider two aspects:

1. Quadratic terms are considered in the operators with $p \neq 0$, thus the Hamiltonian in Eq. [1.24] turns out to be:

$$\mathcal{H} = \sum_{\mathbf{p}} \frac{p^2}{2m} \hat{a}_{\mathbf{p}}^\dagger \hat{a}_{\mathbf{p}} + \frac{1}{2V} V_0 \hat{a}_0^\dagger \hat{a}_0^\dagger \hat{a}_0 \hat{a}_0 + \frac{1}{2V} V_0 \sum_{\mathbf{p} \neq 0} \left(4\hat{a}_0^\dagger \hat{a}_{\mathbf{p}}^\dagger \hat{a}_0 \hat{a}_{\mathbf{p}} + \hat{a}_{\mathbf{p}}^\dagger \hat{a}_{-\mathbf{p}}^\dagger \hat{a}_0 \hat{a}_0 + \hat{a}_0^\dagger \hat{a}_0^\dagger \hat{a}_0 \hat{a}_{-\mathbf{p}} \right) \quad (1.27)$$

2. The higher-order Born approximation must be considered for the relation between the potential V_0 and the scattering length a_{BB} . This gives a_{BB} is calculated as [62]:

$$a_{BB} = \frac{m}{4\pi\hbar^2} \left(V_0 + \frac{V_0^2}{V} \sum_{\mathbf{p} \neq 0} \frac{m}{p^2} \right). \quad (1.28)$$

One should point out that the Hamiltonian in Eq. [1.27] can be rewritten by the equation for number of particles $N = \hat{a}_0^\dagger \hat{a}_0 + \sum_{\mathbf{p} \neq 0} \hat{a}_{\mathbf{p}}^\dagger \hat{a}_{\mathbf{p}}$ yielding:

$$\hat{a}_0^\dagger \hat{a}_0^\dagger \hat{a}_0 \hat{a}_0 = N^2 - 2N \sum_{\mathbf{p} \neq 0} \hat{a}_{\mathbf{p}}^\dagger \hat{a}_{\mathbf{p}}. \quad (1.29)$$

By plugging Eq. [1.29] and Eq. [1.28] into Eq. [1.27] one ends up with:

$$\mathcal{H} = \frac{g_{BB}N_B^2}{2V} + \sum_{\mathbf{p}} \frac{p^2}{2m} \hat{a}_{\mathbf{p}}^\dagger \hat{a}_{\mathbf{p}} + \frac{g_{BB}}{2} n_B \sum_{\mathbf{p} \neq 0} \left(2\hat{a}_{\mathbf{p}}^\dagger \hat{a}_{\mathbf{p}} + \hat{a}_{\mathbf{p}}^\dagger \hat{a}_{-\mathbf{p}}^\dagger + \hat{a}_{\mathbf{p}} \hat{a}_{-\mathbf{p}} + \frac{mg_{BB}n_B}{p^2} \right). \quad (1.30)$$

The previous Hamiltonian is quadratic in the operators $\hat{a}_{\mathbf{p}}^\dagger$ and $\hat{a}_{\mathbf{p}}$ and it can be diagonalized using the Bogoliubov transformation, where operators are written in terms of a set of new operators $\hat{\alpha}_{\mathbf{p}}$ and $\hat{\alpha}_{\mathbf{p}}^\dagger$. By following Bogoliubov's procedure [37] the diagonalized form of the Hamiltonian is

$$\mathcal{H} = E_0 + \sum_{\mathbf{p}} \epsilon(p) \hat{\alpha}_{\mathbf{p}}^\dagger \hat{\alpha}_{\mathbf{p}}, \quad (1.31)$$

here

$$E_0 = \frac{g_{BB}N_B^2}{2V} + \frac{1}{2} \sum_{\mathbf{p} \neq 0} \left(\epsilon(p) - g_{BB}n_B - \frac{p^2}{2m} + \frac{mg_{BB}^2n_B^2}{p^2} \right). \quad (1.32)$$

and the dispersion relation $\epsilon(p)$ is given by:

$$\epsilon(p) = \sqrt{\frac{g_{BB}n_B}{m}p^2 + \left(\frac{p^2}{2m}\right)^2}. \quad (1.33)$$

The Bogoliubov transformation allow us to map a weakly-interacting system into a system of independent quasiparticles with energy $\epsilon(p)$. The operators $\hat{\alpha}_{\mathbf{p}}$ and $\hat{\alpha}_{\mathbf{p}}^\dagger$ are the annihilation and creation operators of these quasiparticles. In fact, $\hat{\alpha}_{\mathbf{p}}|\text{Vacuum}\rangle = 0$ defines the ground state of the interacting system as the vacuum of quasiparticles. Eq. [1.32] gives the ground state energy E_0 after substituting the sum by an integral ($\frac{V}{(2\pi)^3} \sum_{\mathbf{k}} \rightarrow \int d^3\mathbf{k}$). The result is given by

$$E_0 = \frac{g_{BB}N_B^2}{2V} \left[1 + \frac{128}{15\sqrt{\pi}} \left(n_B a_{BB}^3 \right)^{1/2} \right], \quad (1.34)$$

where the lowest-order mean field ground-state energy Eq. [1.26] is now corrected by the Lee-Yang-Huang term [63]. The previous result is valid provided that $n_B a_{BB}^3 \ll 1$.

We refer to $\hat{\alpha}_{\mathbf{p}}|\text{Vacuum}\rangle = 0$ and to Eq. [1.34] as the equation providing the ground-state and the ground-state energy of the system. Actually the true ground-state of the system is a solid and the gas phase can be observed as a metastable phase where thermalization is ensured by two-body collisions and extremely rare events three-body collisions.

1.2.1 Interatomic interactions and Feshbach resonances

In the previous section the s -wave scattering length was introduced. It characterizes the low-energy interactions between pairs of particles. The wave function for the relative motion of two colliding atoms can be written as the sum of an incoming plane wave and a scattered wave

$$\psi(\mathbf{r}) = e^{ikz} + \psi_{sc}(\mathbf{r}). \quad (1.35)$$

One is interested in the behavior of the scattered wave for distances $r \gg R_0$. Under the assumption that the interaction between particles is spherically symmetric. It turns out to be a spherical wave $\psi_{sc}(r \gg R_0) \rightarrow f(\theta) \exp(ikr)/r$, where $f(\theta)$ is the scattering amplitude which depends on the scattering angle θ , that is the angle between the direction of the momentum of the particles before and after the collision. As it was argued before, at very low energies only the s -wave scattering is important. In this limit the wave function displays the asymptotic behaviour

$$\psi(r) = 1 - \frac{a}{r}, \quad (1.36)$$

where a is the s -wave scattering length.

In what follows we will see how the knowledge of the scattering length is enough to describe the interaction between pairs of atoms at low energies. There is a connection between the scattered wavefunction $\psi_{sc}(\mathbf{r})$ in Eq. [1.35] and the scattering T matrix. The latter satisfies the so-called Lippmann-Schwinger (LS) equation (see Ref. [48]).

$$T(\mathbf{k}, \mathbf{k}'; E) = U(\mathbf{k}, \mathbf{k}') + \frac{1}{V} \sum_{\mathbf{k}''} U(\mathbf{k}', \mathbf{k}'') \left(E - \frac{\hbar^2 \mathbf{k}''^2}{m} + i\delta \right)^{-1} T(\mathbf{k}'', \mathbf{k}; E), \quad (1.37)$$

where $U(\mathbf{k}, \mathbf{k}')$ is the Fourier transform of the bare atom-atom interaction. $T(\mathbf{k}, \mathbf{k}'; E)$ is defined in terms of the scattered wave function in the momentum space as:

$$\psi_{sc}(\mathbf{k}') = \left(\frac{\hbar^2 k^2}{m} - \frac{\hbar^2 k'^2}{m} + i\delta \right)^{-1} T(\mathbf{k}, \mathbf{k}'; E), \quad (1.38)$$

and \mathbf{k} and \mathbf{k}' are the momentum of the incoming and outgoing wave respectively. The value δ in the previous equation is introduced to ensure that only outgoing waves are present in the scattered wave. At large distances for zero energy Eq. [1.38] yields:

$$\psi_{sc}(\mathbf{r}) = \frac{m}{4\pi\hbar^2 r} \Gamma(0, 0, 0) \quad (1.39)$$

Therefore, it follows that

$$\Gamma(0, 0, 0) = \frac{4\pi\hbar^2}{m} a \quad (1.40)$$

An approximation for a can be obtained using the Born approximation. It is obtained by coinciding the first term on the right-hand of Eq. [1.37] and yields:

$$a = \frac{m}{4\pi\hbar^2} V(0) = \frac{m}{4\pi\hbar^2} \int d\mathbf{r} V(\mathbf{r}), \quad (1.41)$$

For very low-energies, two body interactions in ultracold gases may be described by a pseudopotential $V(\mathbf{r})$ with the scattering length a taken as an experimental parameter. The scattering length can be either positive or negative corresponding to attractive and repulsive interactions respectively. We now mention how the scattering length can be varied experimentally in order to adjust the interaction between atoms.

The useful way of varying the scattering length is by means of the Feshbach resonances. This mechanism allows one to increase a beyond the mean inter-particle distance. Feshbach resonances were first found in nuclear physics [64]. For cold atoms Feshbach resonances are described in terms of a two-channel model [2]. A Feshbach resonance appears whenever a bound state in a closed channel is coupled resonantly to the open channel corresponding to the scattering continuum (see Fig. 1.6). The channels are related to the internal states of the atoms, for

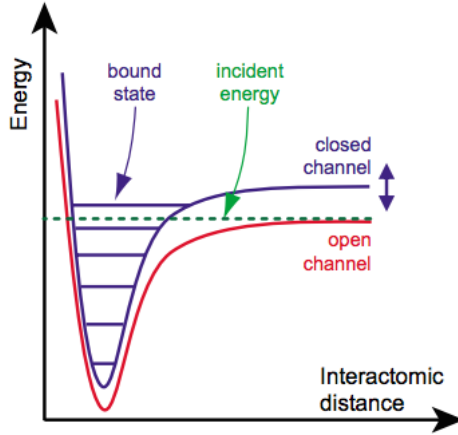


Figure 1.6: Basic two-channel model for a Feshbach resonance: two atoms colliding with energy E (dashed green line) in the open channel (red line) corresponding to the interaction potential is resonantly coupled to a closed channel (purple line). Then a bound state appears on the closed channel with an energy close to zero. The position of the bound state in the closed channel changes with respect to the open channel by varying the magnetic field.

instance, they may correspond to different hyperfine states of the atoms. Feshbach resonances permit tuning of the scattering length by changing a magnetic field [65]. The tunability arises from the difference between the magnetic moments of the close and open channel. In fact, the position of the bound state in the closed channel changes with respect to the open channel by varying an external magnetic field.

Experimentally, the scattering length depends on the external magnetic field according to

$$a(B) = a_{bg} \left(1 - \frac{\Delta B}{B - B_0} \right), \quad (1.42)$$

Here a_{bg} is the off-resonant background scattering length, in the absence of the coupling with the closed channel, B_0 is the magnetic field where the resonance appears, ΔB is the resonance width. For instance, one can consider a collision of two ${}^6\text{Li}$ atoms: they are prepared in the lowest hyperfine state $|\uparrow\rangle = |m_s = -1/2, m_I = 1\rangle$ and $|\downarrow\rangle = |m_s = 1/2, m_I = -1\rangle$ and the magnetic-field dependence of the scattering length for this collision is shown in Fig. [1.7] where the resonance is at $B_0 = 834 \text{ G}$.

It is interesting to consider the strongly-interacting case $n_B a_{BB}^3 \gg 1$, that is obtained near the resonant value of the magnetic field. In this respect, fermions are more favourable than bosons because the Pauli exclusion principle strongly suppresses inelastic processes involving three fermions, whereas these loss mechanisms become very important for bosons when a is large [2]. We notice that for values of a close to the resonance the condition [1.21] is no longer valid and the gas is not weakly interacting. In this regime, the simple theory described in this

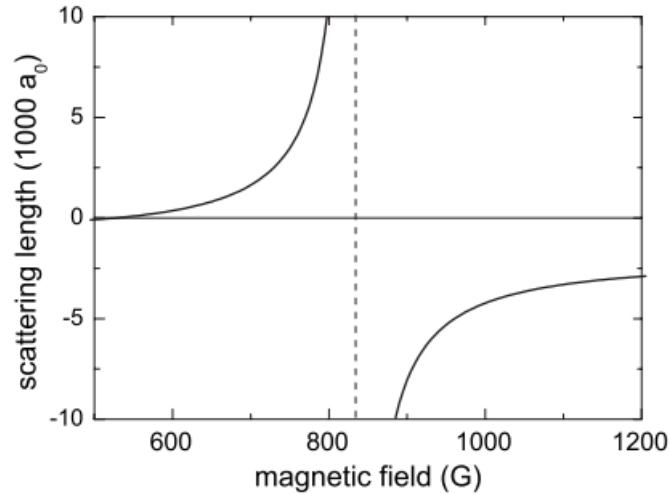


Figure 1.7: Observation of a magnetically tuned Feshbach resonance in an optically trapped BEC of Na atoms. Scattering length normalized to the a_{bg} as a function of the external magnetic field B . The resonant point is placed at $B_0 = 907\text{G}$. Dots represents the experimental data, whereas the solid line is the theoretical formula [2].

chapter breaks down and more sophisticated theoretical tools must be employed.

Quantum gases are used as an excellent test bed for many body theories due to the high degree of controllability of its components such as the density, temperature and interactions [66, 67]. They are particularly useful to investigate strongly correlated system that have remained out of reach in condensed-matter systems [68]. For instance, the polaron problem: a standard problem in condensed-matter physics where the strongly interacting limit in general is inaccessible, but it might be explored by means of ultracold quantum gases. Then, a mark question remains as to whether an ultracold atom system can be used as a quantum simulator of a polaron for all the coupling strengths.

Chapter 2

Impurities and ultracold gases

In this thesis we investigate the ground-state properties of impurities immersed in a bosonic bath. Ground-state properties such as the energy, the pair correlation function and the effective mass. Precisely these properties have been measured and investigated in Fermi polarons. These quasiparticles are found when particles are immersed in a fermionic bath. Nevertheless, since the matter of this thesis is purely theoretical, we warn the lector that the scope of this chapter is a review of the main experiments concerning impurities in ultracold gases. The motivation of this chapter is to familiarize the lector with experimental activity in this field.

In the first part of the chapter, we review the experiments concerning the Fermi polaron, in which ground-state properties such as energy and effective mass are investigated. Subsequently, we review some experiments concerning the manipulation and control of impurities in a Bose-Einstein condensate as well as the polaronic behavior displayed for impurities in one dimensional configurations.

2.1 Fermi Polarons

The dynamics of a single impurity in a bath is a fundamental problem in many-body physics. For instance, in solid-state physics the situation of an electron coupled to a bosonic bath (such as the lattice vibrations) where the impurity and the distortion of the lattice caused by the motion of the electron form a quasiparticle called polaron. The energy and the mass are different from the bare electron (see chapter 1). This quasiparticle is quite important in many branches of physics, for instance it plays an important role in high transition temperature superconductors [69], also in the colossal magnetoresistance in rare-earth manganites [70]. Another example is the Kondo effect where immobile spin impurities give rise to an enhanced resistance in metals below the Kondo temperature [71, 72].

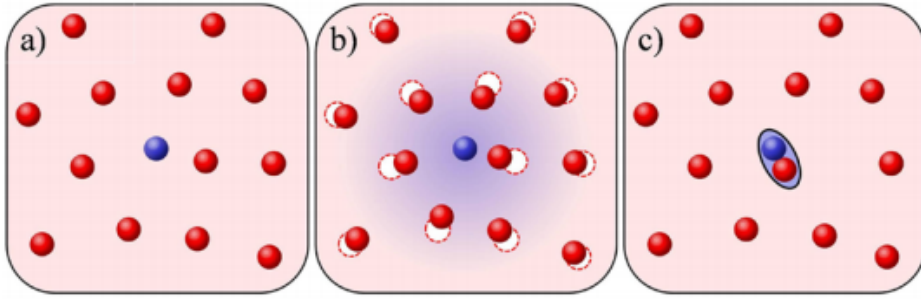


Figure 2.1: **Fermi Polarons**: from polarons to molecules. **(a)** For weak attraction, an impurity (blue) experiences the mean field of the medium (red). **(b)** For stronger attraction, the impurity surrounds itself with a localized cloud of environment atoms, forming a polaron. **(c)** For very strong attraction, molecules of size a are formed despite Pauli blocking of momenta $k < k_F \leq a^{-1}$ by the environment.

In the context of ultracold atoms, both repulsive and attractive polarons are predicted to occur when a particle interact with a degenerate quantum gas. The attractive Fermi polarons have been the first observed: dressed spin-down (up) impurities in a spin-up (down) Fermi sea of ultracold atoms [73]. Experimentally, a remarkable feature of the polaron is a narrow peak in the impurity radio-frequency spectrum that emerges from a broad incoherent background. The fermionic polaron lies in the framework of two fundamental problems in quantum many-body physics: the crossover between a molecular BEC and a superfluid BCS (Barden-Cooper-Schrieffer) pairing with spin-imbalance for attractive interactions [74] and Stoner’s itinerant ferromagnetism for repulsive interactions [75].

The first experimental evidence of fermionic polarons came out from the group of Zwierlein and colleagues in 2009. They used a spin-polarized cloud of ${}^6\text{Li}$ spin-up (\uparrow) atoms in the lower hyperfine state $|1\rangle$ confined in a cylindrically symmetric optical trap in 3D. Then, the spins of a small fraction of atoms are flipped by using a two-photon Landau-Zener sweep into the state $|3\rangle$ (spin-down \downarrow). The polaron energy and the quasiparticle residue for various interaction strengths around a Feshbach resonance have been found with **rf** spectroscopy. There is a characteristic peak that becomes more pronounced at the unitary limit $1/k_F a = 0$ (k_F is the Fermi vector and a is the scattering length). The energy of the peak as well as the quasiparticle residue function Z have been measured [73].

The spin-down impurities are immersed in a degenerate Fermi gas of about 5×10^6 atoms in the state $|1\rangle$ at a temperature of tenths of the Fermi temperature. For weak interactions $1/k_F a \ll 1$ Fig. [2.1, a] there is an impurity that propagates freely in the spin-up background. The impurity experiences the typical mean-field effect, but as soon as the attractive interaction increases, the impurity undergoes in atoms collisions and starts to attract its surrounding atoms Fig.[2.1, b]. The impurity “dressed” with the cloud of scattered fermions defines the Fermi polaron. The dressed impurity can move freely through the environment, with a total energy

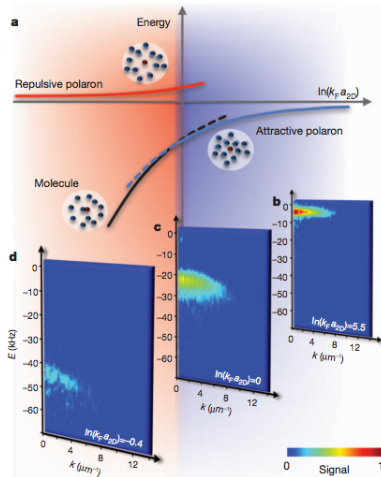


Figure 2.2: **Attractive and repulsive Fermi polarons in 2D:** (a) Energy spectrum displaying the many-body ground state of the system, characterized by both the attractive polaron, the molecular state and the repulsive polaron lying in a metastable branch as a function of the interaction strength written in typical experimental units $\ln(k_F a)$. **The single particle spectral function (b)** displays a well-defined pick for weak attractive interactions, thus characterizing the attractive polaron. When the interaction strength is driven near to the resonance the pick is not well-defined (c) and the single particle spectral function will display an incoherent feature as soon as the resonance is crossed and enters into the molecular branch (d).

shifted away from the mean field result. This polaronic state is stable up to a critical value at strong interactions $1/k_F a \simeq 1$ where the impurity will bind one spin-up atom from the environment forming a tightly bound state Fig. [2.1, c]. Then, the new molecular state forms a bosonic dressed impurity.

After the work carried out by the experimental group of Zwierlein team at the MIT, many theoretical approaches have investigated the Fermi polaron with repulsive interactions [76]. The experimental realization of these polarons faced a huge challenge since the strong interactions between atoms sustains a deeply molecular bound state into which the atoms can decay. In 2012 simultaneously the group in Cambridge led by Köhl and the group of Grimm in Innsbruck succeeded in the realization of the repulsive Fermi polaron. The essential point for studying Fermi polarons is because the Fermi surfaces of the two components in a spin-imbalanced gas are mismatched and bring to light many interesting features.

The Fermi polaron has been studied by Köhl [77] both for attractive and repulsive interactions in two dimensions. They prepared a quantum degenerate gas of ^{40}K atoms in a strongly imbalanced mixture with an impurity concentration $C = a/b$ of the two lowest Zeeman state $a = |F = 9/2, m_F = 9/2\rangle$ and $b = |F = 9/2, m_F = 7/2\rangle$ at low temperatures.

The energy level diagram Fig. [2.2, a] displays two branches: for attractive interactions, the many-body ground state of the system is formed by an attractive polaron and a molecular state

(blue solid line). For strong enough interactions, the attractive polaron decay into this dimer state. In contrast, in the case of an impurity interacting repulsively with the fermionic bath, the strong interaction between the impurity and the bath can be only achieved if the underlying interaction potential is attractive, which implies a two-particle bound state. Therefore the repulsive polaron branch (red dashed line) is metastable and these excitations can decay either into the attractive polaron or the molecular state. The single-particle spectral function have been measured as shown in Fig. [2.2, **b**] and for weak attractive interactions a sharp peak appears revealing the existence attractive polaron as a well defined quasiparticle. In the strong interacting limit Fig. [2.2, **c**], the peak displayed in the single-particle spectral function disappears and it turns into a weak incoherent feature indicating the transition to the molecular state (see Fig. [2.2, **d**]).

The work of Köhl and his team also studied very interesting properties of the fermionic polarons such as: the ground-state energy [77]. This energy is obtained as a function of the interaction parameter $\ln(k_F a_{2D})$ (k_F is the Fermi vector and a_{2D} is the two-dimensional scattering length) as well as theoretical results found in [3] are plotted [2.3, **a**]. On the other hand, the effective mass of fermionic polaron as a function of the interaction strength have been obtained both experimentally and theoretically and the results are plotted in Fig [2.3, **b**] and one observes that the effective mass agrees very well with the theory for weak interactions ($|\ln(k_F a)| \gg 1$), furthermore at the unitary limit where $\ln(k_F a) = 0$, the effective mass is around twice the value of the bare mass.

Furthermore, the effective mass was measured as a function of the temperature in Fig [2.3, **c**] and concentration in Fig [2.3, **d**]. In the former case this dependence is studied for both attractive and repulsive interactions showing no drastic change for the attractive polaron (see red squares in Fig [2.3, **c**]), whereas, for the repulsive case the effective mass ranges from 1 to 5 (see blue circles in Fig [2.3, **c**]).

In addition, the effective mass is investigated as a function of the concentration C , for both attractive and repulsive interactions at finite and very small temperature. In the attractive case (see red squares in Fig [2.3, **d**]), there are no dramatic changes, in fact the effective mass does not overcome a value of two times the bare mass, in contrast with the repulsive polaron where the effective mass is larger than two for the repulsive polaron (see blue circles in Fig [2.3, **d**]). The horizontal red and blue lines represent the theoretical results (see Ref. [3]).

Finally in Fig. [2.3, **e**] the lifetime is investigated as a function of the strength parameter for the metastable repulsive branch.

The metastability and coherence of the repulsive polaron in three dimensions have been investigated by Grimm and coworkers in a resonantly Fermi gas [78] by means of magnetically tuned Feshbach resonances (FR). In this work they found a remarkable increase in the life

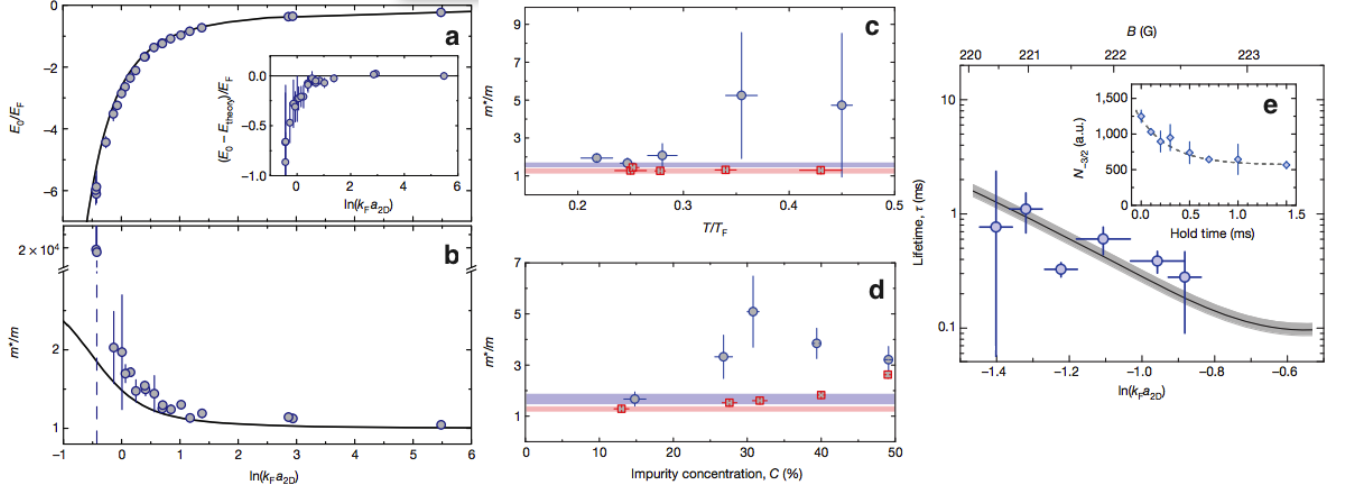


Figure 2.3: Mean results from the Köhl team about 2D fermionic polarons [2.2]: (a) Energy normalized as a function of the strength parameter defined as $\ln(k_F a)$. Theory [3] and experiments are plotted. (b) The effective mass was investigated for both the **attractive (red squares)** and the **repulsive polaron (blue circles)** as a function of the strength parameter as well as a (c) function of the temperature and (d) the impurity concentration. All previous results for the effective mass displays non-self trapping for the impurity. The life-time (e) of the repulsive polaron is plotted as a function of the coupling strength.

time of the repulsive branch when the effective range of the potential is of the order of the inter-particle distance. A sample of fermionic ^{40}K atoms have been immersed in a large Fermi sea of ^6Li atoms at very low temperatures ($T = 290\text{ nK}$). The ^{40}K impurities are prepared in the initial state $|F = 9/2, m_F = -5/2\rangle$, whereas the ^6Li atoms are prepared in the state $|F = 1/2, m_F = +1/2\rangle$. The FR allows to tune the s -wave scattering length $a_{\text{K-Li}}$ using an external magnetic field B . In Fig. [2.4] are displayed the mean features at $T = 0$ for an impurity interacting with the Fermi sea. The energy is obtained as a function of the interaction strength $1/(k_F a_{\text{K-Li}})$ where ($k_F = 1/2850 a_0$) is the Fermi wave vector and a_0 is the Bohr radius. Analogous to the two dimensional case in Fig. [2.2], the three dimensional one also displays two quasiparticle branches and a molecular branch. The lower branch (E_- , green line) corresponds to the attractive polaron. This polaron remains until a critical interaction strength, where the system energetically prefers to form a bosonic molecular state $^6\text{Li}^{40}\text{K}$ by binding the ^{40}K impurity to one ^6Li atoms. The molecular continuum is formed when the impurity has an energy between 0 and ε_F and it can be removed from the Fermi sea. The molecular continuum is represented by the gray zone on Fig. [2.4] limited by the dashed lines and E_m is the energy of the dressed molecule. On the other hand, the attractive polaron may decay into this molecular continuum for $E_- \geq E_m - \epsilon_F$. The red line in Fig. [2.4] depicts the metastable repulsive polaron with an energy $E_+ > 0$. In this branch the strong interactions only can be achieved until a critical value where the polaron becomes unstable and decays either to the lower-lying attractive polaron or to the molecular continuum. The excitation spectrum is

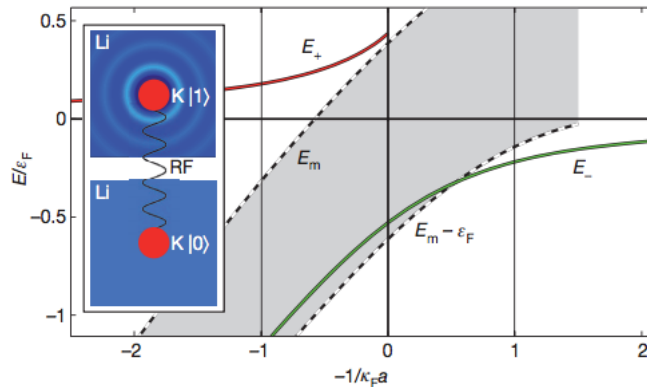


Figure 2.4: **Results from the Grimm team concerning 3D fermionic polarons [2.4]:** similar to the case in two dimensions the energy spectrum displays two polaronic branches as a function of the strength parameter defined here as $1/(k_F a_{k-Li})$: the attractive (green line) and the repulsive polaron (red line). The gray region between E_m and $E_m - \epsilon_F$ is the molecular continuum. The inset illustrates the radio-frequency spectroscopy scheme used in experiments in which the impurity is transferred from a non-interacting state $|0\rangle$ to an interacting state $|1\rangle$.

studied by using radio-frequency spectroscopy (rf), which basically involves the flipping of the spin of the impurity. In particular, samples of ^{40}K atoms are prepared in a non-interacting spin state $|0\rangle = |F = 9/2, m_F = -7/2\rangle$ by using variable frequency ν_{rf} the system is driven from this non-interacting state to the resonant state $|1\rangle = |F = 9/2, m_F = -5/2\rangle$ (see methods in [78]). The energy excitation spectrum is obtained by transferring atoms to the new interacting state as a function of $\nu = \nu_{rf} - \nu_0$ (ν_0 is the frequency of the unperturbed system between the two spin states).

Fermi polarons in two and three dimensions share many interesting features. In fact, the dimensionality plays an important role since quantum fluctuations such as the excitation process of particle-hole creation in the Fermi sea are enhanced in low dimensions. Another interesting feature is concerned to the metastability: in the 3D experiment by Grimm and co-workers the results show that the attractive polaron disappears in the strongly interacting regime and the repulsive polaron survives deeply into the strongly interacting regime; in contrast with the experiments by Zwierlein and colleagues where the attractive polaron is connected adiabatically with the molecular branch and the repulsive polaron was not well defined in the strongly interacting limit.

2.2 Bosonic polaron

In the last section we have reviewed some experiments concerning the Fermi polarons. In this section we will review some advances regarding impurities in a Bose gas. As we have mentioned

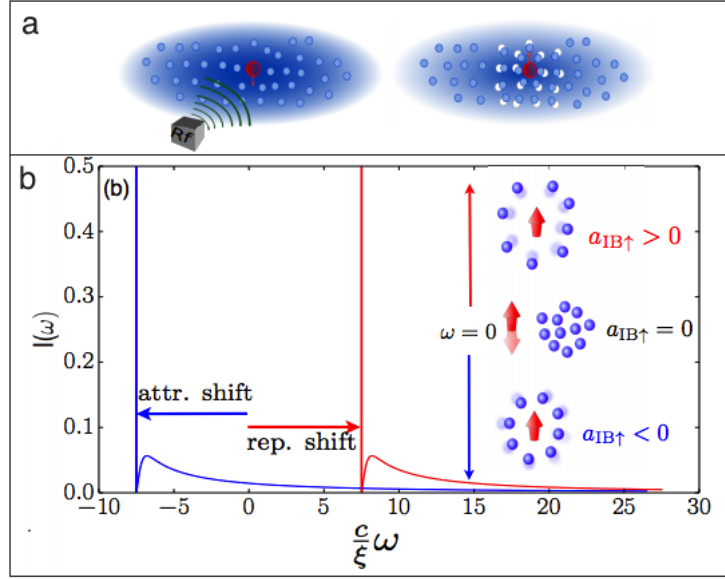


Figure 2.5: Radio Frequency spectroscopy (rf) for investigating the spectral properties of a BEC: The main idea of RF spectroscopy is to drive a non-interacting system to an interacting system from two internal states of the impurity (a) a small concentration of impurities with two internal levels $|\downarrow\rangle$ and $|\uparrow\rangle$ (red spheres) is immersed into a BEC (blue spheres), in which the interaction between the impurity-boson is featured by the s -wave scattering length a_{IB} . A radio frequency pulse transfers impurities from a non-interacting state $|\downarrow\rangle$ to an interacting state $|\uparrow\rangle$. (b) The transition from $|\downarrow\rangle$ to $|\uparrow\rangle$ is made by a coherent well-defined peak centered at a frequency corresponding to the energy of the polaron. The peaks show up for both attractive ($a_{IB\uparrow} < 0$) and repulsive interactions ($a_{IB\uparrow} > 0$). Moreover, the high-frequency power-law tail is associated with the low-energy excitations in the BEC.

In the previous section, radio-frequency spectroscopy (rf) is a quite important technique that allows one to obtain the static and dynamic properties in the case of Fermi polarons. Furthermore, this technique has been applied for both Bose-Bose and Bose-Fermi mixtures [79] and is an important technique also in order to study impurities in a Bose gas.

Experimentally, a small concentration of impurities is considered with two different internal states. The impurities are taken to be initially in the state $|\downarrow\rangle$ which does not interact with the bosons. Then, a radio frequency pulse is applied, transferring these impurities to a final state $|\uparrow\rangle$, where impurities and bosons do interact. In contrast with the particle-hole low-energy excitations present in Fermi polarons, in the bosonic case the free impurities are dressed by the low-energy excitations of the degenerate Bose gas. The remarkable feature that shows the presence of a quasiparticle is a coherent peak in the radio-frequency signal. This peak is centered at a frequency corresponding to the energy of the polaron measured from the transition between the non-interacting $|\downarrow\rangle$ to the interacting $|\uparrow\rangle$ state. This sharp peak is signaling the bosonic polaron corresponding to the impurity dressed by the excitations in the BEC (see Fig. [2.5]). These excitations are associated with a characteristic high-frequency power-law

tail. The same technique can also be extended to the case where both internal states of the impurity are interacting with different interaction strengths. The application of this technique for investigating bosonic polarons has been discussed in [79].

Distinguishable and indistinguishable impurities (bosons and fermions) immersed in BEC, have been studied in some important works. In one dimension, for instance Bloch and colleagues at Munich have tackled the problem of spin impurities and their dynamics in order to understand quantum magnetism [80]. Even though, the polaron physics in this system is not investigated, this work provides a dynamical description of the impurities in the 1D optical lattice. Since the manipulation of single impurities in a Bose gas is still a challenge. Initially atoms of ^{87}Rb were loaded in an optical lattice creating a one-dimensional Mott insulator where all the atoms are in the initial state $|\uparrow\rangle = |F = 1; m_F = -1\rangle$. Subsequently by using single-site addressing (see reference [81]) one flips the spin of one atom changing the hyperfine state from $|\uparrow\rangle$ to $|\downarrow\rangle = |F = 2; m_F = -2\rangle$. The flipped atoms plays the role of the impurity. The coherence of this spin impurity propagating through the one-dimensional spin chain of bosons has been investigated. The system is described by a two-species single-band Hubbard model with the spin-independent single-particle tunneling J and the on-site interaction energy U . The dynamical properties of this impurity are investigated in the Mott insulator regime ($U \gg J$ with filling factor one) where the authors found that spin impurity propagates in defect-free environment except for the presence of thermal excitations, leading to a coherent evolution with its neighbors through superexchange coupling. This coherent evolution is seen when the polar angles (see Fig. [2.6]) in every atom appears to oscillate as a function of the time Fig [2.6]. The impurity initially was “localized” at $t = 0$ in every space lattice. For $t \neq 0$ due to the superexchange mechanism the impurity propagates through of the different lattice space revealing the coherence of the impurity. In contrast in the superfluid regime $J \gg U$, the on-site density of the bath of spin $|\uparrow\rangle$ has quantum fluctuations. These fluctuations are linked with phonon-like excitations, which lead to a Fröhlich-like Hamiltonian (see chapter 1) such that the impurity with the low-energy excitations forms a polaron. In the superfluid regime the polaron can be seen as an impurity propagating coherently together with a dip in the density of the bath that is created by the repulsive interactions between the impurity and the atoms in the bath.

Along the same line of investigating the properties of impurities in one dimension, the quantum dynamics of an impurity in a BEC has been investigated by J. Catani and colleagues [82]. By using a species selective dipolar potential (SSDP) they initially loaded ^{41}K impurities into a bath made by 1D tubes of ^{87}Rb bosonic atoms. The role of the SSDP is to localize the impurities in the center of the ^{87}Rb tubes. The ^{87}Rb atoms are cooled using microwave evaporation and the ^{41}K atoms are sympathetically cooled in a magnetic trap at low temperatures $T = 1.5 \mu\text{K}$. They are then loaded into a dipole trap formed by two orthogonal laser beams (details are found

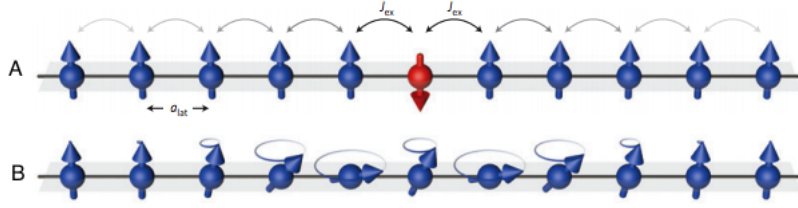


Figure 2.6: (A) single spin impurity is flipped at the center site of a 1D spin chain. Each spin is coherently coupled to its neighbors through the superexchange coupling. (B) Quantum evolution of the spins as a function of the time.

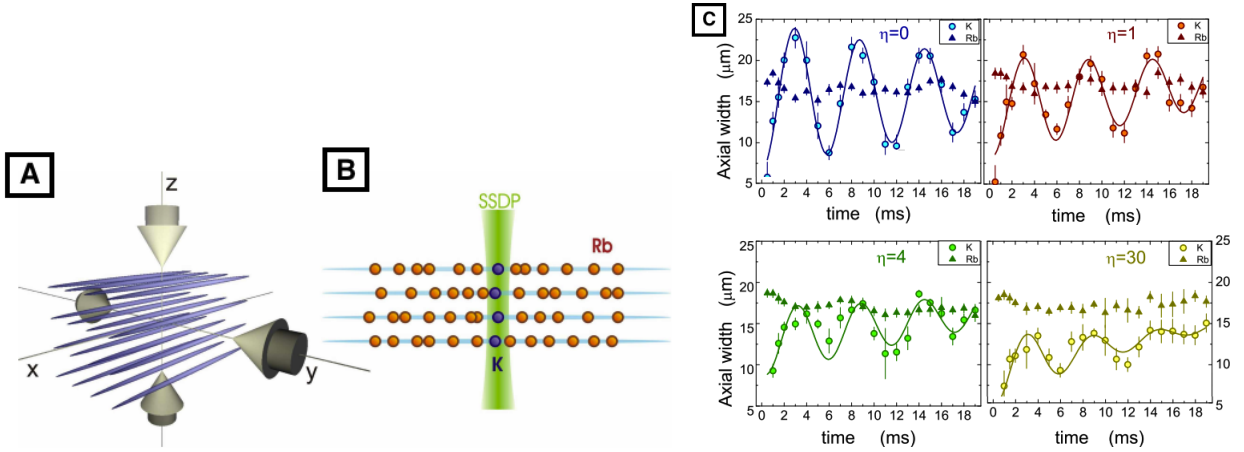


Figure 2.7: **Experimental array for impurities in a one dimensional gas:** (A) species-selective dipolar potential localizes the impurities into the center of a one dimensional Rb atoms. (B) The ultracold Rb atoms with K impurities are loaded into a one dimensional array. (C) The axial width $\sigma = \sqrt{\langle x^2 \rangle}$ is plotted as a function of the time for different ratios $\eta = g_{K,Rb}/g_{Rb}$ displaying the effects of the K impurities on the Rb atoms.

in [82] forming a 1D optical lattice (see [2.7, A]). Both species are polarized in the hyperfine state $|F = 1; m_F = 1\rangle$ allowing for magnetically tunable interspecies interactions $g_{K,Rb}$ atoms. The SSDP only affects one of the components of the mixture: the ^{41}K atoms. They are loaded in the center of the ^{87}Rb tubes, whereas the ^{87}Rb atoms are practically insensitive to the light blade (see Fig. [2.7, B])

The dynamics of the impurities is investigated by analyzing the dependence of the oscillation of the K impurities along the x direction as a function of the interspecies interaction (see [2.7, C]). In fact, the axial width $\sigma = \sqrt{\langle x^2 \rangle}$ is plotted as a function of time for different ratios $\eta = g_{K,Rb}/g_{Rb}$ of the coupling constants. Starting from a configuration where ^{41}K and ^{87}Rb atoms do not interact ($\eta = 0$) up to strongly interacting limit ($\eta = 30$). It is found that the oscillation amplitude decreases with the strength of the interaction, but the oscillation frequency does not change. The solid lines in Fig. [2.7, C] represent the results of the theoretical model describing the phenomenon. The damped oscillation amplitude is fitted by a combination of a linear

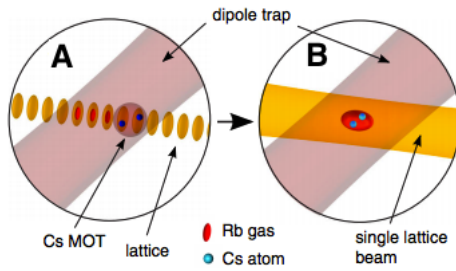


Figure 2.8: ^{133}Cs atoms are immersed in a ultracold gas of ^{87}Rb .

function and a damped-sinusoid function (initially the oscillation amplitude increases linearly over time). The oscillation amplitude plays an important role in the experiment and remarkable information, such as the effective mass of the polaron is extracted. A theoretical model is proposed and its predictions are compared with the experimental observations: the system of the impurity plus the bath is modeled as an harmonic oscillator in contact with a thermal bath. The corresponding Langevin equation is written in terms of quantities renormalized by the interactions, namely, the energy and effective mass. By writing down a 1D version of the Fröhlich Hamiltonian, the effective mass is calculated and its increase is responsible of the attenuation in the oscillation amplitude. In fact, the theoretical model suggests that $\sigma \propto 1/\sqrt{m_K^*}$, where M_K^* is the effective mass of the ^{41}K atoms.

The dynamics of a single neutral impurity immersed in a ultracold gas in three dimensions has been studied by Widera et al. [83] and represents the first step in building an experimental setup aimed to the study the bosonic polaron in a three dimensional configuration. Experimental challenges in the trapping of single atoms concern the detection [84], the preparation of single atoms on individual sites of an optical lattice [85] and the quantum control of the degrees of freedom [86] since the temperature is too high, the atoms cannot undergo in coherent collisions, but their immersion in a bath of ultracold bosons can preserve their internal state coherence.

In the experiment **Cs** atoms are immersed into an ultracold cloud of **Rb** atoms. A rapid thermalization of the impurity inside the **Rb** gas is achieved due to two-body collisions. The system represents the first realization of an ultracold gas doped with a known number of impurities interacting in the s -wave channel. One of the main difficulties for Bose gases is the lost due to three-body recombination processes: **Cs**-**Rb** - **Rb**. The three-body collision rate can be determined with unprecedented precision and it has been studied with single atom resolution event-by-event, yielding a precise value of the decay rate. In fact, for long times, if you look at the survival rate of **Rb** atoms, it is unaffected by the presence of **Cs** atoms. This makes sense, because we are observing the effect of a few **Cs** atoms in a reservoir of about 10^5 **Rb** atoms. However, for the **Cs** atoms the situation is quite different and their survival probability decays exponentially with time and the only mechanism of losses is the molecule formation through a

three-body recombination.

In Fig. [2.8,A] ^{133}Cs atoms are immersed in an ultracold gas of ^{87}Rb (see Ref. [87]). The ^{87}Rb atoms are precooled in a magnetic trap and they are prepared in the initial state $|F = 1, m_F = 0\rangle$. The ^{133}Cs atoms are captured within close vicinity in a magneto-optical trap (MOT). The two species are then loaded in a one-dimensional optical lattice at separated lattices sites (see Fig. [2.8,B]) and the Cs MOT is switched off. The Cs atoms have a temperature of the order of $30\ \mu\text{K}$ which is still too hot for the BEC of ^{87}Rb atoms. In order to lower further the temperature of the ^{133}Cs atoms, the ^{87}Rb cloud is loaded an optical lattice that is adiabatically lowered. The single ^{133}Cs atoms oscillate in the trap together with the ultracold. Then the ultracold cloud is removed and the temperature of the ^{133}Cs atoms is measured. For an interaction time between the atoms and the cloud of $40\ \text{ms}$ the Cs atoms reaches a temperature on the order of $1\ \mu\text{K}$ in the crossed trap. If the interaction time is increased to $150\ \text{ms}$, the ^{133}Cs atoms achieve a temperature of $T = 500\ \text{nK}$. The Rb gas possess on the order of hundreds of nK .

One of the remarkable results of the experiment is the immersion of single Cs atoms into an ultracold gas of Rb atoms despite the strong repulsive interactions which yield to phase separation of the two components for a large number of impurities.

Chapter 3

Quantum Monte-Carlo Methods

This chapter deals with the main features of Quantum Monte-Carlo (QMC) methods. In particular both the Variational Monte-Carlo (VMC) and the Diffusion Monte-Carlo (DMC) techniques are discussed. This chapter opens by recalling some preliminary concepts such as random variables, probability distributions, Markov chains and the Metropolis algorithm. Later on, the details of the QMC methods are explained. The end of the chapter is devoted to the probability distributions, trial wave functions and measurements of observables employed in the QMC algorithms used in this thesis.

3.1 Introduction

The outline of the chapter is as follows: first, we mention the importance of numerical tools in order to address some many-body theoretical problems in physics, in particular the importance of QMC. Subsequently we highlight the advantage of QMC with respect to other widely used tools in theoretical physics. In order to explain the numerical methods used in this thesis, some preliminary concepts are required. We review some basic concepts such as random variables, probability distributions and the Metropolis algorithm.

Once the basic concepts have been reviewed, the details of the QMC methods are explained. We start first with the VMC technique and subsequently DMC is introduced. At the end of the chapter we explain some technical details of the method by applying the QMC method to a specific model: the hard-sphere Bose gas at $T = 0$.

3.2 Analytical vs numerical tools. Why Monte-Carlo methods?

The quantum mechanics of many-body systems is a complex problem that requires powerful methods able to solve the Schrödinger equation. In attempting to solve this equation in a many-body quantum system we deal with many degrees of freedom. For instance, in a system such as a 3D Bose gas in a box, the number of degrees of freedom is $3N$ which is typically a huge number and multi-dimensional integrals in general cannot be computed analytically. Many exotic properties such as superconductivity and superfluidity are consequence of the interactions present in the system. There are many tools that have been derived to tackle the problem of interacting particles. Depend on the specific problem, for instance: long or short-range interactions, few or many-body systems, atoms in a lattice, atoms in a trap. There are methods that can describe some properties with better accuracy compared to others. For instance, the density functional theory (DFT) is a computational method widely used to investigate the electronic structure of many body systems where the relevant quantities are calculated by using an energy functional. However, in more realistic model where exchange and correlation must be included, the method does not provide an accurate description. Moreover, one of the limitation of the method is the number of particles which will increase the computational time. Mean field methods rely on a Hamiltonian that does not include strong correlations. Therefore, the applicability of these methods is limited to regimes of weak interaction between particles. In this thesis we use a numerical method, the quantum Monte-Carlo method, that is intrinsically non perturbative.

The QMC methods are a class of numerical methods based on the use of sequences of random variables and probability distribution functions. QMC methods allows for a direct representation of many body effects using a specific probability distribution function (pdf). The main advantage is, the calculation of multidimensional integrals involving the many-body wavefunction. Moreover, in aiming to calculate the ground-state properties of the many-body system, one finds that the degrees of freedom of the quantum system could be strongly coupled and analytical methods are not reliable anymore. The goal in this thesis is to use QMC methods to study a strongly coupled quantum degenerate Bose system.

The physical properties of various Bose condensed many-body systems have been successfully investigated using QMC methods. In particular, VMC was used to investigate the ground-state properties of superfluid ^4He [88] based on the variational principle. In the VMC method, the modulus square of the wave function of the system gives the probability distribution function in the configuration space. The ground-state properties of superfluid ^4He such as: the ground-state energy, the static structure factor, the momentum distribution and the one-body

density matrix were investigated using another Monte-Carlo technique based on the Green's function formalism: the Green's function Monte-Carlo method (GFMC). This method samples a probability distribution function proportional to the exact ground-state wavefunction and provides the exact value of the ground-state energy within statistical uncertainty. Similarly to the GFMC, the DMC method solves the Schrödinger equation in imaginary time using a short-time approximation for the Green's function. This technique was introduced for the first time in Ref. [89]. In order to address the many-body problem at finite temperatures, the path integral Monte-Carlo (PIMC) has been developed [90, 91]. This method is based on the isomorphism between the partition function of quantum particles in the canonical ensemble and classical polymers. Theoretically it has been shown that the thermodynamic properties of Bose systems are exactly equivalent to those of a type of interacting classical "ring polymers" [92]. More recently, Diagrammatic Monte-Carlo (DiagMC) was introduced as a technique aiming to calculate quantities specified in terms of diagrammatic expansions [7].

The so-called sign problem displayed by Fermi systems, as a consequence of the fundamental quantum mechanical principle which requires antisymmetrization of the many-body wave function with respect to particles exchange, greatly affects both the DMC and GFMC approaches. Nevertheless, the fixed-node diffusion Monte-Carlo method (FNDMC) is used to deal with this problem: the nodes of the ground-state wavefunction are chosen to coincide with the nodes of a trial wave function. Since the nodes of the ground-state wavefunction are generally unknown, the FNDMC method is only capable to provide an upper bound to the exact ground-state energy.

So far, we have seen that QMC techniques are well suited in the study of quantum degenerate systems, exhibiting strong correlations. Before developing the full theory of the specific methods used in this thesis, some preliminary concepts of stochastic methods are introduced.

3.3 Preliminary Concepts

The appropriate probability distribution function that describes a physical system is normally obtained using a (pseudo)-random number generator. The probability distribution function for equilibrium systems is defined for the different thermodynamic ensembles: microcanonical, canonical or grand-canonical. At $T = 0$, the probability distribution function coincides with the modulus square of the ground-state wave function.

A random variable is defined as the result obtained in a stochastic process which has no control on the initial conditions. For instance, the direct result of throwing a die, is one of the numbers contained in the sequence $x = \{1, 2, 3, 4, 5, 6\}$. x is called a *random variable*. Strictly speaking, it might be thought that by analyzing the initial conditions of the motion of the

die this process is deterministic. Nevertheless, due to the partial knowledge of the initial conditions, the process can be associated to a **probability distribution function (pdf)**. In our example, the probability of getting any of the values of x is $1/6$. The random variable x is further characterized by the domain of all the possible values that x can take. The random variable can be either discrete or continuous. In our example, the domain is the set of integers $\{1, 2, 3, 4, 5, 6\}$ and x is a discrete random variable. A random number can be generated by a compiler generator that relies on iterative operations with a long recurrence cycle. In particular, one may produce a (pseudo)-random integer N_1 between $(0, N)$ by using standard routines present in literature. The distribution of numbers generated between 0 and N is homogeneous and approximately random. Nevertheless the series of numbers is deterministically given once starting the generator and repeats itself after a certain period. For this reason the term (pseudo)-random numbers is more appropriate.

We define two **pdf's** that are particularly important in the context of our work: the uniform and the Gaussian distribution.

The **normalized uniform distribution** $U[a, b]$, whose domain is the real interval $[a, b]$ is written as:

$$f(x) = \frac{1}{b-a} \theta(x-a) \theta(b-x), \quad (3.1)$$

in terms of the Heaviside function $\theta(x)$. The most common type is when $a = 0$ and $b = 1$, denoted by $U[0, 1]$. This distribution is obtained by sampling $y = a + (b-a)x$ with $x \in U[0, 1]$.

Another important pdf is the **Gaussian distribution** defined as:

$$f(x) = \frac{1}{\sqrt{2\pi}\sigma} \exp \frac{-(x-\mu)^2}{2\sigma^2}, \quad (3.2)$$

where μ is the mean and σ the standard deviation. An special case is the Gaussian distribution with $\mu = 0$ and $\sigma = 1$, denoted $N(0, 1)$ and it is sampled by using the standard Box-Muller algorithm [93]. The Box-Muller algorithm is summarized as follows:

- Sample u_1 and u_2 independently from the uniform distribution $U[0, 1]$.
- Calculate y_1 and y_2 given by:

$$y_1 = \sqrt{-2 \log u_1} \cos(2\pi u_2). \quad (3.3)$$

$$y_2 = \sqrt{-2 \log u_1} \sin(2\pi u_2). \quad (3.4)$$

- y_1 and y_2 are two independent Gaussian random variables, with $\mu = 0$ and $\sigma = 1$.
- $y_i \rightarrow \sigma y_i + \mu$ with $i = 1, 2$.

The expectation value of a function $h(x)$ weighed by a **pdf** $f(x)$ is given by

$$\langle h \rangle \equiv \int_a^b h(x)f(x)dx, \quad (3.5)$$

where $x \in [a, b]$ the domain of the **pdf**. In particular if $h(x) = x$ one finds that $\langle h \rangle = \langle x \rangle$, the mean value of the **pdf**. On the other hand, if $h(x) = (x - \langle x \rangle)^n$, the expectation value of this function is written as,

$$\langle h \rangle = \int_a^b (x - \langle x \rangle)^n f(x)dx \quad n > 1 \quad (3.6)$$

This expectation value determines the $n - th$ moment of the distribution. In particular

- For $n = 1$, $\langle h \rangle = \langle (x - \langle x \rangle) \rangle = \langle x \rangle - \langle x \rangle = 0$.
- For $n = 2$, $\langle h \rangle = \langle (x - \langle x \rangle)^2 \rangle = \langle x^2 \rangle - \langle x \rangle^2 \equiv \sigma^2$.

The second moment ($n = 2$) is called the variance of the probability distribution and very often its square root is used, which corresponds to the standard deviation $\sigma = \sqrt{\langle x^2 \rangle - \langle x \rangle^2}$.

One of the principal features of the Gaussian distribution is the connection with the **Central limit theorem (CLT)**. The CLT states that the mean value of many random variables independently drawn from the same distribution is distributed according to a Gaussian **pdf** regardless of the form of the original distribution. In other words, let us define $\{x_n\}$ a random sequence of N independent and identically distributed variables drawn from **pdf** $f(x)$ with expectation value μ and standard deviation σ , then the sample average z defined as

$$z = \frac{\sum_{i=1}^N x_i}{N}, \quad (3.7)$$

converge to a Gaussian distribution as N approaches infinity.

$$g(z) \underset{N \rightarrow \infty}{=} \frac{1}{\sqrt{2\pi}(\sigma/\sqrt{N})} \exp \frac{(z - \mu)^2}{2(\sigma/\sqrt{N})^2}. \quad (3.8)$$

In fact, $\langle z \rangle = \mu$ and $\sigma_g^2 = \sigma_f^2/N$.

In other words, the CLT says that the mean of the probability distribution $f(x)$ is found as the average over N realizations of x . The corresponding standard deviation is decreasing with $1/\sqrt{N}$.

The big versatility of the CLT is not limited only to the calculation of expectation values but also to more general integrals. For instance

$$I = \int_b^a h(x) dx, \quad (3.9)$$

that can be rewritten as:

$$I = (b - a) \int_b^a h(x) f(x) dx, \quad (3.10)$$

where $f(x)$ is the uniform **pdf** $U[a, b]$ defined in Eq. [3.1]. So, the previous integral is considered as the expectation value of the function $h(x)$ on the distribution $f(x)$, namely

$$I = (b - a) \langle h \rangle. \quad (3.11)$$

From the CLT follows that the expectation value $\langle h \rangle$ can be estimated as the average of a large set of $h(x_i)$, where the random variable is sampled from a uniform distribution.

$$\langle h \rangle \approx \frac{1}{N} \sum_{i=1}^N h(x_i), \quad (3.12)$$

and the corresponding variance is $\sigma^2 = \sigma_h^2/N$. Where σ_h^2 is given by:

$$\sigma_h^2 \approx \frac{1}{N} \sum_{i=1}^N (h(x_i) - \langle h \rangle)^2, \quad (3.13)$$

is the intrinsic variance associated to $h(x)$.

The main conclusion drawn is that the variance of the integral σ^2 depends on both $h(x)$ and the number of samples N . On the other hand, the variance of the function $h(x)$ depends merely on $h(x)$. Regardless the functional form of $h(x)$, the variance of the integral σ_h^2 could be reduced if the number N is increased. This procedure can be optimized by using **importance sampling** that reduces the variance of the integral significantly. However what is the motivation for this technique?

We would like to address the question in the case of a specific physical problem. In many cases, we are interested in the calculation of the expectation value of a physical observable \mathcal{O} ,

$$\langle \mathcal{O} \rangle = \frac{\int d\mathbf{R} \mathcal{O}(\mathbf{R}) f(\mathbf{R})}{\int d\mathbf{R} f(\mathbf{R})}. \quad (3.14)$$

Here \mathbf{R} is the position vector of the N particles in the system $\mathbf{R} = (\mathbf{R}_1, \mathbf{R}_2, \dots, \mathbf{R}_N)$. In particular, in quantum mechanics $f(\mathbf{R}) = |\psi(\mathbf{R})|^2 / \int d\mathbf{R} |\psi(\mathbf{R})|^2$, where $\psi(\mathbf{R})$ is the wavefunction of the system. In principle, an integral as the one in Eq. [3.14] can be approximated by a sum with a finite number of terms. However, since dealing with many degrees of freedom is synonymous of solving high-dimensional integrals, the previous scheme is not adequate.

The integral Eq. [3.14] can be written as:

$$\langle \mathcal{O} \rangle = \frac{\int d\mathbf{R} \mathcal{O}(\mathbf{R}) f(\mathbf{R})}{\int d\mathbf{R} f(\mathbf{R})} = \frac{1}{M} \sum_{\nu=1}^M \mathcal{O}(\mathbf{R}_\nu). \quad (3.15)$$

In practice, the evaluation of averages by using random numbers is simple. We choose the state of the system characterized by a certain number of parameters, defining the microscopic state. All the possible configurations of these degrees of freedom contribute to the quantum average and are weighted according to a **pdf** $f(\mathbf{R})$. Then, a couple of questions arising are:

- Is it possible to choose, states that are known to be more relevant to the sum Eq.[3.15]?
- Some physical information of the system will give a clue about the a clever sampling in order to reduce the variance and therefore the simulation time?

The answer is yes and it was given by Metropolis [94] by using the importance sampling technique. Next, we will discuss the general idea of this technique.

3.3.1 Importance Sampling

The expectation value of the observable O is given by

$$\langle O \rangle = \int_a^b dx f(x) O(x), \quad (3.16)$$

over a given **pdf** $f(x)$. By means of the CLT, it is possible to estimate the previous integral as:

$$O_N = \frac{1}{N} \sum_{i=1}^N O(x_i), \quad (3.17)$$

and the points x_i are sampled according to the **pdf** $f(x)$. For large values of N , O_N converges to $\langle O \rangle$

$$\langle O \rangle = O_N \pm \sigma_N, \quad (3.18)$$

here $\sigma_N = \sigma_O/\sqrt{N}$ gives the statistical error decreasing with the square root of the number of independent points and σ_O is the variance associated with the expectation value of O , namely:

$$\sigma_O^2 \equiv \int_a^b dx f(x) [O^2(x) - \langle O \rangle^2]. \quad (3.19)$$

There is a way to reduce the variance σ_O associated with the expectation value of $\langle O \rangle$ by introducing a different **pdf** namely $h(x)$ as follows:

$$\langle O \rangle = \int_a^b dx f(x) O(x) = \int_a^b dx h(x) \frac{f(x)}{h(x)} O(x) \equiv \int_a^b dx h(x) G(x), \quad (3.20)$$

where $G(x) \equiv O(x)f(x)/h(x)$. Even though the expectation value does not change: $\langle O \rangle_f = \langle G \rangle_h$ the variance can differ significantly:

$$\sigma_G^2 = \int_a^b dx h(x) [G^2(x) - \langle O \rangle^2] = \int_a^b dx h(x) \left[\frac{f^2(x)}{h^2(x)} O^2(x) - \langle O \rangle^2 \right]. \quad (3.21)$$

In particular $\sigma_G^2 < \sigma_O^2$ if the ratio $f(x)/h(x)$ is on average smaller than 1.

3.3.2 Stochastic Process and Metropolis Algorithm $M(RT)^2$

Sometimes the **pdf** to be sampled is not simple as the Gaussian **pdf** defined in the previous section. Metropolis [94] developed a stochastic algorithm which generates asymptotically a set of random numbers according to a given **pdf**. This algorithm is based on a random walk in a multidimensional space. It relies on the Markov chain concept of stochastic processes. The main advantage of the Metropolis algorithm $M(RT)^2$ is that it can be used to sample any **pdf** regardless of analytic complexity and the disadvantages are that the sampling from a given **pdf** is correct only asymptotically and the sampling is correlated.

A stochastic process is defined as a discrete sequence of random variables, for instance $s = \{s_1, s_2, \dots, s_M, \dots\}$. Each one distributed according to a specified **pdf** $f_n(s_n)$. Let us define the transition matrix of s_n as a probability that depends of the previous elements of the random sequence, i.e $P(s_n | s_{n-1}, s_{n-2}, \dots, s_1)$. Therefore, the sequence s is a Markov process if the transition matrix of $\{s_n\}$ depends exclusively on the previous state s_{n-1} for all n . The previous statement can be formally written in the form:

$$P(s_n | s_{n-1}, s_{n-2}, \dots, s_1) = P(s_n | s_{n-1}). \quad (3.22)$$

In general, the transition matrix P_{ij} to get to the state $s_n = j$ from the state $s_{n-1} = i$, must

fulfill both: 1) $0 \leq P_{ij} \leq 1$ and 2) $\sum_i P_{ij} = 1$. A Markov process is memory-less process: predictions for the future of the process are based solely on its present state.

The evolution of the probability distribution is described by

$$f_n(s_n = j) = \sum_i f_{n-1} P_{ij}(s_{n-1} = i), \quad (3.23)$$

in fact Eq. [3.23] gives the probability $f_n(s_j)$ of being in the state s_j from a previous state s_i with probability $f_{n-1}(s_i)$. The generalization to the continuous is straightforward:

$$f(x) = \int dy P(x \rightarrow y) f(y). \quad (3.24)$$

An initial **pdf** f_0 converges to the equilibrium **pdf** by the application of the transition matrix \mathbf{P} at many successive steps:

$$f_n = \mathbf{P} f_{n-1} = \mathbf{P}^n f_0. \quad (3.25)$$

In order to ensure ergodicity, any state s_j should be reached from a different state s_i , i.e. $P_{ij} > 0$ for at least one $j(\neq i)$. Detailed balance is guaranteed when:

$$f(j)P_{ij} = f(i)P_{ji} \quad \forall i, j \quad (3.26)$$

being f the equilibrium distribution. The Metropolis–Hastings [94] is a Markov chain algorithms for sampling a given probability distribution $f(x)$. Before getting to the sampling in the Metropolis algorithm; we introduce the configuration space used in MC.

In the configuration space, the position of a particle j is described by the vector $\mathbf{R}_j = (x_j, y_j, z_j)$ with $j = 1, \dots, N$; being N the total number of particles in the simulation. However, it would be more convenient from the statistical point of view, rather than using a single configuration, to use W of them. Each configuration represent a possible state for the system. A more suitable configuration space for MC is formed by N particles distributed in W walkers. The configuration space can be represented as:

$$\mathbf{R} = \begin{pmatrix} (\mathbf{R}_1)_1 & (\mathbf{R}_1)_2 & \cdots & (\mathbf{R}_1)_W \\ (\mathbf{R}_2)_1 & (\mathbf{R}_2)_2 & \cdots & (\mathbf{R}_2)_W \\ \vdots & \vdots & \vdots & \vdots \\ (\mathbf{R}_N)_1 & (\mathbf{R}_N)_2 & \cdots & (\mathbf{R}_N)_W \end{pmatrix}, \quad (3.27)$$

here $(\mathbf{R}_j)_m$ is the position of the j – *th* particle in the m – *th* walker with $j = 1, \dots, N$ and $m = 1, \dots, W$. Averages of a given observable can be computed over a large number of walkers.

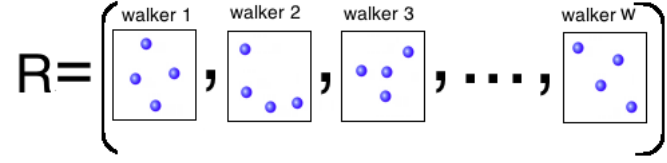


Figure 3.1: Representation of the matrix [3.27]: each column of the matrix is a state where the system lies. In our example we have $N = 4$ particles distributed on W walkers.

The transition matrix in the Metropolis–Hastings algorithm that satisfies detailed balance is obtained as follows

$$P(x \rightarrow y) = T(x \rightarrow y)A(x \rightarrow y), \quad x \neq y \quad (3.28)$$

where $T(x \rightarrow y)$ is defined as an arbitrary conditional probability which one is able to directly sample with a proposed state y , given a previous state x and $A(x \rightarrow y)$ is called the acceptance probability of the move. The acceptance probability is defined as:

$$A(x \rightarrow y) = \min \left(1, \frac{f(y) T(y \rightarrow x)}{f(x) T(x \rightarrow y)} \right). \quad (3.29)$$

This acceptance probability is constructed in such a way that P (defined in Eq. [3.28]) fulfills detailed balance and drives the Markov chain into the equilibrium **pdf**. In particular, we use T as a Gaussian distribution defined as $T(x \rightarrow y) = \frac{1}{\sqrt{2\pi}\sigma} \exp\left(-\frac{(x-y)^2}{2\sigma^2}\right)$ that depends merely on $|x - y|$ and it has a variance σ . The acceptance probability yields a simple expression given by

$$A(x \rightarrow y) = \min \left(1, \frac{f(y)}{f(x)} \right). \quad (3.30)$$

The Metropolis algorithm with the acceptance-rejection step is summarized as follows:

- **Step 1:** Start from a population of W walkers randomly distributed in the space of configurations, example Fig. [3.1].
- **Step 2:** For each walker W at the position $(\vec{x})_W = x$. Sample a “tentative” new vector $(\vec{y})_W = y'$ through the matrix $T(x \rightarrow y')$.
- **Step 3:** Compute the acceptance rate $A = \frac{f(y')T(y' \rightarrow x)}{f(x)T(x \rightarrow y')}$.
- **Step 4:** If A is larger than 1 the move is accepted. Then, the configuration is updated: $y' = y$.
 - Else, a new number z is generated from a uniform distribution $z \in U[0, 1]$.

- if $A = \frac{f(y')T(y' \rightarrow x)}{f(x)T(x \rightarrow y')} \geq z$ the configuration is accepted and the configuration is updated. Otherwise, y' is not accepted and $y = x$.

In the case of continuous process, moves are usually proposed using a simple and fast transition matrix $T(x \rightarrow y)$, where $x = y + \sigma\xi$, with σ a constant and $\xi \in U(-1, 1)$ or $\xi \in N(0, 1)$. The stationary distribution $f(x)$ is reached after some equilibration time. An important number that should be under control is the rate acceptance, defined as $\mathcal{A} = N_{accepted}/N_{total}$, where $N_{acceptance}$ and N_{total} stand for the accepted and the total number of moves respectively. Notice that if σ is small the acceptance rate becomes large, and there is a strong correlation between moves. On the other hand, if σ is large the acceptance rate is small and the point in configuration space rarely moves. In an efficient algorithm σ is tuned such that the acceptance rate is in the range 0.4 – 0.7. For an equilibrium Markov chain, ergodicity claims that the temporal average can be replaced by the average on ensembles. Then, rather than using one single walker it is more efficient to use a large number of them in order to perform the random walks independently. Expectation values of the observables are obtained by averaging over the walkers.

In a Markov chain the current configuration depends on the previous one, therefore correlations always exist. Straightforwardly if one desires to calculate the expectation value of an observable O , the CLT cannot be applied directly since it is based on the calculation of expectation values on a set of independent points in the configuration space. In order to overcome this situation one divides the calculation in Nb blocks such that averages of different blocks are no longer correlated. This is true if the length Nb of a single block is larger than the correlation length of Markov chain for a given observable. The specific algorithm of block averages is explained in appendix A.

The basic preliminary concepts needed in order to address Monte-Carlo techniques have been discussed. Now, we will review the main features of the QMC methods and we will start by discussing the QMC method based on the variational principle.

3.4 Variational Monte-Carlo (VMC)

In this section the Variational Monte-Carlo (VMC) method is discussed. It is based on both the evaluation of multidimensional integrals using the Metropolis algorithm $M(RT)^2$ and on the variational principle. The ground-state properties of a many-body system can be investigated by solving the many-body Schrödinger equation:

$$\mathcal{H}\psi_i(\mathbf{R}) = E_i\psi_i(\mathbf{R}), \tag{3.31}$$

where $\psi(\mathbf{R})$ is the wave function of the system and \mathbf{R} represents the DN -dimensional configuration vector formed by N particles in the D dimensional space. The Hamiltonian can be written as:

$$\mathcal{H} = -\frac{\hbar^2}{2m} \sum_{i=1}^N \nabla_i^2 + \sum_{i=1}^N U(\mathbf{r}_i) + \sum_{i<j} V(\mathbf{r}_i - \mathbf{r}_j), \quad (3.32)$$

where the first term is the kinetic contribution, the second is the one-body potential that describes an external field and the latter term is the two-body potential accounting for the interaction between particles. The study of the ground-state energy and the excitation spectrum of liquid ^4He have been addressed with VMC for first time by Millan [88].

The VMC method is based on the variational principle, which states that the expectation value of the Hamiltonian calculated using a trial wave function ψ_T gives an upper bound to the ground-state energy. Therefore, it is possible to estimate the energy without the complete knowledge of the exact ground-state wavefunction of the system. The previous statement is summarized as:

$$E_T \equiv \frac{\int d\mathbf{R} \psi_T^*(\mathbf{R}) \mathcal{H} \psi_T(\mathbf{R})}{\int d\mathbf{R} |\psi_T(\mathbf{R})|^2} = \frac{\sum_i |c_i|^2 E_i}{\sum_i |c_i|^2} \geq E_0, \quad (3.33)$$

where E_0 is the lowest eigenstate of \mathcal{H} and ψ_T is the trial wave function that can be expanded in terms of eigenfunctions of the Hamiltonian \mathcal{H} , namely, $\psi_T = \sum_i c_i \psi_i$. So, $E_T \geq E_0$ for any ψ_T , and $E_T = E_0$ if and only if $\psi_T = c_0 \psi_0$.

The specific form of the trial wave function will be discussed at the end of this section. Since the variational principle is valid regardless of the statistics of the particles, the VMC method is suitable for both bosons and fermions.

The trial wave function must contain a set of variational parameters $\{a_i\}$ in such a way that the minimization of the energy is performed with respect to these parameters. Namely,

$$\psi_T = \psi_T(\mathbf{R}; a_1, a_2, \dots, a_N). \quad (3.34)$$

In Section 3.6 we will discuss the specific form of the trial wave function used in our study.

Let us suppose we want to calculate the expectation value of the Hamiltonian \mathcal{H} namely

$$\langle \mathcal{H} \rangle = E_T = \int d\mathbf{R} f(\mathbf{R}) E_L(\mathbf{R}), \quad (3.35)$$

where $E_L \equiv \mathcal{H} \psi_T(\mathbf{R}; \{a\}) / \psi_T(\mathbf{R}; \{a\})$ stands for the local energy and the **pdf** is given by:

$f(\mathbf{R}) = |\psi_T(\mathbf{R}; \{a\})|^2 / \int d\mathbf{R} |\psi_T(\mathbf{R}; \{a\})|^2$. Then, the aim of the VMC method is to compute the integral

$$E_T = \frac{\int d\mathbf{R} |\psi_T(\mathbf{R}; \{a\})|^2 \frac{\mathcal{H}\psi_T(\mathbf{R}; \{a\})}{\psi_T(\mathbf{R}; \{a\})}}{\int d\mathbf{R} \psi_T^*(\mathbf{R}; \{a\}) \psi_T(\mathbf{R}; \{a\})}. \quad (3.36)$$

One evaluates this integral by calculating the energy as a function of the variational parameters $\{a\}$ and determinates the values of the parameters corresponding to the lowest energy.

Points from the **pdf** $f(\mathbf{R})$ are sampled using the Metropolis algorithm as follows:

- STEP 1: start from an initial configuration $\mathbf{R} = \mathbf{R}_0$.
- STEP 2: generate a tentative new configuration $\mathbf{R}'^{(m)}$ corresponding to the $(m\text{-th}+1)$ iteration, using $\{\xi_i^{(m)}\}_{i=1}^N$, with $\xi_{ix}^{(m)}, \xi_{iy}^{(m)}, \xi_{iz}^{(m)} \in N(0, 1)$ (see Gaussian distribution $N(0, 1)$ [3.2]):

$$\mathbf{R}^{(m)} = (r_1^{(m)}, r_2^{(m)}, \dots, r_N^{(m)}) \rightarrow \mathbf{R}'^{(m)} \equiv (r_1^{(m)} + \sigma \xi_1^{(m)}, r_2^{(m)} + \sigma \xi_2^{(m)}, \dots, r_N^{(m)} + \sigma \xi_N^{(m)}), \quad (3.37)$$

where the random displacement is chosen to be distributed according to a Gaussian **pdf** with variance σ .

- STEP 3: if $\frac{|\psi_T(\mathbf{R}'^{(m)})|^2}{|\psi_T(\mathbf{R}^{(m)})|^2} \geq 1$, the move is accepted. Otherwise draw $z \in U(0, 1)$ and accept the move if $\frac{|\psi_T(\mathbf{R}'^{(m)})|^2}{|\psi_T(\mathbf{R}^{(m)})|^2} \geq z$.
- STEP 4: If $\mathbf{R}'^{(m)}$ is accepted then the configuration is updated: $\mathbf{R}^{(j+1)} \equiv \mathbf{R}'^{(j)}$, else the configuration remains in the old configuration: $\mathbf{R}^{(j+1)} = \mathbf{R}^{(j)}$.
- STEP 5: Repeat loop from STEP 2 to STEP 4.

After the equilibration time, one carries out the Monte-Carlo estimate:

$$E_T = E_M \pm \sigma_M, \quad (3.38)$$

where

$$E_M = \frac{1}{M} \sum_{i=1}^M E_L(\mathbf{R}_i), \quad (3.39)$$

and

$$\sigma_M = \frac{1}{\sqrt{M}} \left(\frac{1}{M} \sum_{i=1}^M E_L^2(\mathbf{R}_i) - E_M^2 \right)^{1/2}, \quad (3.40)$$

over a collection of statistically independent configurations \mathbf{R}_i ($i = 1, \dots, M$). Where $E_L(\mathbf{R}_i) = \mathcal{H}\psi_T(\mathbf{R}_i; \{a\})/\psi_T(\mathbf{R}_i; \{a\})$ is the local energy.

3.4.1 Time-dependent algorithm in VMC

For a real trial wavefunction $\psi_T(\mathbf{R})$, the **pdf** associated is given by $f(\mathbf{R}) = |\psi_T(\mathbf{R})|^2 / \int d\mathbf{R} |\psi_T(\mathbf{R})|^2$ and it is alternatively sampled by using a process based on the Fokker-Plank equation instead of the acceptance/rejection step used in the last section. The Fokker-Plank equation is given by

$$\frac{\partial f(\mathbf{R}, \tau)}{\partial \tau} = D \sum_{i=1}^N \nabla_i \cdot (\nabla_i - \mathbf{F}_i(\mathbf{R})) f(\mathbf{R}, \tau). \quad (3.41)$$

Here D is the diffusion coefficient $D = -\hbar^2/2m$ and $\mathbf{F}_i(\mathbf{R}) = (2\nabla_i\psi_T)/\psi_T$ is the drift quantum force.

The problem of sampling the time-dependent **pdf** $f(\mathbf{R}, \tau)$ is turned into the problem of finding the asymptotic solution of the Fokker-Planck Eq. [3.41]. The solution of the Fokker-Planck equation is given in terms of the Green's function as

$$f(\mathbf{R}, \tau) = \int d\mathbf{R}' \mathcal{G}(\mathbf{R}, \mathbf{R}', \tau) f(\mathbf{R}', \tau = 0), \quad (3.42)$$

where the Green's function $\mathcal{G}(\mathbf{R}, \mathbf{R}', \tau)$ satisfies the time-dependent equation

$$\frac{\partial \mathcal{G}(\mathbf{R}, \mathbf{R}', \tau)}{\partial \tau} = D \nabla_{\mathbf{R}} \cdot (\nabla_{\mathbf{R}} - \mathbf{F}(\mathbf{R})) \mathcal{G}(\mathbf{R}, \mathbf{R}', \tau), \quad (3.43)$$

with the boundary condition:

$$\mathcal{G}(\mathbf{R}, \mathbf{R}', \tau = 0) = \delta(\mathbf{R} - \mathbf{R}'). \quad (3.44)$$

By using the previous boundary condition, the solution of Eq. [3.43] is given by

$$\mathcal{G}(\mathbf{R}, \mathbf{R}', \tau) = \exp \left[D\tau \left(\nabla_{\mathbf{R}}^2 - \nabla_{\mathbf{R}} \cdot \mathbf{F}(\mathbf{R}) \right) \right] \delta(\mathbf{R} - \mathbf{R}'). \quad (3.45)$$

In general for a pair of non commutating operators $\hat{\mathbf{A}}$ and $\hat{\mathbf{B}}$ one can use the Trotter identity: $\exp \left[\tau (\hat{\mathbf{A}} + \hat{\mathbf{B}}) \right] \simeq \exp \left[\tau (\hat{\mathbf{A}}) \right] \exp \left[\tau (\hat{\mathbf{B}}) \right] \left(1 - \tau^2 [\hat{\mathbf{A}}, \hat{\mathbf{B}}] / 2 \right)$ valid in the limit of $\tau \rightarrow 0$. Then Eq. [3.45] is reduced to

$$\mathcal{G}(\mathbf{R}, \mathbf{R}', \tau) = \exp \left[D\tau \left(\nabla_{\mathbf{R}}^2 \right) \right] \exp \left[-D\tau \nabla_{\mathbf{R}} \cdot \mathbf{F}(\mathbf{R}) \right] \delta(\mathbf{R} - \mathbf{R}') + \mathcal{O}(\tau^2), \quad (3.46)$$

and in the limit of small time-step $\delta\tau$. The total Green's function can be written as:

$$\mathcal{G}(\mathbf{R}, \mathbf{R}', \delta\tau) = \int d\mathbf{R}_1 \mathcal{G}_{Diffusion}(\mathbf{R}, \mathbf{R}_1, \delta\tau) \mathcal{G}_{Drift}(\mathbf{R}_1, \mathbf{R}', \delta\tau) + \mathcal{O}(\delta\tau^2), \quad (3.47)$$

with $\mathcal{G}_{Diffusion}(\mathbf{R}, \mathbf{R}', \tau) = \exp[D\tau(\nabla_{\mathbf{R}}^2)]\delta(\mathbf{R} - \mathbf{R}') = \frac{\exp[-(\mathbf{R}-\mathbf{R}')^2/(4D\tau)]}{(4\pi D\tau)^{3N/2}}$ and $\mathcal{G}_{Drift}(\mathbf{R}, \mathbf{R}', \tau) = \exp[-D\tau\nabla_{\mathbf{R}} \cdot \mathbf{F}(\mathbf{R})]\delta(\mathbf{R} - \mathbf{R}') = \delta(\mathbf{R}(\tau) - \mathbf{R}')$ with $\mathbf{R}(\tau)$ satisfies the equation $d\mathbf{R}(\tau)/d\tau = D\mathbf{F}(\mathbf{R}(\tau))$ and an initial condition $\mathbf{R}(\tau = 0) = \mathbf{R}$. Putting all terms together it yields

$$\mathcal{G}(\mathbf{R}, \mathbf{R}', \delta\tau) = \frac{\exp[-\mathbf{R}(\delta\tau) - \mathbf{R}']^2 / (4D\delta\tau)}{(4\pi D\delta\tau)^{3N/2}} + \mathcal{O}(\delta\tau^2). \quad (3.48)$$

Where the results for the $\mathcal{G}_{Diffusion}(\mathbf{R}, \mathbf{R}', \tau)$ and $\mathcal{G}_{Drift}(\mathbf{R}, \mathbf{R}', \tau)$ are obtained calculating the matrix elements $\langle \mathbf{R} | \exp[D\tau(\nabla_{\mathbf{R}}^2)] | \mathbf{R}' \rangle$ and $\langle \mathbf{R} | \exp[-D\tau\nabla_{\mathbf{R}} \cdot \mathbf{F}(\mathbf{R})] | \mathbf{R}' \rangle$ by projecting the operators on the momentum space $|\mathbf{P}\rangle$ and solving the respective N -dimensional Gaussian integrals.

The Green's function Eq. [3.48] gives the probability of moving from \mathbf{R} to \mathbf{R}' during the time interval $\delta\tau$ and using Eq. [3.42] one can find the temporal evolution of the **pdf** from an initial time τ to a final time $\tau + \delta\tau$. Namely:

$$\begin{aligned} f(\mathbf{R}, \tau + \delta\tau) &= \int d\mathbf{R}' \mathcal{G}(\mathbf{R}, \mathbf{R}', \delta\tau) f(\mathbf{R}', \tau) \\ &= \int d\mathbf{R}' \frac{\exp[-(\mathbf{R}(\delta\tau) - \mathbf{R}')^2 / (4D\delta\tau)]}{(4\pi D\delta\tau)^{3N/2}} f(\mathbf{R}', \tau). \end{aligned} \quad (3.49)$$

Notice that $f(\mathbf{R}, \tau \rightarrow \infty) = |\psi_T(\mathbf{R})|^2 / \int d\mathbf{R} \psi_T(\mathbf{R})|^2$. For the time evolution defined in Eq. [3.49] a linear algorithm can be devised which is correct to order linear in the time step $\delta\tau$. The drift step is carried out by $\mathbf{R} \rightarrow \mathbf{R}(\delta\tau) = \mathbf{R} + D\delta\tau\mathbf{F}(\mathbf{R})$ and the diffusion step by $\mathbf{R}(\delta\tau) \rightarrow \mathbf{R}' = \mathbf{R}(\delta\tau) + \sqrt{2D\delta\tau}\chi$ where $\chi_{x,(y,z)} \in N(0, 1)$ (Gaussian **pdf** with $\mu = 0$ and $\sigma = 1$).

Both the diffusion step and the drift step are affected by a time-step error and require an extrapolation to $\delta\tau = 0$. Nevertheless, the time-step bias can be eliminated by introducing an acceptance/rejection step similar to the Metropolis algorithm. The smart variational Monte-Carlo (SVMC) implements this step.

3.5 Smart Variational Monte-Carlo (SVMC)

The principal motivation of using SVMC is to eliminate the time-step dependence seen previously in the time-dependent algorithms by introducing an acceptance/rejection step similar to

the Metropolis algorithm $\mathbf{M}(\mathbf{R}\mathbf{T})^2$. In the Metropolis algorithm the proposed moves $\mathbf{R} \rightarrow \mathbf{R}'$ are accepted according to the probability:

$$A(\mathbf{R}, \mathbf{R}') = \min \left(1, \frac{f(\mathbf{R}') T(\mathbf{R}' \rightarrow \mathbf{R})}{f(\mathbf{R}) T(\mathbf{R} \rightarrow \mathbf{R}')} \right). \quad (3.50)$$

Since the transfer matrix is symmetric namely, the probability of proposing the move $\mathbf{R} \rightarrow \mathbf{R}'$ is equal to that of propose the move $\mathbf{R}' \rightarrow \mathbf{R}$. One obtains

$$A(\mathbf{R}, \mathbf{R}') = \min \left(1, \frac{|\psi_T(\mathbf{R}')|^2}{|\psi_T(\mathbf{R})|^2} \right). \quad (3.51)$$

Nevertheless, in the time-dependent algorithm the transfer matrix $\mathcal{G}(\mathbf{R}, \mathbf{R}', \tau)$ given by Eq. [3.46] is asymmetric and in general $\mathcal{G}(\mathbf{R}, \mathbf{R}', \tau) \neq \mathcal{G}(\mathbf{R}', \mathbf{R}, \tau)$. The modified acceptance probability must read as:

$$A(\mathbf{R}, \mathbf{R}') = \min \left(1, \frac{\mathcal{G}(\mathbf{R}', \mathbf{R}, \delta\tau) |\psi(\mathbf{R}')|^2}{\mathcal{G}(\mathbf{R}, \mathbf{R}', \delta\tau) |\psi(\mathbf{R})|^2} \right). \quad (3.52)$$

The acceptance/rejection step given by Eq. [3.52] can be implemented with the linear algorithm devised in the last section. Then the Green's function given by Eq. [3.48] is written as

$$\mathcal{G}(\mathbf{R}, \mathbf{R}', \delta\tau) = \frac{\exp[-\mathbf{R} + D\delta\tau\mathbf{F}(\mathbf{R}) - \mathbf{R}']^2 / (4D\delta\tau)}{(4\pi D\delta\tau)^{3N/2}}, \quad (3.53)$$

and the acceptance probability becomes

$$A(\mathbf{R}, \mathbf{R}') = \min \left(1, \exp[Q(\mathbf{R}, \mathbf{R}', \delta\tau)] \frac{|\psi(\mathbf{R}')|^2}{|\psi(\mathbf{R})|^2} \right), \quad (3.54)$$

where

$$Q(\mathbf{R}, \mathbf{R}', \delta\tau) = \frac{[\mathbf{F}(\mathbf{R}) + \mathbf{F}(\mathbf{R}')]}{2} \cdot \left(D\delta\tau \frac{[\mathbf{F}(\mathbf{R}) - \mathbf{F}(\mathbf{R}')]}{2} - (\mathbf{R} - \mathbf{R}') \right). \quad (3.55)$$

The SVMC is called *smart* because it tends to move walkers according to the drift quantum force. The SVMC method was introduced for the first time in addressing the problem of Brownian motion in aqueous solutions [95]. In summary SVMC provides the correct sampling of $f(R)$ with a new transition probability defined by Eq. [3.53] and an acceptance probability defined by [3.54] in order to make the sampling independent of the time step. for instance, in Fig. [3.2] the ground-state energy per particle for $N_B = 64$ bosons in a box with $n_B a^3 = 10^{-5}$ ($n_B = N_B/V$) is calculated with the SVMC algorithm and this energy does not display a dependence with the time.

Now we turn our attention to the specific form of the trial wave function Eq. [3.34] for the

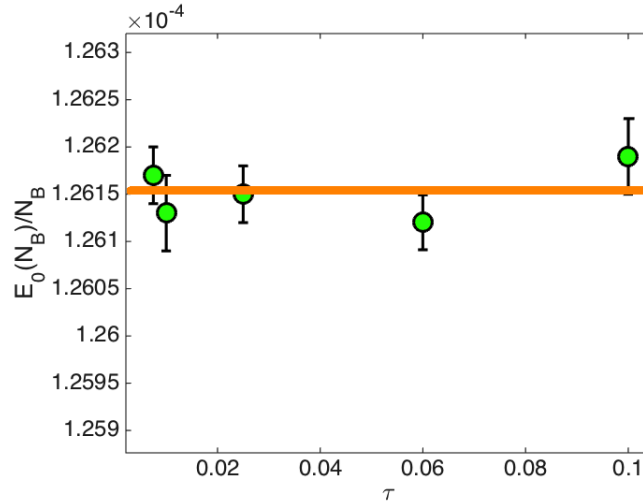


Figure 3.2: **The ground-state energy per particle is calculated with the SVMC.** Green points represent the SVMC data and orange line represents the linear fitting. The time dependent VMC algorithms [3.4.1] are affected by a time-step bias. By using the SVMC that relies on a transition probability defined by Eq. [3.53] and an acceptance probability given by Eq. [3.54] the time-step dependence is eliminated.

different potentials we used in this thesis.

3.6 Trial wave functions

We consider the simulation of an infinite homogeneous system. The calculation is carried out by using the *periodic boundary conditions (p.b.c)*: N particles are placed in a cubic box of size L and the box is virtually repeated in space by considering image particles in the nearest neighboring boxes. Then, when a particle leaves the box on one side an image particle enters the box from the opposite side Fig [3.3]. The use of virtual particles should not introduce

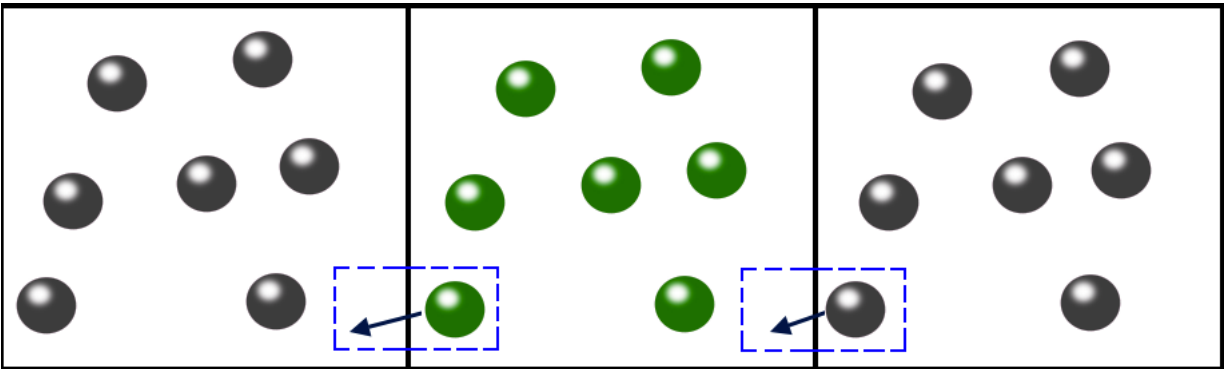


Figure 3.3: **Periodic boundary conditions (p.b.c)**: when a particle (green) leaves the box on the left side, a virtual particle (gray) enters the box on the right side.

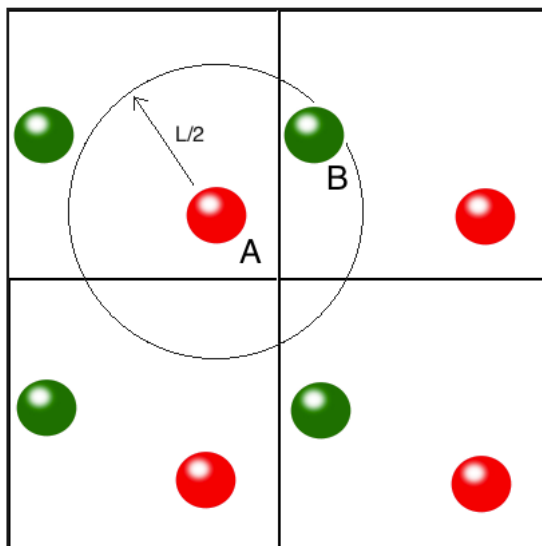


Figure 3.4: Cut off radius $r < L/2$ for inter-particle correlations. Particle B lies inside the radius and images of particle B lies outside.

spurious correlations. Correlations between particles A and the image particle B are real and must be considered, however those between A and the other image particles B are not real and should be neglected. If the inter-particle distance is smaller than the cut-off $L/2$ these spurious correlations can be avoided as it is shown in Fig. [3.4].

We consider a dilute gas of N bosonic particles at $T = 0$ described by the following Hamiltonian:

$$\mathcal{H} = -\frac{\hbar^2}{2m_B} \sum_{i=1}^N \nabla_i^2 + \sum_{i<j} V_B(r_{ij}) \quad (3.56)$$

Here, the Hamiltonian is splitted in the kinetic energy and the interaction energy of the bosonic system consisting of particles of mass m_B and interacting through the two-body potential $V_B(r_{ij})$, which depends on the distance $r_{ij} = |\mathbf{r}_i - \mathbf{r}_j|$ between a pair of bosons.

We can write the trial wave function of bosons in the form

$$\psi_J(\mathbf{R}) \equiv \prod_{i<j} f(r_{ij}), \quad (3.57)$$

where $f(r_{ij})$ is called the *two-body Jastrow correlation function* and it depends on the inter-particle distance $r_{ij} = |\mathbf{r}_i - \mathbf{r}_j|$. In order to be compatible with the **p.b.c** defined above, one must impose a condition at the cut-off radius of correlations by requiring that $f(\mathbf{r}) = \text{constant}$ for $r \geq L/2$. This implies that $df(r = L/2)/dr = 0$ as a boundary condition on the Jastrow factor.

In the following, we will discuss the particular forms of the potential $V_B(r_{ij})$ and their respective Jastrow functions $f(r)$.

3.6.1 Potential 1: Hard sphere (HS)

The inter-boson potential $V_B(r_{ij})$ is modeled by the hard-sphere interaction described by:

$$V_B(r) = \begin{cases} +\infty & r \leq a \\ 0 & r > a \end{cases} \quad (3.58)$$

The main parameter of the system is given by $n_B a^3$ where $n_B = N_B/V$ is the density of the gas and a is the range of the interaction. In the HS potential a coincides with the s -wave scattering length.

The general Jastrow wave function Eq. [3.57] for the **HS** potential is found by solving the two-body Schrödinger equation, namely

$$\left[\frac{-\hbar^2}{2m_R} \nabla^2 + V_B(r) \right] f(r) = E f(r), \quad (3.59)$$

where m_R is the reduced mass $m_R = m_1 m_2 / (m_1 + m_2)$ and $r = |r_1 - r_2|$ is the distance between the particles. The form of the boson-boson wave function is,

$$f(r) = \begin{cases} 0 & r \leq a \\ \sin k(r - a)/r & a \leq r \leq L/2 \\ (2/L) \sin k(L/2 - a) & r \geq L/2 \end{cases} \quad (3.60)$$

where the value of the wave vector k is chosen in such a way that the first derivative of the function vanishes at $r = L/2$ ($f'_B(r = L/2) = 0$) in order to be consistent with **p.b.c** as it was pointed out in the previous section. The wavefunction and its first derivative are continuous functions at $r = L/2$. The value of k is found by solving the transcendental equation

$$\tan [k(L/2 - a)] = kL/2. \quad (3.61)$$

3.6.2 Potential 2: Attractive square-well (ASW) potential

The interaction between the impurity and the bosons can be conveniently modeled by an attractive square well (**ASW**) potential defined by:

$$V(\mathbf{r}) = \begin{cases} -V_0 & r \leq R_0 \\ 0 & r > R_0 \end{cases} \quad (3.62)$$

The **ASW** potential is characterized by the potential range R_0 and the depth V_0 . These values are chosen such as to give the value b of the scattering length which is determined by the transcendental equation:

$$b = R_0 \left[1 - \frac{\tan(K_0 R_0)}{K_0 R_0} \right], \quad (3.63)$$

where $K_0^2 = 2m_R V_0 / \hbar^2$ in terms of the reduced mass $m_R = m_I m_B / (m_I + m_B)$. The impurity-boson scattering length b is tuned by changing either the depth or the range of the potential. In the case of the repulsive **HS** potential the scattering length is always positive, whereas for the **ASW** potential the value of the scattering length can be either positive or negative depending on $K_0 R_0$. In particular, we use values in the range $0 < K_0 R_0 < \pi$, corresponding to no bound state ($0 < K_0 R_0 < \pi/2$) and a single bound state ($\pi/2 < K_0 R_0 < \pi$) for the two-body problem. In this latter case the molecular binding energy ϵ_B is obtained from the transcendental equation

$$\frac{\tan(\kappa R_0)}{\kappa R_0} = \frac{\hbar}{R_0 \sqrt{2m_R |\epsilon_b|}}. \quad (3.64)$$

This equation is obtained by requiring both the continuity of the wave function and of its first derivative at $r = R_0$. In Eq. [3.64], $\kappa^2 = 2m_R (V_0 - |\epsilon_b|) / \hbar^2$. The particular value $K_0 R_0 = \pi/2$ corresponds to the resonance (also known as unitary limit), where the s -wave scattering length diverges and the bound-state energy vanishes.

In other words with the **ASW** potential we can tune the interaction between the two particles either attractive when $K_0 R_0 < \pi/2$ ($b < 0$) or repulsive when $K_0 R_0 > \pi/2$ ($b > 0$).

The interaction between the impurity and the bosons is modeled by either a **HS** or a **ASW** potential. Let us examine the Jastrow functions for the two potentials corresponding to positive, negative or infinite value of the scattering length.

- **HS**: the hard-sphere potential is used to model the interaction between the impurity and the bosons. The two-body solution Eq. [3.59] gives:

$$f_I(r) = \begin{cases} 0 & r < b \\ \sin k(r - b)/r & r > b \end{cases} \quad (3.65)$$

similar to the HS case of Eq. [3.60], but with the difference that the value of the s -wave scattering length is given by b .

- **ASW: Repulsive branch** ($b > 0$): f_I is constructed from the zero-energy scattering solution of the potential [3.62] orthogonal to the bound state existing for two particles when $b > 0$ in the region, where R_m is a matching point. $0 < r < R_m$. In addition, for $R_m < r < L/2$ we use a wavefunction that reduces possible finite-size effects due to the long-range tails of the wavefunction corresponding to $r < R_m$

$$f_I(r) = \begin{cases} A \sin(K_0 r)/r & r \leq R_0 \\ 1 - b/r & R_0 \leq r \leq R_m \\ B [1 - e^{-\alpha r} - e^{-\alpha(L-r)}] & R_m \leq r \leq L/2 \\ 2B e^{-\alpha L/2} & r > L/2 \end{cases} \quad (3.66)$$

The matching point $R_m < L/2$ is introduced and for $r > R_m$ the function f_I goes rapidly to a constant reached at $L/2$ and $f'_I(r = L/2) = 0$. The coefficients A , B and α ensure the continuity of f_I and of its first derivative at the points R_0 and R_m .

- **ASW: Attractive branch** ($b < 0$): f_I is constructed in the same way as for the repulsive branch in Eq. [3.66], with the only difference that the scattering length b is negative.
- **ASW: Attractive branch** ($b > 0$): we use the solution of the two-body bound state with energy ϵ_b for $0 < r < R_m$ and use a functional form similar to Eq. [3.66] for $R_m < r < L/2$

$$f_I(r) = \begin{cases} A \sin(\kappa r)/r & r \leq R_0 \\ [e^{-m|\epsilon_b|r/m}] / r & R_0 \leq r \leq R_m \\ B [e^{-\alpha r} + e^{-\alpha(L-r)}] & R_m \leq r \leq L/2 \\ 2B e^{-\alpha L/2} & r > L/2 \end{cases} \quad (3.67)$$

where $\kappa^2 = m(V_0 - |\epsilon_b|)/\hbar^2$. The coefficients A , B and α ensure the continuity of f_I and of its first derivative at the points R_0 and R_m .

3.7 Diffusion Monte-Carlo (DMC)

In this section a more sophisticated method is discussed. It is called Diffusion Monte-Carlo (DMC) and it was introduced for the first time by J.B Anderson [96, 97]. This method solves the many-body Schrödinger equation in imaginary time by using the analogy with the classical diffusion equation.

The time-dependent Schrödinger equation is written as

$$i\hbar \frac{\partial}{\partial t} \psi(\mathbf{R}, \tau) = -\frac{\hbar^2}{2m} \nabla^2 \psi(\mathbf{R}, \tau) + V(\mathbf{R}) \psi(\mathbf{R}, \tau), \quad (3.68)$$

with $\tau = it/\hbar$ the imaginary time. Let us consider the case of bosons. The system can be described by a Hamiltonian \mathcal{H} . The eigenstates and eigenvalues of the system are $|\phi_\alpha\rangle$ and E_α respectively. In such a way that $\mathcal{H}|\phi_\alpha\rangle = E_\alpha|\phi_\alpha\rangle$.

The ground state $|\phi_0\rangle$ can be found using an iterative procedure which involves the time-evolution operator. One can start from a generic state, say $|\psi_0\rangle$, provided it is not orthogonal to the ground state. i.e $\langle\phi_0|\psi_0\rangle \neq 0$. The temporal evolution from a state $n-1$ to state n is obtained by

$$|\psi_n\rangle = \exp[-\delta\tau(\mathcal{H} - E_T)] |\psi_{n-1}\rangle, \quad (3.69)$$

and the iterative procedure generates a sequence in imaginary time

$$|\psi_n\rangle = \exp[-n\delta\tau(\mathcal{H} - E_T)] |\psi_0\rangle, \quad (3.70)$$

Here $\delta\tau = i\delta t/\hbar$ and E_T is an energy shift. Let us introduce the completeness relation $\sum_\alpha |\phi_\alpha\rangle \langle\phi_\alpha| = \hat{1}$, in the previous equation and let us use the fact that $\mathcal{H}|\phi_\alpha\rangle = E_\alpha|\phi_\alpha\rangle$. Then

$$|\psi_n\rangle = \sum_\alpha \langle\phi_\alpha|\psi_0\rangle \exp[-n\delta\tau(E_\alpha - E_T)] |\phi_\alpha\rangle. \quad (3.71)$$

After many iterations all the contributions orthogonal to the ground state are killed out and the only one which survives is

$$\lim_{n \rightarrow \infty} |\psi_n\rangle = \langle\phi_0|\psi_0\rangle \exp[-n\delta\tau(E_0 - E_T)] |\phi_0\rangle. \quad (3.72)$$

The value of E_T is chosen to maintain the normalization $\langle\psi_n|\psi_n\rangle$ of the state at large times stationary during the iterative process ($E_T = E_0$ for n large).

In coordinate space the temporal evolution of Eq. [3.69] can be written in terms of the Green's function as

$$\psi_n(\mathbf{R}) = \int d\mathbf{R}_n \mathcal{G}(\mathbf{R}, \mathbf{R}_n, \delta\tau) \psi_{n-1}(\mathbf{R}_n), \quad (3.73)$$

and $\mathcal{G}(\mathbf{R}, \mathbf{R}_n, \delta\tau)$ is the Green's function written as:

$$\mathcal{G}(\mathbf{R}, \mathbf{R}', \delta\tau) = \langle\mathbf{R}|\exp[-\delta\tau(\mathcal{H} - E_T)]|\mathbf{R}'\rangle. \quad (3.74)$$

This evolution can be written in terms of convolution integrals over n terms

$$\psi_n(\mathbf{R}) = \int d\mathbf{R}_n \cdots d\mathbf{R}_1 \mathcal{G}(\mathbf{R}, \mathbf{R}_n, \delta\tau) \cdots \mathcal{G}(\mathbf{R}_2, \mathbf{R}_1, \delta\tau) \psi_0(\mathbf{R}_1). \quad (3.75)$$

The Hamiltonian is written in general as $\mathcal{H} = T + V = -\frac{\hbar^2}{2m}\nabla_{\mathbf{R}}^2 + V(\mathbf{R})$, where $V(\mathbf{R})$ includes both inter-particle interactions and external fields. Since in general the operators T and V do not commute, the Trotter formula from section [3.4.1] is used. Therefore, for small a *time step* $\delta\tau$ one obtains:

$$\exp[-\delta\tau(\mathcal{H} - E_T)] = \exp\left[-\frac{\delta\tau}{2}(V - E_T)\right]\exp\left[-\frac{\delta\tau}{2}T\right]\exp\left[-\frac{\delta\tau}{2}(V - E_T)\right] + o(\tau^3). \quad (3.76)$$

The Green's function in the small time-step approximation is written as

$$\begin{aligned} \mathcal{G}(\mathbf{R}, \mathbf{R}', \delta\tau) &= \langle \mathbf{R} | \exp\left[-\frac{\delta\tau}{2}(V - E_T)\right] \exp\left[-\frac{\delta\tau}{2}T\right] \exp\left[-\frac{\delta\tau}{2}(V - E_T)\right] | \mathbf{R}' \rangle + o(\tau^3) \\ &= \exp\left[-\frac{\delta\tau}{2}(V(\mathbf{R}) - E_T)\right] \langle \mathbf{R} | \exp\left[-\frac{\delta\tau}{2}T\right] | \mathbf{R}' \rangle \exp\left[-\frac{\delta\tau}{2}(V(\mathbf{R}') - E_T)\right] + o(\tau^3), \end{aligned} \quad (3.77)$$

and finally, one obtains

$$\mathcal{G}(\mathbf{R}, \mathbf{R}', \delta\tau) = \frac{1}{(4\pi D\delta\tau)^{3N/2}} \exp\left[-\frac{(\mathbf{R} - \mathbf{R}')^2}{4D\delta\tau}\right] \times \exp\left[-\delta\tau\left(\frac{V(\mathbf{R}) + V(\mathbf{R}')}{2} - E_T\right)\right] + o(\tau^3). \quad (3.78)$$

The first term is called *diffusion term*, and the second represents the *branching term*. This latter term modifies the normalization $\int d\mathbf{R}G(\mathbf{R}', \mathbf{R}, \delta\tau) \neq 1$.

3.7.1 How does DMC work?

Let us consider a set of N^W points in the configuration space \mathbf{R} formed by N particles (called walkers see Eq. [3.27]). These positions change according to the diffusion process and their number changes according to the branching term. The moves of the algorithm are summarized:

1. An *initial population of walkers* $N^W(0)$ is distributed according to the function $\psi_0(\mathbf{R})$. For instance, all the walkers can start from the same position $\mathbf{R} = \mathbf{R}_0$ namely, $\psi_0(\mathbf{R}) = \delta(\mathbf{R} - \mathbf{R}_0)$.

2. Produce the n -th generation of walkers with a diffusion and a branching step:

- **Diffusion step:** new positions are generated by the diffusion step found in Sec [3.4.1]:

$$\mathbf{R} \rightarrow \mathbf{R}' = \mathbf{R} + \sqrt{2D\delta\tau}\xi, \quad (3.79)$$

with $\xi \in N(0, 1)$.

- **Branching step:** Since the population of walkers is not constant the number of sons at certain position \mathbf{R}' is calculated as

$$n_i = \text{int} \left[\exp \left\{ -\delta\tau \left(\frac{\mathbf{V}(\mathbf{R}) + V(\mathbf{R}')}{2} - E_T \right) \right\} + \xi' \right]. \quad (3.80)$$

where $\xi' \in U(0, 1)$ and $\text{int}(x)$ is the integer part of x .

- **Population control:** The energy shift is updated every m iterations, $E_T \rightarrow E_T + \delta E_T$ in order to keep the population constant. This energy shift is given by

$$\delta E_T = \log \left(\frac{N^W(n+m)}{N^W(n)} \right). \quad (3.81)$$

Some facts must be highlighted here. The pure diffusion algorithm described above may suffer of large fluctuations in the branching term due to the spatial variations of the potential energy $V(\mathbf{R})$. The calculation is viable only for few particles and for bounded interatomic potentials. In the general case the algorithm is highly inefficient because of large statistical uncertainties in the expectation values. However, as we learned in the past section this problem can be solved by means of *importance sampling*.

3.7.2 Importance Sampling

The previous algorithm can be more efficient if one has some physical knowledge concerning the wavefunction of the system. One uses the following **pdf** corresponding to the n -th step of the iterative procedure

$$f_n(\mathbf{R}) = \psi_T(\mathbf{R})\psi_n(\mathbf{R}), \quad (3.82)$$

where $\psi_T(\mathbf{R})$ is a trial wavefunction. The evolution of $f_n(R)$ is provided by the modified Green's function G_T ,

$$\begin{aligned} f_n(\mathbf{R}) &= \int d\mathbf{R}' \mathcal{G}_T(\mathbf{R}, \mathbf{R}', \delta\tau) f_{n-1}(\mathbf{R}') \\ f_n(\mathbf{R}) &= \int d\mathbf{R}' \psi_T(\mathbf{R}) \mathcal{G}(\mathbf{R}, \mathbf{R}', \delta\tau) \frac{1}{\psi_T(\mathbf{R}')} f_{n-1}(\mathbf{R}'). \end{aligned} \quad (3.83)$$

Where \mathcal{G} is the Green's function defined in Eq. [3.74]. The Green's function and the modified Green's function satisfy the following time-dependent equations

$$\begin{aligned} -\frac{\partial \mathcal{G}(\mathbf{R}, \mathbf{R}', \tau)}{\partial \tau} &= (\mathcal{H} - E_T) \mathcal{G}(\mathbf{R}, \mathbf{R}', \tau) \\ -\frac{\partial \mathcal{G}_T(\mathbf{R}, \mathbf{R}', \tau)}{\partial \tau} &= \left(\psi_T(\mathbf{R}) \mathcal{H} \frac{1}{\psi_T(\mathbf{R})} - E_T \right) \mathcal{G}_T(\mathbf{R}, \mathbf{R}', \tau) = (\mathcal{H}_T - E_T) \mathcal{G}_T(\mathbf{R}, \mathbf{R}', \tau), \end{aligned} \quad (3.84)$$

where the effective Hamiltonian \mathcal{H}_T takes the form

$$\mathcal{H}_T = -D\nabla_{\mathbf{R}}^2 + D\nabla_{\mathbf{R}} \cdot \mathbf{F}(\mathbf{R}) + E_L(\mathbf{R}) = \mathcal{L} + E_L(\mathbf{R}). \quad (3.85)$$

Here $D = \hbar^2/2m$ is the diffusion coefficient and $\mathcal{L} = -D\nabla_{\mathbf{R}}^2 + D\nabla_{\mathbf{R}} \cdot \mathbf{F}(\mathbf{R})$ is the Langevin operator. $\mathbf{F}(\mathbf{R})$ is the quantum drift force defined as $2\nabla_{\mathbf{R}} \log(\psi_T(\mathbf{R}))$ and $E_L = \frac{\mathcal{H}\psi_T(\mathbf{R})}{\psi_T(\mathbf{R})}$ is the local energy. The solution of Eq. [3.84] for a small time step $\delta\tau$ yields

$$\mathcal{G}_T(\mathbf{R}, \mathbf{R}', \delta\tau) = \langle \mathbf{R} | \exp(-\delta\tau\mathcal{L}) | \mathbf{R}' \rangle \exp \left\{ -\delta\tau \left(\frac{E_L(\mathbf{R}) + E_L(\mathbf{R}')}{2} - E_T \right) \right\} + o(\delta\tau^3). \quad (3.86)$$

Recalling now the solution for the Green's function of the Langevin's equation in Eq. [3.48] one finds

$$G(\mathbf{R}, \mathbf{R}', \delta\tau) = \langle \mathbf{R} | \exp(-\delta\tau\mathcal{L}) | \mathbf{R}' \rangle = \frac{\exp - (\mathbf{R}(\delta\tau) - \mathbf{R}')^2 / 4D\delta\tau}{(4\pi D\delta\tau)^{3N/2}} + o(\delta\tau^2). \quad (3.87)$$

The branching term is now much smoother compared to the pure diffusion algorithm because the local energy $E_L(\mathbf{R})$ is in general a slowly varying function in spatial coordinates.

3.7.3 DMC with importance sampling

An algorithm to produce the time evolution can be devised as:

1. Start from $N^W(0)$ walkers distributed according to the function $\psi_0(\mathbf{R}) = \psi_T(\mathbf{R})$.
2. Produce the n -th generation of walkers.

(a) **Diffusion and drift steps** generate the new positions:

$$\mathbf{R} \rightarrow \mathbf{R}' = \mathbf{R} + D\mathbf{F}(\mathbf{R})\delta\tau + \sqrt{2D\delta\tau}\xi, \quad (3.88)$$

with $\xi \in N(0, 1)$.

(b) **Acceptance/rejection step:** In order to reduce the time-step dependence the proposed move is accepted according to the probability given in Eq. [3.54] and Eq. [3.55]. An acceptance rate is evaluated from the ratio of the number of accepted to the total number of moves $r_{acc} = \frac{\#\text{accepted moves}}{\#\text{moves}}$.

i. **Branching** : The time step $\delta\tau$ is modified by accounting for the acceptance rate of the proposed moves $\delta\tau \rightarrow \delta\tau^* = r_{acc}\delta\tau$. The number of sons of a walker that has been moved from \mathbf{R} to \mathbf{R}' is calculated as

$$n_i = \text{int} \left[\exp \left\{ -\delta\tau^* \left(\frac{V(\mathbf{R}) + V(\mathbf{R}')}{2} - E_T \right) \right\} + \xi' \right], \quad (3.89)$$

where $\xi' \in U(0, 1)$ and $\text{int}(x)$ is the integer part of x .

3. **Population control:** The energy shift is updated in every iteration as:

$$E_T(n+1) = \frac{1}{N^W(n)} \sum_{i=1}^{N^W(n)} E_L(\mathbf{R}_i), \quad (3.90)$$

for n iterations. An additional population control is required to maintain N^W within the range $N_- \leq N^W \leq N_+$. This can be obtained by the updated of $E_T(n+1) \rightarrow E_T(n+1) + \delta E_T$. Where

$$\delta E_T = \begin{cases} \frac{1}{\delta\tau^*} \log \frac{\langle N^W \rangle}{N_+} & N^W(n) > N_+ \\ \frac{1}{\delta\tau^*} \log \frac{\langle N^W \rangle}{N_-} & N^W(n) < N_+ \\ 0 & N_+ < N^W < N_+ \end{cases} \quad (3.91)$$

At large times, the obtained **pdf** is proportional to the ground-state of the system

$$\lim_{\tau \rightarrow \infty} f(\mathbf{R}, \tau) = \lim_{n \rightarrow \infty} f_n(\mathbf{R}) = \psi_T(\mathbf{R})\phi_0(\mathbf{R}). \quad (3.92)$$

The Monte-Carlo estimate for the energy is given then by:

$$\frac{1}{N^W} \sum_{i=1}^{N^W} E_L(\mathbf{R}_i) = \frac{\int d\mathbf{R} f(\mathbf{R}, \tau \rightarrow \infty) E_L(\mathbf{R})}{\int d\mathbf{R} f(\mathbf{R}, \tau \rightarrow \infty)}, \quad (3.93)$$

$$= \frac{\int d\mathbf{R} \psi_T(\mathbf{R})\phi_0(\mathbf{R}) \frac{1}{\psi_T(\mathbf{R})} \mathcal{H} \psi_T(\mathbf{R})}{\int d\mathbf{R} f(\mathbf{R}, \tau \rightarrow \infty)} = E_0. \quad (3.94)$$

The previous DMC moves are summarised the Fig. [3.5].

Let us consider an example of the algorithm obtained above: our simulation starts with 3 particles distributed on 4 walkers. A move from \mathbf{R} to \mathbf{R}' is proposed with a diffusion and a drift contribution according to Eq. [3.88]. The number of sons of a walker that has been moved from \mathbf{R} to \mathbf{R}' is calculated with Eq. [3.89]. In particular, for both the first and third walker the number of descendants is zero and the configuration is killed. Whereas, for the second walker one son is obtained and the configuration survives. For the fourth walker two sons appears and the configuration is copied.

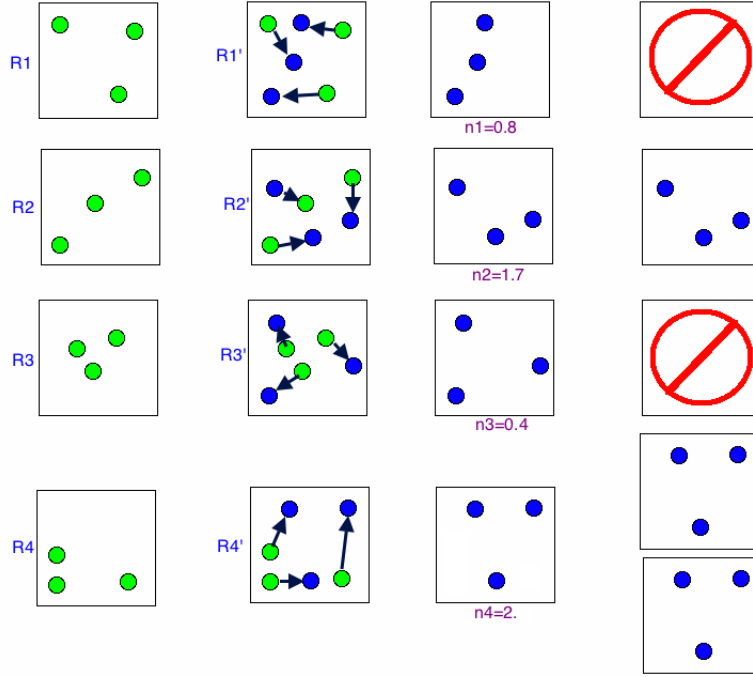


Figure 3.5: DMC moves

3.8 Observables

3.8.1 Energy

The energy is an important and central observable in all QMC methods. In the previous section, we discussed how to calculate expectation values. Let us consider the expectation value of the energy with the Monte-Carlo estimator

$$E_T = E_M \pm \sigma_M, \quad (3.95)$$

where

$$E_M = \frac{1}{M} \sum_{i=1}^M E_L(\mathbf{R}_i), \quad (3.96)$$

and

$$\sigma_M = \frac{1}{\sqrt{M}} \left(\frac{1}{M} \sum_{i=1}^M E_L^2(\mathbf{R}_i) - E_M^2 \right)^{1/2}, \quad (3.97)$$

over a collection of statistically independent configurations \mathbf{R}_i ($i = 1, \dots, M$). The local energy is computed as

$$E_L(\mathbf{R}) = \frac{1}{T} \sum_{j=j'+1}^{j'+T} E_L(\mathbf{R}_j), \quad (3.98)$$

where the total number of iterations is MT .

The local energy associated with the Jastrow wavefunction Eq. [3.57] is written as:

$$E_L(\mathbf{R}) = \frac{\mathcal{H}\psi_J(\mathbf{R})}{\psi_J(\mathbf{R})}, \quad (3.99)$$

then

$$E_L(\mathbf{R}) = -\frac{\hbar^2}{2m} \sum_{i=1}^N \frac{\nabla_i^2 \psi_J(\mathbf{R})}{\psi_J(\mathbf{R})} + V(\mathbf{R}). \quad (3.100)$$

For the Jastrow wavefunction in Eq. [3.57] the above local energy takes the explicit form

$$\begin{aligned} E_L(\mathbf{R}) &= -\frac{\hbar^2}{2m} \sum_{i=1}^N \frac{\nabla_i^2 \psi_J(\mathbf{R})}{\psi_J(\mathbf{R})} + V(\mathbf{R}) \\ &= -\frac{\hbar^2}{2m} \sum_{i=1}^3 \left[\sum_{i \neq j} \left(\frac{\nabla_i^2 f(r_{ij})}{f(r_{ij})} - \left(\frac{\nabla_i f(r_{ij})}{f(r_{ij})} \right)^2 \right) + \left(\sum_{i \neq j} \frac{\nabla_i f(r_{ij})}{f(r_{ij})} \right)^2 \right] + V(\mathbf{R}). \end{aligned} \quad (3.101)$$

By carrying out the calculations, it yields

$$\nabla f(r_{ij}) = \left(\frac{r_i^\alpha - r_j^\alpha}{r_{ij}} \right) f' \quad (3.102)$$

and

$$\nabla_i^2 f(r_{ij}) = \left[\frac{1}{r_{ij}} - \frac{(r_i^\alpha - r_j^\alpha)^2}{r_{ij}^3} \right] f' + \frac{(r_i^\alpha - r_j^\alpha)^2}{r_{ij}^2} f''. \quad (3.103)$$

Finally, the expression for the local energy is reduced to

$$E_L(\mathbf{R}) = \frac{\mathcal{H}\psi_J(\mathbf{R})}{\psi_J(\mathbf{R})} = -D \left\{ \sum_{i \neq j} \left[\frac{f''(r_{ij})}{f(r_{ij})} + \frac{2}{r_{ij}} \frac{f'(r_{ij})}{f(r_{ij})} - \left(\frac{f'(r_{ij})}{f(r_{ij})} \right)^2 \right] + \frac{1}{4} \sum_i \mathbf{F}_i^2(\mathbf{R}) \right\} + V(\mathbf{R}), \quad (3.104)$$

where the diffusion constant D is defined as $D \equiv \hbar^2/2m$. $\mathbf{F}_i(\mathbf{R})$ is defined as the quantum drift force

$$\mathbf{F}_i(\mathbf{R}) = 2 \frac{\nabla_i \psi_J(\mathbf{R})}{\psi_J(\mathbf{R})} = 2 \sum_{i \neq j} \left(\frac{r_i - r_j}{r_{ij}} \right) \frac{f'(r_{ij})}{f(r_{ij})}. \quad (3.105)$$

The previous expression in the case of two particles yields

$$E_L(\mathbf{r}_1, \mathbf{r}_2) = -\left(\hbar^2/m \right) \left[f'' + (2/r_{12}) f'/f \right] + V(r_{12}), \quad (3.106)$$

that is precisely the solution of the two-body-Schrödinger equation.

In the case of the VMC method an alternative estimate of E_T relies on the quantum drift force.

Let us suppose that one can split the Hamiltonian \mathcal{H} as the sum of a kinetic T and a potential V term, namely, $\mathcal{H} = T + V$ (see Eq. [3.56]). The expectation value of \mathcal{H} on the trial wave function ψ_T can be written as

$$\begin{aligned} \langle \mathcal{H} \rangle &= \int d\mathbf{R} \psi_T^* \left(-\frac{\hbar^2}{2m} \nabla_{\mathbf{R}}^2 + V(\mathbf{R}) \right) \psi_T \\ &= -\frac{\hbar^2}{2m} \int d\mathbf{R} \nabla_{\mathbf{R}} \cdot (\psi_T^* \nabla_{\mathbf{R}} \psi_T) + \int d\mathbf{R} \left(\frac{\hbar^2}{2m} (\nabla_{\mathbf{R}} \psi_T^*) \cdot (\nabla_{\mathbf{R}} \psi_T) + V(\mathbf{R}) |\psi_T|^2 \right). \end{aligned} \quad (3.107)$$

In order to be compatible with **p.b.c** we recall that the boundary conditions on the Jastrow term to make the surface term (Ω) vanish, namely the condition $df(r = L/2)/dr = 0$ implies that:

$$\int d\mathbf{R} \nabla_{\mathbf{R}} \cdot (\psi_T^* \nabla_{\mathbf{R}} \psi_T) = \int d\Omega \psi_T^* \nabla_{\mathbf{R}} \psi_T = 0. \quad (3.108)$$

Then E_T can be alternatively written as

$$E_T = \frac{\int d\mathbf{R} \left(\frac{\hbar^2}{2m} (\nabla_{\mathbf{R}} \psi_T^*) \cdot (\nabla_{\mathbf{R}} \psi_T) + V(\mathbf{R}) |\psi_T|^2 \right)}{\int d\mathbf{R} |\psi_T|^2}, \quad (3.109)$$

$$E_T = \int d\mathbf{R} f(\mathbf{R}) \left(\frac{\hbar^2}{2m} \frac{|\nabla_{\mathbf{R}} \psi_T|^2}{|\psi_T|^2} + V(\mathbf{R}) \right) = \int d\mathbf{R} f(\mathbf{R}) E'_L(\mathbf{R}), \quad (3.110)$$

where

$$E'_L(\mathbf{R}) = \left(\frac{\nabla \Psi_T^*(\mathbf{R})}{\Psi_T^*(\mathbf{R})} \right) \cdot \left(\frac{\nabla \Psi_T(\mathbf{R})}{\Psi_T(\mathbf{R})} \right) + V(\mathbf{R}), \quad (3.111)$$

and it can be written in terms of the so called quantum drift force $F_Q = 2 \left(\frac{\nabla \Psi_T(\mathbf{R})}{\Psi_T(\mathbf{R})} \right)$ as

$$E'_L(\mathbf{R}) = \frac{1}{4} |F_Q(\mathbf{R})|^2 + V(\mathbf{R}).$$

Then, the energy can also be estimated by

$$E_T = \int d\mathbf{R} f(\mathbf{R}) \left[\frac{1}{4} |F_Q(\mathbf{R})|^2 + V(\mathbf{R}) \right]. \quad (3.112)$$

The motivation for calculating the energy by using the force estimator in Eq [3.112] and for comparing it with the direct estimator of Eq. [3.107] is to verify the correct implementation of the wave function. Both estimators must be equal within statistical error. Nevertheless, the variance in the force estimator is larger with respect to the direct estimator.

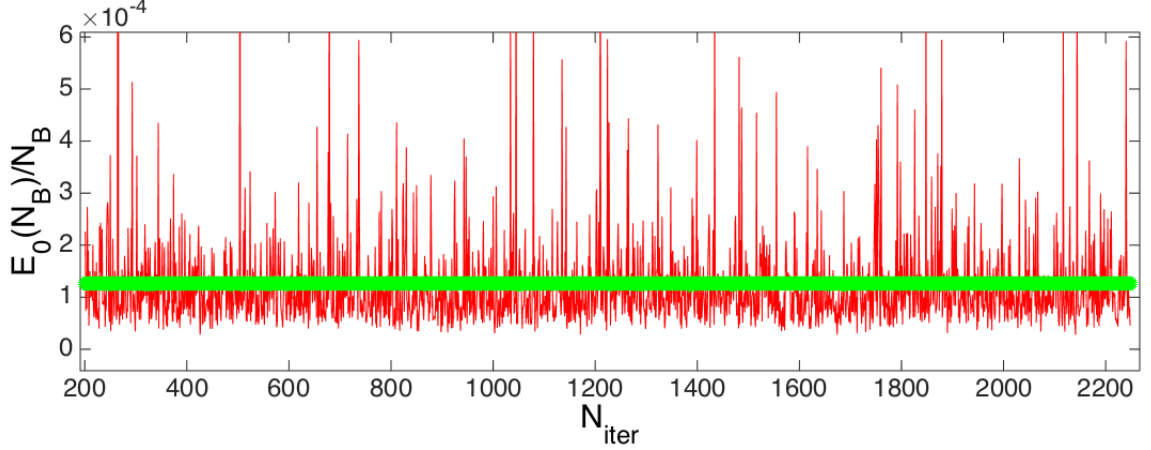


Figure 3.6: **Ground state energy per particle as a function of the iteration number in VMC** for a weakly interacting Bose gas with gas parameter $(n_B a^3) = 10^{-5}$. Green line direct estimator E_D given by Eq. [3.107] and red line, force estimator E_F given by Eq. [3.112].

In Fig. [3.6] the ground-state energy per particle is plotted for a system of interacting bosons with the HS potential at the value of $n_B a^3 = 10^{-5}$. Both the direct \mathbf{E}_D and the force estimator \mathbf{E}_F are computed. The direct estimator gives $E_D^0(N_B)/N_B = (1.262 \pm 0.003) \times 10^{-4}$, whereas the force estimator is $E_F^0(N_B)/N_B = (1.221 \pm 0.20) \times 10^{-4}$ in statistical agreement within the errors bars, but the variance of E_F is much larger.

3.8.2 Pair correlation function

Quantum Monte Carlo methods can be used to calculate not only the ground-state energy of the system, but also other important two-body quantities such as the pair-correlation function. This function can be written by using the Monte-Carlo integral estimator:

$$\mathcal{O}_{MC} = \int d\mathbf{R} O_L(\mathbf{R}) f(\mathbf{R}), \quad (3.113)$$

where $O_L(\mathbf{R}) = \frac{\hat{O}\psi_T(\mathbf{R})}{\psi_T(\mathbf{R})}$ is the local value of the operator \hat{O} and $f(\mathbf{R})$ is the probability distribution. In particular for $\hat{O} = \mathcal{H}$ (the Hamiltonian), we obtain the result [3.100]. In general for operators which do not commute with \mathcal{H} , the DMC method does not provide a pure expectation value on the ground-state, but a “mixed” matrix element involving the ground-state and the trial wavefunction. In fact, one has

$$\frac{1}{NW} \sum_{i=1}^{NW} \mathcal{O}(\mathbf{R}_i) = \frac{\int d\mathbf{R} \psi_T(\mathbf{R}) \phi_0(\mathbf{R}) \mathcal{O}_L}{\int d\mathbf{R} \psi_T(\mathbf{R}) \phi_0(\mathbf{R})} = \frac{\langle \psi_T | \mathcal{O} | \phi_0 \rangle}{\langle \psi_T | \phi_0 \rangle} \equiv \langle \mathcal{O} \rangle_{mix}. \quad (3.114)$$

Pure expectation values, namely $\langle \mathcal{O} \rangle_{pure} \equiv \frac{\langle \phi_0 | \mathcal{O} | \phi_0 \rangle}{\langle \phi_0 | \phi_0 \rangle}$ can be estimated by using an extrapolation

technique which relies on the approximation $|\phi_0\rangle = |\psi_T\rangle + |\delta\psi_T\rangle$. Up to linear order in the real function $|\delta\psi_T\rangle$, one obtains:

$$\langle\mathcal{O}\rangle_{pure} = \langle\mathcal{O}\rangle_{mix} + \frac{\langle\delta\psi_T|\mathcal{O}|\phi_0\rangle}{\langle\psi_T|\psi_T\rangle} - \langle\mathcal{O}\rangle_{var} \frac{\langle\delta\psi_T|\psi_T\rangle}{\langle\psi_T|\psi_T\rangle} \quad (3.115)$$

and

$$\langle\mathcal{O}\rangle_{mix} = \langle\mathcal{O}\rangle_{var} + \frac{\langle\psi_T|\mathcal{O}|\delta\psi_T\rangle}{\langle\psi_T|\psi_T\rangle} - \langle\mathcal{O}\rangle_{var} \frac{\langle\psi_T|\delta\psi_T\rangle}{\langle\psi_T|\psi_T\rangle}, \quad (3.116)$$

where $\langle\mathcal{O}\rangle_{var} \equiv \frac{\langle\psi_T|\mathcal{O}|\psi_T\rangle}{\langle\psi_T|\psi_T\rangle}$ and the term $\frac{\langle\delta\psi_T|\psi_T\rangle}{\langle\psi_T|\psi_T\rangle}$ is eliminated yielding:

$$\langle\mathcal{O}\rangle_{pure} = 2\langle\mathcal{O}\rangle_{mix} - \langle\mathcal{O}\rangle_{var}. \quad (3.117)$$

An example is provided by the pair-correlation function. In general the pair-correlation function is defined as:

$$g(\mathbf{r}) = \frac{1}{n^2} \langle \Psi^\dagger(\mathbf{r}') \Psi^\dagger(\mathbf{r}' + \mathbf{r}) \Psi(\mathbf{r}' + \mathbf{r}) \Psi(\mathbf{r}') \rangle, \quad (3.118)$$

where $\Psi^\dagger(\mathbf{r}')$ and $\Psi(\mathbf{r}')$ are the standard creation and annihilation fields operators and n is the density. The previous expression describes the process of removing two particles from the position \mathbf{r}' and $\mathbf{r}' + \mathbf{r}$, returning back to the same state after replacing the particles in the same positions. In this work, we consider two pair-correlation functions: the boson-boson and the impurity-boson pair correlation functions denoted by $g_{BB}(r)$ and $g_{IB}(r)$ respectively. A simple algorithm is devised for the former case. For instance, for a Bose gas with N particles, one choose a particle i , then, one counts the number of particles $j > 1$ bounded between the interval $(r, r + dr)$, normalized by the number ndV , associated with a uniform density enclosed in a spherical shell of width dr . Statistics is carrying out by averaging over all the particles $i = 1, \dots, N$ and after the data is drawn in a hystogram such as Fig. [3.7, **B**].

A Monte- Carlo estimate of Eq. [3.118] is provided by

$$g_{BB}(r) = V(1 - 1/N) \frac{\sum_{i < j}^N \int d\mathbf{R} \delta(r - |\mathbf{r}_i - \mathbf{r}_j|) \psi_T(\mathbf{r}_i, \mathbf{r}_j, \mathbf{R}) \phi_0(\mathbf{r}_i, \mathbf{r}_j, \mathbf{R})}{\int d\mathbf{R} \psi_T(\mathbf{R}) \phi_0(\mathbf{R})}. \quad (3.119)$$

The boson boson pair-correlation function $g_{BB}(r)$ will be also used for describing the distribution of bosonic impurities in the chapter 5: this is called the impurity-impurity pair correlation function denoted by $g_{II}(r)$. The same algorithm used above is employed since the impurities are bosons as well.

On the other hand, the impurity-boson correlation function $g_{IB}(r)$ is related with the density profile. In other words, this function establishes how the density of the bosons looks in the

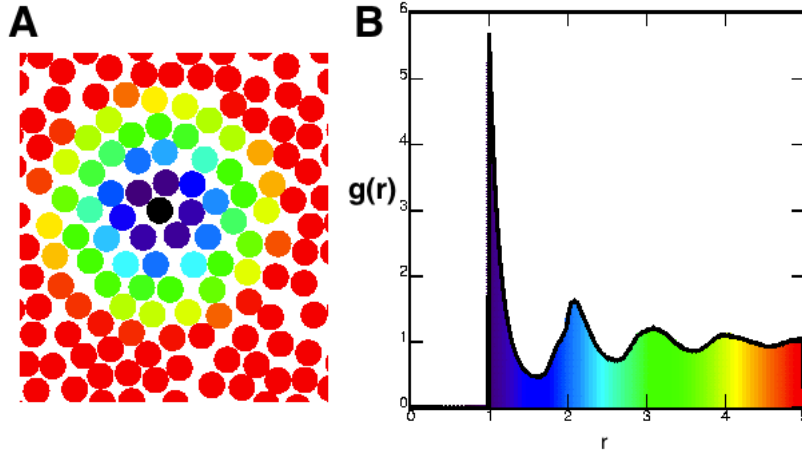


Figure 3.7: **Example of the boson-boson pair correlation function $g_{BB}(r)$:** (A) For short distances, this is related to how the particles are distributed in the simulation box. For example, consider hard spheres (bosons). The spheres can't overlap (**HS** potential), so the closest distance between two centers is equal to the diameter of the spheres. Further away, the bosons get more diffuse, and so for large distances, the probability of finding two bosons with a given separation is essentially constant. This is represented by the boson-boson correlation function. (B) histogram representing the statistics.

presence of the impurity. A similar algorithm used in the $g_{BB}(r)$ case can be devised for the $g_{IB}(r)$: in the system of a Bose gas with N particles and one impurity, one choose the impurity as a fixed reference, then one counts the number of bosons $j > 1$ bounded between the interval $(r, r + dr)$ enclosed in a spherical shell of width dr and the data is drawn in a histogram normalized with respect to the number ndV . The density of the bosons as a function of the r can be obtained by integrating $g_{IB}(r)$ over the spherical shell as follows

$$n(r) = n_B \frac{\int_0^r dr' 4\pi r'^2 g_{IB}(r')}{4\pi r^3/3}. \quad (3.120)$$

3.8.3 Effective mass

Let us consider a system formed by a weakly interacting Bose gas at $T = 0$ composed by N bosons and one distinguishable impurity. The energy of the system of $N + 1$ particles can be expanded in terms of the impurity momentum denoted by \mathbf{p}_α as

$$E(N + 1; \mathbf{p}_\alpha) = E_0(N) + \mu + \frac{\mathbf{p}_\alpha^2}{2m^*} + \dots, \quad (3.121)$$

where E_0 is the ground-state energy of the Bose gas without impurity (see Eq. [1.34]) and μ is the binding energy, defined as the difference between the energy of the system of $N + 1$ particles, $E(N + 1)$, and the ground-state energy of the Bose gas $E_0(N)$. It means:

$$\mu = E(N + 1) - E_0(N). \quad (3.122)$$

In a DMC calculation let $(\mathbf{R}, \mathbf{r}_a)$ be the $3(N + 1)$ -dimensional vector of the positions of the $N + 1$ particles. According to Eq. [3.49], the temporal evolution of a **pdf** $f(\mathbf{R}, \mathbf{r}_a, \tau)$ of the walkers at the time $\tau = \tau_0 + \Delta\tau$ after a large interval $\Delta\tau$ is given by

$$f(\mathbf{R}, \mathbf{r}_a, \tau) = \int d\mathbf{R}' d\mathbf{r}'_a f(\mathbf{R}', \mathbf{r}'_a, \tau_0) \frac{\psi_T(\mathbf{R}, \mathbf{r}_a)}{\psi_T(\mathbf{R}', \mathbf{r}'_a)} \langle \mathbf{R}, \mathbf{r}_a | e^{-\Delta\tau(\mathcal{H}-E_T)} | \mathbf{R}', \mathbf{r}'_a \rangle. \quad (3.123)$$

By using Eq. [3.121] one obtains:

$$f(\mathbf{R}, \mathbf{r}_a, \tau) = e^{-\Delta\tau(E_0(N)+\mu-E_T)} \int d\mathbf{r}'_a f(\mathbf{R}, \mathbf{r}'_a, \tau_0) \frac{\psi_T(\mathbf{R}, \mathbf{r}_a)}{\psi_T(\mathbf{R}, \mathbf{r}'_a)} \langle \mathbf{r}_a | e^{D^* \Delta\tau \nabla_a^2} | \mathbf{r}'_a \rangle, \quad (3.124)$$

$$= e^{-\Delta\tau(E_0(N)+\mu-E_T)} \int d\mathbf{r}'_a f(\mathbf{R}, \mathbf{r}'_a, \tau_0) \frac{\psi_T(\mathbf{R}, \mathbf{r}_a)}{\psi_T(\mathbf{R}, \mathbf{r}'_a)} \frac{e^{-(\mathbf{r}_a - \mathbf{r}'_a)^2 / 4D^* \Delta\tau}}{(4\pi D^* \Delta\tau)^{3/2}}, \quad (3.125)$$

where r_α is the position of the impurity, $\mathbf{p}_a = i\hbar\nabla_a$ and $D^* = -\hbar^2 / (2m^*)$. By introducing the winding number estimator associated with the impurity $W_a^2(\tau) = \int_{\tau_0}^{\tau} d\tau' \frac{d\mathbf{r}_a(\tau')}{d\tau'}$ and by noticing that $\psi_T(\mathbf{R}, \mathbf{r}_a) = \psi_T(\mathbf{R}, \mathbf{r}'_a)$ when averaged over \mathbf{r}_a and \mathbf{r}'_a , one finds that the mean square value is written as

$$\langle \mathbf{W}_a^2(\tau) \rangle = \frac{1}{N^W} \int d\mathbf{R} d\mathbf{r}_a f(\mathbf{R}, \mathbf{r}_a, \tau) [\mathbf{r}_a(\tau) - \mathbf{r}_a(\tau_0)]^2 = 6D\Delta\tau \frac{m}{m^*}. \quad (3.126)$$

The previous estimator is distributed for large intervals of time $\Delta\tau$ according to a Gaussian whose width increases linearly with $\Delta\tau$ and the proportionality coefficient depends on the ratio m/m^* between the bare and the effective mass of the impurity. Therefore, the effective mass can be estimated by

$$\frac{m}{m^*} = \lim_{\tau \rightarrow \infty} \frac{\langle |\mathbf{r}_a(\tau) - \mathbf{r}_a(0)|^2 \rangle}{6D\Delta\tau}. \quad (3.127)$$

3.9 Test case: Bose gas

In this section we consider a Bose gas in a cubic box of size L , density $n_B = N_B/V$ and gas parameter given by $n_B a^3$, where a is the s -wave scattering length. We investigate the dependence of the ground-state energy on the different sources of systematic errors in the DMC algorithm. Namely:

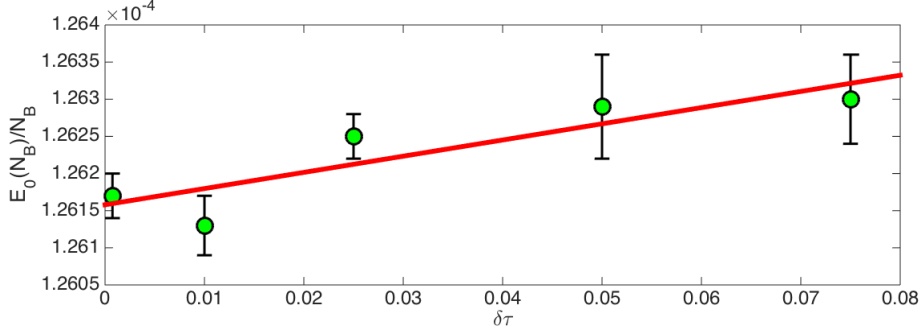


Figure 3.8: **SDMC ground-state energy per particle as a function of the time-step:** For $\delta\tau \rightarrow 0$ we obtain $E_{\mathbf{D}}^0(N_B)/N_B = (1.2617 \pm 0.0020) \times 10^{-4}$

- Zero time-step limit.
- Infinite population of walkers.
- Thermodynamic limit.

3.9.1 Time step

By using the Smart Variational Monte-Carlo SVMC we eliminated the time-step dependence displayed in the VMC when a time-dependent algorithm is implemented (Sec. [3.4.1]). A similar implementation can be done in the DMC. However, the time-dependence in DMC is reduced rather than eliminated because of the presence of the branching term (see Eq. [3.78]). The inclusion of the acceptance/rejection step improves significantly the convergence. In Fig. [3.8] we plot the dependence of the ground-state energy per particle as a function of the time step. We use a value of $\delta\tau = 5 \times 10^{-2}/D$ that turns out to be within the error bars of the value extrapolated for $\delta\tau \rightarrow 0$: $E_{\mathbf{D}}^0(N_B)/N_B = (1.2617 \pm 0.0020) \times 10^{-4}$.

3.9.2 Number of Walkers

Additionally to the $\delta\tau \rightarrow 0$ extrapolation in the time-step the DMC is exact for a number of walkers that can grow unbounded, namely $1/N^W = 0$. The ground-state energy per particle is plotted as a function of the inverse of the walkers number N^W in Fig. [3.9]. One extrapolates to $1/N^W = 0$ and obtains the value for the ground-state energy given by $E_{\mathbf{D}}^0(N_B)/N_B = (1.2625 \pm 0.0100) \times 10^{-4}$. If one uses $N^W = 50$, the corresponding energy agrees with the extrapolated value. However, the optimal N^W parameter also depends on the specific physical situation. Indeed, for a weakly interacting Bose gas with $n_B a^3 = 1 \times 10^{-5}$, a safe value is $N^W = 50$, whereas we find that for a system where the impurity is resonantly interacting with the bosonic bath, the value of N^W is significantly larger.

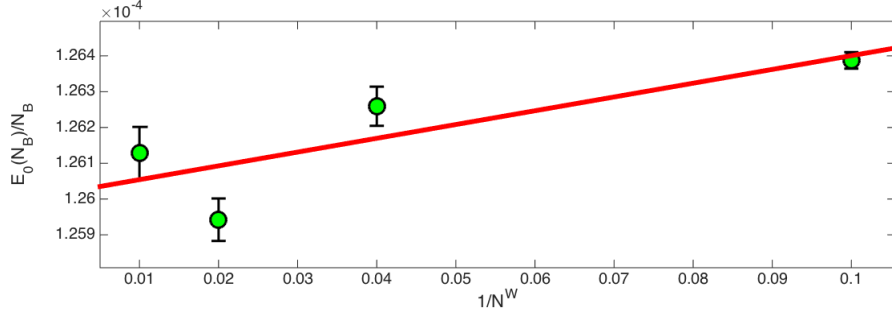


Figure 3.9: **Number of walkers dependence:** ground-state energy per particle of a Bose gas with $n_B a^3 = 10^{-5}$ as a function the inverse on the number walkers. For $1/N^W \rightarrow 0$ we obtain a value $E_D^0(N_B)/N_B = (1.2625 \pm 0.0010) \times 10^{-4}$.

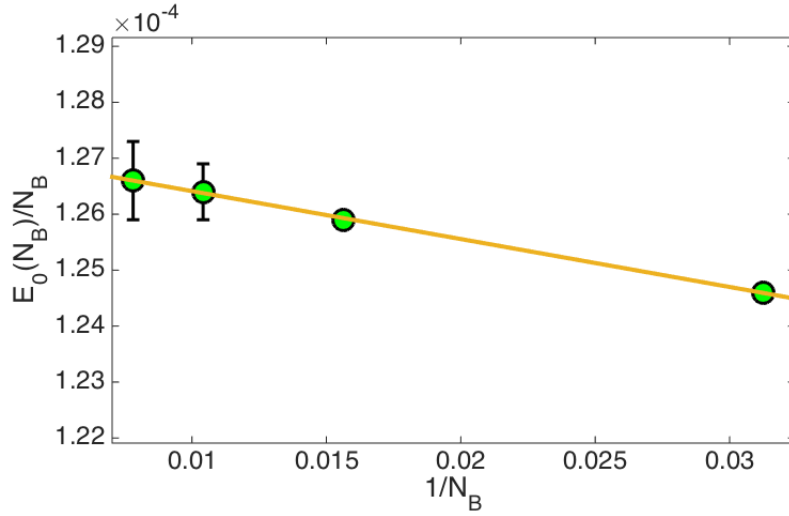


Figure 3.10: **Finite-size effects:** ground-state energy per particle as a function $1/N_B$ of a weakly interacting Bose gas with $n_B a^3 = 10^{-5}$. For $n_B = \frac{N_B \rightarrow \infty}{V \rightarrow \infty} = \text{constant}$, one gets $E_D^0(N_B)/N_B = (1.266 \pm 0.010) \times 10^{-4}$

3.9.3 Finite-size Effects

The properties in the thermodynamic limit must be checked as well. This limit is searched for a very large number of particles ($N_B \rightarrow \infty$) and large volume ($V \rightarrow \infty$), such that the density $n_B = \frac{N_B}{V}$ is constant. The ground-state energy should be computed as a function of $1/N_B$ and the results extrapolated to $1/N_B \rightarrow 0$ (see Fig. [3.10]). One obtains $E_D^0(N_B)/N_B = (1.266 \pm 0.010) \times 10^{-4}$. In these simulations we used the values of time-step $\delta\tau = 5 \times 10^{-2}/D$ and walker number $N^W = 50$.

We now turn our attention for two interesting properties.

- The ground-state energy as a function of the gas parameter $(n_B a^3)^{1/3}$.
- The boson-boson pair correlation function .

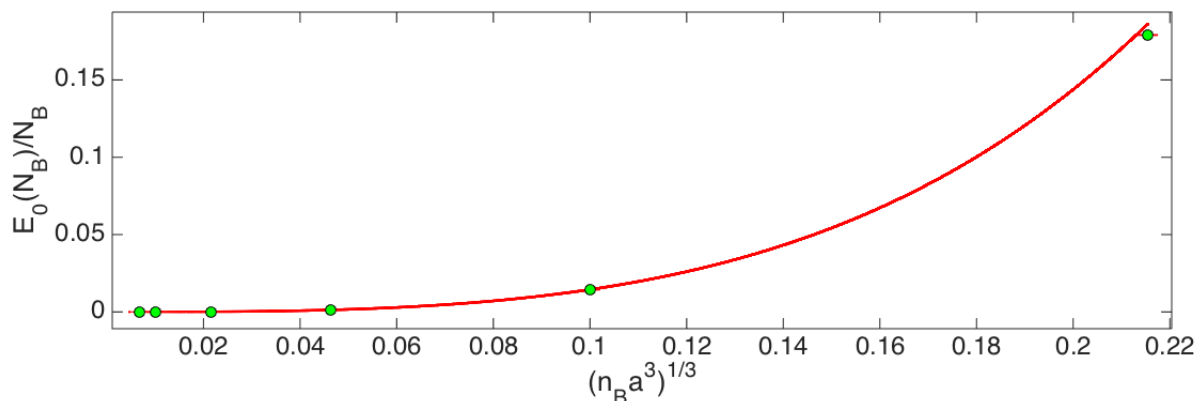


Figure 3.11: **Ground-state energy per particle of a Bose gas as a function of parameter $(n_B a^3)^{1/3}$.** Red line from the Bogoliubov theory Eq. [1.34] and green points are the DMC simulations.

3.9.4 Equation of state. Gas parameter $n_B a^3$

In Fig. [3.11] we plot the ground-state energy per particle as a function of $(n_B a^3)^{1/3}$. The parameter $n_B a^3$ is ranging from the very dilute regime, $n_B a^3 = 10^{-6}$ to $n_B a^3 = 0.1$. We observe a good agreement between the Monte-Carlo results (green points) and the Bogoliubov theory (solid red line) obtained from Eq. [1.34]. The Bogoliubov theory is applicable only on a dilute system of bosons, whereas QMC simulations have no restrictions on the parameter $n_B a^3$. In fact, small deviations start to appear between the Bogoliubov theory and the QMC data for values of $n_B a^3 > 10^{-2}$.

3.9.5 Pair correlation function

In Fig [3.12] we plot the boson-boson pair correlation function $g_{BB}(r)$ for a weakly interacting Bose gas with gas parameter $n_B a^3 = 10^{-5}$, time-step $\delta\tau = 5 \times 10^{-2}/D$ and walker number $N^W = 50$. Notice that the $g_{BB}(r)$ is zero for $0 \leq r \leq 1$ due to the HS potential between the bosons. In addition, for large distances, it approaches to the value $g_{BB}(r) = 1$ indicating that particles are no longer correlated.

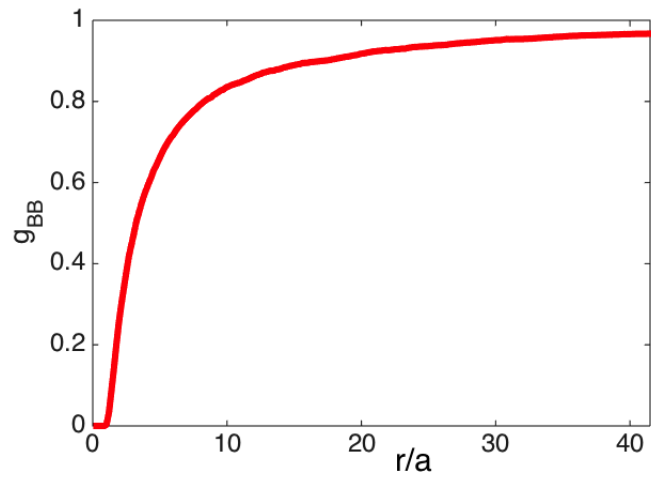


Figure 3.12: **boson-boson correlation pair function** as a function of the inter-boson distance. For a Bose gas with $n_B a^3 = 10^{-5}$.

Chapter 4

Single impurity problem

4.1 Statement of the problem

In this chapter we investigate the properties of an impurity immersed in a dilute and homogeneous Bose gas ($V_{ext} = 0$) at zero temperature with gas parameter $n_B a^3 \ll 1$. We use both mean-field techniques and quantum Monte-Carlo methods. The interaction between bosons are modeled by the hard-sphere potential (**HS**) defined in Eq. [3.58] and characterized by the s -wave scattering length a , whereas the interaction between the impurity and the bosons is modeled by a short-range, attractive square-well (**ASW**) potential defined in Eq. [3.62]. Both the sign and the strength of the s -wave scattering length b can be varied by adjusting the well depth in Eq. [3.63]. The ground-state properties such as the ground-state energy, the effective mass and the pair correlation functions are studied as a function of the coupling strength b/a .

In the weakly interacting regime, $n_B a^3 \ll 1$, the Bogoliubov theory is suitable to describe the properties of a weakly interacting Bose gas (see Chapter 1). On the other hand, the ground-state properties of an electron interacting with a bosonic bath such as the lattice vibrations (see chapter 1) was addressed with perturbative methods. It turns out that the problem of an impurity immersed into a Bose-Einstein condensate can be mapped onto the Fröhlich Hamiltonian (see Eq.[1.1] in chapter 1) where the Bogoliubov excitations of the bosonic bath play the role of the phonons. The ground-state properties will depend on the parameter b/a and the gas parameter $n_B a^3$.

The Hamiltonian of a neutral single atom in the presence of a BEC is given by:

$$\mathcal{H} = \frac{\hat{p}^2}{2m_I} + \sum_{\mathbf{k}} \varepsilon_{\mathbf{k}} \hat{a}_{\mathbf{k}}^\dagger \hat{a}_{\mathbf{k}} + \frac{1}{2} \sum_{\mathbf{k}, \mathbf{k}', \mathbf{q}} V_{BB}(\mathbf{q}) \hat{a}_{\mathbf{k}'-\mathbf{q}}^\dagger \hat{a}_{\mathbf{k}+\mathbf{q}} \hat{a}_{\mathbf{k}}^\dagger \hat{a}_{\mathbf{k}'} + \sum_{\mathbf{k}, \mathbf{q}} V_{IB}(\mathbf{q}) \hat{\rho}_I(\mathbf{q}) \hat{a}_{\mathbf{k}'-\mathbf{q}}^\dagger \hat{a}_{\mathbf{k}'} \quad (4.1)$$

The first term represents the kinetic energy of the impurity atom with mass m_I and momentum p . The second term is the energy of the bosons, where $\hat{a}_{\mathbf{k}}^\dagger$ ($\hat{a}_{\mathbf{k}}$) creates (annihilates) a boson with mass m_B , wave vector \mathbf{k} , and energy $\varepsilon_{\mathbf{k}} = \hbar^2 k^2 / 2m_B - \mu$ with μ the chemical potential of the bosons. The third term depicts the interaction between bosons, where $V_{BB}(\mathbf{q})$ is the Fourier transform of the boson-boson interaction potential. Finally the interaction between the impurity and the bosons is given by the last term, where $V_{IB}(\mathbf{q})$ is the coupling potential between the boson density and the impurity density $\hat{\rho}_I(\mathbf{q})$ written as:

$$\rho_I(\mathbf{q}) = \exp(-i\mathbf{q} \cdot \mathbf{r}_I). \quad (4.2)$$

Under the same assumptions used in the first chapter for the weakly interacting Bose gas, the Bogoliubov approximation can be used on the Hamiltonian describing the impurity interacting with the bosonic bath. The Bogoliubov transformation applied on the Hamiltonian in Eq. [4.1] yields:

$$\mathcal{H} = E_0 + \sum_{\mathbf{k} \neq \mathbf{0}} E_{\mathbf{k}} \hat{b}_{\mathbf{k}}^\dagger \hat{b}_{\mathbf{k}} + \frac{\hat{p}^2}{2m_I} + n_B V_{IB}(\mathbf{0}) + \sum_{\mathbf{k} \neq \mathbf{0}} \sqrt{\frac{\xi_{\mathbf{k}} n_B}{E_{\mathbf{k}}}} V_{IB}(\mathbf{k}) \hat{\rho}_I(\mathbf{k}) (\hat{b}_{-\mathbf{k}}^\dagger + \hat{b}_{\mathbf{k}}). \quad (4.3)$$

Here $b_{\mathbf{k}}^\dagger$ and $b_{\mathbf{k}}$ represent the creation and annihilation Bogoliubov excitations with momentum \mathbf{k} and dispersion relation $E_{\mathbf{k}}$ given by:

$$E_{\mathbf{k}} = \sqrt{\xi_{\mathbf{k}} (\xi_{\mathbf{k}} + 2n_B V_{BB}(\mathbf{k}))}. \quad (4.4)$$

Where $\xi_{\mathbf{k}} = \hbar^2 k^2 / 2m_B$ and n_B is the density of the bosonic gas. The Hamiltonian Eq. [4.3] is divided as follows: the first two terms represent the Hamiltonian of a standard BEC without impurity, with E_0 the ground-state energy of the BEC given by Eq. [1.34]. Whereas the remaining terms are the contributions of the impurity, namely: the third term is the kinetic energy of the impurity with momentum p and the last two terms represent the interaction between the impurity and the BEC mediated by interaction potential between the impurity and the bosons V_{IB} .

For both the boson-boson and the impurity-boson interactions, one assumes the contact pseudo-potential written as $V_{BB}(\mathbf{r} - \mathbf{r}') = g_{BB} \delta(\mathbf{r} - \mathbf{r}')$ and $V_{IB}(\mathbf{r} - \mathbf{r}') = g_{IB} \delta(\mathbf{r} - \mathbf{r}')$. The g_{BB} and the g_{IB} can be written in terms of the s -wave boson-boson scattering length a and the impurity-boson scattering length b through the Lippmann-Schwinger equation (see Chapter 1). By using these results, the Hamiltonian Eq. [4.3] is simplified to

$$\mathcal{H} = \mathcal{H}_{pol} = \frac{\hat{p}^2}{2m_I} + \sum_{\mathbf{k} \neq \mathbf{0}} E_{\mathbf{k}} \hat{b}_{\mathbf{k}}^\dagger \hat{b}_{\mathbf{k}} + \sum_{\mathbf{k} \neq \mathbf{0}} V_{\mathbf{k}} \exp(i\mathbf{k} \cdot \mathbf{r}_I) (b_{-\mathbf{k}}^\dagger + b_{\mathbf{k}}), \quad (4.5)$$

with

$$E_{\mathbf{k}} = c\hbar |\mathbf{k}| \sqrt{1 + (\xi k)^2 / 2}, \quad (4.6)$$

and

$$V_k = \sqrt{n_B} \left[\frac{(\xi k)^2}{(\xi k)^2 + 2} \right]^{1/4} g_{IB}. \quad (4.7)$$

In the previous expressions $\xi = 1/\sqrt{8\pi a n_B}$ is the healing length and $c = \hbar/(\sqrt{2}m_B\xi)$ is the speed of the sound in the Bose-Einstein condensate.

The Hamiltonian in Eq. [4.5] is identical in structure to the Fröhlich Hamiltonian originally devised to investigate the interaction between electron/hole and longitudinal optical phonons in a crystal (see Eq. [1.9]). However, for the Fröhlich Hamiltonian in Eq. [4.5], one finds that the dispersion relation of the quasiparticles at low-momenta describes acoustic phonons. The acoustic polarons have been investigated in the context of solid-state physics see [98, 99].

As it was discussed in the first chapter, the Fröhlich Hamiltonian has been a difficult problem since it resists exact diagonalization. In our particular problem, when the impurity interacts with a BEC, the solution of the Fröhlich Hamiltonian also becomes a difficult task and many techniques have been proposed to address the problem. For instance, perturbation theory is suitable for describing the ground-state properties of the system where the impurity interacts weakly with the bosonic bath [100]. In the context of Bose-Fermi mixtures, where the fermions play the role of impurities, the ground-state properties have been also investigated with perturbative methods [101]. A variational Gaussian wave function has also been used in order to address this problem in the strongly interacting regime, where the impurity is expected to exhibit self-localization [102]. A trial wavefunction similar to that used for the fermionic polaron has been proposed and by means of variational methods the ground-state properties of the impurity immersed in a Bose bath have been investigated [103]. A Variational method based on Feynman's path integral formalism have been used to treat both the weak and the strong coupling [104, 105, 106] and features analogue to the acoustic polaron case are predicted to occur including a transition between free to self-trapped polarons [98, 107]. On the other hand, the problem has also been tackled using beyond mean-field techniques [103, 108]. In contrast with variational methods, the self-trapping of the impurity has not been found with the beyond mean-field techniques.

In this chapter we will address the problem using some of the methods mentioned above. In particular, perturbative and variational methods based on the path integral formalism are applied for the regime of weak coupling between the impurity and the BEC. Furthermore,

quantum Monte-Carlo methods are used in order to investigate the ground-state properties for any value of the coupling strength.

4.2 Perturbation Theory

4.2.1 Ground-state energy and effective mass

If the interaction between the impurity and the bosonic bath is small, a perturbative calculation can provide a reliable description of the ground-state properties of the system such as the energy and the effective mass.

One starts with the impurity-BEC Hamiltonian Eq. [4.5] written as:

$$\mathcal{H} = \mathcal{H}_0 + \mathcal{H}' \quad (4.8)$$

Where \mathcal{H}_0 is the Hamiltonian of the system without any perturbation (i.e the interaction impurity-boson vanishes) and \mathcal{H}' is the perturbation, given in terms of the impurity-BEC coupling. The Hamiltonian is split as follows:

$$\begin{aligned} \mathcal{H}_0 &= \frac{p^2}{2m_I} + E_0 + \sum_{\mathbf{k} \neq 0} E_{\mathbf{k}} b_{\mathbf{k}}^\dagger b_{\mathbf{k}} \\ \mathcal{H}' &= n_B g_{IB}(\mathbf{0}) + \sum_{\mathbf{k} \neq 0} V_{\mathbf{k}} \exp(i\mathbf{k} \cdot \mathbf{r}_I) (b_{\mathbf{k}}^\dagger + b_{\mathbf{k}}) \end{aligned} \quad (4.9)$$

Up to second-order, the correction to the energy can be written as

$$E(N_B, 1) = E_0(N_B) + \langle 0 | \mathcal{H}' | 0 \rangle + \sum_n \frac{\langle 0 | \mathcal{H}' | n \rangle \langle n | \mathcal{H}' | 0 \rangle}{E_0^0 - E_n^0} + \dots, \quad (4.10)$$

where $|0\rangle$ represents the state formed by the ground-state of the BEC and the impurity with momentum p . Whereas $|n\rangle$ is an excited state represented by the collision between one phonon of the bosonic bath and the impurity (see Fig. [4.1]). The first-order term yields the mean-field energy of the system characterized by the coupling strength g_{IB} :

$$\langle 0 | \mathcal{H}' | 0 \rangle = g_{IB} n_B. \quad (4.11)$$

A relevant detail concerning the coupling strengths g_{BB} and g_{IB} must be considered with care. The proper relation between g_{IB} and the s -wave scattering length b is obtained by solving the Lippmann-Schwinger equation Eq. [1.37] up to second-order. The proper relation between g_{IB} and b is written as:

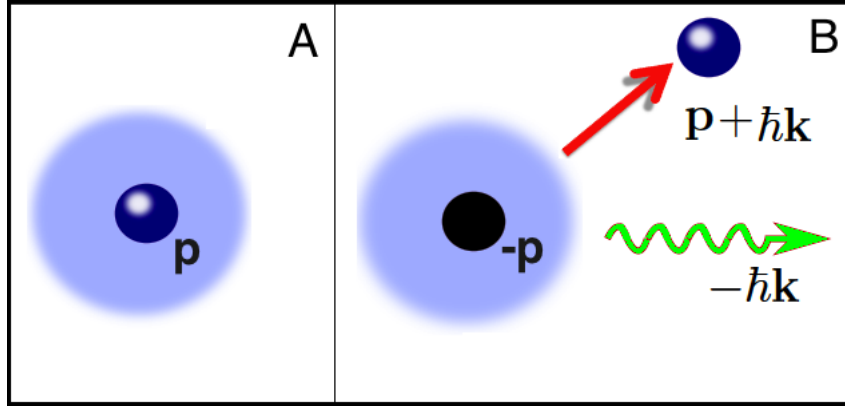


Figure 4.1: **Perturbation of the impurity in the bosonic bath:** **A)** The initial state has an impurity of momentum p and no phonons **B)** an excited state is represented by the impurity with momentum $\mathbf{p} + \hbar\mathbf{k}$ and a phonon with momentum $-\hbar\mathbf{k}$.

$$\frac{2\pi\hbar^2b}{m_r} = g_{IB} - g_{IB}^2 \sum_{k' \neq 0} \frac{2m_r}{(\hbar k')^2}, \quad (4.12)$$

where m_r is the reduced mass ($m_r^{-1} = m_B^{-1} + m_I^{-1}$). Therefore g_{IB} must be replaced by:

$$g_{IB} \rightarrow \frac{2\pi\hbar^2b}{m_r} + g_{IB}^2 \sum_{k' \neq 0} \frac{2m_r}{(\hbar k')^2}. \quad (4.13)$$

The second-order correction to the energy is given by

$$\Delta E^{(2)} = \sum_{n \neq 0} \frac{|\langle 0 | \mathcal{H}' | n \rangle|^2}{E_0 - E_n} + \frac{n_B g_{IB}^2}{V} \sum_k \frac{2m_R}{\hbar^2 k^2}. \quad (4.14)$$

Fig. [4.1] shows the process involved in the second-order term of Eq. [4.14]: the initial state consists of one impurity with momentum p and the BEC in the ground-state [4.1.A] and $E_0 = p^2/2m_I$. Then, in an excited state the impurity has a momentum $\mathbf{p} + \hbar\mathbf{k}$ and an excitation with momentum $-\hbar\mathbf{k}$ is present. The second-order process is represented by the collision of the impurity with one excitation of the bosonic bath. The energy of this excited state is $E_n^0 = (\mathbf{p} + \hbar\mathbf{k})^2/2m_I + E_k$. Therefore

$$\langle n | \mathcal{H}' | 0 \rangle = \left\langle n \left| \sum_{\mathbf{k} \neq 0} V_{\mathbf{k}} \exp(i\mathbf{k} \cdot \mathbf{r}_I) \hat{b}_{\mathbf{k}}^\dagger \right| \mathbf{p}, \text{No phonons} \right\rangle. \quad (4.15)$$

In addition, if $|n\rangle = |p', 1 \text{ phonon}\rangle$ and using the fact that $\exp(i\mathbf{k} \cdot \mathbf{r}) |\mathbf{p}\rangle = |\mathbf{p} + \hbar\mathbf{k}\rangle$. One obtains

$$\begin{aligned}\langle n|\mathcal{H}'|0\rangle &= \sum_{\mathbf{k}\neq\mathbf{0}} V_{\mathbf{k}} \langle \mathbf{p}', 1 \text{ phonon} | \hat{b}_{\mathbf{k}}^\dagger | \mathbf{p} + \hbar\mathbf{k}, \text{ No phonons} \rangle \\ &= \sum_{\mathbf{k}\neq\mathbf{0}} V_{\mathbf{k}} \delta_{\mathbf{p}', \mathbf{p} + \hbar\mathbf{k}},\end{aligned}\quad (4.16)$$

where $\hat{b}_{\mathbf{k}}^\dagger$ creates a phonon with energy $E_{\mathbf{k}}$. The momentum conservation requires that $\mathbf{p}' = \mathbf{p} + \hbar\mathbf{k}$. We obtain for the second-correction to the energy

$$\Delta E^{(2)} = \sum_{\mathbf{k}} \frac{V_{\mathbf{k}}^2}{\frac{(\mathbf{p}+\mathbf{k})^2}{2m_I} + E_{\mathbf{k}} - \frac{\mathbf{p}^2}{2m_I}} + \frac{n_B g_{IB}^2}{V} \sum_{\mathbf{k}} \frac{2m_R}{\hbar^2 k^2} \quad (4.17)$$

with

$$V_{\mathbf{k}}^2 = n_B g_{IB}^2 \left(\frac{\varepsilon_{\mathbf{k}}}{E_{\mathbf{k}}} \right). \quad (4.18)$$

The second-order correction turns out to be

$$\Delta E^{(2)} = \frac{n_B g_{IB}^2}{V} \left[\sum_{\mathbf{k}} \frac{2m_R}{\hbar^2 k^2} - \sum_{\mathbf{k}} \left(\frac{\varepsilon_{\mathbf{k}}}{E_{\mathbf{k}}} \right) \frac{1}{\frac{\hbar^2}{2m_I} (|\mathbf{k}|^2 + \mathbf{p} \cdot \hbar\mathbf{k}) + E_{\mathbf{k}}} \right]. \quad (4.19)$$

The previous expression can be expanded for small impurity momentum p . The sum over wave vectors becomes

$$\begin{aligned}& \sum_{\mathbf{k}} \left(\frac{\varepsilon_{\mathbf{k}}}{E_{\mathbf{k}}} \right) \frac{1}{\frac{\hbar^2}{2m_I} \mathbf{p} \cdot \hbar\mathbf{k} + \frac{\hbar^2}{2m_I} |\mathbf{k}|^2 + E_{\mathbf{k}}} \\ &= \sum_{\mathbf{k}} \left(\frac{\varepsilon_{\mathbf{k}}}{E_{\mathbf{k}}} \right) \left[\frac{1}{\frac{\hbar^2}{2m_I} |\mathbf{k}|^2 + E_{\mathbf{k}}} - \frac{\frac{\hbar^2}{2m_I} |\mathbf{k}| \cos \theta}{\left(\frac{\hbar^2}{2m_I} |\mathbf{k}|^2 + E_{\mathbf{k}} \right)} |\mathbf{p}| - \frac{\left(\frac{\hbar^2}{2m_I} \right)^2 |\hbar\mathbf{k}|^2 \cos^2 \theta}{\left(\frac{\hbar^2}{2m_I} |\mathbf{k}|^2 + E_{\mathbf{k}} \right)^3} \mathbf{p}^2 + \mathcal{O}(\mathbf{p}^3) \right].\end{aligned}\quad (4.20)$$

The term independent of \mathbf{p} gives the connection to the ground-state energy. After replacing the sum with an integral, $\sum_{\mathbf{k}} \rightarrow \frac{V}{(2\pi)^3}$ one finds

$$\Delta E^{(2)} = n_B g_{IB}^2 \frac{1}{(2\pi)^3} \int d\mathbf{k} \left(\frac{2m_R k^2}{\hbar^2 k^2} - \frac{\varepsilon_{\mathbf{k}}^B \hbar^2 k^2}{E_{\mathbf{k}} \left(E_{\mathbf{k}} + \frac{\hbar^2}{2m_I} k^2 \right)} \right), \quad (4.21)$$

then,

$$\Delta E^{(2)} = \frac{n_B 16\pi^2 \hbar^4 b^2 (m_B + m_I)^2}{(m_B m_I)^2 (2\pi)^3} \underbrace{\int_{4\pi} d\varphi \int \sin \theta d\theta}_{4\pi} \int_0^\infty dk \left(\frac{2m_B m_I}{(m_B + m_I) \hbar^2} - \frac{\varepsilon_{\mathbf{k}}^B k^2}{E_{\mathbf{k}} \left(E_{\mathbf{k}} + \frac{\hbar^2}{2m_I} k^2 \right)} \right), \quad (4.22)$$

$$\Delta E^{(2)} = \underbrace{\frac{n_B 64 \pi^3 \hbar^4 b^2 (m_B + m_I)^2 2 m_B m_I}{(m_B m_I)^2 (2\pi)^3 (m_B + m_I) \hbar^2}}_{A_0} \int_0^\infty dk \left(1 - \frac{\hbar^2 (m_B + m_I) \frac{\hbar^2}{2m_B} k^4}{2 (m_B m_I) E_k \left(E_k + \frac{\hbar^2}{2m_I} k^2 \right)} \right). \quad (4.23)$$

The previous integral can be performed by using the following substitutions $E_k = \frac{\hbar^2}{2m_B} k \sqrt{k^2 + \alpha^2}$, with $\alpha^2 = \frac{16\pi n_B a^3}{a^2}$ and $\chi = \frac{m_I}{m_B}$. Finally one needs to calculate the following integral

$$\Delta E^{(2)} = A_0 \int_0^\infty dk \left[1 - \frac{(1 + \chi) k^2}{\sqrt{k^2 + \alpha^2} (\chi \sqrt{k^2 + \alpha^2} + k)} \right]. \quad (4.24)$$

In our specific case, one considers the balanced case where the masses of the bosons are equal to the mass of the impurity ($\chi = 1$). Additionally a change of variable is done $\zeta = \alpha/k$ yielding

$$\Delta E^{(2)} = A_0 \alpha \underbrace{\int_0^\infty d\zeta \left[1 - \frac{2\zeta^2}{\sqrt{\zeta^2 + 1} (\sqrt{\zeta^2 + 1} + \zeta)} \right]}_{=4/3}. \quad (4.25)$$

Finally, the second-order correction is given by

$$\Delta E^{(2)} = \left[\frac{256}{3} \sqrt{\pi} (n_B a^3)^{3/2} \left(\frac{\mathbf{b}}{\mathbf{a}} \right)^2 \right] \frac{\hbar^2}{2ma^2}. \quad (4.26)$$

For the total to the ground-state energy one finds:

$$E(N_B, 1) = E_0(N_B) + 8\pi (n_B a^3) \left[\left(\frac{\mathbf{b}}{\mathbf{a}} \right) + \frac{32}{3\sqrt{\pi}} (n_B a^3)^{1/2} \left(\frac{\mathbf{b}}{\mathbf{a}} \right)^2 \right] \frac{\hbar^2}{2ma^2}. \quad (4.27)$$

Valid to order b^2 . This total energy depends on both the gas parameter $n_B a^3$ and the coupling strength b/a .

The **binding energy** of the impurity is defined as:

$$\mu = E(N_B, 1) - E_0(N_B), \quad (4.28)$$

where $E_0(N_B)$ is the ground-state energy of the system of bosons without impurity (see Eq. [1.34]) and $E(N_B, 1)$ is the energy of the system of N_B bosons plus the impurity at the same volume V . For the perturbative case, one finds

$$\mu = 8\pi (n_B a^3) \left[\left(\frac{\mathbf{b}}{\mathbf{a}} \right) + \frac{32}{3\sqrt{\pi}} (n_B a^3)^{1/2} \left(\frac{\mathbf{b}}{\mathbf{a}} \right)^2 \right] \frac{\hbar^2}{2m a^2}. \quad (4.29)$$

A useful quantity is also **the reduced binding energy** defined as the binding energy once the mean-field shift has been removed:

$$F = E(N_B, 1) - E_0(N_B) - 8\pi (n_B a^3) \left(\frac{\mathbf{b}}{\mathbf{a}} \right). \quad (4.30)$$

For the perturbative case, the previous expression is:

$$F = \left[\mu - 8\pi (n_B a^3) \left(\frac{\mathbf{b}}{\mathbf{a}} \right) \right] = \frac{256}{3} \sqrt{\pi} (n_B a^3)^{3/2} \left(\frac{\mathbf{b}}{\mathbf{a}} \right)^2. \quad (4.31)$$

written in units of $\left(\frac{\hbar^2}{2m_B a^2} \right)$.

4.2.2 Effective mass

In the previous section we calculated the ground-state energy of a system of one impurity coupled to a bath of non-interacting bosonic quasiparticles. From the energy as a function of the polaron momentum \mathbf{p} in Eq. [4.19] is possible to obtain the effective mass of the polaron.

The energy of the system can be expanded in the following form

$$E(N_B + 1, \mathbf{p}) = E_0(N_B) + \mu + \underbrace{\frac{\mathbf{p}^2}{2m^*}}_{\Delta E^{(2)}} \cdots \quad (4.32)$$

where $E(N_B + 1, \mathbf{p})$ and $E_0(N_B)$ are the energy of the bosonic bath with an impurity of momentum \mathbf{p} and the ground-state energy of the system without the impurity and μ stands for the binding energy of the impurity (see Eq. [4.28]). The effective mass m^* is related to the kinetic energy of the quasiparticle with momentum \mathbf{p} [109]. From the expansion Eq. [4.19] and Eq. [4.20]. One gets that

$$\Delta E^{(2)} = n_B g_{BF}^2 \frac{1}{(2\pi)^3} \int d^3 \mathbf{k} \sqrt{\frac{(\xi k)^2}{(\xi k)^2 + 2} \frac{\left(\frac{\hbar^2}{2m_I} \right)^2 k^2 \cos^2 \theta}{\left(\hbar \omega_k + \frac{\hbar^2 \mathbf{k}^2}{2m_I} \right)^3}} \mathbf{p}^2 = \frac{\mathbf{p}^2}{2m^*}. \quad (4.33)$$

By carrying out the calculations on the angular part and by using the substitutions $\alpha^2 = 16\pi n_B a = 2\xi^{-2}$, $y = \alpha k$ and $\gamma = m_I/m_B$ one ends up with

$$\Delta E^{(2)} = \frac{8\hbar^2}{3m_I} (1 + \gamma)^2 \mathbf{p}^2 \int_0^\infty \alpha dy \frac{(\alpha y)^2}{\alpha\sqrt{y^2+1} (\alpha\gamma\sqrt{y^2+1} + \alpha y)^3}. \quad (4.34)$$

By using the fact that $\int_0^\infty dy \frac{y^2}{\sqrt{y^2+1}(\sqrt{y^2+1}+y)^3} = \frac{2}{15}$, one obtains

$$\frac{m}{m^*} = 1 + \frac{64}{45\sqrt{\pi}} \sqrt{(n_B a^3)} \left(\frac{b}{a}\right)^2. \quad (4.35)$$

Independently of the sign of the coupling strength b/a there is an increase of the effective mass. In other words, either attractive and repulsive interactions produce an increase of the effective mass. Apart from the trivial first-order contribution $g_{IB}n_B$ to the ground-state energy, the second-order corrections in Eq. [4.27] and Eq. [4.35] scale in terms of the same dimensionless parameter $\sqrt{n_B a^3} \left(\frac{b}{a}\right)^2$. The condition

$$\sqrt{n_B a^3} \left(\frac{b}{a}\right)^2 \ll 1, \quad (4.36)$$

therefore must be satisfied in order to ensure the validity of the perturbation approach. For the strongly interacting limit where $\sqrt{n_B a^3} \left(\frac{b}{a}\right)^2 > 1$ mean-field methods are not reliable, we will employ QMC methods (see Chapter 3).

We made use of perturbation methods to calculate the polaron binding energy (see Eq. [4.31]) and its effective mass (see Eq. [4.35]) in the weakly interacting regime. In the following subsection a variational principle based on the path integral formalism is used to investigate the problem. This formalism has been widely employed in the problem of impurities interacting with a BEC [104] not only restricted to the weak coupling regime between the impurity and the bosons, but also exploring the regime where correlations are strong [106, 107].

Starting from the general Hamiltonian of the impurity interacting with the BEC in Eq. [4.5], an expression for the reduced binding energy at finite temperature in terms of the action of the system is derived. Then, the reduced binding energy is minimized with respect to certain variational parameters. In this work, the particular case of zero temperature is considered. We will determine the reduced binding energy at zero temperature with the variational formalism showing that it agrees with the result of perturbation theory. Using the variational method, one finds a behaviour similar to acoustic polarons in solid-state physics, including a transition between free to self-trapped polarons [104, 107].

4.3 Variational principle: the Jensen-Feynman formalism

The literature about polarons in a BEC investigated using the path integral variational method is reviewed in [104]. In the following we will summarize the main features of the method.

The variational principle considered here states the following inequality involving the free energy

$$F \leq F_0 + \langle \mathcal{H} - \mathcal{H}_0 \rangle_0, \quad (4.37)$$

where F and \mathcal{H} represent respectively the free energy and the Hamiltonian given by Eq. [4.5] of the real system. The subscript “0” in the previous expression stands for the model system that will be introduced in the following. It can be shown (see Ref.[21]) that the free energy of the system can be written

$$F \leq F_0 + \frac{1}{\hbar\beta} \langle S - S_0 \rangle_0. \quad (4.38)$$

Here S is the action of the system described by the Hamiltonian in Eq. [4.5]. This action S is found by integrating out the degrees of freedom corresponding to the Bogoliubov excitations [23]. One obtains

$$S = \int_0^{\hbar\beta} \frac{1}{2} m_I \dot{r}^2(\tau) d\tau - \sum_{\mathbf{k} \neq 0} \frac{|V_{\mathbf{k}}|^2}{2\hbar} \int_0^{\hbar\beta} d\tau \int_0^{\hbar\beta} d\sigma \mathcal{G}(\mathbf{k}, |\tau - \sigma|) \exp(i\mathbf{k} \cdot [\mathbf{r}(\tau) - \mathbf{r}(\sigma)]), \quad (4.39)$$

where $\beta = 1/K_B T$, m_I is the mass of the impurity, \dot{r} is the velocity of the impurity, $\tau = it$ is the imaginary time and \mathcal{G} denotes the Green’s function of the Bogoliubov excitations. The latter function is given by:

$$\mathcal{G}(\mathbf{k}, u) = \frac{\cosh[\omega_{\mathbf{k}}(u - \hbar\beta/2)]}{\sinh(\hbar\beta\omega_{\mathbf{k}}/2)}. \quad (4.40)$$

The system composed of an impurity interacting with the Bogoliubov excitations of the bosonic bath is modeled by a mass m coupled to another mass M through a spring with spring constant MW^2 (see Fig. [4.2]). Both M and W are variational parameters. The action corresponding to this trial system is given by:

$$S_0 = \int_0^{\hbar\beta} \frac{1}{2} m_I \dot{r}^2(\tau) d\tau + \frac{MW^3}{8} \int_0^{\hbar\beta} d\tau \int_0^{\hbar\beta} d\sigma \frac{\cosh[\omega_{\mathbf{k}}(u - \hbar\beta/2)]}{\sinh(\hbar\beta\omega_{\mathbf{k}}/2)} |\mathbf{r}(\tau) - \mathbf{r}(\sigma)|^2. \quad (4.41)$$

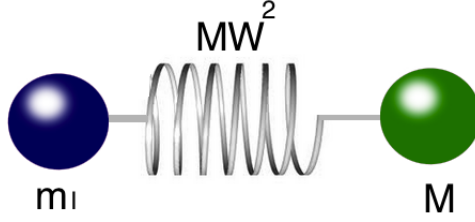


Figure 4.2: **Variational model for an impurity interacting with a BEC:** the impurity with mass m_I harmonically coupled to the bosonic bath with total mass M with spring constant MW^2 .

By plugging Eq. [4.39], Eq. [4.41] and Eq. [4.38] into the Jensen-Feynman inequality (see Refs. [21, 104]), one ends up with an expression for the free energy

$$\begin{aligned}
F(M, \Omega) \leq & -\frac{3}{2\beta} \ln \left[\frac{m_I + M}{m_I} \right] - \frac{3}{2\beta} \left[\frac{M}{m_I + M} \right] \left(\frac{\hbar\beta\Omega}{2} \coth \left[\frac{\hbar\beta\Omega}{2} \right] - 1 \right) \\
& + \frac{3}{\beta} \left\{ \ln \left[2 \sinh \left(\frac{\hbar\beta\Omega}{2} \right) \right] - \ln \left[2 \sinh \left(\frac{\hbar\beta\Omega}{2\sqrt{1+M/m_I}} \right) \right] \right\} \\
& - \sum_k \frac{|V_k|^2}{\hbar} \int_0^{\hbar\beta} du \left(1 - \frac{u}{\hbar\beta} \right) \mathcal{G}(\mathbf{k}, u) \mathcal{M}(\mathbf{k}, u; M, \Omega).
\end{aligned} \tag{4.42}$$

Here Ω a variational parameter that contains M and W , defined as $\Omega = W\sqrt{1 + M/m_I}$ and $\mathcal{M}(\mathbf{k}, u; M, \Omega)$ is called memory function and is given by

$$\mathcal{M}(\mathbf{k}, u; \mathbf{M}, \Omega) = \exp \left[-\frac{\hbar k^2}{2(m_I + M)} \left(u - \frac{u^2}{\hbar\beta} - \frac{M \cosh [\Omega\hbar\beta/2] - \cosh [\Omega(\hbar\beta/2 - u)]}{\Omega \sinh (\Omega\hbar\beta/2)} \right) \right]. \tag{4.43}$$

As it was discussed in the previous section, the proper relation between the coupling strength g_{IB} and the s -wave scattering length must be introduced. In addition, by plugging Eq. [4.6] and Eq. [4.7] into Eq. [4.42], one finds

$$\begin{aligned}
F \leq & \frac{3}{2\beta} \ln (1 + M) + \frac{3}{\beta} \left\{ \ln \left[2 \sinh \left(\frac{\beta\Omega}{2} \right) \right] - \ln \left[2 \sinh \left(\frac{\beta\Omega}{2\sqrt{1+M}} \right) \right] \right\} \\
& - \frac{3}{2\beta} \left[\frac{M}{1+M} \right] \left(\frac{\beta\Omega}{2} \coth \left[\frac{\beta\Omega}{2} \right] - 1 \right) \\
& + \frac{\mathbf{b}^2}{\mathbf{a}\xi} \left(\frac{1+\chi}{\chi} \right)^2 \frac{1}{4\pi} \int dk \left[\left(\frac{2\chi}{1+\chi} \right) - \frac{k^3}{\sqrt{2+k^2}} \int_0^{\beta/2} \mathcal{G}(\mathbf{k}, u) \mathcal{M}(\mathbf{k}, u; M, \Omega) \right].
\end{aligned} \tag{4.44}$$

The Green's function and the memory function respectively are given by:

$$\mathcal{G}(\mathbf{k}, u) = \frac{\cosh \left[k\sqrt{k^2 + 2} (2u - \beta) / 4\chi \right]}{\sinh \left(\beta k\sqrt{k^2 + 2} / 4\chi \right)}. \tag{4.45}$$

and

$$\mathcal{M}(\mathbf{k}, u; M, \Omega) = \exp \left[-\frac{k^2}{2(1+M)} \left(\frac{u(\beta-u)}{\beta} + M \frac{\cosh[\Omega\beta/2] - \cosh[\Omega(\beta/2-u)]}{\Omega \sinh(\Omega\beta/2)} \right) \right]. \quad (4.46)$$

Where $\hbar = m_I = \xi = 1$ and the ratio between masses is defined as $\chi = m_B/m_I = 1$ and the energy is in units of $\hbar^2/(m_I\xi^2)$. The integration variables k and u as well as the variational parameters M and Ω are dimensionless.

Let us turn our attention to the $T = 0$ case. The corresponding expression for the Green's function in Eq. [4.45] and the memory function at zero temperature ($\beta \rightarrow \infty$) in Eq. [4.46] reads

$$\lim_{\beta \rightarrow \infty} \mathcal{G}(\mathbf{k}, u) = \mathcal{G}^{T=0}(\mathbf{k}, u) = \exp \left[\frac{-k}{2m_B} \sqrt{2+k^2} u \right], \quad (4.47)$$

$$\lim_{\beta \rightarrow \infty} \mathcal{M}(\mathbf{k}, u; M, \Omega) = \mathcal{M}^{T=0}(\mathbf{k}, u; M, \Omega) = \exp \left[-\frac{k^2}{2(1+M)} \left(u + M \frac{1 - \exp[-\Omega u]}{\Omega} \right) \right]. \quad (4.48)$$

By plugging these expressions in Eq. [4.46] one obtains the following results for the free energy at $T = 0$

$$F = \frac{3\Omega(\sqrt{1+M}-1)^2}{4(1+M)} + \left[\frac{K_c}{\pi} - \frac{1}{\pi} \int_0^{K_c} dk \frac{k^3}{\sqrt{k^2+2}} \int_0^\infty du \mathcal{G}^{T=0}(\mathbf{k}, u) \mathcal{M}^{T=0}(\mathbf{k}, u; M, \Omega) \right] \left(\frac{b^2}{a\xi} \right). \quad (4.49)$$

Here K_c is a cut-off that depends on the physical parameters of the system. The above free energy is known as the **Jensen-Feynman polaron energy or Jensen-Feynman reduced binding energy**.

The weak coupling limit is recovered by taking the limit $M \rightarrow 0$ in Eq. [4.49] corresponding to the trial action $S_0 = \int_0^{\hbar\beta} m_I \dot{r}^2(\tau)/2$. The Jensen-Feynman reduced binding energy in this regime is written as:

$$E_{pol}^{weak} = \left[\frac{4\sqrt{2}}{3\pi} \frac{b^2}{a\xi} \right] \left(\frac{\hbar^2}{m_I\xi^2} \right). \quad (4.50)$$

After the transformation

$$\left(\frac{\hbar^2}{m_I\xi^2} \right) = 8\pi n_B a \left(\frac{\hbar^2}{m_I} \right) = 16\pi n_B a^3 \left(\frac{\hbar^2}{2m_I a^2} \right), \quad (4.51)$$

one recovers the perturbation theory result given (see Eq. [4.31]). Within this formalism the strong coupling regime has been discussed in Ref. [106].

The effective mass of the polaron can be derived from the propagation of the particle from $R(\tau = 0)$ to $R(\tau) = R(\tau = 0) + v\tau$ by using a transition probability of the form $e^{m_{pol}v^2\tau/2}$ [see 4.49]. The value of m_{pol} ranges between 1 and $1 + M$ (for the case of equal masses) with M the variational parameter defined previously [104]. According to the Jensen-Feynman calculation of the effective mass, there is a critical value of the interaction strength where the effective mass increases rapidly. This behavior qualitatively agrees with the jump of several orders of magnitude in the effective mass of electron interacting with acoustic phonons in solid-state physics.

4.4 Strongly interacting regime: mean-field techniques and QMC calculation

So far we have discussed the problem of an impurity immersed in a bosonic bath by means of mean-field methods such as perturbation theory. We also have used methods addressing the problem from a variational point of view: namely the Jensen-Feynman approach. The results obtained using perturbation theory for the ground-state energy and for the effective mass of the polaron are restricted to the weak-coupling regime between the impurity and the bosonic bath. More interesting features are expected to appear when one enters the strongly interacting limit. In this regime QMC methods can provide a reliable description of the ground-state properties. We now discuss the specific implementation of QMC methods for the problem of the impurity coupled to the bosonic bath.

The ground-state properties are investigated for a specific value of the gas parameter, $n_B a^3 = 10^{-5}$, which is realistic for ultracold atoms experiments.

4.4.1 Local energy for the impurity problem

In the previous chapter we learned how to calculate the energy of the weakly interacting Bose gas with QMC methods (see Eq. [3.95]). For the system of an impurity interacting with a Bose gas at zero temperature, we consider the impurity plus N_B bosons in a cubic box of size L with periodic boundary conditions. In the simulation box we have $N_B + 1$ particles with a bosonic density $n_B = N_B/V$ and a gas parameter given by $n_B a^3$, where a is the s -wave boson-boson scattering length.

The trial wave function for this system can be written as:

$$\psi_T(\mathbf{R}) = \prod_{i=1}^{N_B} f_I(r_{i\alpha}) \prod_{i<j} f(r_{ij}), \quad (4.52)$$

with $\mathbf{R} = \{\mathbf{r}_\alpha, \mathbf{r}_1, \dots, \mathbf{r}_i, \dots, \mathbf{r}_N\}$. Here, \mathbf{r}_α is the position of the impurity and \mathbf{r}_i is the position of the i -th boson. The functions f and f_I describe respectively, the inter-boson and impurity-boson correlations. Both correlation functions were discussed in the previous chapter (see Sec. 3.6).

The local energy (see Eq. [3.99]) associated with the trial wave function in Eq. [4.52] yields:

$$E_L(\mathbf{R}) = -D \left\{ \sum_{i=1}^{N_B} \left[\frac{f_I''(r_{i\alpha})}{f_I(r_{i\alpha})} + \frac{2}{r_{i\alpha}} \frac{f_I'(r_{i\alpha})}{f_I(r_{i\alpha})} - \left(\frac{f_I'(r_{i\alpha})}{f_I(r_{i\alpha})} \right)^2 \right] + \sum_{i<j}^{N_B} \left[\frac{f''(r_{ij})}{f(r_{ij})} + \frac{2}{r_{ij}} \frac{f'(r_{ij})}{f(r_{ij})} - \left(\frac{f'(r_{ij})}{f(r_{ij})} \right)^2 \right] \right. \\ \left. + \frac{1}{4} \sum_i \mathbf{F}_I^2 + \frac{1}{4} \sum_i \mathbf{F}_{B,i}^2 + \frac{1}{2} \sum_i \mathbf{F}_I \cdot \mathbf{F}_{B,i} \right\} + V(\mathbf{R}), \quad (4.53)$$

where $r_{i\alpha} = |\mathbf{r}_i - \mathbf{r}_\alpha|$ and $r_{ij} = |\mathbf{r}_i - \mathbf{r}_j|$. The quantum drift force are given by:

$$\mathbf{F}_I = 2 \sum_{i=1}^{N_B} \left(\frac{r_i - r_\alpha}{r_{i\alpha}} \right) \frac{f_I'(r_{i\alpha})}{f_I(r_{i\alpha})} \quad (4.54)$$

and

$$\mathbf{F}_{B,i} = 2 \sum_{i \neq j} \left(\frac{r_i - r_j}{r_{ij}} \right) \frac{f'(r_{ij})}{f(r_{ij})}. \quad (4.55)$$

From the local energy in Eq. [4.53] and by using Eq. [3.95] we determine $E^{DMC}(N_B, 1)$. Then, the binding energy can be calculated as:

$$\mu = E^{DMC}(N_B, 1) - E_0^{DMC}(N_B), \quad (4.56)$$

and accordingly to Eq. [4.30], we define the DMC reduced binding energy as:

$$F = E^{DMC}(N_B, 1) - E_0^{DMC}(N_B) - 8\pi \left(n_B a^3 \right) \frac{b}{a}, \quad (4.57)$$

where $E_0^{DMC}(N_B)$ is the DMC energy for the system without impurity. The study of the bias from the time-step ($\delta\tau$) and number of walkers (N^w) has been carried out as explained in the section [3.9].

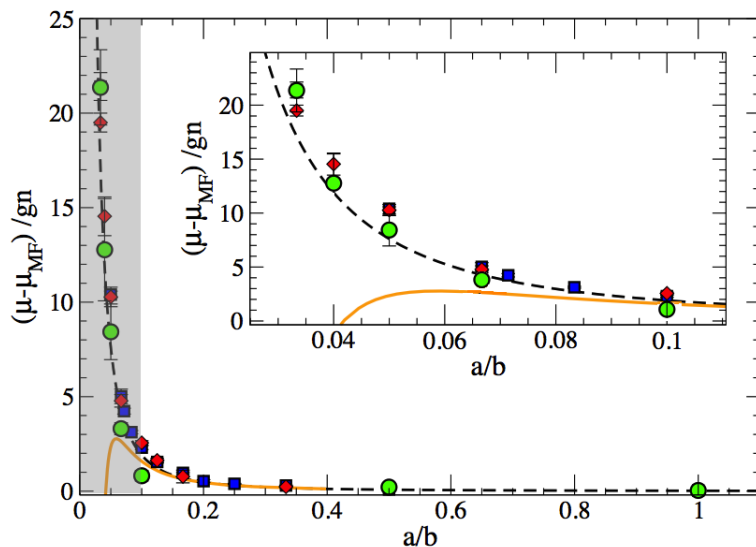


Figure 4.3: **Reduced binding energy** ($F = \mu - \mu_{MF}$) **in units of** $\frac{4\pi\hbar^2 n_B a}{m}$ **as a function of the coupling strength** a/b computed with perturbation theory (dashed black line), using the Jensen-Feynman variational formalism (solid orange line) and the DMC method for two different ASW potential ranges $a/R_0 = 5$ (filled green circles) and $a/R_0 = 20$ (filled red diamonds) and the HS potential (blue square).

4.4.2 Binding energy of the polaron

The binding energy of the impurity interacting with the bosonic bath displays two branches. The **repulsive branch** is present only for $a/b > 0$ and represents an excited state of the impurity. The **attractive branch** is present for any value of a/b and represents the many body ground-state. We remind that b is the s -wave scattering length between the impurity and the bosons of the bath. In particular, following the **attractive branch** one can enter the **unitary limit** where the impurity-boson scattering length b diverges ($a/b = 0$). This regime will be investigated separately in chapter 5.

In this section we compare the results of the reduced binding energy obtained from perturbation theory, from the Jensen-Feynman variational approach and from QMC calculations. The reduced binding energy F is given by Eq. [4.31] in the approach of perturbation theory, by Eq. [4.44] in the Jensen-Feynman approach and given by Eq. [4.57] within the QMC method.

The results for the reduced binding energy $F = \mu - \mu_{MF}$ in units of $gn_B = \frac{4\pi\hbar^2 n_B a}{m}$ are shown in Fig. [4.3] for the **repulsive branch**. In the weakly interacting limit ($a/b \gtrsim 0.1$) all calculations are in a good agreement. In this regime, the most important contribution comes from the mean-field term μ_{MF} and the correction is tiny and positive. Notice that, in the DMC simulations we used for the impurity-boson interaction both a HS potential (see Eq. [3.58]) and a short-range ASW potential (see Eq. [3.66]) with two different ranges: $R_0 = 0.2a$ and $R_0 = 0.05a$. We

observe no effects due the range R_0 confirming that the short-range details of the potential are not important, provided that it gives the proper value of the s -wave scattering length b .

On the contrary in the strongly interacting regime ($a/b \lesssim 0.1$) shown by both the shadow region and the inset in Fig. [4.3], significant deviations appear between perturbation theory, the Jensen-Feynman variational approach and DMC simulations. The deviations between perturbation theory and DMC calculation are smaller compared with the ones shown with respect to the Jensen-Feynman approach. Both the DMC and the perturbation theory results of the reduced binding energy increase with a/b , whereas the Jensen-Feynman result decreases becoming negative at a certain value of the coupling strength. The deviations between the QMC results and perturbation theory is explained in terms of the range of validity of the latter, in fact perturbation theory is expected to work only if $\left|\frac{a}{b}\right| \ll (n_B a^3)^{-1/4}$ (see Sec [4.2]). The deviations between the Jensen-Feynman approach and the DMC simulations can be explained as follows. On one side, the Jensen-Feynman results are obtained from the minimization of the energy functional associated with the Fröhlich's Hamiltonian. The Fröhlich Hamiltonian described the impurity coupled to the low-energy excitations of the bosonic bath and for a certain critical value $\frac{a}{b} < 0.068$, the Fröhlich polaron undergoes a transition from a mobile to a self-localized state. On the other side, a question mark remains as to whether the Fröhlich Hamiltonian, being a low-energy effective Hamiltonian, still provides a correct description of the system in the regime of strong coupling.

For the repulsive branch, we used for the impurity-boson interaction an ASW potential and the trial wavefunction f_I (see Eq. 3.66). which corresponds to the scattering solution of the two-body problem. The ASW potential also admits a bound state with energy $\epsilon_B < 0$. The function f_I is orthogonal to this bound state and decay into the ground state is avoided for the two-body problem. At the many-body level the trial wavefunction we use contains a nodal surface that allows one to follow the excited branch of the polaron preventing its decay into the ground-state attractive branch. We can only follow this repulsive branch up to values of $\frac{a}{b} \sim 0.03$. Beyond that point large fluctuations in the energy make the calculation unfeasible. The energy we obtain with the DMC algorithm is the lowest compatible with the nodal surface fixed with the choice of the trial wave function.

We discuss now the attractive branch corresponding to the ground-state of the polaron. We use both perturbation theory and QMC methods to investigate this branch. For the impurity-boson interaction in the DMC calculations we use a short-range ASW potential (see Eq. [3.66]) with two different ranges $R_0 = 0.2a$ and $R_0 = 0.05a$. The trial wave function f_I for the attractive branch is given by Eq. [3.66] for the $a/b < 0$ side which corresponds to scattering states at negative scattering length and by Eq. [3.67] for the $a/b > 0$ side, which corresponds to a two-body bound state with energy ϵ_B . For $a/b = 0$, namely the **unitary limit**, both Eq. [3.66] and Eq. [3.67] give the same result.

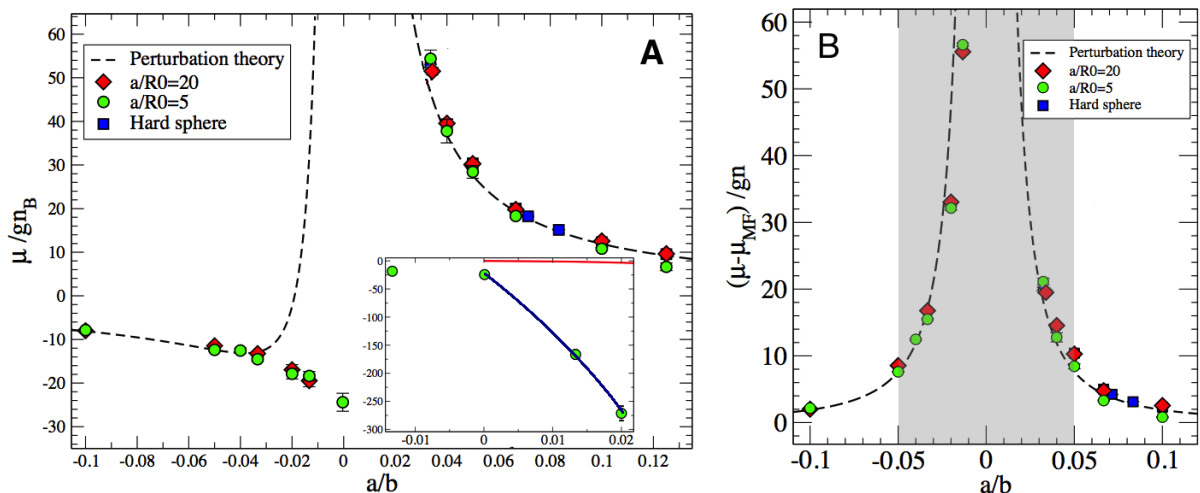


Figure 4.4: **(A) Binding energy** as a function of the strength interaction, for both the attractive and repulsive branch. In the inset we show the binding energy for $a/b > 0$ along the attractive branch. The red line shows the two-body binding energy **(B) Reduced binding energy** as a function of the coupling strength a/b for both the attractive and the repulsive branch.

The binding energy μ in units of gn_B defined by Eq. [4.28] in the perturbation theory approach and by Eq. [4.56] within the DMC method are plotted in Fig. [4.4, A] for both the repulsive and the attractive branch. Similar to the repulsive branch we observe no dependence of the energy on the range R_0 of the ASW potential. In the attractive branch we find that DMC calculations and perturbation theory (see Eq. [4.31]) are in good agreement in the weakly interacting limit ($\frac{a}{b} \lesssim -0.03$). On the contrary, for values of ($\frac{a}{b} \gtrsim -0.03$) one observes deviations. In particular, perturbation theory predicts that the binding energy increases as one approaches the resonance $a/b \rightarrow 0$ and diverges at the resonance. DMC results gives instead $\mu = (-23.95 \pm 0.70) gn_B$ at the resonant point.

In Fig. [4.4, B] we plot the reduced binding energy defined as the binding energy once the mean-field term μ_{MF} is subtracted. The reduced binding energy is plotted for both the repulsive and the attractive branch. We notice that the results on the attractive branch seem to be in better agreement with perturbation theory once the mean-field contribution μ_{MF} linear in b/a has been subtracted. By approaching the resonance, however, the reduced binding energy lies well below the second-order contribution of perturbation theory.

Once the resonance is crossed on the $a/b > 0$ side the energy decreases very rapidly with a/b reaching values that are very below the two-body binding energy ϵ_B (see Fig. [4.4, A]). This result can be explained with the presence of deep cluster states as soon as one crosses the resonance.

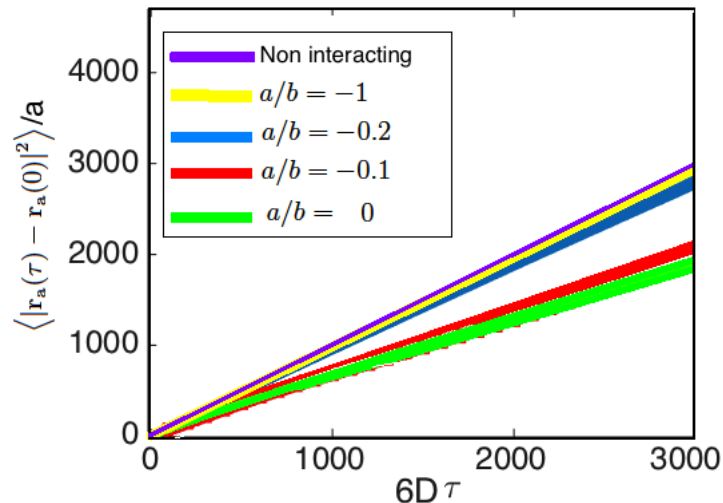


Figure 4.5: **Mean square displacement of the impurity as a function of the imaginary time** for the case where the impurity and the bosons do not interact (purple), $a/b = -1$ (yellow); $a/b = -0.2$ (blue), $a/b = -0.1$ (red) and $a/b = 0$ (green).

4.5 Effective mass

Another important property is the effective mass of the polaron. We studied the dependence of the effective mass as a function of the coupling strength a/b . We investigated this dependence both along the repulsive **branch** $a/b > 0$ and along the **attractive branch** for values $-1 < a/b < 0$. On the repulsive branch, we compared results of perturbation theory (see Eq. [4.35]), of the Jensen-Feynman approach (see Sec. [4.3]) and of DMC simulations (see Sec 3.8.3). For the attractive branch we use instead both perturbation theory and DMC simulations. At the **unitary limit**, $a/b = 0$, the value of the effective mass and its dependence in the gas parameter $n_B a^3$ (see chapter 5) is obtained using QMC calculations.

As it was discussed in Sec. [3.8] in a DMC calculations the effective mass of the impurity can be calculated from the mean square displacement in imaginary time. According to Eq. [3.127] we calculate the slope of Δr as a function of the imaginary time. In Fig. [4.5] we show Δr for different values of a/b along the attractive branch.

In Fig. [4.6] we plot the results for the effective mass as a function of the coupling strength a/b . Good agreement is found between all the approaches at weak coupling. In contrast, at strong coupling the perturbative result diverges (see Eq. [4.35]) and the Jensen-Feynman approach predicts a sharp transition from a mobile to a localized impurity. Instead, DMC calculations provide a value of m^*/m which is always smaller than 2. In particular, at unitary limit we find $m^*/m = 1.63 \pm 0.03$

Similar results for the attractive branch were obtained in Ref. [108] using various T -matrix

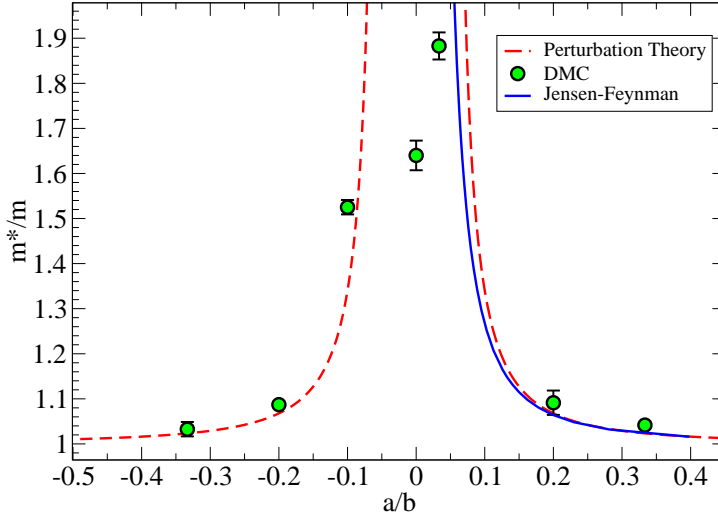


Figure 4.6: **Effective mass as a function of a/b** : perturbation theory (red dashed line), Jensen-Feynman (solid blue line), DMC simulations with ASW potential (green points). The range of the potential in the DMC simulations is $R_0 = 0.2a$.

approximation schemes.

4.6 Pair correlation functions

The pair correlation functions are investigated in this section by means of QMC methods. In particular, we consider both the boson-boson $g_{BB}(\mathbf{r})$ and the impurity-boson $g_{IB}(\mathbf{r})$ pair correlation function. In Fig. [4.7] we plot $g_{BB}(r)$ for three values of the coupling strength both on the repulsive and on the attractive branch. In all cases we find that there are no significant differences compared with the $g_{BB}(\mathbf{r})$ when the impurity is absent. This implies that the structure of bosonic bath is not appreciably altered by the presence of the impurity.

The situation is completely different for the impurity-boson $g_{IB}(r)$ pair correlation function. In fact, the distribution of bosonic atoms around the impurity is greatly affected by the impurity-boson interaction.

In order to investigate the spatial distribution of the bosons for different coupling strengths a/b , we compute the impurity-boson pair correlation function $g_{IB}(\mathbf{r})$ as a function of the distance in units of the healing length $\xi = \frac{1}{\sqrt{8\pi n_B a}}$. From $g_{IB}(\mathbf{r})$ one obtains the density profile of the bosons around the impurity:

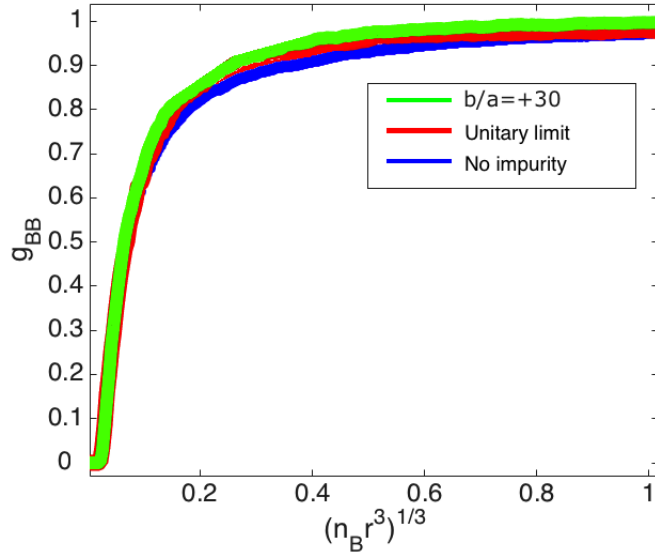


Figure 4.7: **Boson-boson pair correlation function $g_{BB}(\mathbf{r})$ on the repulsive branch ($\frac{b}{a} = +30$) (green solid line), at the unitary limit (red solid line) on the attractive branch and for the case where the impurity is absent (blue solid line).**

$$n(r) = n_B \frac{\int_0^r dr' 4\pi r'^2 g_{IB}(r')}{4\pi r^3/3}. \quad (4.58)$$

In Fig. [4.8] we plot the density profile $n(r)$ (in logarithmic scale) as a function of the distance in units of the healing length ξ for both the attractive and the repulsive branch. The pair correlation functions are calculated for values of $b/a = \pm 10, \pm 20$ and $b/a = \pm 30$. One of the main features of the $g_{IB}(\mathbf{r})$ function is a very large peak for distances $r \ll \xi$. It means that there is a very large probability of finding a boson close to the impurity as a consequence of the attractive nature of the ASW potential that mediates the impurity-boson interaction.

We observe a smooth behavior in the density profile for the **attractive branch**. The density gradually decreases with the distance until the equilibrium density n_B is reached at distances $r > \xi$. On the contrary, along the **repulsive branch**, the density profile is characterized by a minimum at distances $r \lesssim \xi$. For larger distances, the density approaches the equilibrium value remaining always smaller than n_B .

In the insets in Fig. [4.8] we plot the number of bosons surrounding the impurity defined as $N_B(r) = n_B \int_0^r dr 4\pi r'^2 g_{IB}(r')$ as a function of the distance (in units of the healing length) for the attractive and repulsive branch. We notice that at short distances the quantity $N_B(r)$ increases faster on the repulsive branch than on the attractive one. On the contrary, we also notice that for the largest values of $|b|/a$ the average number of bosons surrounding the impurity reaches the values $N_B(r) = 1$ already at distances on the order of $r \simeq 0.30\xi$. For very large distances, the number of bosons for the repulsive case is always lower than for the attractive case.

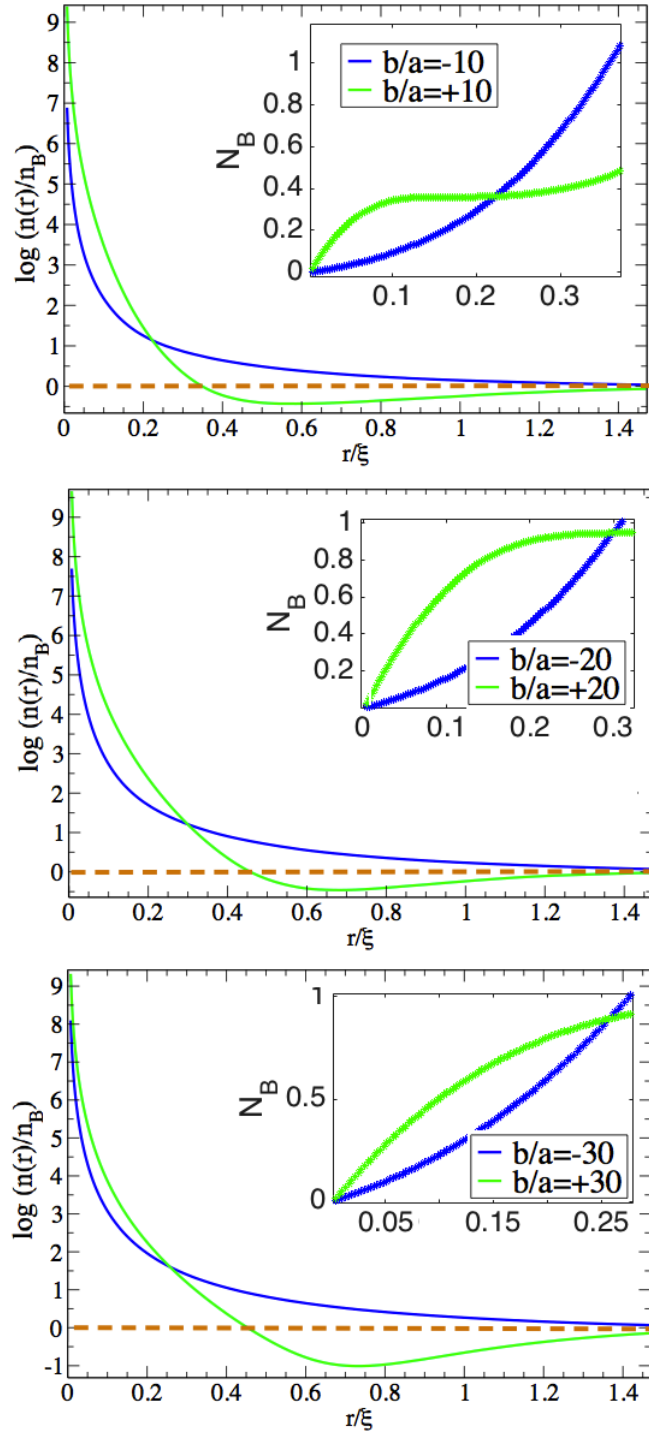


Figure 4.8: **Density profiles $n(r)$ (in logarithmic scale) as a function of the distance in units of the healing length ξ .** The profiles are computed for both the attractive (solid blue line) and the repulsive (green solid line) branches for coupling strengths: $b/a = \pm 10$, ± 20 and $b/a = \pm 30$. The dashed line represents the equilibrium density n_B . In the insets the number of bosons as a function of the distance in units of the healing length for the attractive and repulsive branch.

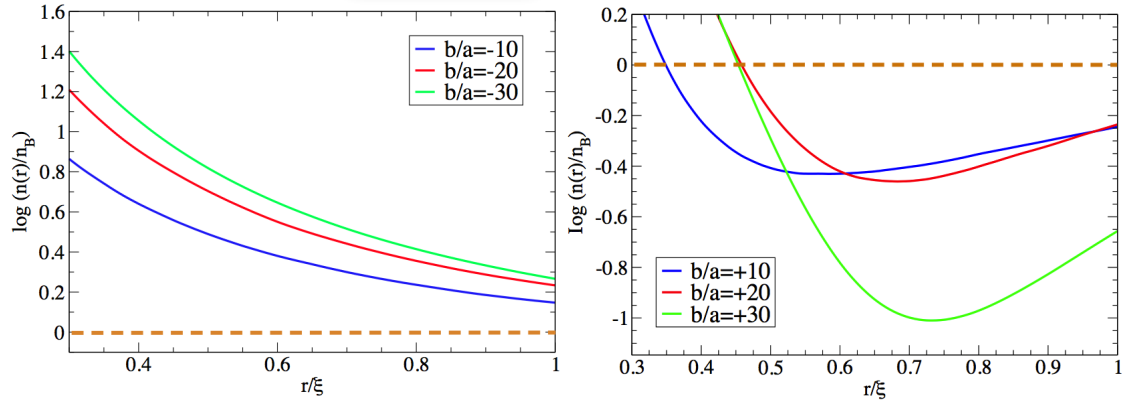


Figure 4.9: **Enhancement for the attractive branch (right) and depletion for the repulsive branch (left) of the density profile.** The dashed line represents the equilibrium density n_B .

In Fig. [4.9] we plot separately the density profile for three values of a/b focusing on the behavior at large distances. This regime of large distance and small deviations from the equilibrium density can be appropriately described using the mean-field theory. On the contrary, the regime of small distances and large deviations from n_B can not be described neither by the mean-field theory nor by the effective low-energy Fröhlich Hamiltonian.

Along the attractive branch we find an enhancement of the bosonic density at large distances from the impurity, whereas along the repulsive branch, we find a significative reduction. This modification of the bosonic bath far away from the impurity is caused by the impurity-boson effective interaction that is attractive in the former case and repulsive in the latter.

Chapter 5

Impurity interacting resonantly with the bosonic bath

In the **unitary limit** the value of the s -wave scattering length b can be several orders of magnitude larger than the range of the potential R_0 and one enters into a new strongly correlated regime. In dilute systems for which the effective range of the interaction R_0 is much smaller than the mean interparticle distance, namely $n_B R_0^3 \ll 1$, the unitary regime should not depend on details of the impurity boson interaction [110]. In this regime the only natural parameter should be for the problem of an impurity interacting with a bosonic bath given by $n_B a^3$.

The impurity-boson interaction is modeled using the ASW potential ($R_0 = 0.2a$) corresponding to the resonant condition $k_0 R_0 = \pi/2$. (see Section 3.6)

We investigate the binding energy, the effective mass and the correlation pair functions as a function of $n_B a^3$.

The sources of systematic errors of the DMC algorithm are explicitly analyzed for the special case of the unitary limit. We carry out a systematic study of both the number of walkers and the time step for different values of the gas parameter. For instance, at $n_B a^3 = 3.375 \times 10^{-6}$ (see Fig. [5.1, **A**]) and $n_B a^3 = 10^{-6}$ (see Fig. [5.1, **B**]), the binding energy μ (in units of gn) is calculated as a function of the inverse of the number of walkers ($1/N^W$). For the values of the gas parameter $n_B a^3 = 3.0 \times 10^{-7}$ (see Fig. [5.1, **C**]) and $n_B a^3 = 10^{-6}$ (see Fig. [5.1, **D**]) the binding energy is calculated as a function of the time step ($\delta\tau$).

5.1 Binding energy of the impurity

Once the extrapolations to $1/N^W = 0$ and $\delta\tau = 0$ are carried out for all the values of the gas parameter $n_B a^3$, we determine the binding energy as a function of $n_B a^3$. The binding energy

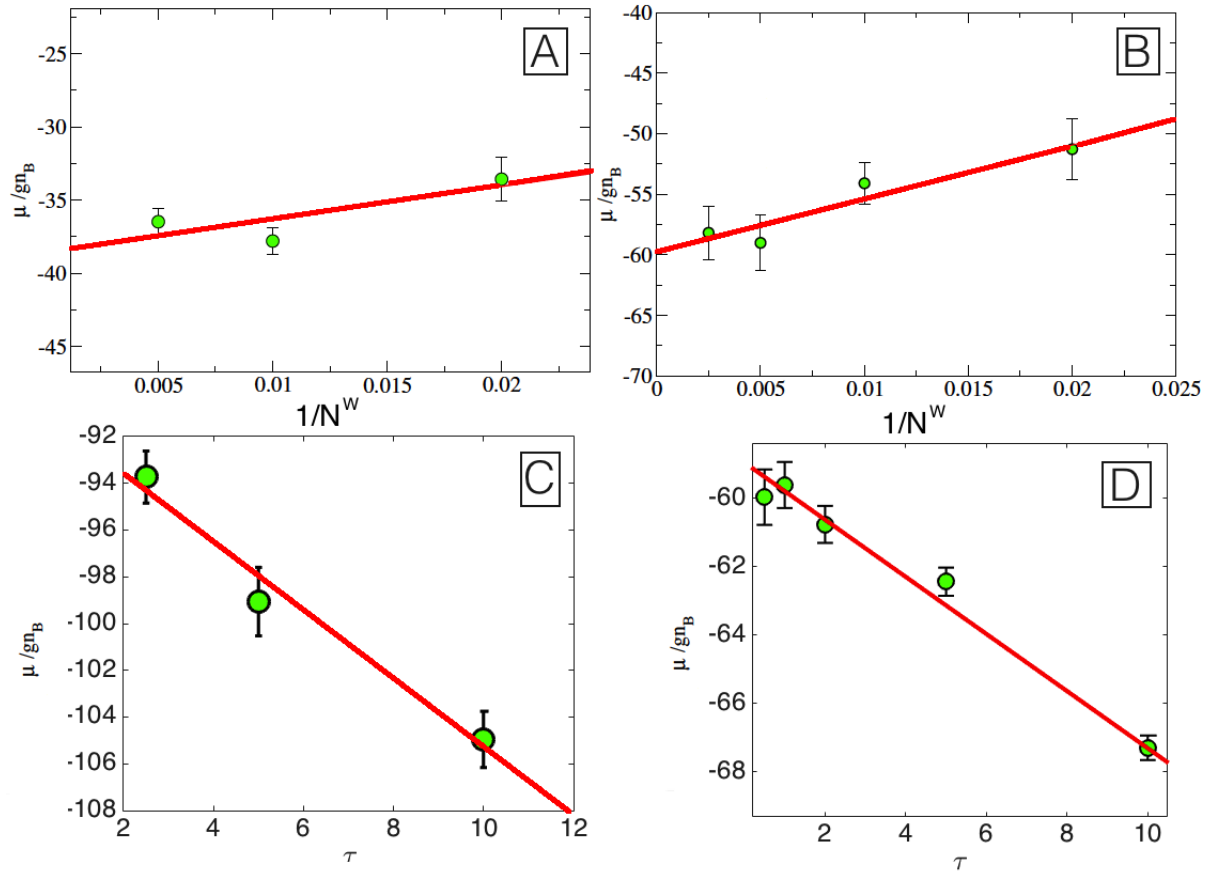


Figure 5.1: **Binding energy at the unitary limit as a function of the inverse number of the walker** (time-step fixed $\delta\tau = 0.05$) (A) $n_B a^3 = 3.375 \times 10^{-6}$ and (B) $n_B a^3 = 10^{-6}$ and **as a function of the time step** $\delta\tau$ (number of walkers $N_W = 400$) (C) $n_B a^3 = 3.0 \times 10^{-7}$ and (D) $n_B = 10^{-6}$.

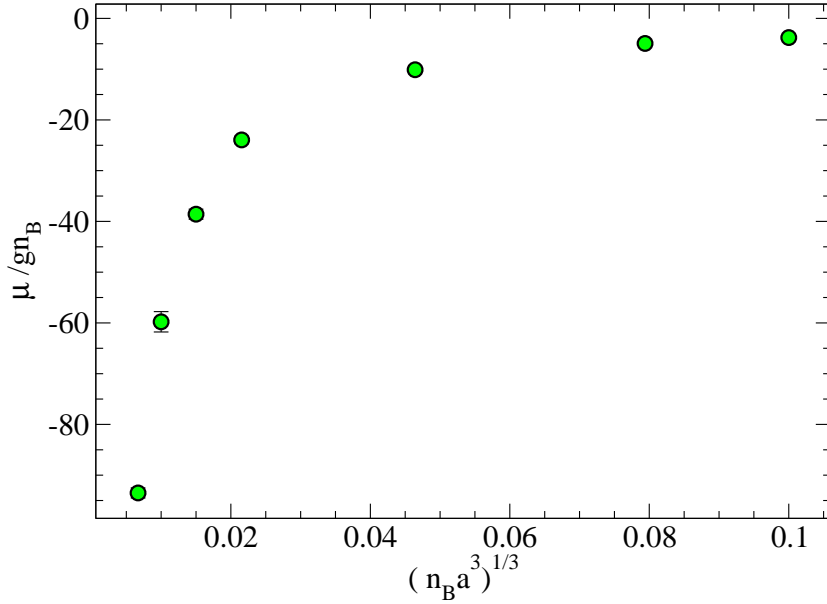


Figure 5.2: **Binding energy as a function of the gas parameter $(n_B a^3)^{1/3}$ at the unitary.** Green points represent DMC simulations.

in units of gn_B is shown in Fig. [5.2]. The gas parameter is ranging from the very dilute regime i.e $n_B a^3 = 3 \times 10^{-7}$ to $n_B a^3 = 10^{-4}$. We notice that the binding energy $|\mu|$ is always significantly larger than the chemical potential of the bosonic atoms approximatively given by gn_B . For the smallest value of $n_B a^3$, $|\mu|$ can become as larger as $90gn_B$.

In Fig. [5.3] we plot the same binding energy in units of $\frac{\hbar^2}{m} n_B^{2/3}$ which corresponds to an energy scale similar to the Fermi energy in the Fermi polaron problem. A good fitting law is provided by the following expression

$$\mu = \frac{\hbar^2}{m} n_B^{2/3} \left(\frac{a_0}{x} + a_1 + a_2 x + a_3 x^2 \right), \quad (5.1)$$

where $x = (n_B a^3)^{1/3}$. The best fit results for the parameters is given by:

$$\begin{aligned} a_0 &= -0.0069, \\ a_1 &= 7.13, \\ a_2 &= 35.97, \\ a_3 &= -106.43. \end{aligned} \quad (5.2)$$

It is interesting to notice that for $x = 0$, the binding energy diverges. Therefore the interactions

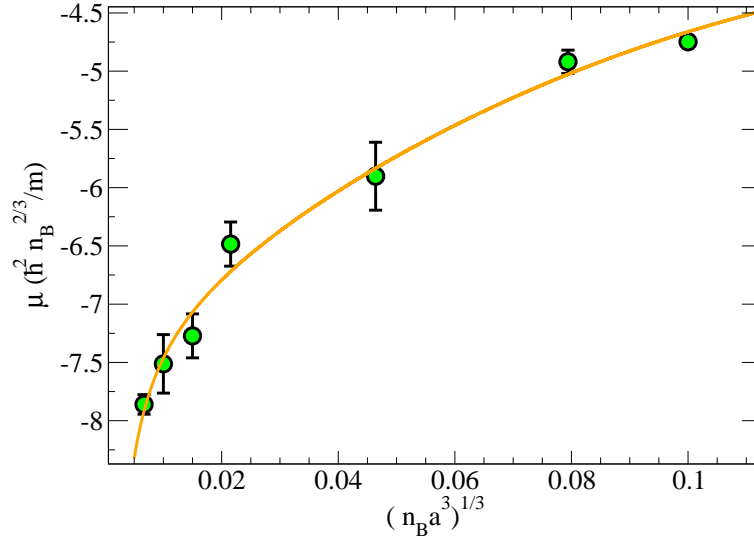


Figure 5.3: **Dependence on the binding energy with $(n_B a^3)^{1/3}$ at the unitary limit:** Green points stand for DMC, whereas the red line is a power law fitting.

between bosons are crucial in order to guarantee a well defined binding energy. From the binding energy calculation one observes that the coupling between the impurity and the bosonic bath gets stronger when the bosonic bath is dilute.

The problem of an impurity resonantly interacting with a bosonic bath was addressed in the work by Rath and Schmidt [111] using various T-matrix formalisms. At the density $n_B a^3 = 10^{-3}$ the value of μ at unitarity obtained from their calculation agrees quite well with the result of our DMC simulation. Nevertheless the results of [111] seem to depend very little on the value of a (s -wave boson-boson scattering length), while from the expansion law of Eq. [5.1] the dominant contribution to μ at small $n_B a^3$ is provided by $\hbar^2 n_B^{1/3} / ma$.

5.2 Effective mass

As it was discussed in the previous section the only dimensionless parameter that describes the ground-state properties of the impurity interacting resonantly with the bosonic bath is given by $n_B a^3$. Then, the effective mass should also scale with this parameter. Following Eq. [3.127] we calculate the slope of the the mean square displacement of the impurity as a function of the imaginary time. We follow a similar procedure carried out for the study of the effective mass as a function of a/b at the value of the gas parameter $n_B a^3 = 10^{-5}$.

The results are shown in Fig. [5.4] we plot the effective mass as a function of the gas parameter

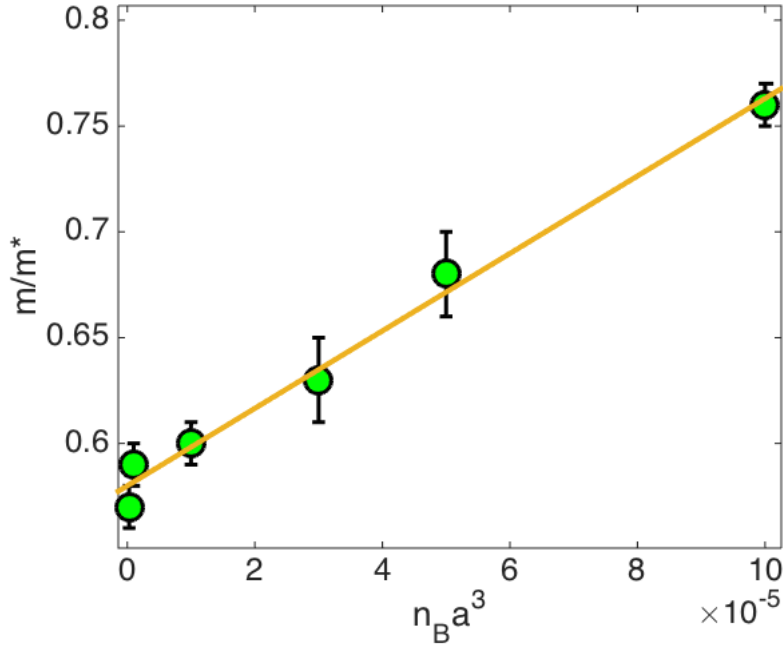


Figure 5.4: **Effective mass of the polaron at the unitary limit as a function of the gas parameter $n_B a^3$ of the bosonic bath.**

$n_B a^3$. We find a linear dependence of m/m^* with the gas parameter according to the law

$$\frac{m}{m^*} = \alpha (n_B a^3) + \beta, \quad (5.3)$$

where the values

$$\begin{aligned} \alpha &= 1.83 \times 10^3 \text{ and} \\ \beta &= 0.58 \end{aligned} \quad (5.4)$$

are determined from a best fit analysis.

It is worth noting that for the limit $n_B a^3 \rightarrow 0$ the effective mass retains a defined value: $m^*/m = 1.72 \pm 0.03$, even though the binding energy increases as $\frac{\hbar^2}{ma} n_B^{1/3}$.

The effective mass at the unitary limit was calculated with the T -matrix formalism in Ref. [111]. The value $m^*/m = 1.17$ is obtained at $n_B a^3 = 10^{-3}$, to be compared in Ref. [111] with $m^*/m = 1.23$ from our DMC simulations. On the other hand, when the special case of non-interacting bosons (i.e $n_B a^3 \rightarrow 0$) is considered the value $m^*/m = 1.2$ is obtained. As already mentioned, our DMC simulations give instead the slightly large value $m^*/m = 1.72 \pm 0.03$.

In Ref. [103] the impurity problem at resonance is addressed similar beyond-mean field techniques based on a variational ansatz that relies on a wave function similar to the one introduced for the first time in the context of Fermi polarons. In this work the value of the effective

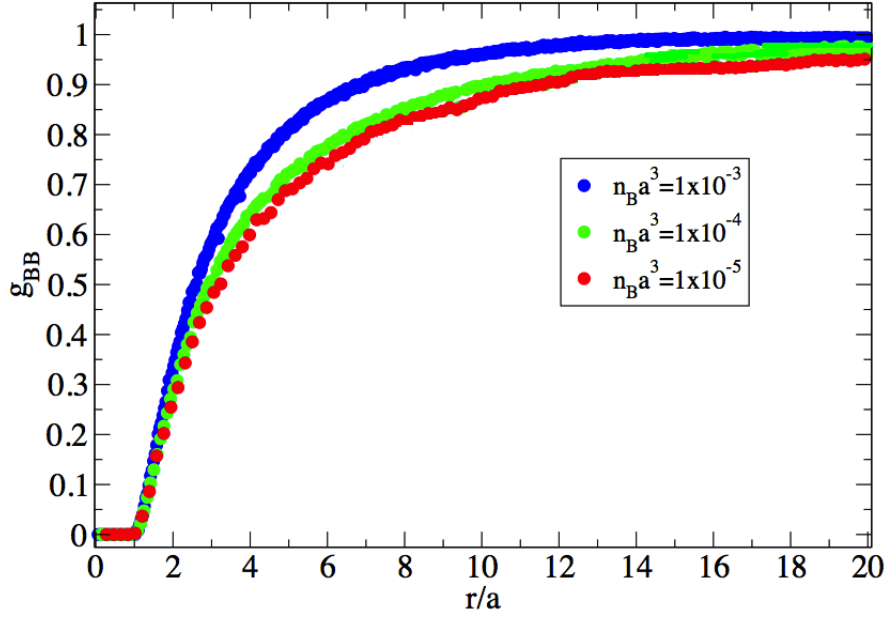


Figure 5.5: **Boson-boson pair correlation function at the $a/b = 0$ for different values of the gas parameter $n_B a^3$.**

mass was calculated both at the density $n_B a^3 = 1.35 \times 10^{-4}$ and for vanishing interactions ($n_B a^3 \rightarrow 0$). In the first case $m^*/m = 1.2$ was obtained, whereas in the latter case a slightly difference $m^*/m = 1.17$ was reported.

At the finite density $n_B a^3 = 1.35 \times 10^{-4}$ we calculate an effective mass in good agreement with the result in Ref. [103], while for vanishing interactions our result is larger.

5.3 Pair correlation functions

The boson-boson pair correlation function $g_{BB}(r)$ is computed as a function of the distance in units of a for different values of the gas parameter $n_B a^3$. The function $g_{BB}(r)$ is plotted for three different values of $n_B a^3$ in Fig. [5.5]. We observe that, by increasing the gas parameter, the probability of finding two bosons at certain distance r slightly increases. The reason is that the average interparticle distance decreases by increasing the $n_B a^3$ and, as a consequence, the regime of uniform density of surrounding particles, corresponding to $g_{BB}(r) = 1$, is reached for shorter distances. According to the results of Fig. [5.5], we notice that the function $g_{BB}(r)$ is only very slightly affected by the presence of the impurity.

More interesting features are related with the pair correlation function $g_{IB}(r)$ such as the density profile, that is obtained by using Eq. [3.120]. In Fig. [5.6] we plot the density profile in a logarithmic scale as a function the distance in units of the healing length $\xi = (8\pi n_B a)^{-1/2}$

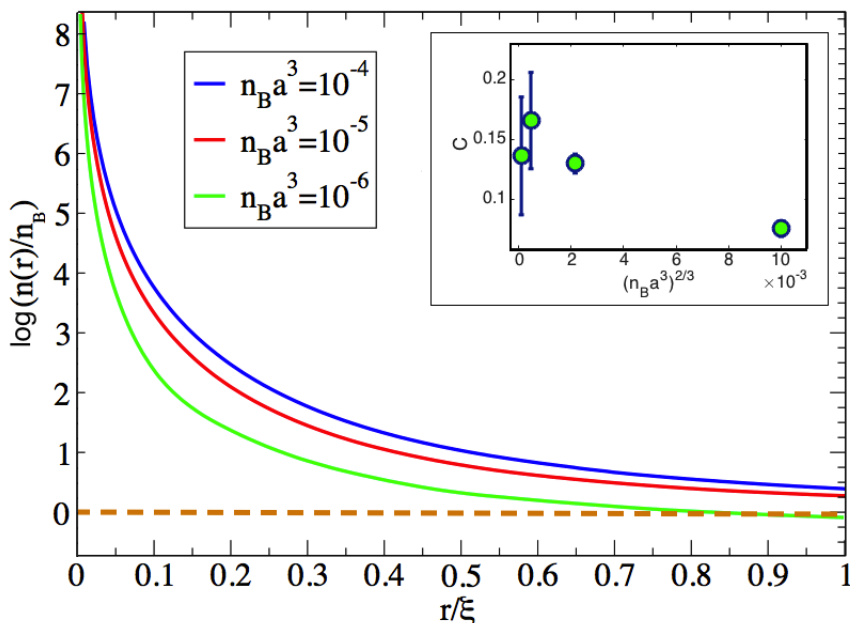


Figure 5.6: Density profile (in logarithmic scale) at the unitary limit as a function of the inter particle distance for different values of $n_B a^3$: green ($n_B a^3 = 3 \times 10^{-6}$), red ($n_B a^3 = 1 \times 10^{-5}$), blue ($n_B a^3 = 1 \times 10^{-4}$). Inset: parameter C contact as a function of $(n_B a^3)^{2/3}$. The dashed line represents the equilibrium density n_B .

for different values of the gas parameter $n_B a^3$. We observe that the density reaches the bulk value for distances larger than the healing length.

For shorter distances a sharp peak is visible which becomes narrower as the density is decreased.

In the inset of Fig. [5.6] we plot the dimensionless contact parameter defined as:

$$C = \lim_{r \rightarrow 0} g_{IB}(r) \frac{r^2}{a^2} (n_B a^3)^{2/3}, \quad (5.5)$$

as a function of $(n_B a^3)^{2/3}$. This quantity, also known as Tan's parameter C Ref. [112], corresponds to the coefficient, determined by many-body effects, multiplying the short-range behavior of the pair correlation function fixed by the two-body physics. In the above equation, the limit $r \rightarrow 0$ should be intended as the regime $R_0 < r \ll n_B^{-1/3}$.

5.4 Efimov physics

Efimov states [113], i.e three-body bound states with peculiar scaling behavior, exist for the problem of two bosons and one distinguishable particle with resonant interspecies interaction [114]. The lowest Efimov state has an energy given by $E_{trimer} \sim 4 \exp(-2\pi/s_0) = -10^{-6} \frac{\hbar^2}{mR^2}$

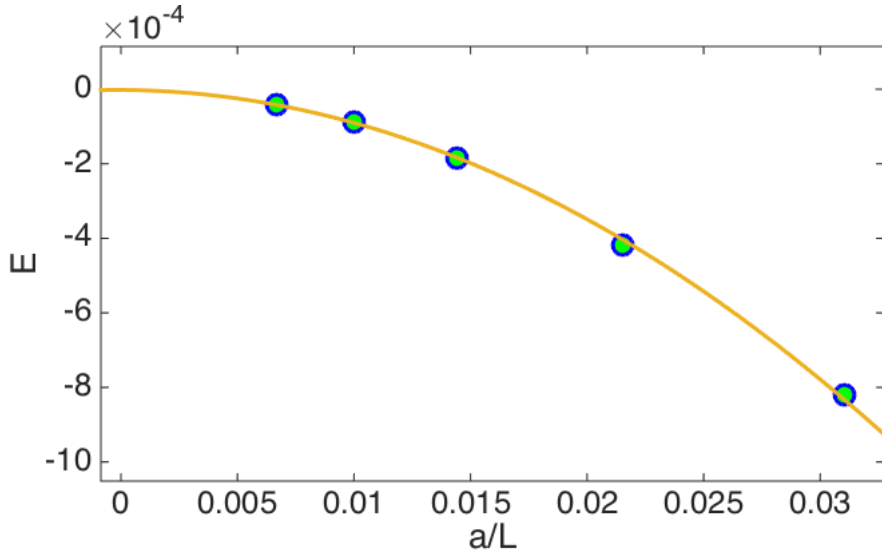


Figure 5.7: **Total energy in units of \hbar^2/ma^2 for a system consisting of two bosons and one impurity with resonant interspecies interaction as a function of the inverse of the size of the simulation box a/L .**

when $a/b = 0$ (see Ref. [114]). Where R is the typical 3-body length and s_0 is the parameter associated with Efimov's scaling law. For equal masses of the bosons and the distinguishable particles one has that $\exp(\pi/s_0) \sim 1986$ and assuming $R \sim a$, one can estimate $E_{trimer} \sim -10^{-6} \frac{\hbar^2}{ma^2}$.

We have calculated the energy of the system of three particles as a function of the size of the simulation box and the results are shown in Fig. 5.7. The extrapolation to $a/L = 0$ gives an energy that can not exceed $E \sim -10^{-6} \frac{\hbar^2}{ma^2}$ in agreement with the above estimate. Bound states more than three particles should also occur at the resonant point $a/b = 0$, but we estimate similarly to the 3-body bound-state that their energy should be much smaller than the binding energy of the polaron.

5.5 Discussion

In this chapter we studied the ground-state properties of the impurity interacting resonantly with the bosonic bath. These ground-state properties were investigated as a function of the dimensionless scale provided by the gas parameter of the bosonic bath. We computed the binding energy as a function of $(n_B a^3)^{1/3}$ and we found that the effects between the impurity and the bosons are more relevant for dilute systems. In particular, when of $a \rightarrow 0$, the binding energy diverges signaling that interactions in the Bose gas play an important role for the stability of the system. We compare our results with the findings of the T -matrix calculation in Ref. [111] obtaining good agreement at $n_B a^3 = 10^{-3}$, but significant disagreements when

$n_B a^3 \rightarrow 0$.

The effective mass was also calculated as a function of $(n_B a^3)$. We found a linear dependence between the effective mass and the gas parameter in the dilute regime. The DMC results give the value $m^*/m = 1.72 \pm 0.03$ of the effective mass in the limit $n_B a^3 \rightarrow 0$. This value indicates that there is no self-localization of the polaron at the unitary limit regardless of the density. Even though the coupling between the impurity and the bosonic bath is very strong for a dilute system, the effective mass of the polaron is not larger than twice the mass of the impurity. We computed the density profile obtained from the impurity-boson pair correlation function $g_{IB}(r)$ as a function of the gas parameter and one realizes that for distances smaller than the healing length, there is a large peak in the density and there is a large probability to find a boson in the neighbourhood of the impurity. The effective mass was compared also with the T -matrix calculation in Ref. [111] and good agreement is found at $n_B a^3 = 10^{-3}$, but important deviations emerge when $n_B a^3 \rightarrow 0$.

Chapter 6

Many impurities in a Bose-Einstein condensate

In the previous chapter we discussed the ground-state properties of one impurity immersed in a Bose-Einstein condensate at zero temperature by using the perturbation theory, the variational Jensen-Feynman approach and QMC methods. We found that QMC techniques provide a strong and robust tool for describing the ground-state properties of the impurity interacting with the bosonic bath beyond the mean-field regime. Now, we turn our attention to the case of many impurities where the statistics plays an important role. In this chapter we investigate the ground-state properties when M bosonic impurities are immersed in a Bose-Einstein condensate at zero temperature by using both mean-field and QMC techniques.

From the experimental point of view a system of few impurities immersed in a quantum gas is more realistic than the case of a single impurity. In the context of ultracold atoms, binary mixtures have already been realized experimentally. In these mixtures the two species can either be two different hyperfine states of the same atoms [115, 116] or different atoms [117]. In particular, mixtures of bosonic species have been realized and unveil a range of interesting phenomena such as the dynamics of coupled Bose-Einstein condensates [118], the phase coherence and instability [119]. On the other hand, binary mixtures in a three dimensional optical lattice have also been realized [120]. As for as fermionic impurities are concerned, Bose-Fermi mixtures have been widely studied in the literature [121, 122, 123].

The many-impurity problem has been addressed by many theoretical approaches. One of them is inspired by the idea of the Fröhlich polaron for the single impurity. According to this approach, M distinguishable charged impurities in a polarizable medium form polarons and a bound state arises called the Fröhlich multipolaron state [124]. The energy and the effective mass of this state show a strong dependence on the number of impurities. In particular, the special case of two impurities has been studied and the formation of bipolarons is predicted:

a bound state of two polarons. The formation of bipolarons is related with the mechanism of pairing in high temperature superconductivity [27, 69, 125].

In the context of ultracold atoms, the problem of many impurities has been tackled in the weak [126] and in the strong-coupling regime [68] by using the Jensen-Feynman formalism. In the latter case, for very large coupling strengths between the impurities and the bosonic bath, the system can lead to clusterization of the impurities. Whereas, polaronic self-localization occurs for lower values of the impurity–boson interaction strength [127].

In the following we discuss the Hamiltonian of the system within the Bogoliubov approximation. Then, in order to investigate the ground-state energy of the system, we apply second-order perturbation theory.

6.1 Theoretical model

The Hamiltonian of M impurities immersed in homogeneous Bose gas of N atoms at $T = 0$ is given by:

$$\mathcal{H} = \underbrace{\sum_{i=1}^M \frac{\hat{\mathbf{p}}_i^2}{2m_I}}_{\text{Impurities}} + \underbrace{\sum_{i<j}^M V_{II}(\mathbf{r}_i - \mathbf{r}_j)}_{\text{Impurities}} + \underbrace{\sum_{\mathbf{k}} E_{\mathbf{k}} \hat{b}_{\mathbf{k}}^\dagger \hat{b}_{\mathbf{k}} + \frac{1}{2} \sum_{\mathbf{k}, \mathbf{k}', \mathbf{q}} V_{BB}(\mathbf{q}) \hat{b}_{\mathbf{k}'-\mathbf{q}}^\dagger \hat{b}_{\mathbf{k}+\mathbf{q}}^\dagger \hat{b}_{\mathbf{k}} \hat{b}_{\mathbf{k}'}}_{\text{BEC}} + \underbrace{\sum_{\mathbf{k}, \mathbf{q}} V_{IB}(\mathbf{q}) \hat{\rho}_I(\mathbf{q}) \hat{b}_{\mathbf{k}-\mathbf{q}}^\dagger \hat{b}_{\mathbf{k}}}_{\text{Impurities-BEC interaction}}. \quad (6.1)$$

The first term represents the Hamiltonian of the M particles (impurities) with momentum \mathbf{p}_i and mass m_I . The impurity-impurity interaction is described by the interparticle potential $V_{II}(\mathbf{r}_i - \mathbf{r}_j)$. The second term is the usual Hamiltonian describing uniform and dilute Bose gas (see Eq. [1.22]) where $\hat{b}_{\mathbf{k}}^\dagger$ and $\hat{b}_{\mathbf{k}}$, respectively, creates and annihilate a boson with mass m_B , wave vector \mathbf{k} , and energy $E_{\mathbf{k}} = \frac{\hbar^2 k^2}{2m_B} - \mu_B$, with μ_B the chemical potential of the bosons and $V_{BB}(\mathbf{q}) = \int V_{BB}(r) \exp[-i\mathbf{q} \cdot \mathbf{r}/\hbar] d\mathbf{r}$ is the Fourier transform of the boson-boson interatomic potential. Finally, the last term in Eq. [6.1] represents the interaction between the impurities and the bosons mediated by $V_{IB}(\mathbf{q})$, which is the Fourier transform of the impurity-boson interatomic potential that couples the boson density to the impurity density $\rho_I(\mathbf{q}) = \sum_{i=1}^M \exp[-i\mathbf{q} \cdot \mathbf{r}_i]$.

The M impurities can be distinguishable and the ground-state properties such as the energy and the effective mass were investigated in [128]. In this work we are interested to the case of *indistinguishable bosonic impurities*. Therefore, we consider bosonic impurities (***bosons of***

type A) immersed in a bosonic bath (**bosons of type B**) at $T = 0$. The Hamiltonian of the system can be written as:

$$\mathcal{H} = \underbrace{\sum_{\mathbf{k}} E_{\mathbf{k}}^A \hat{a}_{\mathbf{k}}^\dagger \hat{a}_{\mathbf{k}} + \frac{1}{2} \sum_{\mathbf{k}, \mathbf{k}', \mathbf{q}} V_{AA}(\mathbf{q}) \hat{a}_{\mathbf{k}'-\mathbf{q}}^\dagger \hat{a}_{\mathbf{k}+\mathbf{q}}^\dagger \hat{a}_{\mathbf{k}} \hat{a}_{\mathbf{k}'}}_{\text{BEC OF ATOMS A}} + \underbrace{\sum_{\mathbf{k}} E_{\mathbf{k}}^B \hat{b}_{\mathbf{k}}^\dagger \hat{b}_{\mathbf{k}} + \frac{1}{2} \sum_{\mathbf{k}, \mathbf{k}', \mathbf{q}} V_{BB}(\mathbf{q}) \hat{b}_{\mathbf{k}'-\mathbf{q}}^\dagger \hat{b}_{\mathbf{k}+\mathbf{q}}^\dagger \hat{b}_{\mathbf{k}} \hat{b}_{\mathbf{k}'}}_{\text{BEC OF ATOMS B}} + g_{AB} \int dr n_A(r) n_B(r), \quad (6.2)$$

where $\hat{a}_{\mathbf{k}}^\dagger$ and $\hat{a}_{\mathbf{k}}$ respectively create and annihilate a boson of type A, with mass m_A , vector \mathbf{k} , and energy $E_{\mathbf{k}}^A = \frac{\hbar^2 k^2}{2m_A} - \mu_A$, with μ_A the chemical potential of the bosons of type A. The interaction term $V_{AA}(\mathbf{q}) = \int V_{AA}(r) \exp[-i\mathbf{q} \cdot \mathbf{r}/\hbar] d\mathbf{r}$, is the Fourier transform of the interatomic potential for the bosons of type A. Bogoliubov theory can be used if one assumes that both bosonic gases are dilute. The Bogoliubov transformation for the species A and B yields

$$\text{type A : } \begin{cases} \hat{a}_k = u_k^A \hat{\alpha}_k + v_k^A \hat{\alpha}_{-k}^\dagger \\ \hat{a}_k^\dagger = u_k^A \hat{\alpha}_k^\dagger + v_k^A \hat{\alpha}_{-k}^\dagger \end{cases} \quad (6.3)$$

and

$$\text{type B : } \begin{cases} \hat{b}_k = u_k^B \hat{\beta}_k + v_k^B \hat{\beta}_{-k}^\dagger \\ \hat{b}_k^\dagger = u_k^B \hat{\beta}_k^\dagger + v_k^B \hat{\beta}_{-k}^\dagger \end{cases}, \quad (6.4)$$

the operators $\hat{\alpha}_k^\dagger$ ($\hat{\alpha}_k$) are the creation (annihilation) quasiparticle operators for bosons of type A and $\hat{\beta}_k^\dagger$ ($\hat{\beta}_k$) are the creation (annihilation) quasiparticle operators for bosons of type B. The following mixed commutation relations are satisfied, $[\hat{a}_k, \hat{b}_k] = [\hat{a}_k, \hat{b}_k^\dagger] = 0 \Rightarrow [\hat{\alpha}_k, \hat{\beta}_k] = [\hat{\alpha}_k, \hat{\beta}_k^\dagger] = 0$. In addition,

$$\begin{aligned} (u_k^A)^2 &= 1 + (v_k^A)^2 = \frac{(\varepsilon_k^A + gn_A + \omega_k^A)}{2\omega_k^A} \\ (u_k^B)^2 &= 1 + (v_k^B)^2 = \frac{(\varepsilon_k^B + gn_B + \omega_k^B)}{2\omega_k^B}. \end{aligned} \quad (6.5)$$

With $\varepsilon_k^A = \frac{\hbar^2}{2m_A} k^2$ and $\varepsilon_k^B = \frac{\hbar^2}{2m_B} k^2$. Plugging Eqs. [6.3] and [6.4] into Eq. [6.2] one ends up with

$$\mathcal{H} = \underbrace{E_0^A + \sum_k \omega_k^A \hat{\alpha}_k^\dagger \hat{\alpha}_k}_{\text{BEC-A}} + \underbrace{E_0^B + \sum_k \omega_k^B \hat{\beta}_k^\dagger \hat{\beta}_k}_{\text{BEC-B}} + g_{AB} \int dr n_A(r) n_B(r). \quad (6.6)$$

The previous expression is written as the Hamiltonian of bosons of type A, plus the Hamiltonian of bosons of type B and the last term represents the interaction between the two condensates. Here

$$E_0^A = \frac{1}{2} M g_A n_A \left(1 + \frac{128}{15\sqrt{\pi}} \sqrt{n_A a_A^3} \right) \quad (6.7)$$

and

$$E_0^B = \frac{1}{2} N g_B n_B \left(1 + \frac{128}{15\sqrt{\pi}} \sqrt{n_B a_B^3} \right), \quad (6.8)$$

represent the ground-state energy of the bosons of type A and type B respectively. The corresponding densities of each component are given by $n_A = M/V$ for the bosons of type A and $n_B = N/V$ for the bosons of type B.

For the interparticle interactions we assume contact pseudo-potentials, namely

$$\begin{aligned} V_{II}(\mathbf{r}) &= g_A \delta(\mathbf{r}_A - \mathbf{r}'_A), \\ V_{BB}(\mathbf{r}) &= g_B \delta(\mathbf{r}_B - \mathbf{r}'_B), \\ V_{IB}(\mathbf{r}) &= g_{AB} \delta(\mathbf{r}_{AB} - \mathbf{r}'_{AB}). \end{aligned} \quad (6.9)$$

The interaction strengths g_A , g_B , and g_{AB} are related to the corresponding scattering lengths a_A , a_B and a_{AB} through the Lippmann-Schwinger (LS) equation (see Eq. [1.37]). The inter-bosonic coupling strengths in Eqs. [6.7] and [6.8] are given by the first-order result in the LS equation

$$\begin{aligned} g_A &= \frac{4\pi\hbar^2}{m_A} a_A \\ g_B &= \frac{4\pi\hbar^2}{m_B} a_B \end{aligned} \quad (6.10)$$

The second-order correction in the LS equation for the impurity-boson interaction reads

$$\frac{2\pi\hbar^2}{m_r} a_{AB} = g_{AB} - g_{AB}^2 \sum_{\mathbf{k} \neq 0} \frac{2m_r}{(\hbar k)^2}, \quad (6.11)$$

where $m_r^{-1} = m_A^{-1} + m_B^{-1}$ is inverse of the reduced mass. The dispersion relations in Eq. [6.6] are given by:

$$\omega_k^A = \sqrt{(\varepsilon_k^2)_A + 2g_A n_A (\varepsilon_k)_A} \quad (6.12)$$

and

$$\omega_k^B = \sqrt{(\varepsilon_k^2)_B + 2g_B n_B (\varepsilon_k)_B} \quad (6.13)$$

where n_A and n_B are the density of the bosons of the species A and B respectively.

The inter-species interaction is written as:

$$g_{AB} \int d\mathbf{r} n_A(\mathbf{r}) n_B(\mathbf{r}) = g_{AB} V n_A n_B + g_{AB} \sum_k \rho_k^A \rho_{-k}^B \quad (6.14)$$

with

$$\begin{aligned} \rho_k^A &= \frac{1}{\sqrt{V}} \int d\mathbf{r} \exp(i\mathbf{k} \cdot \mathbf{r}) [n_A(\mathbf{r}) - n_A] \\ \rho_k^B &= \frac{1}{\sqrt{V}} \int d\mathbf{r} \exp(i\mathbf{k} \cdot \mathbf{r}) [n_B(\mathbf{r}) - n_B]. \end{aligned} \quad (6.15)$$

By using the Bogoliubov approximation the bosonic density fluctuation operator can be written as a linear combination of quasi-particle operators:

$$\begin{aligned} \rho_k^A &= \frac{1}{\sqrt{V}} \sum_q \hat{a}_q^\dagger \hat{a}_{q+k} \cong \sqrt{n_A} (u_k^A + v_k^A) (\hat{\alpha}_k + \hat{\alpha}_{-k}^\dagger) \\ \rho_k^B &= \frac{1}{\sqrt{V}} \sum_q \hat{b}_q^\dagger \hat{b}_{q+k} \cong \sqrt{n_B} (u_k^B + v_k^B) (\hat{\beta}_k + \hat{\beta}_{-k}^\dagger), \end{aligned} \quad (6.16)$$

and we neglected quantum depletion effects in the condensate of both components A and B. Where we used Eq [6.3] and Eq. [6.4]. Then, the Hamiltonian Eq. [6.6] can be written as:

$$\begin{aligned} \mathcal{H} &= E_0^A + E_0^B + g_{AB} V n_A n_B + \sum_k (\omega_k^A \hat{\alpha}_k^\dagger \hat{\alpha}_k + \omega_k^B \hat{\beta}_k^\dagger \hat{\beta}_k) \\ &+ g_{AB} \sqrt{n_A n_B} \sum_k (u_k^A + v_k^A) (v_k^B + v_k^B) (\hat{\alpha}_k + \hat{\alpha}_{-k}^\dagger) (\hat{\beta}_k + \hat{\beta}_{-k}^\dagger). \end{aligned} \quad (6.17)$$

6.2 Perturbation theory

In this section we address the problem of M bosonic impurities immersed in a BEC by using second-order perturbation theory. One assumes from now on, the case of equal masses $m_A = m_B = m$. The Hamiltonian for this system (see Eq. [6.17]) can be written as:

$$\mathcal{H} = \mathcal{H}_0 + \mathcal{H}', \quad (6.18)$$

where:

$$\mathcal{H}_0 = E_0^A + E_0^B + \sum_k (\omega_k^A \hat{\alpha}_k^\dagger \hat{\alpha}_k + \omega_k^B \hat{\beta}_k^\dagger \hat{\beta}_k), \quad (6.19)$$

and

$$\mathcal{H}' = g_{AB} V n_A n_B \left[1 + \frac{1}{V} (n_A n_B)^{-1/2} \sum_k (u_k^A + v_k^A) (u_k^B + v_k^B) (\hat{\alpha}_k + \hat{\alpha}_{-k}^\dagger) (\hat{\beta}_k + \hat{\beta}_{-k}^\dagger) \right]. \quad (6.20)$$

The total correction to the ground-state energy up to second-order in the impurity-boson coupling can be written as

$$E = E_0^A + E_0^B + \langle 0 | \mathcal{H}' | 0 \rangle + \sum_n \frac{\langle 0 | \mathcal{H}' | n \rangle \langle n | \mathcal{H}' | 0 \rangle}{E_0^0 - E_n^0}. \quad (6.21)$$

where $|0\rangle$ is the vacuum and $|n\rangle$ are states with defined number of quasiparticles consisting of excitations of the bosons of type A and type B. Here E_0^A and E_0^B are given by Eqs. [6.7] and [6.8] respectively. The first-order correction is easy to evaluate and gives

$$\Delta E_0^{(1)} = |\langle 0 | \mathcal{H}' | 0 \rangle| = g_{AB} V n_A n_B. \quad (6.22)$$

The second-order term can be written as

$$\Delta E_0^{(2)} = \sum_{n \neq 0} \frac{|\langle n | \mathcal{H}' | 0 \rangle|^2}{E_0 - E_n} + n_A n_B g_{AB}^2 \sum_k \frac{m}{\hbar^2 k^2}. \quad (6.23)$$

Where last term provides the regularization of the ultraviolet divergence (see Eq. [6.11]). By plugging the perturbation Hamiltonian Eq. [6.20] into the matrix element entering second-order correction of the energy, one finds that in sum

$$\sum_k \left| \langle n | (u_k^A + v_k^A) (u_k^B + v_k^B) (\hat{\alpha}_k \hat{\beta}_k + \hat{\alpha}_k \hat{\beta}_{-k}^\dagger + \hat{\alpha}_{-k}^\dagger \hat{\beta}_k + \hat{\alpha}_{-k}^\dagger \hat{\beta}_{-k}^\dagger) | 0 \rangle \right|^2, \quad (6.24)$$

the only term that survives is

$$= \sum_k (u_k^A + v_k^A)^2 (u_k^B + v_k^B)^2 \left| \langle n | \hat{\alpha}_{-k}^\dagger \hat{\beta}_{-k}^\dagger | 0 \rangle \right|^2. \quad (6.25)$$

In the previous equation the excited state $|n\rangle = |1_\alpha, 1_\beta\rangle$ represent the creation of one excitation of type A and of type B. The energy difference between the unperturbed ground-state and excited state is given by

$$E_0 - E_n = -(\omega_k^A + \omega_k^B). \quad (6.26)$$

Thus, the second-order correction of the energy turns out to be

$$\Delta E_0^{(2)} = -g_{AB}^2 n_A n_B \sum_k \left[\frac{(u_k^A + v_k^A)^2 (u_k^B + v_k^B)^2}{\omega_k^A + \omega_k^B} - \frac{1}{2\varepsilon_k} \right]. \quad (6.27)$$

Recalling that $(u_k^A + v_k^A)^2 = \frac{\varepsilon_k}{\omega_k^A}$ and $(u_k^B + v_k^B)^2 = \frac{\varepsilon_k}{\omega_k^B}$, one finds

$$\Delta E_0^{(2)} = -g_{AB}^2 n_A n_B \sum_k \left[\frac{\varepsilon_k^2}{\omega_k^A \omega_k^B} \frac{1}{(\omega_k^A + \omega_k^B)} - \frac{1}{2\varepsilon_k} \right]. \quad (6.28)$$

By using the expressions in Eqs. [6.12] and [6.13] one obtains the following integral

$$\begin{aligned} \Delta E_0^{(2)} = & -g_{AB}^2 n_A n_B \frac{4\pi V}{(2\pi)^3} \int_0^\infty dk k^2 \left[\frac{\varepsilon_k^2}{\sqrt{\varepsilon_k^2 + 2g_A n_A \varepsilon_k} \sqrt{\varepsilon_k^2 + 2g_B n_B \varepsilon_k}} \right. \\ & \left. \times \frac{1}{\left(\sqrt{\varepsilon_k^2 + 2g_A n_A \varepsilon_k} + \sqrt{\varepsilon_k^2 + 2g_B n_B \varepsilon_k} \right)} - \frac{1}{2\varepsilon_k} \right]. \end{aligned} \quad (6.29)$$

Where one replaces the sum by an integral, $\sum_{\mathbf{k}} \rightarrow \frac{V}{(2\pi)^3} \int d^3 \mathbf{k}$. In addition, by substituting $\varepsilon_k = \frac{\hbar^2 k^2}{2m} = x$ one ends up with

$$\begin{aligned} \Delta E_0^{(2)} = & -g_{AB}^2 n_A n_B \frac{4\pi}{(2\pi)^3} \left(\frac{m}{\hbar^2} \right) V \frac{1}{\sqrt{2}} \int_0^\infty dx \frac{1}{\sqrt{x}} \left[\frac{2x^{3/2}}{\sqrt{(x+2g_A n_A)(x+2g_B n_B)}} \right. \\ & \left. \times \frac{1}{\sqrt{x+2g_A n_A} + \sqrt{x+2g_B n_B}} - 1 \right]. \end{aligned} \quad (6.30)$$

Let us consider the particular case where both species have the same scattering length, namely $a_A = a_B = a$ and therefore $g_A = g_B = g$. Additionally, the previous integral is simplified by using the fact that $\int_0^\infty \frac{1}{\sqrt{x}} \left[\frac{2x^{3/2}}{\sqrt{(x+a)\sqrt{x+b}(\sqrt{x+a}+\sqrt{x+b})}} - 1 \right] dx = -\frac{8(a^{3/2}-b^{3/2})}{3(a-b)}$. After carrying out the substitutions, we have that the second-order correction to the energy reads

$$\Delta E_0^{(2)} = \frac{1}{6\pi^2} \left(\frac{2m}{\hbar^2} \right)^{3/2} n_A n_B g_{AB}^2 V \frac{(2gn_A)^{3/2} - (2gn_B)^{3/2}}{g(n_A - n_B)}. \quad (6.31)$$

The final result for the ground-state energy of the system of M impurities and N bosons is given by

$$\begin{aligned} E(M, N) = & \frac{1}{2} g n_A^2 V \left(1 + \frac{128}{15\sqrt{\pi}} \sqrt{n_A a^3} \right) + \frac{1}{2} g n_B^2 V \left(1 + \frac{128}{15\sqrt{\pi}} \sqrt{n_B a^3} \right) \\ & + g_{AB} n_A n_B V \left[1 + g_{AB} \frac{\sqrt{2}}{3\pi^2} \left(\frac{2m}{\hbar^2} \right)^{3/2} \frac{(gn_A)^{3/2} - (gn_B)^{3/2}}{g(n_A - n_B)} \right]. \end{aligned} \quad (6.32)$$

Now we substitute the expressions for the pseudo-potential $g = 4\pi\hbar^2 a/m$ and $g_{AB} = 4\hbar^2 b/m$, where $b = a_{AB}$ is the impurity-boson scattering length. The result reads

$$\begin{aligned}
E(M, N) &= 4\pi M (n_A a^3) \left(1 + \frac{128}{15\sqrt{\pi}} \sqrt{n_A a^3}\right) \left(\frac{\hbar^2}{2ma^2}\right) + 4\pi N (n_B a^3) \left(1 + \frac{128}{15\sqrt{\pi}} \sqrt{n_B a^3}\right) \left(\frac{\hbar^2}{2ma^2}\right) \\
&\quad + 8\pi n_B a^3 M \left[\frac{b}{a} + \frac{32}{3\sqrt{\pi}} \frac{(n_A)^{3/2} - (n_B)^{3/2}}{(n_A - n_B)} a^{3/2} \frac{b^2}{a^2}\right] \left(\frac{\hbar^2}{2ma^2}\right).
\end{aligned} \tag{6.33}$$

We define the generalized binding energy of the mixture as:

$$\begin{aligned}
\frac{\mu(M, N)}{N} &= \frac{E(M, N) - E_0(N)}{N} \\
&= 4\pi n_A a^3 \left(1 + \frac{128}{15\sqrt{\pi}} \sqrt{n_A a^3}\right) \frac{M}{N} + 8\pi n_B a^3 \frac{M}{N} \left[\left(\frac{b}{a}\right) + \frac{32}{3\sqrt{\pi}} \frac{(n_A)^{3/2} - (n_B)^{3/2}}{(n_A - n_B)} a^{3/2} \frac{b^2}{a^2}\right].
\end{aligned} \tag{6.34}$$

We use units of $\left(\frac{\hbar^2}{2ma^2}\right) = 1$. In the case of small concentration, $x = M/N \ll 1$, the previous equation can be written as:

$$\frac{\mu(N, M)}{N} = g n_B \left(\frac{b}{a} + \frac{32}{3\sqrt{\pi}} \sqrt{n_B a^3} \frac{b^2}{a^2}\right) x + g n_B \left(1 + \frac{64}{3\sqrt{\pi}} \sqrt{n_B a^3} \frac{b^2}{a^2}\right) \frac{x^2}{2}, \tag{6.35}$$

which in terms of the binding energy of the single impurity (see Eq. [4.28]) turns out to be

$$\frac{\mu(N, M)}{N} = \mu^{\text{single}} x + F(x). \tag{6.36}$$

where

$$\mu^{\text{single}} = 8\pi n_B a^3 \left(\frac{b}{a} + \frac{32}{3\sqrt{\pi}} \sqrt{n_B a^3} \frac{b^2}{a^2}\right), \tag{6.37}$$

and

$$F(x) = 8\pi n_B a^3 \left(1 + \frac{64}{3\sqrt{\pi}} \sqrt{n_B a^3} \frac{b^2}{a^2}\right) \frac{x^2}{2}. \tag{6.38}$$

The function $F(x)$ gives information about the interaction between polarons. One observes that for $x \rightarrow 0$ one recovers M times the binding energy of the single polaron. The previous equations are valid for $x \ll 1$ and

$$\sqrt{n_B a^3} \frac{b^2}{a^2} \ll 1. \tag{6.39}$$

6.3 Collective variables method

In this section we use the results of Balabanyan [129] concerning the ground-state properties of binary mixtures of weakly interacting Bose gases by using the method of collective variables

developed for first time by Bogoliubov and Zubarev [130]. One considers a mixture of an interacting Bose gas in a volume V at $T = 0$. The mixture is formed by M particles of the type A and N particles of the type B . We also assume here the case of $a_A = a_B = a$, $a_{AB} = b$ and the equal masses case $m_A = m_B = m$. The result for the ground-state energy of the mixture is given by

$$E(N, M) = \frac{M^2}{2V}g + \frac{N^2}{2V}g + \frac{NM}{V}g_{AB} + \frac{4\pi V}{(2\pi)^3} \left(\frac{2m}{\hbar^2}\right)^{3/2} \frac{1}{15} [(\beta - \gamma)^{5/2} + (\beta + \gamma)^{5/2}]. \quad (6.40)$$

Here $g = 4\pi\hbar^2 a/m$ and $g_{AB} = 4\hbar^2 b/m$. The above energy in units of $\hbar^2/2ma^2$ is then given by

$$E(N, M) = (4\pi M n_A a^3 + 4\pi N n_B a^3 + 8\pi M n_B a^2 b) \left(\frac{\hbar^2}{2ma^2}\right) + \frac{4\pi V}{(2\pi)^3 a^3} \left(\frac{2ma^2}{\hbar^2}\right)^{3/2} \frac{1}{15} [(\beta - \gamma)^{5/2} + (\beta + \gamma)^{5/2}], \quad (6.41)$$

where $n_A = M/V$ and $n_B = N/V$. From now on, we use units of $\left(\frac{\hbar^2}{2ma^2}\right) = 1$. The coefficients β and γ are given by:

$$\beta = 8\pi a^3 (n_A + n_B) \quad \text{and} \quad \gamma = 8\pi a^3 \sqrt{(n_A - n_B)^2 + 4n_A n_B \left(\frac{b^2}{a^2}\right)}. \quad (6.42)$$

The stability condition, requiring a real value for the ground-state energy, one gets:

$$\frac{g^2}{g_{AB}} > 1 \Rightarrow \frac{a^2}{b^2} > 1. \quad (6.43)$$

Therefore, the mixture is stable under the condition $a > 0$ and $-a \leq b \leq a$.

6.3.1 Low concentration limit $x = M/N \ll 1$

Now we investigate the limit of small concentration of the above theoretical treatment $M \ll N$. The terms $(\beta \mp \gamma)^{5/2}$ entering Eq. [6.41]

$$(\beta \mp \gamma)^{5/2} = \left(8\pi n_B a^3\right) \left[(1+x) \mp \sqrt{x^2 + 2x(2\alpha^2 - 1) + 1}\right]^{5/2}, \quad (6.44)$$

in terms of x and $\alpha = b/a$. The previous expressions can be expanded for small concentration $x \ll 1$ one finds

$$(\beta - \gamma)^{5/2} \approx (8\pi n_A a^3)^{5/2} \left[\underbrace{[4\sqrt{2}(1 - \alpha^2)^{5/2}]}_{A_1} x^{5/2} + \mathcal{O}(x^{7/2}) \right], \quad (6.45)$$

and

$$(\beta + \gamma)^{5/2} \approx (8\pi n_B a^3)^{5/2} \left[\underbrace{4\sqrt{2}}_{A_0} + \underbrace{10\sqrt{2}x}_{A_2} + \underbrace{10\sqrt{2}\alpha^2 x^2}_{A_3} + \mathcal{O}(x^3) \right]. \quad (6.46)$$

Plugging both Eq. [6.45] and Eq. [6.46] into the ground state energy Eq. [6.41] we obtain

$$E(N, M) = 4\pi M n_A a^3 + 4\pi N n_B a^3 + 8\pi M n_B a^2 b + \frac{4\pi V}{15(2\pi)^3 a^3} (8\pi n_B a^3)^{5/2} (A_0 + A_2 x + A_3 x^2 + A_1 x^{5/2}). \quad (6.47)$$

It is convenient to split the previous expression as follows:

$$E(N, M) = 4\pi M n_A a^3 + 4\pi N n_B a^3 + 8\pi M n_B a^2 b + \frac{4\pi V}{15(2\pi)^3 a^3} (8\pi n_B a^3)^{5/2} (A_0 + A_2 x) + \frac{4\pi V}{15(2\pi)^3 a^3} (8\pi n_B a^3)^{5/2} (A_3 x^2 + A_1 x^{5/2}), \quad (6.48)$$

in such a way that

$$E(N, M) = 4\pi M n_A a^3 + 4\pi N n_B a^3 + 8\pi M n_B a^2 b + \frac{512\sqrt{\pi}}{15} N (n_B a^3)^{3/2} + \frac{256\sqrt{\pi}}{3} M (n_B a^3)^{3/2} \left(\frac{b^2}{a^2}\right) + \frac{4\pi V}{15(2\pi)^3 a^3} (8\pi n_B a^3)^{5/2} (A_3 x^2 + A_1 x^{5/2}). \quad (6.49)$$

Where A_0 and A_2 were substituted. After reorganizing the terms one ends up with

$$E(N, M) = E_0(N) + 8\pi M n_B a^2 b + \frac{256\sqrt{\pi}}{3} M (n_B a^3)^{3/2} \left(\frac{b^2}{a^2}\right) + 4\pi M n_A a^3 + \frac{4\pi V}{15(2\pi)^3 a^3} (8\pi n_B a^3)^{5/2} (A_3 x^2 + A_1 x^{5/2}), \quad (6.50)$$

where $E_0(N)$ is the ground-state energy of the weakly interacting Bose gas (bosons type B). In addition, by using the definition of the binding energy for the single polaron μ^{single} (see Eq. [4.28]) and inserting the coefficients A_1 and A_3 into Eq. [6.50] we find the generalized binding energy of the mixture as:

$$\frac{\mu(N, M)}{N} = \mu^{\text{single}} x + 8\pi a^3 n_B \left(1 + \frac{32}{3\sqrt{\pi}} \sqrt{n_B a^3} \left(\frac{2b^2}{a^2} - \frac{1}{2} \frac{b^4}{a^4} \right) \frac{x^2}{2} \right), \quad (6.51)$$

or alternatively:

$$\boxed{\frac{\mu(N, M)}{N} = \mu^{\text{single}} x + F(x).} \quad (6.52)$$

Where

$$\begin{aligned}\mu^{\text{single}} &= 8\pi n_B a^3 \left(\frac{b}{a} + \frac{32}{3\sqrt{\pi}} \sqrt{n_B a^3} \frac{b^2}{a^2} \right), \\ F(x) &= 8\pi n_B a^3 \left(1 + \frac{32}{3\sqrt{\pi}} \sqrt{n_B a^3} \left(\frac{2b^2}{a^2} - \frac{1}{2} \frac{b^4}{a^4} \right) \right) \frac{x^2}{2}.\end{aligned}\tag{6.53}$$

The previous expression coincides with the perturbative result Eq. [6.35] in the limit of both small concentration x and weak impurity-boson coupling.

The perturbative result can be used for arbitrary concentration of impurities but only when the impurity-boson coupling is weak. On the other hand, the collective variable results are valid for $-a \leq b \leq a$ with $a > 0$. In the next section we use DMC simulations in order to investigate the ground-state energy of the system as a function of the ratio b/a of scattering lengths and of the concentration x .

6.4 Monte-Carlo calculation

In this section we use QMC methods to calculate the energy of the system of M impurities in a bosonic bath of $N = 64$ particles. In the QMC simulations we use $64 + M$ particles in a cubic box of size L with periodic boundary conditions. The density of the impurities (**bosons of type A**) is $n_A = M/V$, whereas for the bosons of the bath (**bosons of type B**), is $n_B = N/V$. The general Hamiltonian of the system is written as

$$\mathcal{H} = \underbrace{-\frac{\hbar^2}{2m_A} \sum_{\alpha=1}^M \nabla_{\alpha}^2 + \sum_{\alpha<\beta} V(r_{\alpha\beta})}_{\text{Bosons A}} - \underbrace{\frac{\hbar^2}{2m_B} \sum_{i=1}^N \nabla_i^2 + \sum_{i<j} V(r_{ij})}_{\text{Bosons B}} + \sum_{\alpha,i}^{N,M} V(r_{i\alpha}),\tag{6.54}$$

The previous expression is splitted in terms of the Hamiltonian of the bosons of type A and type B. The last term represent the interaction between the two bosonic components. Where $r_{\alpha\beta} = |\mathbf{r}_{\alpha} - \mathbf{r}_{\beta}|$ is the inter-particle distance of the bosons of type A, $r_{ij} = |\mathbf{r}_i - \mathbf{r}_j|$ is the inter-particle distance of the bosons of type B and $r_{i\alpha} = |\mathbf{r}_i - \mathbf{r}_{\alpha}|$ is the distance between particles of type A and B. In addition, we use a trial wave function for this system written as:

$$\psi_T(\mathbf{R}_A, \mathbf{R}_B) = \Psi_A(\mathbf{R}_A) \Psi_B(\mathbf{R}_B) \Psi_{AB}(\mathbf{R}_A, \mathbf{R}_B),\tag{6.55}$$

where \mathbf{R}_A and \mathbf{R}_B represents the positions of the bosons of type A and type B respectively. Here $\Psi_A(\mathbf{R}_A)$ is the trial wavefunction of the bosons of type A, $\Psi_B(\mathbf{R}_B)$ is the trial wavefunction of the bosons of type B and $\Psi_{AB}(\mathbf{R}_A, \mathbf{R}_B)$ is the trial wavefunction describing the correlations between the bosons of type A and type B. The explicit form of the above trial wavefunctions is in terms of Jastrow functions is

$$\begin{aligned}
\Psi_A(\mathbf{R}_A) &= \prod_{\alpha < \beta} f_A(r_{\alpha\beta}), \\
\Psi_B(\mathbf{R}_B) &= \prod_{i < j} f_B(r_{ij}) \text{ and} \\
\Psi_{AB}(\mathbf{R}_{AB}) &= \prod_i \prod_\alpha f_{AB}(r_{i\alpha}).
\end{aligned} \tag{6.56}$$

We also assume that each species interact via a HS potential (see Eq. [3.58]) with the same scattering length, namely $a_A = a_B = a$. The Jastrow functions f_A and f_B are given by Eq. [3.60] for each species and f_{AB} is given by Eq. [3.66]. The impurity-boson potential is modeled by a ASW potential similar to the case of a single impurity.

The local energy (see Eq. [3.99]) associated with the trial wavefunction in Eq. [6.55] reads:

$$E_L = -\frac{\hbar^2}{2m} \frac{(\nabla_{\mathbf{R}_A}^2 + \nabla_{\mathbf{R}_B}^2) \psi_T(\mathbf{R}_A, \mathbf{R}_B)}{\psi_T(\mathbf{R}_A, \mathbf{R}_B)} + V(\mathbf{R}_A, \mathbf{R}_B). \tag{6.57}$$

Carrying out the calculations, one obtains

$$\begin{aligned}
\nabla_{\mathbf{R}_A}^2 \psi_T(\mathbf{R}_A, \mathbf{R}_B) &= \Psi_B(\mathbf{R}_B) \left[(\nabla_{\mathbf{R}_A}^2 \Psi_A(\mathbf{R}_A)) \Psi_{AB}(\mathbf{R}_A, \mathbf{R}_B) + \Psi_A(\mathbf{R}_A) (\nabla_{\mathbf{R}_A}^2 \Psi_{AB}(\mathbf{R}_A, \mathbf{R}_B)) \right. \\
&\quad \left. + 2 \nabla_{\mathbf{R}_A} \Psi_A(\mathbf{R}_A) \cdot \nabla_{\mathbf{R}_A} \Psi_{AB}(\mathbf{R}_A, \mathbf{R}_B) \right]
\end{aligned} \tag{6.58}$$

and

$$\begin{aligned}
\nabla_{\mathbf{R}_B}^2 \psi_T(\mathbf{R}_A, \mathbf{R}_B) &= \Psi_A(\mathbf{R}_A) \left[(\nabla_{\mathbf{R}_B}^2 \Psi_B(\mathbf{R}_B)) \Psi_{AB}(\mathbf{R}_A, \mathbf{R}_B) + \Psi_B(\mathbf{R}_B) (\nabla_{\mathbf{R}_B}^2 \Psi_{AB}(\mathbf{R}_A, \mathbf{R}_B)) \right. \\
&\quad \left. + 2 \nabla_{\mathbf{R}_B} \Psi_B(\mathbf{R}_B) \cdot \nabla_{\mathbf{R}_B} \Psi_{AB}(\mathbf{R}_A, \mathbf{R}_B) \right].
\end{aligned} \tag{6.59}$$

Therefore the local energy is written as:

$$\begin{aligned}
E_L &= -D \left\{ \frac{\nabla_{\mathbf{R}_A}^2 \Psi_A(\mathbf{R}_A)}{\Psi_A(\mathbf{R}_A)} + \frac{\nabla_{\mathbf{R}_B}^2 \Psi_B(\mathbf{R}_B)}{\Psi_B(\mathbf{R}_B)} + \frac{(\nabla_{\mathbf{R}_A}^2 + \nabla_{\mathbf{R}_B}^2) \Psi_{AB}(\mathbf{R}_A, \mathbf{R}_B)}{\Psi_{AB}(\mathbf{R}_A, \mathbf{R}_B)} \right. \\
&\quad \left. + \left[\frac{2 \nabla_{\mathbf{R}_A} \Psi_A(\mathbf{R}_A)}{\Psi_A(\mathbf{R}_A)} \cdot \frac{\nabla_{\mathbf{R}_A} \Psi_{AB}(\mathbf{R}_A, \mathbf{R}_B)}{\Psi_{AB}(\mathbf{R}_A, \mathbf{R}_B)} + \frac{2 \nabla_{\mathbf{R}_B} \Psi_B(\mathbf{R}_B)}{\Psi_B(\mathbf{R}_B)} \cdot \frac{\nabla_{\mathbf{R}_B} \Psi_{AB}(\mathbf{R}_A, \mathbf{R}_B)}{\Psi_{AB}(\mathbf{R}_A, \mathbf{R}_B)} \right] \right\} + V(\mathbf{R}_A, \mathbf{R}_B)
\end{aligned} \tag{6.60}$$

with $D = \frac{\hbar^2}{2m}$ and finally,

$$\begin{aligned}
E_L &= E_L^A(\mathbf{R}_A) + E_L^B(\mathbf{R}_B) + E_L^A(\mathbf{R}_{AB}) + E_L^B(\mathbf{R}_{AB}) \\
&\quad + [\mathbf{F}_A \cdot \mathbf{F}_{AB} + \mathbf{F}_B \cdot \mathbf{F}_{BA}] + V(\mathbf{R}_A, \mathbf{R}_B)
\end{aligned} \tag{6.61}$$

with the local energies

$$\begin{aligned}
E_L^A(\mathbf{R}_A) &= -D \left(\frac{\nabla_{\mathbf{R}_A}^2 \Psi_A(\mathbf{R}_A)}{\Psi_A(\mathbf{R}_A)} \right), \\
E_L^B(\mathbf{R}_B) &= -D \left(\frac{\nabla_{\mathbf{R}_B}^2 \Psi_B(\mathbf{R}_B)}{\Psi_B(\mathbf{R}_B)} \right), \\
E_L^A(\mathbf{R}_{AB}) &= -D \frac{\nabla_{\mathbf{R}_A}^2 \Psi_{AB}(\mathbf{R}_A, \mathbf{R}_B)}{\Psi_{AB}(\mathbf{R}_A, \mathbf{R}_B)}, \\
E_L^B(\mathbf{R}_{AB}) &= -D \frac{\nabla_{\mathbf{R}_B}^2 \Psi_{AB}(\mathbf{R}_A, \mathbf{R}_B)}{\Psi_{AB}(\mathbf{R}_A, \mathbf{R}_B)}.
\end{aligned} \tag{6.62}$$

Whereas, the quantum drift forces are defined as:

$$\begin{aligned}
\mathbf{F}_A &= -D \frac{2\nabla_{\mathbf{R}_A} \Psi_A(\mathbf{R}_A)}{\Psi_A(\mathbf{R}_A)}, \\
\mathbf{F}_B &= -D \frac{2\nabla_{\mathbf{R}_B} \Psi_B(\mathbf{R}_B)}{\Psi_B(\mathbf{R}_B)}
\end{aligned} \tag{6.63}$$

and

$$\mathbf{F}_{AB} = -D \frac{\nabla_{\mathbf{R}_A} \Psi_{AB}(\mathbf{R}_A, \mathbf{R}_B)}{\Psi_{AB}(\mathbf{R}_A, \mathbf{R}_B)}, \quad \mathbf{F}_{BA} = -D \frac{\nabla_{\mathbf{R}_B} \Psi_{AB}(\mathbf{R}_A, \mathbf{R}_B)}{\Psi_{AB}(\mathbf{R}_A, \mathbf{R}_B)}.$$

The DMC energy associated with the local energy in Eq. [6.57] is denoted by $E^{DMC}(N, M)$. According to the definition of **generalized binding energy** as:

$$\boxed{\frac{\mu(M, N)}{N} = \frac{E^{DMC}(M, N) - E_0^{DMC}(N)}{N}}, \tag{6.64}$$

where $E_0^{DMC}(N)$ is the DMC energy of the system without impurities.

The generalized binding energy in units of gn_Bx is plotted in Fig. [6.1] as a function of b/a for different number of bosons of type A ($M = 3, 5, 7$ and 9). The results refer to the repulsive branch and the density of bosons of type B is fixed $n_B a^3 = 10^{-5}$. We plot both the perturbation result given by Eq. [6.34] and the DMC result obtained from Eq. [6.64]. The known sources of systematic errors of the DMC algorithm, namely the dependence on the number of walkers and the time step have been analyzed.

In Fig. [6.1] one observes a good agreement between perturbation theory and the DMC results for both small concentrations and weak coupling between the two bosonic species. In contrast, deviations appear for both large concentrations x and large coupling strengths b/a .

In Fig. [6.2] we summarize the results for the generalized binding energy in units of gn_Bx as a function of b/a . We observe that for values of the coupling strength $\frac{b}{a} \gtrsim 7$ a dependence of the generalized binding energy on the concentration showed.

In Fig. [6.3] we plot the generalized binding energy once the mean-field contribution $\mu_{MF} = 8\pi(n_B a^3) \frac{b}{a}$ is subtracted as a function of b/a for different concentrations x . In the weakly interacting and low concentration regime, the perturbation theory is in good agreement with

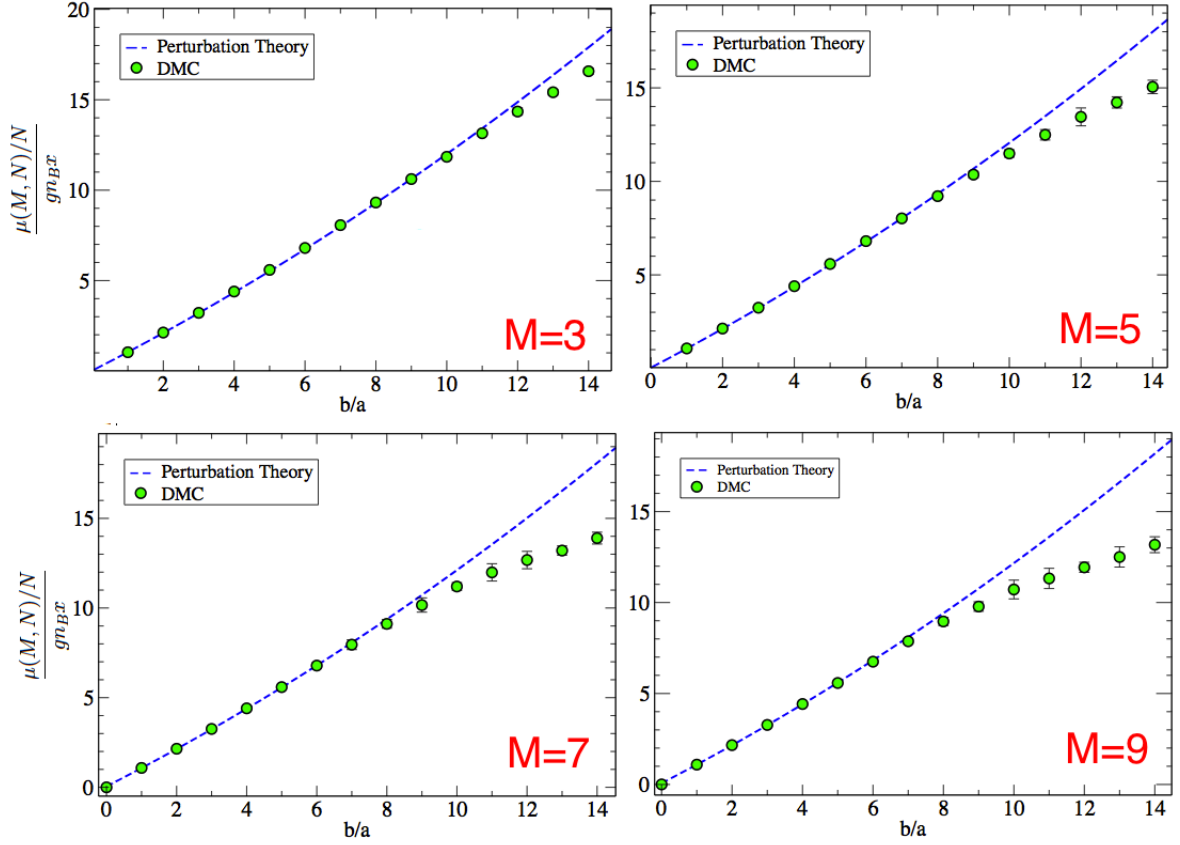


Figure 6.1: Generalized binding energy in units of gn_Bx as a function of b/a along the repulsive branch for different concentrations $x = 3/64, 5/64, 7/64$ and $x = 9/64$. Both perturbation theory (blue dashed line) and DMC results (filled green circles).

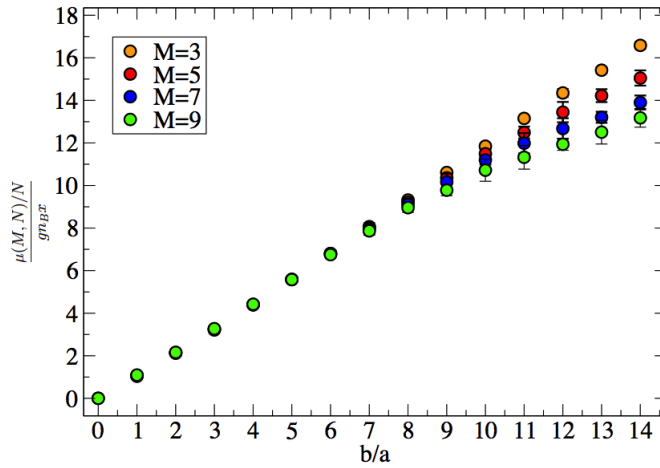


Figure 6.2: Generalized binding energy (in units of gn_Bx) as a function of b/a for different concentrations $x = 3/64, 5/64, 7/64$ and $x = 9/64$.

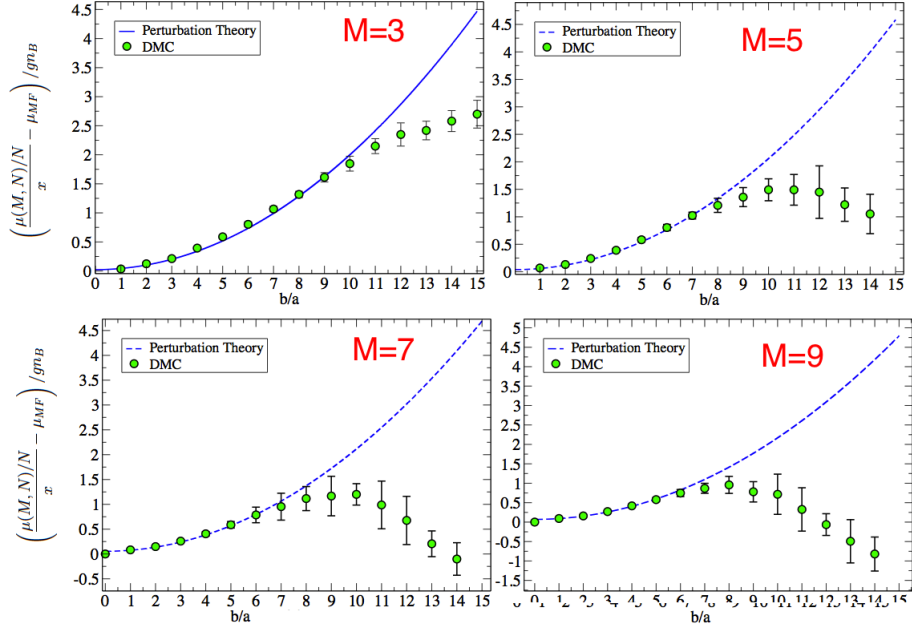


Figure 6.3: **Generalized binding energy (in units of gn_Bx) once the mean-field term (μ_{MF}) is subtracted as a function of b/a for different concentrations $x = 3/64, 5/64, 7/64$ and $x = 9/64$. Perturbation theory (blue dashed line) and DMC results (filled green circles).**

the DMC calculations. At small concentrations $x \lesssim \frac{9}{64}$, deviations are found for values of b/a larger than $b/a \gtrsim 10$. For these values, the energy defined above decreases as x increases.

6.5 Energy dependence on the concentration of impurities

In this section we consider a fixed value of the ratio b/a and we investigate the dependence of the energy on the concentration $x = M/N$. For values of $b/a = \pm 5$, belonging to the repulsive and attractive branches. We plot the generalized binding energy in units of Ngn_B in Fig. [6.4] as a function of the concentration x . Differences between DMC and perturbative results are not visible

6.6 Interaction between polarons

From perturbation theory and the collective variables method we learned that for both small coupling strength b/a and small concentration x , the generalized binding energy of the mixture can be written as

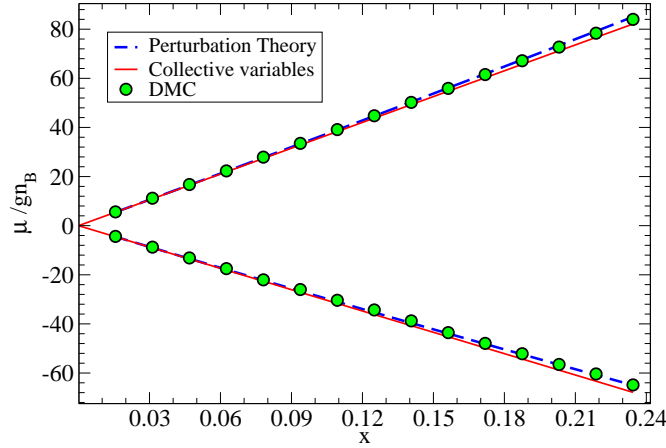


Figure 6.4: **Generalized binding energy in units of $gn_B N$ as a function of the concentration x .** For $b/a = -5$ (lower branch) and $b/a = +5$ (upper branch) computed with perturbation theory (blue dashed line), collective variables method (solid red line) and DMC results (filled green circles).

$$\frac{\mu}{Ngn_B} = \mu^{single}x + F(x), \quad (6.65)$$

where μ^{single} is the binding energy of the single polaron and $F(x)$ is called the residual function. The residual function describes the interaction between polarons.

Accordingly to Eq. [6.36] in perturbation theory, Eq. [6.52] in the collective variables method and Eq. [6.64] in the DMC, we find that the residual functions are written as follows:

- Perturbation theory

$$F(x) = 8\pi (n_B a^3) \left[1 + \frac{64}{3\sqrt{\pi}} (n_B a^3)^{1/2} \left(\frac{b^2}{a^2} \right) \right] \frac{x^2}{2}. \quad (6.66)$$

- Collective variables

$$F(x) = 8\pi (n_B a^3) \left(1 + \frac{32}{3\sqrt{\pi}} (n_B a^3)^{1/2} \left[2 \left(\frac{b^2}{a^2} \right) - \frac{1}{2} \left(\frac{b^2}{a^2} \right)^2 \right] \right) \frac{x^2}{2}. \quad (6.67)$$

- DMC calculation

$$F(x) = \frac{\mu_{\text{DMC}}}{N} - (\mu^{single})_{\text{DMC}} x. \quad (6.68)$$

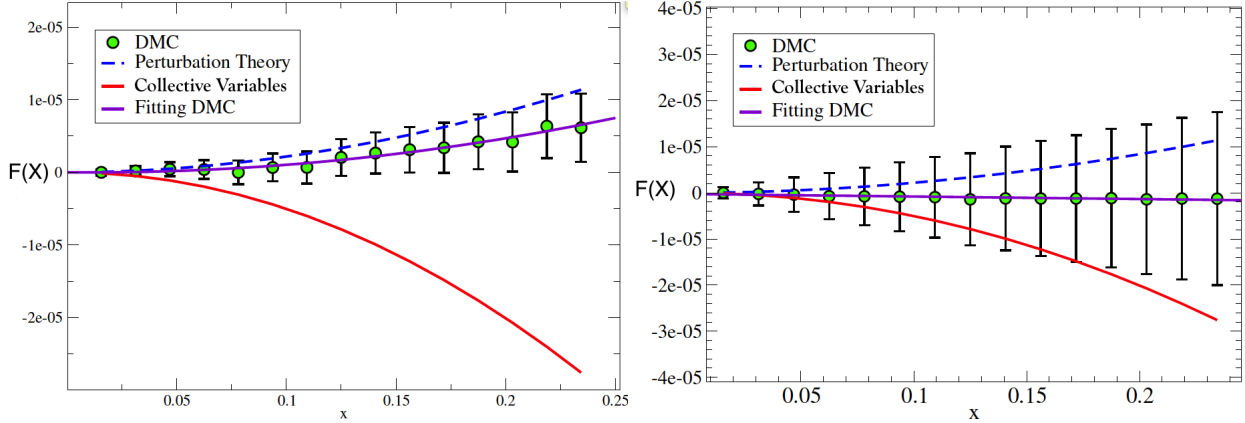


Figure 6.5: **Residual function $F(x)$ as a function of the concentration x for both (left) attractive interactions $b/a = -5$ and (right) repulsive interactions $b/a = +5$.** Perturbation theory (blue dashed line), collective variables method (solid red line) and DMC results (filled green circles).

In Fig. [6.5] we plot the residual function $F(x)$ corresponding to perturbation theory, to the collective variable method and the results of DMC calculations. The function is plotted as a function of the concentration x for two different values $b/a = \pm 5$ of the coupling strength. We obtain a very good agreement between perturbation theory and the DMC results for both values of b/a and for all values of x .

6.7 Stability conditions and phase diagram

In the past section we calculated the generalized binding energy of the mixture as a function of the concentration x for fixed values of coupling strength $b/a = \pm 5$.

Based on the generalized equation of state we calculate the phase diagram of the mixture in the regime of small concentration. By using the information about the equation we determine the phase diagram as a function of both the parameter $n_B a^3$ and the coupling strength b/a for the two possible phases in the system: homogeneous and phase separated state.

6.7.1 Phase I: homogeneous mixture

We investigate the condition for which an homogeneous phase can exist. This phase consists of both bosons of type A and of type B distributed uniformly in a cubic box of size L as is shown in Fig. [6.6].

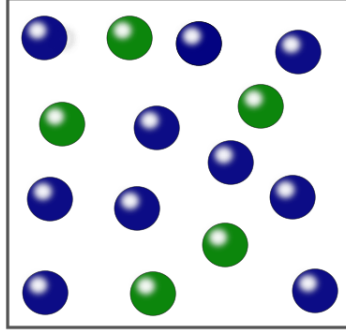


Figure 6.6: **Homogeneous phase:** M bosons of type A (green balls) and N bosons of type B (blue balls) immersed in a cubic box of size L .

Mechanical equilibrium

In order to investigate the mechanical equilibrium of the homogeneous mixture we calculate the compressibility matrix defined as

$$\beta = \begin{pmatrix} \frac{\partial \mu_A}{\partial n_A} & \frac{\partial \mu_A}{\partial n_B} \\ \frac{\partial \mu_B}{\partial n_A} & \frac{\partial \mu_B}{\partial n_B} \end{pmatrix}, \quad (6.69)$$

where μ_A and μ_B are the chemical potentials of the bosons of type A and type B respectively.

The ground-state energy of the homogeneous mixture can be parametrized in general as

$$E(N, M) = E_0(N) + gn_B N \left[A \left(\frac{b}{a}, n_B a^3 \right) x + F \left(\frac{b}{a}, n_B a^3 \right) x^2 \right], \quad (6.70)$$

where A is the binding energy of a single polaron, F is the residual function and $x = M/N$ is the concentration of the mixture.

The chemical potential of each component is written as:

$$\begin{aligned} \mu_A &= \frac{\partial E(N, M)}{\partial M} = gn_B (A + 2xF) \text{ and} \\ \mu_B &= \frac{\partial E(N, M)}{\partial N} = \mu_0 + gAn_A + gA'n_A n_B + gF'n_A^2, \end{aligned} \quad (6.71)$$

where

$$\begin{aligned} \mu_0 &= gn_B \left(1 + \frac{32}{3\sqrt{\pi}} \sqrt{n_B a^3} \right), \\ A' &= \frac{\partial A}{\partial n_B}, \\ F' &= \frac{\partial F}{\partial n_B}. \end{aligned} \quad (6.72)$$

The derivatives involved in Eq. [6.69] can be readily computed, providing the results

$$\begin{aligned}
\frac{\partial \mu_A}{\partial n_A} &= 2gF, \\
\frac{\partial \mu_A}{\partial n_B} &= gA + gA'n_B + 2gF'n_A, \\
\frac{\partial \mu_B}{\partial n_A} &= gA + gA'n_B + 2gF'n_A, \\
\frac{\partial \mu_B}{\partial n_B} &= \frac{\partial \mu_0}{\partial n_B} + 2gA'n_A + gA''n_An_B + gF''n_A^2,
\end{aligned} \tag{6.73}$$

and the compressibility matrix is given by:

$$\beta = \begin{pmatrix} g \left[1 + \frac{16}{\sqrt{\pi}} \sqrt{n_B a^3} + (2n_B A' + n_B^2 A'') x + n_B^2 F'' x^2 \right] & g(A + n_B A' + 2n_B F' x) \\ g(A + n_B A' + 2n_B F' x) & 2gF \end{pmatrix}. \tag{6.74}$$

The mechanical stability of the mixture is obtained for $\det(\beta) > 0$. It means:

$$\begin{aligned}
2F \left(1 + \frac{16}{\sqrt{\pi}} \sqrt{n_B a^3} + (2n_B A' + n_B^2 A'') x + n_B^2 F'' x^2 \right) \\
- (A + n_B A' + 2n_B F' x)^2 > 0,
\end{aligned} \tag{6.75}$$

for small concentration, $x \ll 1$, one obtains

$$h_1(n_B a^3, b/a) \equiv 2F \left(1 + \frac{16}{\sqrt{\pi}} \sqrt{n_B a^3} \right) - (A + n_B A')^2 > 0. \tag{6.76}$$

From perturbation theory (see Eq. [6.35]) one can derive analytic expressions for the quantities A , A' and F yielding

$$\begin{aligned}
A &= \frac{b}{a} + \frac{32}{3\sqrt{\pi}} \sqrt{n_B a^3} \frac{b^2}{a^2}, \\
n_B A' &= \frac{16}{3\sqrt{\pi}} \sqrt{n_B a^3} \frac{b^2}{a^2}, \\
F &= \frac{1}{2} \left(1 + \frac{64}{3\sqrt{\pi}} \sqrt{n_B a^3} \frac{b^2}{a^2} \right).
\end{aligned} \tag{6.77}$$

In Fig. [6.7] we plot the function $h_1(n_B a^3, b/a)$ obtained from perturbation theory as a function of b/a for different values of the gas parameter $n_B a^3$.

We observe that for values of $n_B a^3 \leq 10^{-4}$ the homogeneous mixture is stable in the range (see inset of Fig. [6.7])

$$-1 \lesssim b/a \leq 1. \tag{6.78}$$

However, for larger values of the gas parameter $n_B a^3 \gtrsim 10^{-3}$, the range where the mixture is stable becomes significantly wider when $b/a < 0$.

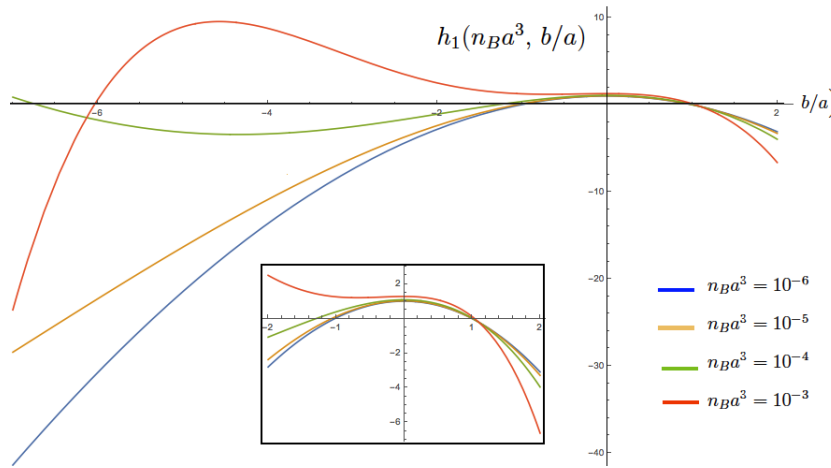


Figure 6.7: Representation of $h_1(n_B a^3, \frac{b}{a})$ for different values of $\frac{b}{a}$ and $n_B a^3$. For values of $h_1 > 0$, the homogeneous phase is stable.

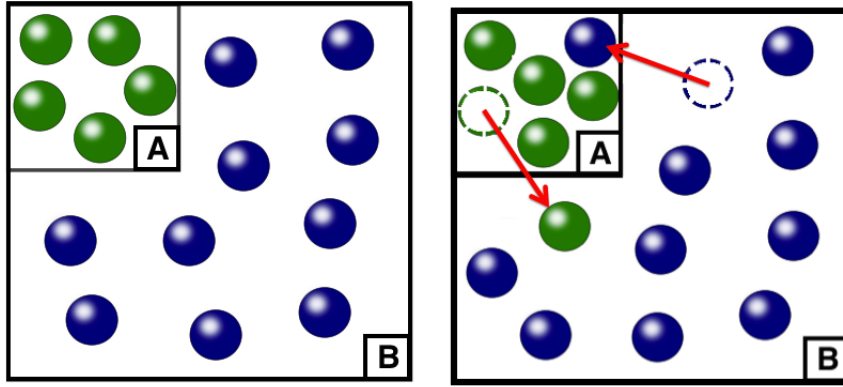


Figure 6.8: **Phase II:** (left) M bosons in the region A and N bosons in the region B distributed in different volumes $V_A \neq V_B$. (right) stability of the phase separated state,

A problem remains through with the predictions at large values of $n_B a^3$: first of all perturbation theory might not be applicable when bosons of B are so strongly interacting and secondly even DMC might not be reliable because at high densities results become model dependent (e.g. on the use of the Hard-sphere potential).

6.7.2 Phase II: phase separated state

In this phase we consider that the bosons of type A and of type B are distributed in two separate sectors: M bosons of type A lie in a volume V_A and N bosons of type B lie in a volume V_B such that $V_A + V_B = V$ (see Fig. [6.8]).

The equation of state of every sector

$$\begin{aligned} E_A(M) &= \frac{1}{2}g\tilde{n}_A M \left(1 + \frac{128}{15\sqrt{\pi}}\sqrt{\tilde{n}_A a^3}\right), \\ E_B(N) &= \frac{1}{2}g\tilde{n}_B N \left(1 + \frac{128}{15\sqrt{\pi}}\sqrt{\tilde{n}_B a^3}\right). \end{aligned} \quad (6.79)$$

Where $\tilde{n}_A = M/V_A$ and $\tilde{n}_B = N/V_B$. Mechanical equilibrium requires that the pressure in both sectors is equal. This means

$$p_A = -\left(\frac{\partial E_A(M)}{\partial V_A}\right)_N = -\left(\frac{\partial E_B(N)}{\partial V_B}\right)_M = p_B, \quad (6.80)$$

$$\frac{1}{2}\tilde{n}_A^2 g \left(1 + \frac{64}{5\sqrt{\pi}}\sqrt{\tilde{n}_A a^3}\right) = \frac{1}{2}\tilde{n}_B^2 g \left(1 + \frac{64}{5\sqrt{\pi}}\sqrt{\tilde{n}_B a^3}\right). \quad (6.81)$$

Eq. [6.81] yields $\tilde{n}_A = \tilde{n}_B = \tilde{n}$ and therefore,

$$\frac{M}{V_A} = \frac{N}{V_B} \rightarrow \frac{V_A}{V_B} = x. \quad (6.82)$$

From the previous relation one obtains that

$$\begin{aligned} \tilde{n}_A &= n_B (1 + x) \text{ and} \\ \tilde{n}_B &= n_B (1 + x). \end{aligned} \quad (6.83)$$

where $n_B = N/V$. The total energy can be written as

$$\begin{aligned} E(N, M) &= E_A(M) + E_B(N) \\ &= \frac{1}{2}Ngn_B (1 + x)^2 \left(1 + \frac{128}{15\sqrt{\pi}}\sqrt{n_B(1 + x)a^3}\right). \end{aligned} \quad (6.84)$$

For small concentrations, $x \ll 1$, one ends up with:

$$\begin{aligned} E(N, M) &= \frac{1}{2}gNn_B \left(1 + \frac{128}{15\sqrt{\pi}}\sqrt{n_B a^3}\right) \\ &+ gNn_B \left[\left(1 + \frac{32}{3\sqrt{\pi}}\sqrt{n_B a^3}\right)x + \left(1 + \frac{16}{\sqrt{\pi}}\sqrt{n_B a^3}\right)\frac{x^2}{2}\right]. \end{aligned} \quad (6.85)$$

Now, let us suppose that the energy to take a boson of the type A out of the sector A and put it in sector B (right side of Fig. [6.8]) is positive. This process is energetically suppressed and can not happen. In other words

$$-\mu_A + \mu^{\text{single}} > 0. \quad (6.86)$$

where μ_A is the chemical potential of the bosons in the sector A and μ is the binding energy of the impurity atom (boson of type A) in the bath of type B bosons. By writing the above

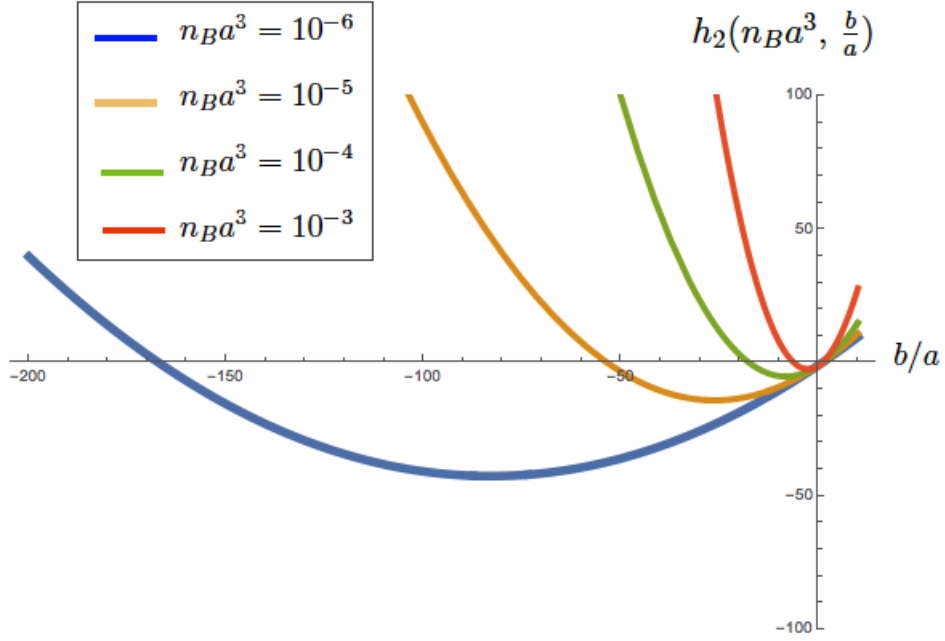


Figure 6.9: Plot of $h_2(n_B a^3, \frac{b}{a})$ as a function of $\frac{b}{a}$ for different values of $n_B a^3$. For values of $h_2 < 0$, the phase separated state is unstable.

condition using the result in Eq. [4.28] for μ^{single} one gets

$$-g\tilde{n}_A \left(1 + \frac{32}{3\sqrt{\pi}} \sqrt{\tilde{n}_A a^3} \right) + 8\pi\tilde{n}_B a^3 \left(\frac{b}{a} + \frac{32}{3\sqrt{\pi}} (\tilde{n}_B a^3)^{1/2} \frac{b^2}{a^2} \right) > 0. \quad (6.87)$$

Using the fact $\tilde{n}_A = \tilde{n}_B$ the previous equation can be written as

$$\left(\frac{b}{a} - 1 \right) \left[1 + \frac{32}{3\sqrt{\pi}} \sqrt{n_B a^3} \left(\frac{b}{a} + 1 \right) \right] > 0. \quad (6.88)$$

Therefore if

$$h_2(n_B a^3, \frac{b}{a}) \equiv \left(\frac{b}{a} - 1 \right) \left[1 + \frac{32}{3\sqrt{\pi}} \sqrt{n_B a^3} \left(\frac{b}{a} + 1 \right) \right] < 0, \quad (6.89)$$

the phase separated state is unstable. In Fig. [6.9] we plot the function h_2 as a function of the coupling strength b/a and the gas parameter $n_B a^3$.

In the phase diagram Fig. [6.9] we observe that for values of $n_B a^3 \lesssim 10^{-5}$ the phase separated state is stable for large values of the coupling strength b/a on the attractive branch. Namely $b/a \lesssim -150$ (for $n_B a^3 = 10^{-6}$) and $b/a \lesssim -50$ (for $n_B a^3 = 10^{-5}$). Whereas for the repulsive branch the phase is stable for for $b/a > 1$.

In Fig. [6.10] we collect the results from Figs. [6.7] and [6.9]. The phase diagram in Fig. [6.10] represents the stability of both the homogeneous phase (green region) and the phase separated

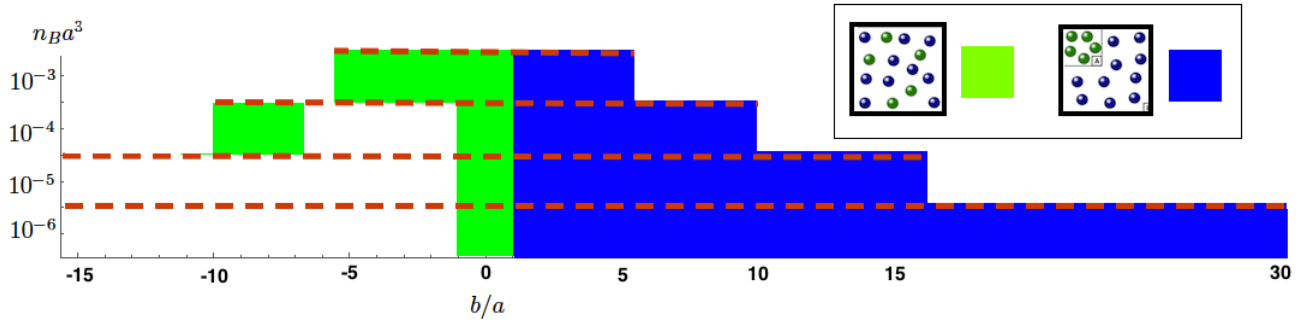


Figure 6.10: Phase diagram for different values of $n_B a^3$ as a function of the coupling strength b/a . The stable homogeneous phase is represented by the green region, whereas the stable phase separated state is represented by the blue region. The horizontal dashed lines represent the interval where perturbation theory works.

state (blue region) as a function of the gas parameter $n_B a^3$ and the coupling strength b/a . The horizontal dashed lines represent the values where perturbation theory is applicable i.e $\sqrt{n_B a^3} \left(\frac{b^2}{a^2} \right) \ll 1$.

Chapter 7

Conclusions and Perspectives

7.1 Conclusions

In this work we used quantum Monte-Carlo (QMC) methods to investigate the ground-state properties of bosonic impurities coupled to a bosonic bath at $T = 0$. The ground-state properties studied here are the energy, the effective mass and the pair correlation functions. We also used mean-field and variational approaches to address the single impurity problem aiming to compare them with the QMC. This work is inspired by the recent experiments concerning Fermi-polarons with ultracold atoms, which permit to investigate scenarios that are not accessible in solid-state physics. Even though, QMC methods provide different results for the ground-state properties compared with those predicted by the Fröhlich Hamiltonian in the strongly-interacting regime, a question mark remains as to whether this system can be used as a quantum-simulator for polarons in solid state physics.

- In this thesis we calculated the ground-state properties of a single impurity interacting with a dilute bosonic bath as a function of the coupling strength a/b with perturbation theory, the Jensen-Feynman variational method and QMC techniques. We found two branches, one corresponding to the repulsive branch ($0.03 \lesssim a/b \leq 1$) which is an excited state of the system and to the attractive branch that represents the many body ground-state of the system ($-\infty \lesssim a/b < 0$). The ground-state energy and effective mass are found in good agreement with perturbation theory and variational methods (Jensen-Feynman approach) in the weakly-interacting regime, where the so-called Fröhlich Hamiltonian describes the low-energy excitations of the bosonic bath coupled to the impurity. On the other hand, for strong interactions between the impurity and the bosons, QMC methods provide results that are completely different from those predicted by mean field and variational methods. For instance, self-localization of the impurity

does not occur, the binding energy at the unitary limit is finite and the density profile obtained from the impurity-boson correlation function displays a large deviations from the equilibrium density of the bosonic bath.

- The special case of an impurity interacting resonantly with the bosonic bath (unitary limit, $a/b = 0$) is investigated as a function of the gas parameter $n_B a^3$. We found a power-law dependence of the binding energy with the gas parameter in the limit of a dilute bosonic bath. On the other hand, the effective mass shows a linear dependence with the gas parameter. The problem of the impurity interacting resonantly with the bosonic bath has also been investigated T -matrix techniques. The QMC results for the binding energy and effective mass are in good agreement at relatively large values of $n_B a^3$. In the limit of a very dilute bosonic bath the above two techniques present differences. According to the results of the pair correlation functions, the structure of the bosonic bath is not largely modified by the presence of the impurity, whereas the density of bosons around the impurity is significantly modified over distances smaller than the healing length. The Efimov effect was studied for a system of two bosons and one distinguishable particle with resonant species interaction. Even though, a trimer bound state is predicted to occur, we found that the energy of this state is not larger than the binding energy of the polaron.
- We also investigated the ground-state energy of a system of many impurities in a bosonic bath. For small concentrations of the impurities and small values of the coupling strength b/a in the phase we found good agreement with mean-field methods. The values of both concentration and coupling strength for which the homogeneous mixture is stable are limited. We determine the phase diagram.

7.2 Perspectives

- To investigate the ground-state properties of the the impurity coupled with the bosonic bath as a function of the temperature. For instance, by using Monte-Carlo techniques at finite temperature.
- To consider the case of different masses is interesting, since experimentally many bosonic binary mixture of different components have been realized. On the other hand, concerning the single polaron problem, the Efimov effect in the unbalanced case brings more interesting features. Such as possible N -body bound states.
- The study of fermionic impurities immersed in the bosonic bath.

Appendix A: Error estimates for Markov chains

The QMC algorithms used in this thesis rely on the Markov chains concept. In a markov chains the statistical errors are correlated and it must be treated in a proper way. Along this thesis we used a bunching method that allow us to estimate the true error of a detemined observables both VMC and DMC.

The idea of the bunching method algorithm is cutting-up the Markov chain in blocks. For instance, one produces bunches of size 2, 4 or 8,..., especially if the number of data points is a power of two. The bunching into sets of increasing length can be done iteratively, by repeatedly replacing two adjacent samples by their average value (see Fig. [7.1]) and the algorithm in Fig. [7.2]. One starts with a sample of 2^N correlated data, at each block, we compute the apparent error, as if the data were independent. The average value remains unchanged. Bunching makes the data become increasingly independent, and makes the apparent error approach the true error of the Markov chain.

The question is how bunched data becomes less correlated? In the M block, bunches of size 2^M are generated: let us suppose that the samples are correlated on a length scale $\epsilon < 2^M$, but that original samples distant by more than 2^M are fully independent. It follows that, at the block M , these correlations still affect neighboring bunches, but not next-nearest ones: the correlation length of the data decreases from length 2^M to a length 2.

The bunching algorithm makes the data become increasingly independent and makes the apparent error approach the true error of the Markov chain for a determined number of blocks M for which the data is no longer correlated. This is related with the correlation length ϵ .

For example let us consider Fig. [7.1] one considers a sample of 64 correlated data. One bunchs two adjacent samples. Then, the first block ($M = 1$) contains 32 data and one calculates the average and the error as if they were independent data. The procedure of bunching into blocks is done again in such a way that for the second block ($M = 2$) we obtain 16 data. The average and the error are estimated and so on. The bunching algorithm is summarized as:

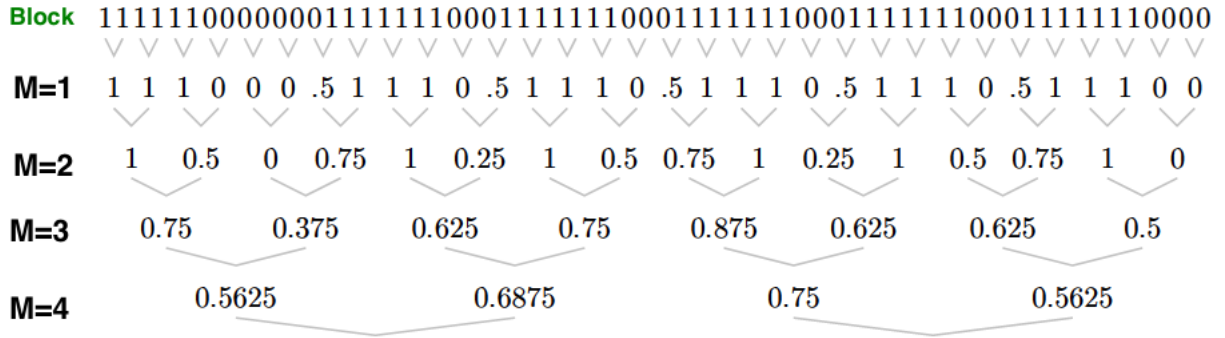


Figure 7.1: Bunching data algorithm for a sample of correlated data. Taking from Ref. [4].

```

input  $\{x_1, \dots, x_{2N}\}$  (Markov-chain data)
 $\Sigma \leftarrow 0$ 
 $\Sigma' \leftarrow 0$ 
for  $i = 1, \dots, N$  do
   $\Sigma \leftarrow \Sigma + x_{2i-1} + x_{2i}$ 
   $\Sigma' \leftarrow \Sigma' + x_{2i-1}^2 + x_{2i}^2$ 
   $x'_i \leftarrow (x_{2i-1} + x_{2i})/2$ 
error  $\leftarrow \sqrt{\Sigma'/(2N) - (\Sigma/(2N))^2}/\sqrt{2N}$ 
output  $\Sigma/(2N), \text{error}, \{x'_1, \dots, x'_N\}$ 

```

Figure 7.2: Bunching data algorithm taking from Ref. [4].

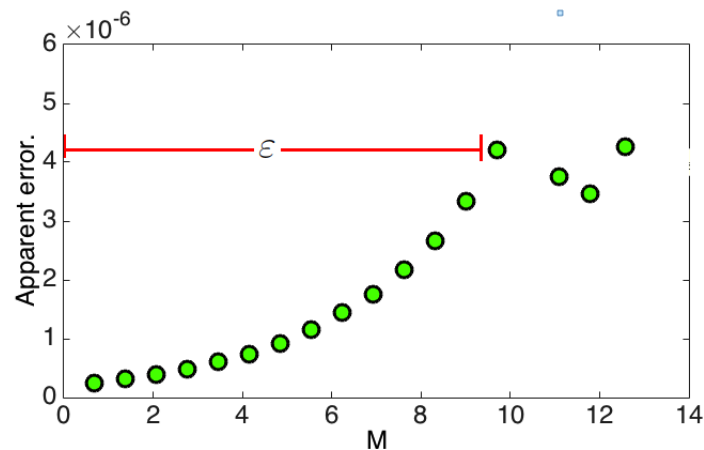


Figure 7.3: Estimation of the true error in a DMC simulation for 10000 iterations of the total energy for a system of bosons in a cubic box.

The question now is how to determinate the correlation length ϵ . In our previous example, the number of samples is very small the data is correlated for any number of blocks. Instead we use a realistic simulation with 10000 data. In Fig. [7.3] we plot the apparent error as a function of M for a total sample of 8192 MC data (equilibrated data). We use the bunching data algorithm (see Fig. [7.2]) . We observe that for $M = 10$ the data is not longer correlated since the bunching of uncorrelated data does not change the expected variance of the data.

Appendix B: The two-body problem.

The interaction between the impurity and the bosons can be modeled by an attractive square well (**ASW**) potential defined by:

$$V(\mathbf{r}) = \begin{cases} -V_0 & r \leq R_0 \\ 0 & r > R_0 \end{cases} \quad (7.1)$$

The two body-Schrödinger equation reads as:

$$f''(r) + \frac{2}{r}f'(r) + V(r)f(r) = Ef(r) \quad (7.2)$$

Plugging Eq. [7.1] in to the previous equation and considering the scattering states for $E \geq 0$. One obtains

$$f_I(r) = \begin{cases} A \sin(K_0 r)/r & r \leq R_0 \\ 1 - b/r & R_0 \leq r \leq R_m \\ B [1 - e^{-\alpha r} - e^{-\alpha(L-r)}] & R_m \leq r \leq L/2 \\ 2Be^{-\alpha L/2} & r > L/2 \end{cases} \quad (7.3)$$

f_I is constructed from the zero-energy scattering solution of the potential [7.1] orthogonal to the bound state existing for two particles when $b > 0$ in the region, where R_m is a matching point. $0 < r < R_m$. Continuity of the wavefunction and its first derivative at $r = R_0$

$$\left. \frac{f'_I}{f_I} \right|_{r=R_0} \rightarrow \text{continuous} \quad (7.4)$$

yields that

$$b = R_0 \left[1 - \frac{\tan(K_0 R_0)}{K_0 R_0} \right], \quad (7.5)$$

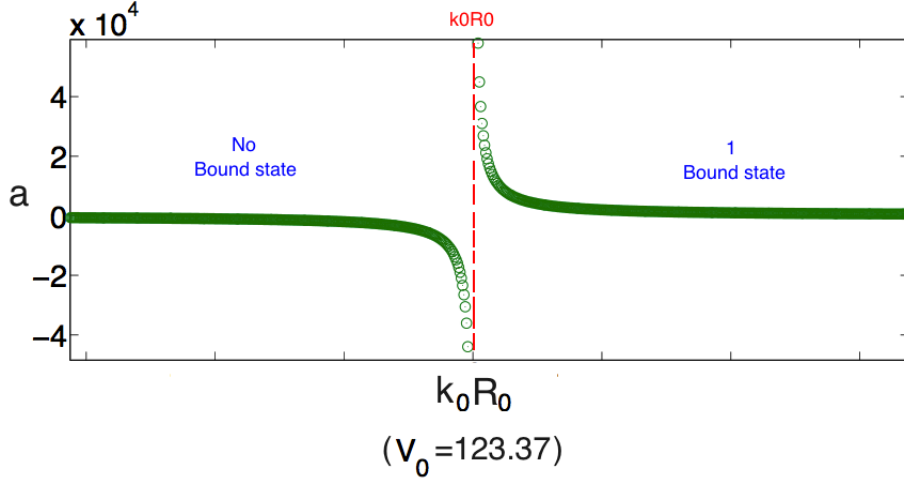


Figure 7.4: Plotting of Eq. [3.63]. For $R_0/a = 0.2$. By tuning the deep and range of the **ASWP**, one can access either to attractive interactions when $K_0 R_0 < \pi/2$ ($a < 0$) and or repulsive when, $K_0 R_0 > \pi/2$ ($a > 0$) and there is one bound state.

where $K_0^2 = 2m_R V_0/\hbar^2$ in terms of the reduced mass $m_R = m_I m_B/(m_I + m_B)$. Eq [7.5] is plotted in Fig. [7.4]. Continuity of the wavefunction and its first derivative at $r = R_m$ yields the transcendental equation

$$1 - \alpha x \frac{\exp(-\alpha x) - \exp(-\alpha [2 - x])}{\exp(-\alpha x) + \exp(-\alpha [2 - x])} = 0. \quad (7.6)$$

The impurity-boson scattering length b is tuned by changing either the depth or the range of the potential. for the **ASW** potential the value of the scattering length can be either positive or negative depending on $K_0 R_0$. In particular, we use values in the range $0 < K_0 R_0 < \pi$, corresponding to no bound state ($0 < K_0 R_0 < \pi/2$) and a single bound state ($\pi/2 < K_0 R_0 < \pi$) for the two-body problem (see Fig. [7.4]). In this latter case the molecular binding energy ϵ_B is obtained from the transcendental equation:

$$\frac{\tan(\kappa R_0)}{\kappa R_0} = \frac{\hbar}{R_0 \sqrt{2m_R |\epsilon_b|}} \quad (7.7)$$

This equation is obtained by requiring both the continuity of the wave function and of its first derivative at $r = R_0$. In Eq. [7.7], $\kappa^2 = 2m_R (V_0 - |\epsilon_b|)/\hbar^2$. The particular value $K_0 R_0 = \pi/2$ corresponds to the resonance (also known as unitary limit), where the s -wave scattering length diverges and the bound-state energy vanishes. The corresponding Jastrow wave function is given by the solution of the two-body bound state with energy ϵ_b for $0 < r < R_m$ and use a functional

form similar to Eq. [3.66] for $R_m < r < L/2$:

$$f_I(r) = \begin{cases} A \sin(\kappa r)/r & r \leq R_0 \\ [e^{-m|\epsilon_b|r/m}] /r & R_0 \leq r \leq R_m \\ B [e^{-\alpha r} + e^{-\alpha(L-r)}] & R_m \leq r \leq L/2 \\ 2Be^{-\alpha L/2} & r > L/2 \end{cases} \quad (7.8)$$

where $\kappa^2 = m(V_0 - |\epsilon_b|)/\hbar^2$. The coefficients A , B and α ensure the continuity of f_I and of its first derivative at the points R_0 and R_m through of the equation

$$\sqrt{\frac{|\epsilon_b|}{2a^2}} \frac{Lx}{2} + 1 - \frac{\alpha Lx}{2} \frac{\exp(-\frac{\alpha Lx}{2}) - \exp(-\frac{\alpha L}{2} [2-x])}{\exp(-\frac{\alpha L}{2} x) + \exp(-\frac{\alpha L}{2} [2-x])} = 0 \quad (7.9)$$

Bibliography

- [1] M. R. Matthews C. E. Wieman E. A. Cornell M. H. Anderson, J. R. Ensher. Observation of bose-einstein condensation in a dilute atomic vapor. *Science*, 269(5221):198–201, 1995.
- [2] Paul Julianne Cheng Chin, Rudolf Grimm and Eite Tiesinga. Feshbach resonances in ultracold gases. *Rev.Mod.Phys.*, 82(1225), 2010.
- [3] Ville Pietilä Richard Schmidt, Tilman Enss and Eugene Demler. Fermi polarons in two dimensions. *Phys. Rev. A.*, 85, 2012.
- [4] Werner Krauth. *Statistical Mechanics Algorithms and Computations*. Oxford university Press, 2006.
- [5] L.D. Landau and S.I Pekar. *Zh.Eksp.Teor.Fiz.*, 18,(419), 1948.
- [6] H. Fröhlich. *Adv.Phys.*, 3(325), 1954.
- [7] gerald D. Mahan. *Many-Particle Physics.*, volume 1. Plenum Press-New york and London, 1990.
- [8] F. M. Peeters and J.T. Devreese?. Acoustical polaron in three dimensions: The ground-state energy and the self-trapping transition. *Phys.Rev.B*, 32(6), 1985.
- [9] G. D. Mahan and J. J. Hopfield. Piezoelectric polaron effects in cds. *Phys.Rev.Lett*, 12(241), 1964.
- [10] S. A. Jackson and P. M. Platzman. Polaronic aspects of two-dimensional electrons on. *Phys.Rev.B*, 24(400), 1981.
- [11] P.M Studart S.A Jackson. Polaronic state of electrons on the surface of liquid helium films: A self-consistent treatment. *Phys.Rev.B*, 39(4133-4139), 1989.
- [12] Motohiko Saitoh Takaaki Kawaguchi, Tomi Ohtsuki. Two-rippion processes of electrons on the liquid 4he surface. *ELSEVIER*, 263(1-2), 1992.

- [13] I.F.Silvera J.T Devreese J. Tempere, S.N. Klimin. Wigner lattice of ripplopolarons un a multielectron bubble in helium. *Eur.Phys.J.32*, 2003, 329.
- [14] P.Longe A.J.Glick. *Phys.Rev.Lett*, 15(589), 1965.
- [15] S Lundqvist L.Hedin, B.I Lundqvist. *Solid state Comm*, 5(237), 1967.
- [16] B.I.Lundqvist. Single-particle spectrum of teh degenerate electron gas. *Physik der Kondensierten Materie*, 6(193), 1967.
- [17] Y.Toyozawa. Theory of the electronic polaron and ionizationof a trapped electronby an exciton. *Prog.Theor.Phys.*, 12(421), 1954.
- [18] C.T.C A.B. Kunz, J.T.Devreese. The role of the electronic polaron in the soft ray xabsorption of lithium halides. *J.Phys.C: Solid state Phys.*, 3259, 1072.
- [19] C.T.C. J.T.Devreese, A.B. Kunz. A resonace of the electronic polaron appearing in the optical absortion of alkaline halides. *Solid state Comm*, 11(673), 1972.
- [20] S.V Tyablikov N.N Bogoliubov. *Zh.Eksp.Teor.Fiz.*, 18(419), 1949.
- [21] R.P. Feynman. *Statistical Mechanics*. W.A. BENJAMIN, INC., 1972.
- [22] R.P. Feynman. Space-time approach to non-relativistic quantum physics. *Rev.Mod.Phys.*, 20(2):367–387, April 1948.
- [23] R.P. Feynman. Slow electrons in a polar crystal. *Phys.Rev.*, 97(3), 1955.
- [24] A. Sakamoto A. S. Mishchenko, N. V. Prokof'ev and B. V. Svistunov. Diagrammatic quantum monte carlo study of the fröhlich polaron. *Phys.Rev.B*, 62(6317), 2000.
- [25] Nikolay Prokof'ev Boris Svistunov Kris Van Houcke, Evgeny Kozik. Diagrammatic monte carlo. *arXiv:0802.2923*, 2008.
- [26] Nikolai V. Prokof'ev and Boris V. Svistunov. Polaron problem by diagrammatic quantum monte carlo. *Phys.Rev.Lett*, 81(2514), 1998.
- [27] F. M. Peeters G. Verbist and J. T. Devreese. Large bipolarons in two and three dimensions. *Phys.Rev.B*, 43(2712), 1991.
- [28] F. M. Peeters M. A. Smondyrev, G. Verbist and J. T. Devreese. Stability of multipolaron matter. *Phys.Rev.B*, 47(2596), 1993.
- [29] V. K. Mukhomorov C. A. Perroni, G. Iadonisi. Formation of polaron clusters. *Eur.Phys.B*, 41(163-170), 2004.

- [30] *Polarons and excitons*. New York, Plenum Press, 1963.
- [31] F. M. Peeters J. T. Devreese J. W. Hodby, G. P. Russell and D. M. Larsen. Cyclotron resonance of polarons in the silver halides: AgBr and AgCl. *Phys.Rev.Lett*, 58(1471), 1987.
- [32] S.N.Bose. *Z. Phys.*, 26(178), 1924.
- [33] A. Einstein. *Sitzber. Kgl. Preuss. Akad. Wiss*, 3(261), 1925.
- [34] A.D. Misener. J.F, Allen. *Nature*, 141(75), 1938.
- [35] F. London. *Nature*, 141:643, 1938.
- [36] L. Landau. Theory of the superfluidity of helium ii. *Phys.Rev.Lett*, 60:356, 1941.
- [37] N.N Bogoliubov. *J.Phys. (USSR)*, 11(23), 1947.
- [38] E.M. Lifshitz L.D. Landau. *The Classical Theory of Fields*. Addison-Wesley, 1951.
- [39] O. Penrose. *Philos.Mag*, 42:1373, 1951.
- [40] Lars Onsager Oliver Penrose. Bose-einstein condensation and liquid helium. *Phys.Rev.Lett*, 104(576), 1956.
- [41] A. P Keesom. W.H Keesom. New measurements on the specific heat of liquid helium". *Physica 2*, (557), 1935.
- [42] L. Onsager. *Nuovo Cimento*, suppl. 2(249 and 281), 1949.
- [43] R. Feynman. *Progress in Low temperature Physics*, volume 1. C.J Gorter, North-Holland, amsterdam, 1955.
- [44] W.F Vinen H.E Hall. *Proc. Roy . Soc. A*, (238):204, 1956.
- [45] T. W. Hansch ; A. L. Schawlow. Cooling of gases by laser radiation. *Optics Communications*, 13, 1975.
- [46] D. J. Wineland and Wayne M. Itano. Laser cooling of atoms. *Phys. Rev. A.*, 1979.
- [47] Alex Cable S. Chu D. Pritchard. E.L. Raab, M. Prentiss. Trapping of neutral sodium atoms with radiation pressure. *Phys.Rev.Lett*, 59(23), 1987.
- [48] C.J.Pethich and H.Smith. *Bose-Einstein Condensation In Dilute Gases*. CAMBRIDGE UNIVERSITY PRESS, 2002.

- [49] M.R. Andrews N.J. van Druten D.S. Durfee D.M. Kurn K.B. Davis, M.O. Mewes and W. Ketterle. Bose-einstein condensation in a gas of sodium atoms. *Phys.Rev.Lett*, 75(22):3969–3973, 1995.
- [50] J. J. Tollett C. C. Bradley, C. A. Sackett and R. G. Hulet. Evidence of bose-einstein condensation in an atomic gas with attractive interactions. *Phys.Rev.Lett*, page 1687, 75.
- [51] C. A. Sackett C. C. Bradley and R. G. Hulet. Bose-einstein condensation of lithium: Observation of limited condensate number. *Phys.Rev.Lett*, 78(985), 1997.
- [52] Lorenz Willmann David Landhuis Stephen C. Moss Daniel Kleppner Dale G. Fried, Thomas C. Killian and Thomas J. Greytak. Bose-einstein condensation of atomic hydrogen. *Phys.Rev.Lett*, 81(3811), 1998.
- [53] Junmin Wang C. J. Barrelet F. Perales E. Rasel C. S. Unnikrishnan M. Leduc F. Pereira Dos Santos, J. Léonard and C. Cohen-Tannoudji. Bose-einstein condensation of metastable helium. *Phys.Rev.Lett*, 86(16), 2001.
- [54] G. Roati R. J. Brecha A. Simoni M. Inguscio G. Modugno, G. Ferrari. Bose-einstein condensation of potassium atoms by sympathetic cooling. *Science*, 294(5545):1320–1322, 2001.
- [55] Michael Mark Hanns-Christoph Nägerl Rudolf Grimm Tino Weber, Jens Herbig. Bose-einstein condensation of cesium. *Science*, 299(10):232–235, 2002.
- [56] Seiji Sugawa Takeshi Fukuhara and Yoshiro Takahashi. Bose-einstein condensation of an ytterbium isotope. *Phys. Rev. A.*, 76(051604(R)), 2007.
- [57] Bo Huang-Rudolf Grimm Simon Stellmer, Meng Khoon Tey and Florian Schreck. Bose-einstein condensation of strontium. *Phys.Rev.Lett*, 103, 2009.
- [58] M. Mark S. Baier A. Rietzler R. Grimm K. Aikawa, A. Frisch and F. Ferlaino. Bose-einstein condensation of erbium. *Phys.Rev.Lett*, (108), 2012.
- [59] C. H. Schunck S. M. F. Raupach S. Gupta Z. Hadzibabic M. W. Zwierlein, C. A. Stan and W. Ketterle. Observation of bose-einstein condensation of molecules. *Phys.Rev.Lett*, 91, 2003.
- [60] A. Altmeyer G. Hendl S. Riedl C. Chin¹ J. Hecker Denschlag¹ R. Grimm. S. Jochim, M. Bartenstein. Bose-einstein condensation of molecules. *Science*, 302(19), 2003.
- [61] Lev Pitaevskii-Sandro Stringari. *Bose-Einstein Condensation*, volume 1. OXFORD SCIENCE PUBLICATIONS, 2003.

- [62] E.M. Lifshitz L.D. Landau. *Quantum Mechanics*, volume 3. Pergamon Press 1965.
- [63] K. Huang T. D. Lee and C. N. Yang. *Phys.Rev.Lett*, (106):1135, 1957.
- [64] Herman Feshbach. Unified theory of nuclear reactions. *Ann.Phys.*, 5(4):357–390, 1958.
- [65] B. J. Verhaar E. Tiesinga and H. T. C. Stoof. Threshold and resonance phenomena in ultracold ground-state collisions. *Phys. Rev. A.*, 47(4114), 1993.
- [66] J. Dalibard I. Bloch and W. Zwerger. Many-body physics with ultracold gases. *Rev.Mod.Phys.*, 80(885), 2008.
- [67] Sylvain Nascimbène. Immanuel Bloch, Jean Dalibard. Quantum simulations with ultracold quantum gases. *Nature Physics.*, (8):267–276, 2012.
- [68] Jozef T. Alexandrov, Alexandre S. Devreese. *Advances in polaron physics*. Springer series in solid-state sciences, 2010.
- [69] A. Alexandrov E. K. Salje and W. Liang. *Polarons and bipolarons in high-Tc superconductors and related materials*. Cambridge University Press, 2005, 2005.
- [70] B. Holzapfel L. Schultz R. von Helmolt, J. Wecker and K. Samwer. Giant negative magnetoresistance in perovskitelike $\text{La}_{2/3}\text{Ba}_{1/3}\text{MnO}_x$ ferromagnetic films. *Phys.Rev.Lett*, 71(2331), 1993.
- [71] Jun Kondo. Resistance minimum in dilute magnetic alloys. *Prog.Theor.Phys.*, 32(37-49), 1964.
- [72] J. Kondo. Resistance minimum in dilute magnetic alloys. *Prog.Theor.Phys.*, 32(37-49), 1964.
- [73] Ariel Sommer André Schirotzek, Cheng-Hsun Wu and Martin W. Zwierlein. Observation of fermi polarons in a tunable fermi liquid of ultracold atoms. *Phys.Rev.Lett*, 102, 2009.
- [74] Frédéric Chevy and Christophe Mora. Ultra-cold polarized fermi gases. *Rep. Prog. Phys.*, 73, 2010.
- [75] R. A. Duine and A. H. MacDonald. Itinerant ferromagnetism in an ultracold atom fermi gas. *Phys.Rev.Lett*, 95, 2005.
- [76] Matteo Zaccanti Pietro Massignan and Georg M Bruun. Polarons, dressed molecules and itinerant ferromagnetism in ultracold fermi gases. *Rep. Prog. Phys.*, 77, 2014.
- [77] Enrico Vogt Bernd Fröhlich Michael Feld Marco Koschorreck, Daniel Pertot and Michael Köhl. Attractive and repulsive fermi polarons in two dimensions. *Nature*, 485.

- [78] M. Jag A. Trenkwalder P. Massignan G. M. Bruun F. Schreck C. Kohstall, M. Zaccanti and R. Grimm. Metastability and coherence of repulsive polarons in a strongly interacting fermi mixture. *Nature*, 485, 2012.
- [79] Dmitry A. Abanin Aditya Shashi, Fabian Grusdt and Eugene Demler. Radio-frequency spectroscopy of polarons in ultracold bose gases. *Phys. Rev. A.*, 2014.
- [80] Manuel Endres Marc Cheneau Peter Schauß Sebastian Hild David Bellem Ulrich Schollwöck Thierry Giamarchi Christian Gross Immanuel Bloch Takeshi Fukuhara, Adrian Kantian and Stefan Kuhr. Quantum dynamics of a mobile spin impurity. *Nature*, 2013.
- [81] Jacob F. Sherson Marc Cheneau Peter Schauß Takeshi Fukuhara Immanuel Bloch Christof Weitenberg, Manuel Endres and Stefan Kuhr. Single-spin addressing in an atomic mott insulator. *Nature*, 2011.
- [82] D. Naik M. Gring M. Inguscio F. Minardi A. Kantian J. Catani, G. Lamporesi and T. Giamarchi. Quantum dynamics of impurities in a one-dimensional bose gas. *Phys. Rev. A.*, 85, 2012.
- [83] Shincy John Claudia Weber Dieter Meschede Nicolas Spethmann, Farina Kindermann and Artur Widera. Dynamics of single neutral impurity atoms immersed in an ultracold gas. *Phys. Rev. A.*, 109, 2012.
- [84] J. M. Choi W. Alt A. Widera M. Karski, L. Förster and D. Meschede. Nearest-neighbor detection of atoms in a 1d optical lattice by fluorescence imaging. *Phys.Rev.Lett*, 2009.
- [85] Jai-Min Choi Andreas Steffen Noomen Belmechri Wolfgang Alt Dieter Meschede Michał Karski, Leonid Förster and Artur Widera. Imprinting patterns of neutral atoms in an optical lattice using magnetic resonance techniques imprinting patterns of neutral atoms in an optical lattice using magnetic resonance techniques. *NJP*, 12, 2010.
- [86] Jai-Min Choi Andreas Steffen Noomen Belmechri Wolfgang Alt Dieter Meschede Michał Karski, Leonid Förster. Quantum walk in position space with single optically trapped atoms. *Science*, 10, 2009.
- [87] S. John C. Weber D. Meschede A. Widera N. Spethmann, F. Kindermann. Inserting single cs atoms into an ultracold rb gas. *Applied Physics B*, 106(3), 2012.
- [88] W. L. McMillan. Ground state of liquid he4. *Phys.Rev.Lett*, 138(A422), 1965.
- [89] R.G Storer R.C Grimm. Monte-carlo solution of schrödinger's equation. *Journal of Computational Physics*, 7(1):134–156, 1971.

- [90] E.L. Pollock. and D.M.Ceperley. Simulation of quantum many-body systems by path integral methods. *Phys.Rev.B*, 30(5):2555–2568, September 1984.
- [91] Kenneth Paul Esler. *Advancements in the Path integral Monte Carlo method for many-body quantum systems at finite temperature*. PhD thesis, Massachusetts Institute of Technology, MIT, 1999.
- [92] D. M. Ceperley. *Rev.Mod.Phys.*, 67(2), April 1995.
- [93] G.E.P. Box and Mervin Muller. A note on the generation of random normal deviates. *The Annals of Mathematical Statistics*, 29(2), 1958.
- [94] N. Metropolis, A.W Roenbluth, A. H Teller, and E. Teller. Metropolis. *J. Chem. Phys*, 21, 1087.
- [95] H. L. Friedman. Download PDF P. J. Rossky¹, J. D. Doll. Brownian dynamics as smart monte carlo simulation. *J. Chem. Phys.*, 69(4628), 1978.
- [96] J.B. Anderson. A random-walk simulation of the schrödinger equation. *The journal of Chemical Physics*, 63(4)(1499), 1975.
- [97] J.B. Anderson. Quantum chemistry by random walk, h+ 3 d3h 1a0 1, h2 3+u , h4 1+g , be 1s. *The journal of Chemical Physics*, 65(4121), 1976.
- [98] F. M. Peeters and J. T. Devreese. Acoustical polaron in three dimensions: The ground-state energy and the self-trapping transition. *Phys.Rev.B*, 32(3515), 1985.
- [99] G.D. Mahan and J.J Hopfield. *Phys.Rev.Lett*, 12(241), 1964.
- [100] W.F Saam. Dilute mixture of fermions in a bose gas,. *Ann.Phys.(Paris)*, 53(239-252), (1969).
- [101] L. Viverit and S. Giorgini. Ground-state properties of a dilute bose-fermi mixture. *Phys.Rev.A*, 66(063604), 2002.
- [102] F. M. Cucchietti and E. Timmermans. Strong-coupling polarons in dilute gas bose-einstein condensates. *Phys.Rev.Lett*, 2006.
- [103] S. Das Sarma Weiran Li. Variational study of polarons in bose-einstein condensates. *arXiv.org*.
- [104] M.K.Oberthaler S.Knoop E Timmermans J.Tempere, W. Casteels and J.T.Devreese. Feynman path-integral treatment of the bec-impurity polaron,. *Physical Review B*, 2009.

- [105] J.T Devreese W. Casteels J. Tempere. Many-polarons description of impurities in a bose-einstein condensate in the weak-coupling regime. *Phys.Rev.A*, 84(063612), 2011.
- [106] J. Tempere W. Casteels, T. Van Cauteren and J. T. Devreese. Strong coupling treatment of the polaronic system consisting of an impurity in a condensate. *Laser Phys.*, 21(1480), 2011.
- [107] M. Bruderer. W. Bao and D. Jaksch. Self-trapping of impurities in bose-einstein condensates: Strong attractive and repulsive coupling. *EPL*, 82(30004):6, 2008.
- [108] Steffen Patrick Rath and Richard Schmidt. Field-theoretical study of the bose polaron. *Phys. Rev. A.*, 2013.
- [109] Neil W. Ashcroft and N. David Mermin. *Solid State Physics*. Saunders College, 1976, 2007.
- [110] Henning Heiselberg. Fermi systems with long scattering lengths. *Phys. Rev. A.*, 63, 2001.
- [111] Steffen Patrick Rath and Richard Schmidt. Field-theoretical study of the bose polaron. *Phys. Rev. A.*, 88(053632), 2013.
- [112] S. Tan. Energetics of a strongly correlated fermi gas. *Annals of Physics*, 323(2952), (2008).
- [113] V. N. Efimov. *Phys. Lett. B*, 33(563), 1970.
- [114] D. S. Petrov and F. Werner. Three-body recombination in heteronuclear mixtures at finite temperature. *arXiv.org.*, (1502.04092v1), 2015.
- [115] R. W. Ghrist E. A. Cornell C. J. Myatt, E. A. Burt and C. E. Wieman. Production of two overlapping bose-einstein condensates by sympathetic cooling. *Phys.Rev.Lett*, 78(586), 1997.
- [116] A. P. Chikkatur S. Inouye H.-J. Miesner J. Stenger D. M. Stamper-Kurn, M. R. Andrews and W. Ketterle. Optical confinement of a bose-einstein condensate. *Phys.Rev.Lett*, 80(2027), 1998.
- [117] F. Riboli G. Roati G. Modugno, M. Modugno and M. Inguscio. Two atomic species superfluid. *Phys.Rev.Lett*, 89(190404), 2002.
- [118] J. R. Ensher C. E. Wieman D. S. Hall, M. R. Matthews and E. A. Cornell*. Dynamics of component separation in a binary mixture of bose-einstein condensates. *Phys.Rev.Lett*, 1998.

- [119] A. Sinatra and Y. Castin. Binary mixtures of bose-einstein condensates: Phase dynamics and spatial dynamics. *Eur. Phys. J. D*, 8:319–332, 2000.
- [120] G. Barontini F. Minardi J. Catani, L. De Sarlo and M. Inguscio. Degenerate bose-bose mixture in a three-dimensional optical lattice. *Phys. Rev. A.*, 77, 2008.
- [121] B. A. Heringa M. J. Bijlsma and H. T. C. Stoof. Phonon exchange in dilute fermi-bose mixtures: Tailoring the fermi-fermi interaction. *Phys. Rev. A.*, 61, 2000.
- [122] C. J. Pethick L. Viverit and H. Smith. zero-temperature phase diagram of binary boson-fermion mixture. *Phys. Rev. A.*, 61, 2000.
- [123] K. Dieckmann S. Gupta M. W. Zwierlein A. Görlitz Z. Hadzibabic, C. A. Stan and W. Ketterle. Two-species mixture of quantum degenerate bose and fermi gases. *Phys.Rev.Lett*, 88(16), 2002.
- [124] M. A. Smondryev E. A. Kochetov. Fröhlich multipolarons. *Theoretical and Mathematical Physics*, 85(1062-1072), 1990.
- [125] A S Alexandrov and N F Mott. Bipolarons. *Rep. Prog. Phys.*, 57(1197), 1994.
- [126] J. Tempere W. Casteels and J. T. Devreese. Many-polaron description of impurities in a bose-einstein condensate in the weak-coupling regime. *Phys. Rev. A.*, 84, 2011.
- [127] D H Santamore and Eddy Timmermans. Multi-impurity polarons in a dilute bose–einstein condensate. *NJP*, 13, 2011.
- [128] W. Casteels J. Tempere and J. T. Devreese. Bipolarons and multipolarons consisting of impurity atoms in a bose-einstein condensate. *Phys. Rev. A.*, 88, 2013.
- [129] G.O Balabanyan. *Theoretical and Mathematical Physics*, Volume 71(1):418–428, April 1987.
- [130] N.N Bogoliubov and D.N Zubarev. *Zh.Eksp.Teor.Fiz.*, 28(129), 1955.